Ikasketa automatikoan eta seinalearen prozesaketan oinarritutako ekarpenak zirkulazio-egoera identifikatzeko ospitalez kanpoko bihotz-biriketako geldialdietan

Egilea

Andoni Elola Artano

Zuzendariak:

Elisabete Aramendi Ecenarro

Unai Irusta Zarandona

Doktorego tesia

eman ta zabal zazu

Universidad del País Vasco
Euskal Herriko Unibertsitatea

Komunikazioen ingeniaritza saila

Bilbo, 2021eko apirila

AURKIBIDEA

IRUDIEN ZERRENDA

TAULEN ZERRENDA

LABURDUREN ZERRENDA

AHA	American Heart Association
AS	Asistolia
BBB	Bihotz-biriketako berpiztea
BEA	Bihotz-erritmoaren aldakortasuna
BBG	Bihotz-biriketako geldialdia
BI	Bular-inpedantzia
BPGAE	Benetako pultsurik gabeko aktibitate elektrikoa
BPP	Balio prediktibo positiboa
BPN	Balio prediktibo negatiboa
BZI	Berezko zirkulazioaren itzulera
CO_2	Karbono dioxidoa
DPA	Desfibrilazio publikorako atzipena
EBM	Euskarri bektoredun makinak
EKG	Elektrokardiograma
ERC	European Resuscitation Council
FB	Fibrilazio bentrikularra
KAA	Kurbaren azpiko azalera
KDA	Kanpoko desfibriladore automatikoa
LOS	Larrialdi osasun sistema
OKBBG	Ospitalez-kanpoko bihotz-biriketako geldialdia
PE	Pultsudun erritmoa
PGAE	Pultsurik gabeko aktibitate elektrikoa

PRKAA	PR kurbaren azpiko azalera
ROC	Receiver operating characteristic
RF	Random forest
Se	Sentsibilitatea
Sp	Espezifikotasuna
SPGAE	Sasi-pultsurik gabeko aktibitate elektrikoa
SS	Sakaden sakontasuna
TB	Takikardia bentrikularra
ZO	Zehaztasun orekatua

1 SARRERA

1.1 Ospitalez kanpoko bihotz-biriketako geldialdia

Bat-bateko bihotz geldialdia (BBG) ustekabeko bihotz jardueraren etenaldi gisa definitzen da [9], non odol perfusioa ez baita iristen ez burmuinera, ez beste ezinbesteko organoetara. BBGa ahalik eta azkarren tratatu behar da berpizte terapien bidez bat-bateko bihotz heriotza (BBH) ekiditeko [10, 11]. Ohikoena BBGa ospitalez kanpoko inguruneetan gertatzea da [12] eta kasu gehienetan ez da lekukorik egoten [13]. Horregatik, berpizte terapien aplikazio goiztiarra erronka mediku eta soziala da gaur egun.

BBGaren etiologia oso ongi ezagutzen ez den arren, kasuen %80a gaixotasun koronarioen ondorioz gertatzen direla estimatzen da [14], eta geratzen den %20a faktore genetikoei eta kardiopatia desberdinen ondorioz [14, 15]. Gaixotasun horiek bihotz-erritmo desberdinak sortzen dituzte, fibrilazio bentrikularra (FB) izanik ohikoena ospitalez kanpoko BBGan (OKBBG). Gaixoak FB erritmo bat aurkezten duenean, bentrikuluen uzkurtze-maiztasuna azkarra eta irregularra da, beraz, bihotza uzkurtzen den arren, ez du nahikoa odol banatzen gorputzera. Beste batzuetan bihotz-maiztasuna asko jaisten da eta bihotza geratu egiten da.

Herrialde industrializatuetan BBGa heriotza kausa nagusienetako bat da, baina bere intzidentzia estimatzea ez da erraza, definizioa eta kasuak kontutan hartzeko irizpideak desberdinak izan baitaitezke ikerketa zientifikoaren arabera. Urteko kasu kopurua 150 000 eta 530 000 tartean estimatzen da Estatu Batuetan [10, 16] eta 275 000 Europan [17, 18], hau da, 55 eta 38 kasu 100 000 biztanleko hurrenez hurren. Espainian 29 eta 40 kasu tartean estimatzen dira 100 000 biztanleko [19, 20], eta Euskal Autonomia Erkidegoan 34 inguru [21].

Azken urteetan komunitate zientifikoa asko saiatu da BBGa aurresaten eta hobeto tratatzen. Hala ere, biziraupen-tasa egoera neurologiko funtzionalarekin %9 inguruan dago pertsona helduetan [22]. Egun, atentzioa merezi duen osasun publikoko arazo larri bat kontsideratzen da, bere bat-bateko portaeragatik eta biziraupen-tasa baxuengatik.

1.2 Berpizte terapiak

Hainbat nazioarteko elkarte daude gaur egun BBG terapien definizioak eta protokoloak bateratzeko, *American Heart Association* (AHA) eta *European Resuscitation Council* (ERC) dira garrantzi eta inpaktu handiena dutenak mundu mailan. Munduko elkarte desberdinek batera lan egiteko *International Liaison Committee on Resuscitation* (ILCOR) sortu zen 1992an; zeinek 5 urtero berpizte terapia gauzatzeko gidak eguneratzen dituen azken urteetako ebidentzia zientifikoetan oinarrituta.

OKBBG kasuetan egungo gidek 5 erritmo mota bereizten dituzte [23, 24]: FB, takikardia bentrikularra (TB, bentrikuluen aktibitate elektriko ezegokiak bihotz-maiztasun altuak eragiten ditu), asistolia (AS, aktibitate elektriko falta), pultsurik gabeko aktibitate elektrikoa (PGAE, disoziazio elektromekanikoa) eta pultsudun erritmoa (PE, nahikoa odol fluxu sortzen duen erritmo organizatua). Erritmo bakoitzaren adibide bat 1.1. irudian erakusten da. Oro har, FB eta TB erritmoek desfibrilazio elektrikoa behar dute bihotzaren ohiko funtzionamendua berreskuratzeko, AS eta PGAE erritmoek berriz, bihotz-biriketako berpiztea (BBB) eskatzen dute.

BBB terapia bular-sakadez eta aireztapenez osatzen da. Horien helburua da oxigeno nahikoa duen odol fluxu minimo bat eskaintzea oinarrizko organoei, batik bat bihotzari eta burmuinari [25]. Soroslea gaixoaren ondoan jartzen da BBB terapia gauzatzen duen bitartean, 1.2. irudian erakusten den moduan. Behin BBGa identifikatuta, BBB terapia ahalik eta azkarren hastea komeni da eta larrialdi osasun sistemaren (LOS) protokoloa aktibatu behar da. Kasu gehienetan,

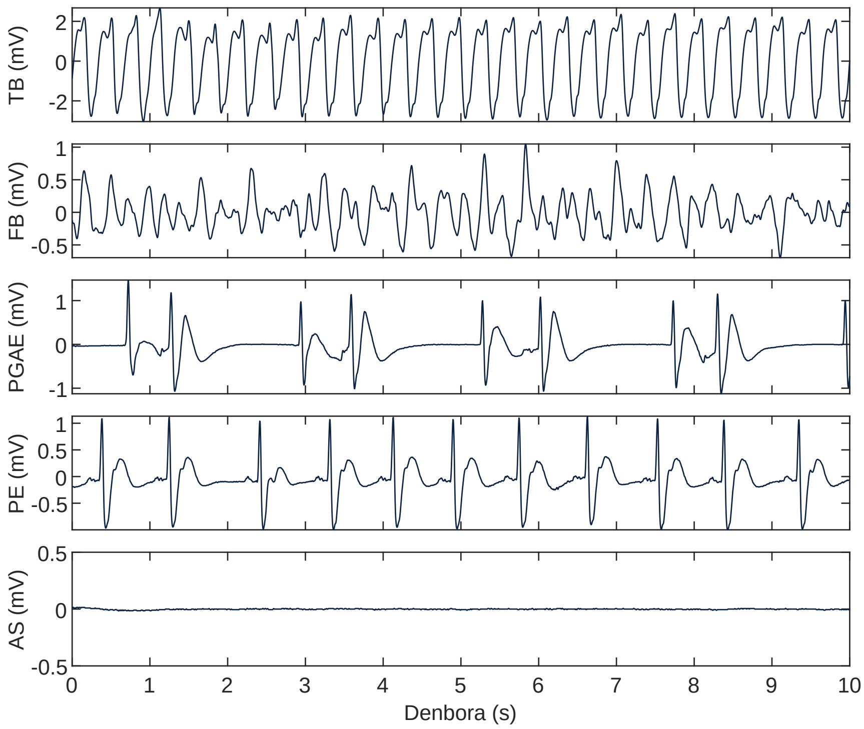

1.1. Irudia. Bihotz-biriketako geldialdian aurkitu daitezken bost erritmoen adibideak. Goitik behera: takikardia bentrikularra (TB), fibrilazio bentrikularra (FB), pultsurik gabeko aktibitate elektrikoa (PGAE), pultsudun erritmoa (PE) eta asistolia (AS).

BBB terapia soilik ez da nahikoa gaixoa BBGtik ateratzeko, eta bai intubazioa bai tratamendu farmakologikoa beharrezkoak dira.

Biziraupen-kateak (1.3 irudia) lau maila definitzen ditu gaixoaren biziraupen-probabilitatea handitzeko [26, 27], gidek azaltzen dituzten honako lau oinarrizko faseak adieraziz:

- **Sarbide goiztiarra:** Aurreneko gakoa BBGa ahalik eta azkarren antzematea da, eta LOS protokoloa aktibatzea. Horrek biziraupen-probabilitatea igotzen duela frogatuta dago [28].
- **BBB goiztiarra:** Bular-sakadak eta aireztapenak ahalik eta azkarren hastea beharrezkoa da gaixoaren biziraupen-probabilitatea igotzeko. Hainbat ikerketek frogatu duten moduan, lekukoek BBB terapia aplikatzen dutenean biziraupen-probabilitatea

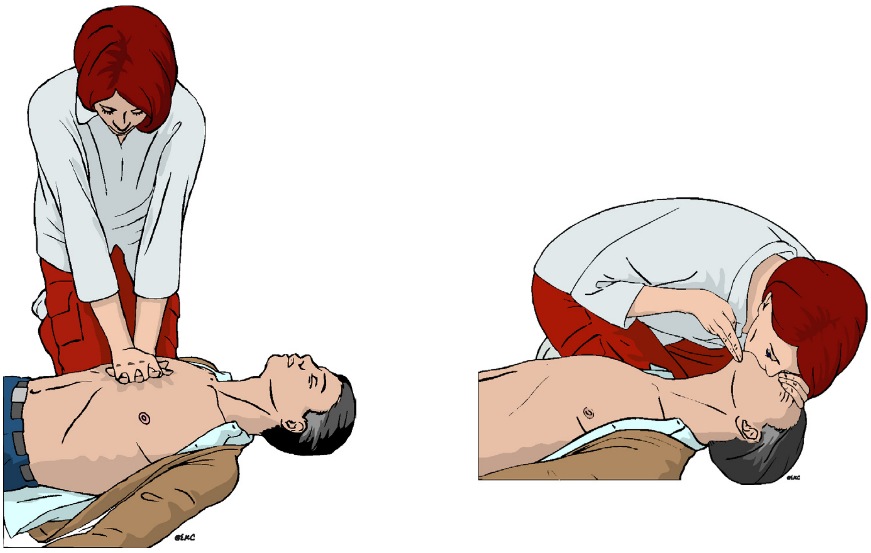

1.2. **Irudia.** Soroslearen kokapena bular-sakadak eta aireztapenak emateko, gaixoari BBB aplikatzen dion bitartean. Iturria: ERC gidak 2015 [23].

handiagoa da [29, 30, 31]. Horregatik, biztanleriak lehen sorospen ikastaroak eta BBB ikastaroak egitea beharrezkoa da. AHAren arabera, biztanleriaren %20a prestatzeak biziraupen-tasak nabarmenki igoko lituzke [32]. Beste ikerketa baten arabera, lekukoek lehen 4 minutuetan BBBa aplikatzen badute eta desfibrilazio elektrikoa aurreneko 8 minutuetan eman, biziraupen-tasa bikoiztu daiteke [33].

- **Desfibrilazio goiztiarra:** Desfibrilazio elektriko bat behar duen erritmoa agertzen denetik, aurreneko desfibrilazio elektrikoa eman arte igarotako denborak eragin handia dauka gaixoaren biziraupen-probabilitatean [34, 35]. Desfibrilazio publikorako atzipen (DPA) programen helburua desfibrilazio elektrikoa eskuragarria izatea da kanpoko desfibriladore automatikoen (KDA) bidez [36]. Lekukoek BBB terapia aplikatzen ez dutenean, biziraupen-tasa %10-12 jaisten da desfibrilazio elektrikoa atzeratzen den minuturo [37, 38].
- **Bizi-euskarri aurreratu (BEA) goiztiarra:** Baliteke BBBa eta desfibrilazio elektrikoa nahikoa ez izatea eta gaixoak medikuak

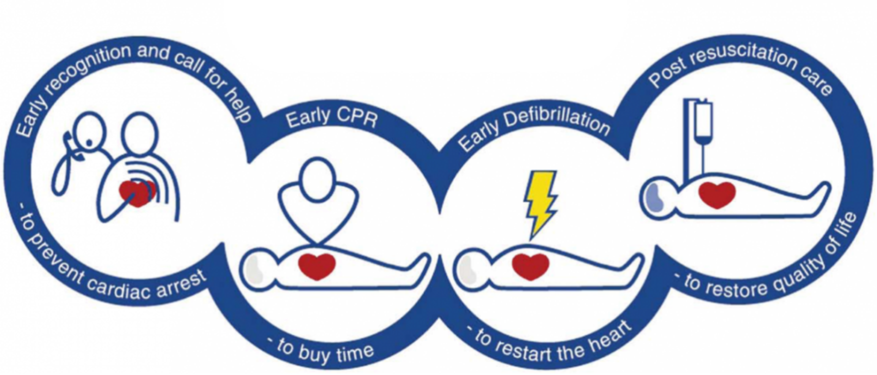

1.3. Irudia. Biziraupen-katearen oinarrizko lau urratsak: sarbide goiztiarra, BBB goiztiarra, desfibrilazio goiztiarra eta bizi-euskarri aurreratu goiztiarra. Iturria: ERC gidak 2015 [23].

emandako tratamendua behar izatea. Hala nola, medikamentu desberdinen administrazioa edo intubazioa [39].

Terapiaren helburu nagusia gaixoak PEa berreskuratzea da, hots, berezko zirkulazioaren itzulera (BZI) lortzea. Horren ondoren datorren terapiari geldialdi ondoko zaintza ere deitzen zaio, eta guztiz beharrezkoak da gaixoaren biziraupen-probabilitatea igotzeko [39]. Egungo giden arabera, gaixoak BZI lortu bezain laster, gertuen dagoen zainketa intentsiboko zentrora eraman behar da etengabeko diagnostiko, monitorizazio eta tratamendurako [24, 40].

1.3 Monitorizazioa eta datuen bilketa OKBBGan

Soroslea terapiaren fase desberdinen zehar gidatu ahal izateko, gaixoaren oinarrizko bizi-zeinuak eta seinale fisiologiko desberdinak monitorizatzea ezinbestekoa da. Gailu mota desberdinak erabili daitezkeen arren, arruntenak KDA eta monitore/desfibriladoreak dira.

KDA oinarrizko gailua da, medikuntza arloan heziketa edo ezagutza minimo batzuk dituen jendeak erabiltzeko modukoa [23]. KDA piztu ondoren, desfibrilazio txaplatak behar bezala eransteko eskatzen du (1.4. irudian erakusten den moduan). Ondoren, gailuak BBBa aplikatzeko eskatzen du edo bestela etenaldi bat egiteko, KDAk erritmoa aztertu dezan eta beharrez gero, desfibrilazio

1.4. Irudia. Kanpoko desfibriladore automatiko (KDA) komertzial bat eta txaplaten kokapen egokia.

elektrikoa aplikatu dezan. Soroslea audio- edo ikusmen-oharren bidez gidatzen du gailuak. Normalean KDA batek bi seinale jasotzen ditu: EKGa (bihotzaren aktibitate elektrikoaren adierazpena) eta bular inpedantzia (BI). Bigarren hau azala eta elektrodoaren arteko lotura egiaztatzeko erabiltzen zen hasiera batean, baina gaur egun erabilera gehiago ditu. Maiztasun altuko korronte elektriko bat txertatzen da (20-100 kHz, 1-5 mA) eta bi txaplaten arteko potentzial diferentzia neurtzen da. Azkenik, Ohm-en legea aplikatuz bularrak duen inpedantzia kalkulatzen da [41].

KDAen erabilera nahiko zabala da gaur egun DPA programei esker [36]. Arrakastaz inplementatu dira aireportuetan [42], kiroldegietan, kasinoetan [34] edo unibertsitateetan, eta hainbat ikerketen arabera BBGaren hasieraren eta aurreneko desfibrilazio elektrikoaren arteko tartea murrizten dute, biziraupen-probabilitatea igoz [43, 44, 45].

Monitore/desfibriladoreak eskarmentu gehiago daukaten profesionalentzat daude pentsatuta, ospitalez kanpoko eta ospitale barruko eszenarioetan erabiltzeko. Gailu horiek seinale fisiologikoak etengabe bistaratzen dituzte, baita bizi-zeinu desberdinak ere. EKG eta BI seinaleez gain, modulu gehigarriak edukitzen dituzte seinale gehiago jaso ahal izateko, adibidez, pulsioximetria, kapnografia edo odolaren presioa. Pulsioximetria sentsore optiko baten bidez lortzen da, behatzean, sudurrean edo belarrian kokatzen dena, eta odolean dagoen oxigenoaren saturazioa neurtzen du (%94tik gora izaten dute hemodinamikoki egonkorrak diren pertsonek). Kapnografia ahoan edo sudurrean jasotzen da, eta gaixoak botatzen dituen gasetan dagoen karbono dioxidoaren (CO_2) presio partziala irudikatzen du denboran [46]. Azken urteetan kapnografia seinalearen erabilera asko zabaldu da, eta egungo berpizte gidek bere erabilera sustatzen dute intubazioa zuzen egin dela baieztatzeko, BBBaren kalitatea bermatzeko [47, 48] edo aireztapenen maiztasuna monitorizatzeko [49]. Gainera, BZI baieztatzeko ere erabilgarria izan daitekeela frogatu da [50, 48, 51, 52, 53, 54, 46].

Dispositibo berriagoek sakaden kalitatea monitorizatzeko modulu gehigarriak ere badituzte. Honela, sakaden maiztasuna eta sakontasuna kalkulatzen dute azelerometroei edo indar-sentsoreei esker. Sakaden sakontasun (SS) seinaleak sakada bakoitzaren eboluzioa erakusten du eta bertatik metrika desberdinak kalkulatzea erraza da. Sorosleari sakaden kalitateari buruzko informazioa emateak berauen kalitatea hobetzen du, biziraupen-probabilitatea handituz [55].

Azaldutako seinale batzuen adibideak 1.5. irudian erakusten dira. Sakadak oso erraz identifikatzen dira SS seinaleari edo BI seinaleari begiratuz, gorabeherak erakusten baitituzte sorosleak gaixoaren bularra bultzatzen duen bakoitzean [56]. Bular-sakadek artefaktu bat sortu dezakete EKG edo kapnografia seinaleetan, seinale horien interpretazio egokia zailduz. Kapnografia seinaleak gorabeherak erakusten ditu aireztapen bakoitzarekin (BI seinalean ere antzeman daitezke), eta gaixoak arnasketaren bukaeran botatzen duen CO_2 mailari $EtCO_2$ deritzo.

Gailu mota horiek jasotzen dituzten seinaleak eta datuak ordegailura jaisteko aukera dago normalean, KDA edo monitore/desfibriladorearen ekoizleak eskaintzen duen softwarea erabiliz (CODE-STAT adibidez Strykerrek egiten dituen gailuentzat). Hala ere, tresna gehigarriak behar dira normalean informazio hori irekia den formatu batetara esportatzeko, zeinak beharrezkoak diren ikerketa-proposamenak garatzeko.

Seinaleez gain, geldialdiari buruzko hainbat informazio bildu eta jasotzen da BBG erregistro handiak sortzeko. Informazio hori era uniforme batetan biltzeko Utstein ereduak sortu ziren ospitalez kanpoko eta barruko BBGentzat [57, 58, 59]. Eredu horiek informazio anitz gehitzen dute, hala nola, BBG bakoitzaren testuinguruari

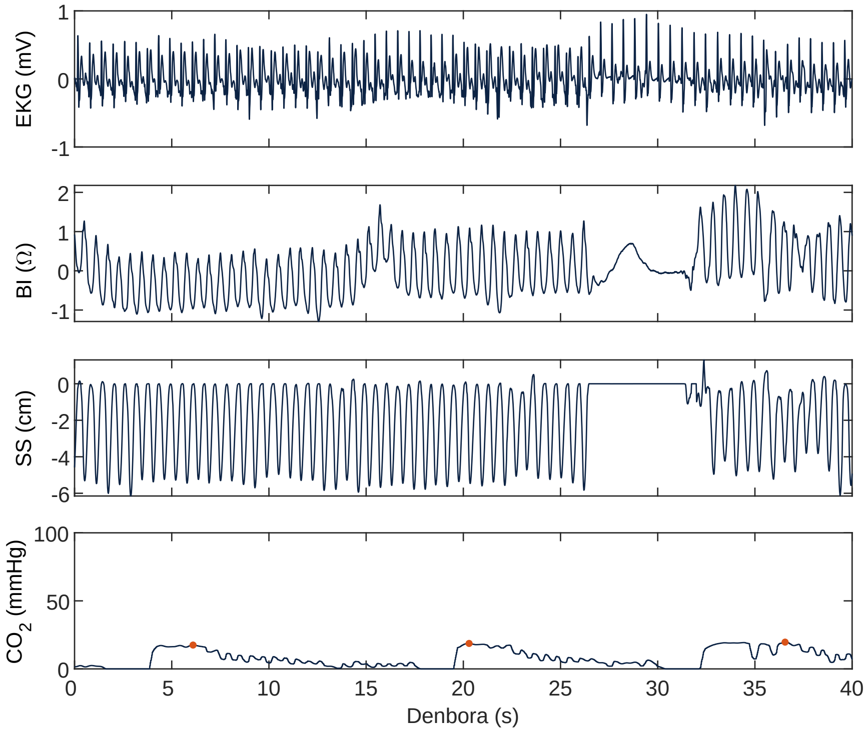

1.5. Irudia. Monitore/desfibriladoreek jasotzen dituzten seinaleen adibideak. Goitik behera: EKG, bular inpedantzia (BI), sakaden sakontasuna (SS) eta kapnografia. Sakadek fluktuazio azkarrak induzitzen dituzte BI eta SS seinaleetan. Aldiz, aireztapenen ondoriozko fluktuazio makalagoak ikusten dira kapnografian edo BI seinalean.

buruz, gaixoaren informazio pertsonala, etiologia, bistaratu den lehen bihotz-erritmo mota, sakada mekanikoei edo eskuzkoei buruzko informazioa edo gaixoaren pronostikoa. Tesi hau gauzatzeko garrantzitsuena BZIari lotutako informazioa da, eta Utstein ereduak ondokoak gehitzen ditu: ea BZIa egon den edo ez, egon bada noiz (unea), berriro galdu den edo ez, eta gaixoaren egoera momentu desberdinetan (geldialdiaren tokian bertan, ospitalera iristean, ospitaletik irtetean, ...).

1.4 Pultsua antzematea

Gaixoak pultsua daukan edo ez jakitea ezinbestekoa da biziraupen-katearen pausuak jarraitu ahal izateko. Berpizte maniobra guztiak

BZIa lortzeko daude pentsatuta, beraz, pultsua noiz berreskuratzen den edo galtzen den jakiteak asko laguntzen du, berpizte lanak bideratuz gehienbat ondoko hiru fasetan:

- BBGaren hasieran beharrezkoa da BBGa identifikatzea, berpizte terapia ahalik eta azkarren hasteko.
- Berpizte terapia aplikatzen den bitartean, BZIa antzemateko eta berpizte ondoko terapia aplikatzeko.
- BZIaren ondoren, gaixo batzuek pultsua galtzen dute berriro, bigarren geldialdi bat jasanez. Kasu horietan berpizte terapiak aplikatu behar dira berriro, baina horretarako ezinbestekoa da pultsu falta ahalik eta azkarren antzematea.

BBGa antzemateko lehen aukera telefono bidez da, lekukoek larrialdi zerbitzuetara deitzen dutenean. Larrialdiak erantzuten dituen pertsonak deitzen duenari asistentzia eskaini behar dio OKBBGa identifikatzen. Ikerketa batzuen arabera, lekukoek BBB terapia maizago aplikatzen dute horri esker [60]. Hala ere, larrialdietan jasotzen diren dei guztietatik portzentaia txiki bat dira OKBBGaren ondorioz, eta berauen identifikazioa ez da erraza. Estimazioen arabera, kasuen %25 inguru ez dira ongi detektatzen [61, 62, 63].

BBGaren tokian, pultsua antzemateko bular-sakadak emateari utzi behar zaio eta horrek biziraupen-probabilitatea jaisten du. 1998.urtera arte, gidek karotidaren haztapena gomendatzen zuten pultsua antzemateko, baina beranduago frogatu den bezala ez da metodo fidagarria eta horretarako behar den denbora luzeegia da [64, 65, 66, 67, 68, 69, 70, 71, 72]. Ikerketen arabera, pultsu falta kasuen %50-70 tartean identifikatzen da pultsu falta gisa, eta ondorioz paziente horiei ez zaie BBB terapia aplikatzen, gehien behar duten unean. Gainera, egungo giden arabera sorosleak ez lituzke 10 s baino gehiago erabili behar pultsua antzematen, eta ikerketen arabera hori baino gehiago erabiltzen da. Egun, karotidaren haztapena eskarmentu handiko jendearentzat soilik gomendatzen da [24].

Beranduago bizi-zeinak bilatzea proposatu zen, adibidez, arnasketa, mugimendua edo eztula, baina ez dago ebidentzia zientifikorik metodo hori karotidaren haztapena baino hobea dela frogatzen duenik. Alde batetik, arnasketa normala eta agonalaren artean bereiztea ez da erraza [73, 74, 75, 76]. Arnasketa agonala ohikoa da BBGaren hasieran eta ez litzateke bizi-zeinu gisa interpretatu behar; arnasketa mantso eta sakonak dira eta orokorrean zurrunga moduko soinu bereizgarri bat ageri da. Bestalde, BBGa gertatzen denean burmuinak jasotzen duen odol fluxua asko jaisten da, eta horrek epilepsiarekin nahastu daitezken konbultsio-gertaerak sortzen ditu [77, 78].

Pultsua antzemateko beste proposamen bat kapnografiaren erabilera da. Hainbat ikerketen arabera, $EtCO_2$ mailak igo egiten dira BZI lortzen den unean [53, 54, 52, 48], eta egungo gidek kapnografiaren erabilera gomendatzen dute BZI baieztatzeko [24]. 1.6. irudiak BZI gabeko kasu bat eta BZIdun kasu bat erakusten ditu, non bigarren kasuan argi ikusten den $EtCO_2$ maila nola igotzen den. Metodo horren abantaila nagusia da bular-sakadak ez direla eten behar, $EtCO_2$ igoera sakadak eten gabe antzeman baitaiteke. Hala ere, bi desabantaila ere aurkezten ditu metodo horrek. Alde batetik, BZI detektatzeko soilik erabili daiteke, baina ez pultsua antzemateko oro har. Hau da, BBGa den edo ez bereizteko ez du balio, ezta ere bigarren BBG bat detektatzeko. Bestalde, ez dago atalase-balio unibertsal bat BZI detektatzeko kapnografia erabiliz. Horregatik, egungo gidek EKG seinalea begiratzea gomendatzen dute kapnografian BZIa antzemandakoan [24].

Metodo berriago bat ultrasoinuen erabilera da, bihotzaren aktibitate mekanikoa begiz ikusteko aukera ematen baitu eta PEa errazago detektatzen da irudien bidez [79]. Gainera, PGAE-erritmoak beste bi azpi-erritmotan sailkatzeko aukera ematen du: benetako-PGAE (BPGAE) edo sasi-PGAE (SPGAE) [80]. Oro har, PGAE ondoko eran definitzen da: pultsua ezin da haztatu baina bihotzak aktibitate elektriko organizatua dauka. Hala ere, baliteke bihotzak aktibitate mekanikorik ez izatea (BPGAE) edo aktibitate mekaniko minimo bat izatea (SPGAE), nahikoa ez dena gaixoaren kontzientzia eta organoen perfusio egokia mantentzeko [81]. Ikerketen arabera, bi erritmoek ez dituzte biziraupen-probabilitate berdinak eta gaixoari aplikatu behar zaion terapia desberdina da [82, 83, 84], horregatik ezinbestekoa da bi erritmo mota horiek bereiztea. Ultrasoinuek dituzten bi desabantaila

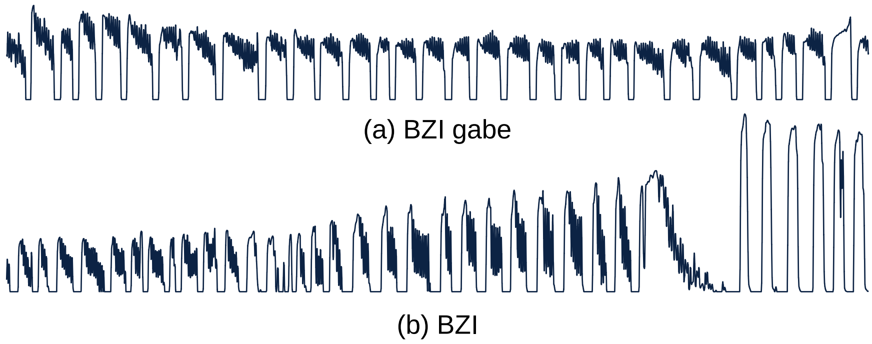

1.6. Irudia. Kapnografiaren uhin forma BZI gabeko eta BZIdun gaixo banatan. $EtCO_2$ balioek gora egiten dutela ikus daiteke BZI duen gaixoaren kasuan. BZI ez dagoenean berriz, $EtCO_2$ balioak konstante mantentzen dira.

nagusiak ondokoak dira: OKBBGaren tokian ez dira eskuragarri egoten normalean, eta teknologia horren erabilerak bular-sakaden etenaldien iraupena handitzen du [85, 86].

Ondorengo analisiak egiteko ere BZIa detektatzeko metodoak erabilgarriak izan daitezke. Datu-base handiak zentro desberdinetatik datoz eta milaka episodio prozesatu behar izaten dira. Ohiko aplikazioak metrikak alderatzea edo tratamendu desberdinak alderatzea izaten da, eta alderatzeko taldeak maiz BZI duten eta ez duten gaixoenak izaten dira [87, 88, 89]. Egungo anotazioak ez dira zehatzak eta informazioa falta dute, beraz, metodo automatikoek eskuzko lan ordu asko aurreztuko lituzkete asmo handiko ikerketa lanetan.

1.5 Tesi lanaren motibazioa

Oraindik 2020an hainbat protokolo berri proposatzen ari dira pultsua antzemateko [90], oraindik metodo hobeak behar direnaren seinale. Ukimen edo ikusmenean oinarrituta dauden metodoak ez dira behar bezain zehatzak, eta azken urteetan komunitate zientifikoak ahalegin handiak egin ditu metodo automatikoak garatzeko [1, 91, 92, 7, 93]. Metodo automatikoek sorosleari laguntza eskaintzea dute helburu, BBB terapia lehenago asteko, berpizte ondorengo terapia ahalik eta azkarren aplikatzeko, eta bular-sakaden etenaldiak ahalik eta gehien murrizteko, biziraupen-probabilitateak igoz.

Ingeniaritzaren ikuspuntutik, pultsua antzemateko erronka nagusia PE eta PGEA erritmoen arteko diskriminazio automatikoa da, biek aktibitate elektriko organizatua erakusten dutelako eta begiz antzematen diren ezaugarriak antzekoak direlako. Metodo automatikoek OKBBGaren tokian ohikoak diren seinaleekin egin behar lukete lan, hala nola, EKG, BI edo kapnografia bezalako seinaleekin. Hainbat metodo proposatu dira EKG eta BI seinaleetan oinarrituta KDAtan funtzionatu dezaten eta horrela esperientzia murritzeko sorosleei laguntzeko, baina egun ez dago gailu komertzialik PE eta PGEA erritmoak bereizten dituenik. Metodo zehatzagoak behar dira eta analisi sakonagoak [94].

PE eta PGEA erritmoak bereizteaz gain, PGEA desberdinen diskriminazioa ere oso erabilgarria izan daiteke. BPGEA eta SPGEA erritmoak automatikoki diskriminatzeak ultrasoinuen teknologiaren beharra murriztuko luke.

Azkenik, gaixoen %40ak bigarren geldialdi bat jasan dezake, eta gertaera hori biziraupen-tasa baxuagoekin erlazionatzen dute hainbat ikerketek [95, 96, 97, 98, 99]. Egun, fenomeno horren mekanikak ezezagunak dira eta ez dago metodo automatikorik bigarren geldialdi bat aurresateko eta sorosleak lehenago jakinaren gainean jartzeko.

Tesi honetan ekarpen esanguratsuak egingo dira pultsuaren detekzio automatikoan eta BZIaren anotazio automatikoan. Gainera, urrunago joaten da PGEA egoera gehiago automatikoki diskriminatuz (BPGEA eta SPGEA) ohiko seinaleak erabiliz eta bigarren geldialdiak aurresanez.

2 ARTEAREN EGOERA

2.1 Ikasketa automatikoa OKBBGetako erritmoen sailkapenerako

Adimen artifizialari esker, hainbat aurrerapen lortu dira ingeniaritzako arlo desberdinetan, ikusmen artifiziala edo ahotsaren prozesatze automatikoa izanik ezagunenetakoak. Berpiztearen arloa ez da salbuespen bat izan, ikasketa automatikoa desfibrilazio elektrikoa behar duten erritmoak diskriminatzeko edo desfibrilazio elektrikoaren arrakasta aurresateko baliagarria dela frogatu da. Tesi honetan, ikasketa automatiko gainbegiratuan oinarritutako sailkapen teknikak erabiltzen dira zirkulazio-maila desberdinak detektatzeko edo bigarren geldialdiak aurresateko.

2.1.1 Sailkapenerako algoritmoak

Ezaugarrien espazio bat edukita ($\mathbf{v}$), ikasketa automatikoan oinarritutako sailkatzaileek irteerako klasea (y) aurresaten dute. Klase horiei *etiketa* ere esaten zaie. Oro har, f funtzioaren hurbilketa bat estimatzea da helburua, zeinak $\mathbf{v}$ onartzen duen sarrera gisa eta y funtzioaren emaitza den ($y = f(\mathbf{v})$). Hurbilketa hori egiteko sailkatzailearen $\boldsymbol{w}$ parametroak estimatu behar dira kostu- edo errore-funtzio bat minimizatuz ($\mathcal{L}$). Behin $\boldsymbol{w}$ doituta, klasea estimatzea zuzena da sarrerako ezaugarriak ezagututa.

Sailkatzaile bat nola diseinatu eta erabiltzen den ulertzeko, adibide baten bidez azalduko da. Demagun PGAE eta PE erritmoen arteko bereizketa automatikoa gauzatu nahi dugula EKG seinaletik erausten diren ezaugarriak erabiliz. Ezagutzen den seinalea EKGa da (s_{ecg}), eta $\mathbf{v} = \mathcal{T}\{s_{ecg}\}$ transformatua aplikatuz esanguratsua den $\mathbf{v}$ ezaugarrien espazioa lortu daiteke. Demagun kalkulatutako ezaugarriak ($\mathbf{v} = \{v_1, v_2\}$) bihotz-maiztasuna ($v_1$) eta batezbesteko anplitudea (v_2) direla. Bi ezaugarrien diseinurako aplikazio esparruko adituen parte-hartzea beharrezkoa da. Irteera $y = \{0 : \text{PGAE}, 1 : \text{PE}\}$ izanik, instantzia gisa definitzen da $\{\mathbf{v}, y\}$ bikote bakoitza. Erregresio logistikoan oinarritutako sailkatzaile batek irteera PEa izateko *probabilitatea* (p) estimatuko luke ezaugarrien bektorea ezagututa ondoko formula jarraituz:

$$p = \frac{1}{1 + e^{-(w_0 + w_1 \cdot v_1 + w_2 \cdot v_2)}} \tag{2.1}$$

non w_0 eta $\boldsymbol{w} = \{w_1, w_2\}$ estimatu beharreko parametroak diren sailkatzailearen entrenamendu prozesuan zehar. Ondoren, p estimatzen da eta PGAE/PE erabakia atalase-balio bat ezarriz gauzatu daiteke. Adibidez, $\hat{y} = 0$ kontsideratu daiteke $p < 0.5$ bada. Hala ere, instantzia kantitate minimo bat behar da w_0 eta $\boldsymbol{w}$ estimatu ahal izateko entrenamenduko datuak erabiliz, $\mathbf{V}^{(\text{tr})} = \{\mathbf{v}_1^{(\text{tr})}, \ldots, \mathbf{v}_M^{(\text{tr})}\}$ eta $\boldsymbol{y}^{(\text{tr})} = \{y_1, \ldots, y_M\}$. Kasu horretan, maximizatu behar den funtzioa ondokoa da:

$$\arg\max_{w_0, \boldsymbol{w}} \{\sum_{i=1}^{M} [y_i^{(\text{tr})} (w_0 + \boldsymbol{w}^T \mathbf{v}_i^{(\text{tr})}) + \ln(1 + e^{-(w_0 + \boldsymbol{w}^T \mathbf{v}_i^{(\text{tr})})})]\} \tag{2.2}$$

Sailkatzaile desberdinen arteko desberdintasun nagusia $f(\mathbf{v})$ funtzioan eta funtzio hori estimatzeko prozeduran dago. Adibidez, gure kasuan, ezaugarrien eta irteerako klasearen arteko erlazioa lineala dela suposatu da. Sailkatzaile ez-linealak, nukleo desberdinetako euskarri bektoredun makinak (EBM) edo azaleko sare neuronalak bezalakoak, datu-patroi konplexuagoak ikasteko gai dira, eta horregatik dira hain erabiliak gaur egun. Beste algoritmo batzuek sailkatzaile sinple asko konbinatzen dituzte sendotasuna lortzeko; horien artean, *random forest* (RF) da ezagunenetako estrategia bat eta tesi honetan zehar asko erabiltzen da.

Oro har, aipatutako algoritmoek giza-ezagutzak behar dituzte ezaugarrien diseinua gauzatzeko (bihotz-maiztasuna eta batezbesteko anplitudea gure adibidean), sailkatzaileak elikatzeko behar baitira. Beraz, arloan aditua den norbait behar da ezaugarri horiek diseinatzeko.

Bihotz-arritmia desberdinak detektatzeko hainbat ezaugarri proposatu dira literaturan. EKG seinalean agertzen diren osagaietan edo puntu fiduzialetan (ikus 2.1 irudia) daude oinarrituta. Bihotz-arritmia desberdinak EKG seinalean era desberdinetan ageri dira, batzuetan anomaliak agertzen dira puntu fiduzialetan edo punturen bat falta izaten da. Beste ohiko metodo bat bi taupaden arteko denboraren aldakortasuna aztertzea da (RR tarteak), bihotz-erritmoaren aldakortasuna (BEA) gisa ere ezagutzen dena.

Azken urteetan, ikasketa sakonean (*deep learning* ingelesez) oinarritutako algoritmoak ospe handia lortu dute. Algoritmo horiek ikasketa automatikoaren azpi-familia bat dira, eta abantaila nagusia ezaugarrien diseinuaren pausua ezabatzen dutela da, ezaugarrien erauzketa eta sailkatzailearen optimizazioa aldi berean doitzen baitira. Gure adibideari helduz, PGAE eta PE erritmoen arteko bereizketa gauzatzeko ikasketa sakonean oinarritutako algoritmo batek EKG seinalea onartuko luke sarrera gisa. Horrek v_1 eta v_2 ezaugarrien diseinua ezabatuko luke, $\mathbf{v} = \mathcal{T}\{s_{ecg}\}$ eragiketa ez bailitzateke beharrezkoa izango. 2.2. irudian ikasketa automatiko tradizionalean oinarritutako algoritmoen funtzionatzeko modua eta ikasketa sakonean oinarritua dauden algoritmoen funtzionatzeko modua laburbiltzen dira. Algoritmo horien funtzionamendua antzekoa da, instantzia kopuru bat erabiliz ereduaren parametroak estimatzen dira. Hala ere, beraien desabantaila nagusia behar duten datu kopurua da, parametroak estimatzeko behar den instantzia kopurua handiagoa baita. Datu nahikoa daudenean, giza-begiak ikusi

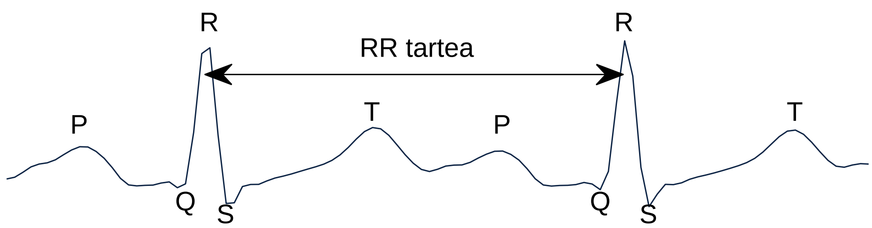

2.1. Irudia. EKG seinalearen taupaden arteko RR tartea, eta bakoitzaren puntu fiduzialak.

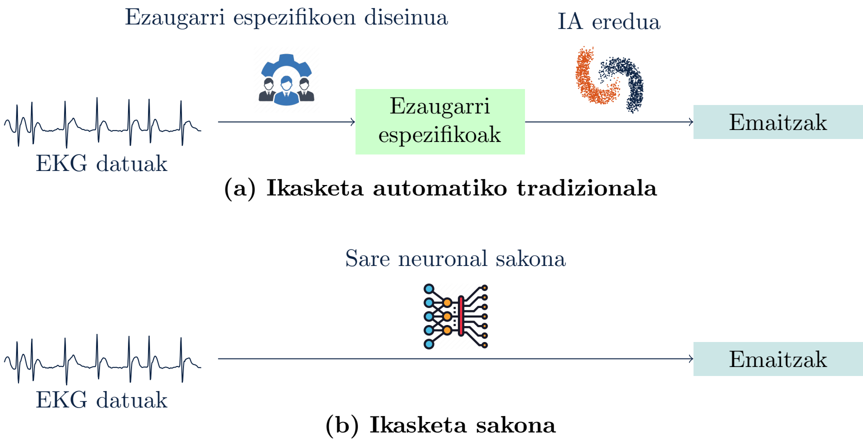

2.2. Irudia. Ikasketa automatiko tradizionalaren (a) eta ikasketa sakonean (b) oinarritutako algoritmoen arteko desberdintasunak. Bigarrenak eskuzko ezaugarrien diseinuaren pausua ezabatzen du.

ezin dituen ezaugarriak kalkulatzeko gai dira, sailkatze-algoritmo oso sendoak eskainiz.

2.1.2 Ezaugarrien aukeraketa

Ezaugarrien aukeraketari esker esanguratsuak diren ezaugarri-familia bat aukeratzen da eredua diseinatzeko. Pausu hori oso garrantzitsua da, izan ere, ereduak sinplifikatzen ditu, entrenatzeko behar den denbora murrizten du eta sarritan errendimendu hobea lortzen da. Oro har, hiru metodo-familia daude ezaugarrien aukeraketa gauzatzeko: iragazkietan oinarrituta, bilgarri-metodoak eta sailkatzailean txertatutako metodoak.

Iragazkietan oinarrituta dauden metodoak neurri estatistikoak erabiltzen dituzte sarrerako ezaugarrien erabilgarritasuna neurtzeko. Algoritmo mota horiek ez dira sailkatzailearen menpekoak eta ezaugarriak bere garrantziaren arabera ordenatzeko gaitasuna dute, garrantzi baxuena duten ezaugarriak ezabatzeko helburuarekin. Adibide klasiko bat erredundantzia minimoa gailentasun maximoa (*minimum redundancy maximum relevance*) algoritmoa da, zeinak erredundantzia gutxien eta gailentasun gehien dituen ezaugarriak aukeratzen dituen neurri estatistiko batean oinarrituta (elkarrekiko informazio minimoa ezaugarrien artean eta elkarrekiko informazio maximoa ezaugarrien eta irteeraren artean, adibidez).

Bilgarri-metodoak, aldiz, sailkatzailearen errendimenduan oinarritzen dira. Algoritmo oinarrizkoena *exhaustive search* gisa ezagutzen dena da, zeinak konbinazio posible guztiak probatzen dituen, eta errendimendu metrika altuena eskaintzen duen familia aukeratzen den. Hala ere, hori ez da bideragarria ezaugarri edo datu kopurua handia denean, eta literaturan bi familietan banatzen diren metodo eraginkorragoak proposatu dira: metodo deterministikoak (ezaugarrien aukeraketa sekuentziala) edo zorizkoak (zorizko bilaketa edo algoritmo genetikoak). Oro har, bilgarri-metodoak konputazionalki astunagoak diren arren, iragazkietan oinarrituta dauden metodoak baino emaitza hobeak eskaintzen dituzte.

Azkenik, sailkatzailean txertatutako metodoek ezaugarrien aukeraketa eredua entrenatzeko garaian burutzen dute. Zuhaitz-sailkatzaileek adibidez ezaugarri esanguratsuenak aukeratzen dituzte pausu bakoitzean, edo erregresio logistikoak erregularizazioarekin erredundanteak diren ezaugarriak ezabatzeko gaitasuna dauka.

Familia bakoitzak bere abantailak eta desabantailak ditu, eta metodo hibridoak ere proposatu dira literaturan. Adibidez, posiblea da ezaugarri kopurua murriztea hasieran iragazkietan oinarrituta dauden metodoak erabiliz, eta bilgarri-metodoekin aukeratu beste ezaugarrien erdiak (karga konputazionala murrizteko). Beste aukera bat sailkatzailean txertatutako metodoak erabiltzea da ezaugarrien garrantziak neurtzeko, eta ondoren sailkatzailea ezaugarri gutxiagorekin entrenatzen da.

2.1.3 Hiper-parametroen optimizazioa

Sailkatzaile bat diseinatzeko garaian, parametro batzuk eredua entrenatu baino lehen aukeratu behar dira, horiek definitzen baitute ereduaren egitura. Parametro-multzo horiei hiper-parametro deritze. Adibide gisa, demagun sare neuronal bat dugula ezkutuko geruza bakarrarekin L unitatez osatuta, honako diskriminazio-funtzioa duena:

$$f(\mathbf{v}) = g(\sum_{i=1}^{L} \beta_i \cdot h_i(\boldsymbol{w}_i, \mathbf{v})) \tag{2.3}$$

non $g(\cdot)$ irteerako geruzaren aktibazio-funtzioa den, β_i i.unitatearen irteerako pisua, eta $h_i(\boldsymbol{w}_i, \mathbf{v})$ aktibazio funtzioa. Entrenamendu prozesuan zehar, $\boldsymbol{w}_i$ eta β_i estimatzen dira (modeloaren parametroak), baina L balioaren arabera modeloaren parametro kopurua eta horien balioak desberdinak dira. Adibide honetan beraz, L hiper-parametro bat da, eta modeloa entrenatu aurretik erabaki behar da bere balioa.

Hiper-parametroak aukeratzeko metodo oinarrizkoena eskuzko diseinua da, hau da, nahi den emaitza lortu arte diseinatzaileak hiper-parametroen balio desberdinak probatzen ditu. Hala ere, hiper-parametroen kopurua handia denean ez da prozesu egingarri bat, eta eskuzko diseinuak metodo automatikoek baino emaitza okerragoak eskaintzen ditu normalean. Metodo automatiko oinarrizkoena berriz, aurretik ezarritako balioak automatikoki probatzea da, edo hiper-parametroei ausazko balioak ezartzea automatikoki frogak egiteko. Metodo aurreratuagoak algoritmo genetikoak edo optimizazio bayestarra dira.

Optimizazio bayestarra da metodo eraginkorrenetako bat. Metodo probabilistiko horrek balio erreal bati lotutako helburu-funtzio bat minimizatzea du helburu (errendimendu-metrika bat sailkatzaileen kasuan). Hiper-parametro multzo bat emanda ($\boldsymbol{\vartheta}$), helburu-funtzioaren hurbilketa bat gauzatzen da, $\hat{f}(\boldsymbol{\vartheta})$, zeina benetako funtzioa baino errazagoa den ebaluatzeko. Iterazioen bidez $\hat{f}(\boldsymbol{\vartheta})$ funtzioaren hurbilketa bat egiten da, gero eta hobea izanez iterazio kopurua handituz gero. Optimizazio bayestarraren barruan, algoritmo-familia desberdinak existitzen dira hurbilketa hori gauzatzeko.

2.1.4 Ereduaren ebaluazioa

Ikasketa automatikoaren edozein aplikaziotan, azken eredua ebaluatu egin behar da bere erabilgarritasuna bermatzeko. Hainbat metodo daude horretarako, baina gakoa ondoko kontzeptua da: ebaluazio prozesuan erabilitako datuak eta entrenamendu prozesuan erabilitako datuak desberdinak izan behar dute. Are eta gehiago, ingeniaritza biomedikoko aplikazioetan entrenatzeko eta ebaluatzeko erabili diren gaixo multzoak desberdinak izan behar dute (gaixoarentzat espezifikoki diseinatutako modeloak salbuespena izanik). Hori aplikagarria da baita ezaugarrien aukeraketa eta hiper-parametroen optimizazioa gauzatzeko erabiltzen diren datuekin; prozesu horietan erabilitako gaixo-multzoa ezin da ebaluazio prozesuan erabili.

Metodo ohikoena datu-basea bi multzotan banatzea da, multzo bat entrenatzeko erabiltzen da (entrenamendu-multzoa) eta bestea ebaluatzeko (ebaluazio-multzoa). Metodo honen arazoa emaitzak hasierako banaketarekiko oso menpekoak direla da. Hau ekiditeko modu klasiko bat datu-basea k multzotan banatzea da k-multzotako ebaluazio gurutzatua aplikatzeko. Modeloa $k-1$ multzo erabiliz entrenatzen da eta k. multzoan ebaluatzen da. Prozesua k aldiz errepikatzen da eta errendimendu-metriken banaketak aztertzen dira. Prozesu horri esker algoritmoa datu-base guztian zehar entrenatu eta ebaluatzen da, baina ez aldi berean. Entrenatzeko erabilitako datu multzoa ere k multzotan banatu daiteke ezaugarriak aukeratzeko edo hiper-parametroak optimizatzeko. Edozein kasutan, y-ren banaketak antzekoak izan behar dute multzo guztietan.

Ikasketa automatikoan oinarritutako algoritmoak ebaluatzeko hainbat errendimendu-metrika existitzen dira. Klase anitzeko problemetan (irteera posibleak bi baino gehiago direnean), sentsibilitatea (Se) klase konkretu bat detektatzeko probabilitatea da. Balio prediktibo positiboa (BPP) berriz, sailkatzaileak klase bat detektatzen duenean benetan klase hori izatearen probabilitatea da. Bien arteko batezbesteko harmonikoari F_1 deritzo. Sailkatzailearen errendimendua laburbiltzeko, Se guztien batezbesteko aritmetikoa kalkulatzen da eta horri zehaztasun orekatua (ZO) deritzo. Era berean, F_1 guztien batezbestekoa kalkulatzea ere ohikoa da.

Irteera posibleak bi direnean, Se klase positiboarentzat erabiltzen da (PE izaten da klase positiboa normalean) eta klase negatiboaren Se-ari espezifikotasuna (Sp) deritzo. Berdina gertatzen da BPParekin, klase negatiboaren BPPari balore prediktibo negatiboa (BPN) deritzo.

Diseinatutako eredua lan-puntu desberdinetan ebaluatzeko (gure adibidean p-ren atalase-balio desberdinak ezarrita lortuko genuke) Se marrazten da $1 - Sp$-ren kontra, eta kurba horri ROC (*receiver operating characteristic*) kurba deritzo. Kurbaren azpiko azalerak (KAA) errendimendu orokorra laburbiltzen du. Zorizko irteerak sortzen dituen sailkatzaile batek KAA$= 0.5$ eskaintzen du, eta 1etik gertuago egoteak sailkatzailea hobea dela esan nahi du. Era berean, Se BPParen kontra marraztuta PR kurba lortzen da, eta beronen azpiko azalerari PRKAA (PR kurbaren azpiko azalera) deritzo.

2.2 Pultsuaren detekzio automatikoa OKBBGan

Pultsua detektatzeko metodo automatikoak OKBBGaren tokira egokitu behar dira, eskuragarri dauden gailuak ez baitira beti berdinak. Hala nola, fase goiztiarretan KDA egon ohi da eskuragarri, beraz, pultsu detektoreak KDAren txaplaten bidez jasotako seinaleekin lan egiteko gai izan behar du. Aurrerago, monitore/desfibriladoreak eskuragarri daudenean, seinale gehiago erabiltzen dituen algoritmoak aplikatu daitezke. Tesi honetan zehar KDAk jasotako seinaleak eta kapnografia erabiltzen dira zirkulazio-egoerak automatikoki bereizteko.

2.2.1 Pultsu detekzioa KDA erabiliz

KDA askok EKG eta BI seinaleak jasotzen dituzte aldi berean desfibrilazio txaplaten bidez. BI seinalean gorabeherak antzeman daitezke taupada eraginkor bakoitzarekin, taupadek sortzen duten odol-fluxuak konduktibitatea aldatzen baitu. Hala ere, osagai hori iragaztea ez da erraza, mugimenduak edo aireztapenek sortzen dituzten gorabeherak handiagoak baitira. 2.3. irudian PE baten EKG eta BI seinaleak ageri dira. Bertan ikus daiteke taupada bakoitzak gorabeherak sortzen dituela BI seinalean, baina dauden bi aireztapenek anplitude handiagoko gorabeherak sortzen dituzte.

Urte asko dira gorabehera horiek antzeman eta kuantifikatu daitezkeela frogatu zenetik [100, 101], baina pultsua detektatzeko aurreneko algoritmoa Risdal et aliik [1] proposatutakoa da. Autoreen arabera, PGAE eta PE erritmoen arteko bereizketa automatikoa

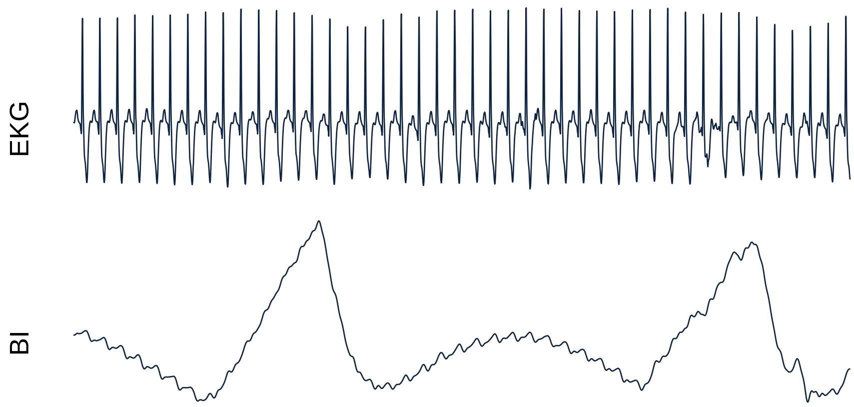

2.3. Irudia. 20 segundoko iraupena duten EKG eta BI seinaleak PE erritmoa duen gaixo batean. BI seinalean ikusten diren gorabehera handiak aireztapenak dira, eta gorabehera txikiak berriz taupada eraginkor bakoitzak sortutakoak.

da erronka nagusia. Izan ere, desfibrilazio elektrikoa behar duten erritmoak (FB edo TB) detektatzeko metodo oso zehatzak existitzen dira gaur egun, eta AS erritmoak erraz bereizi daitezke erritmo organizatuengandik (PGAE eta PE) seinalearen potentzia edo anplitudea neurtuta.

Risdal et aliik [1] erabilitako datu-basea 127 PGAE eta 91 PE segmentuz osaturik zegoen, iraupen minimoa 10 s izanik. Beraien metodoa 2.4. irudian laburbiltzen da. Lehendabizi, QRSak detektatzen zituzten Kohama et aliik [102] proposatutako metodoa erabiliz; informazio hori BI seinaletik zirkulazio osagaia iragazteko ($z_{EA}[n]$) eta EKG seinaletik ($x[n]$) ezaugarriak kalkulatzeko erabiltzen da beranduago. Azkenik, ezaugarri gehiago kalkulatu zituzten $z_{EA}[n]$ erabiliz sare neuronal batean oinarritutako sailkatzaile bat diseinatzeko.

Zirkulazio osagaia kalkulatzeko, BI seinalearen batezbestekoa kalkulatzen zuten taupada guztiak erabiliz:

$$z_{EA}[m] = \frac{1}{K} \sum_{k=1}^{K} z[p[k] + m - 1] \quad 1 \leq m \leq M \tag{2.4}$$

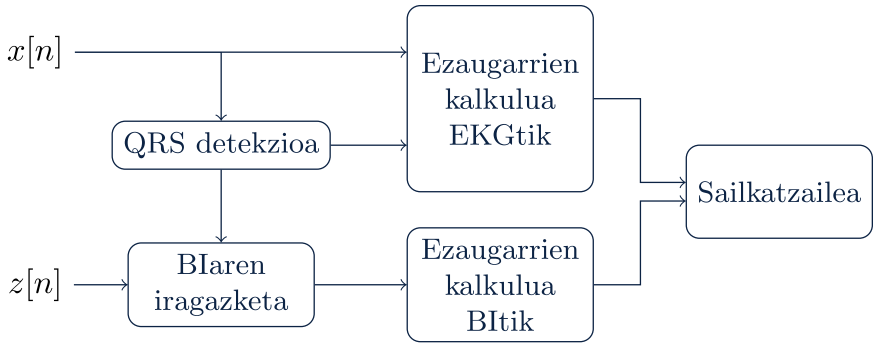

2.4. Irudia. Risdal et aliik [1] proposatutako metodoa pultsua automatikoki detektatzeko, non $x[n]$ EKG seinalea den eta $z[n]$ aurreprozesatutako BI seinalea.

non K detektatutako taupada kopurua den, $z[n]$ aurreprozesatutako BI seinalea, $p[k]$ QRS uneak eta m, berriz, M luzeradun z_{EA} seinalearen lagin zenbakia. Kasu honetan M batezbesteko bihotz-maiztasunaren berdina da. Guztira 17 ezaugarri kalkulatu zituzten (v_1-v_{17}):

- QRS zabaleraren batezbestekoa (v_1).
- QRS bakoitzarentzat seinalearen luzera (SL), ondoko eran kalkulatzen dena:

$$SL = \frac{\sum_{n=0}^{N-1} w[n] \cdot y^2[n]}{\sum_{n=0}^{N-1} y^2[n]} \tag{2.5}$$

  non $y[n]$ QRS bakoitzaren MPCa (*minimum phase correspondent*) den eta $w[n]$ funtzio positibo gorakor bat. SL guztien batezbestekoa da v_2.

- EKG segmentuaren batezbestekoa (v_3).
- Seinalea 0 eta 1 balioen artean normalizatu ondoren, horren mediana eta bariantza ziren v_4 eta v_5, hurrenez hurren.
- RR tarteen batezbestekoa eta bariantza (v_6 eta v_7).
- $z_{EA}[n]$ osagaiaren maximoaren eta minimoaren diferentzia bere iraupenarekiko (v_8).

- $z_{EA}[n]$-ren lehen diferentziaren maximoaren eta minimoaren arteko diferentzia $z_{EA}[n]$ (v_9).
- $z_{EA}[n]$-ren azpiko azalera (v_{10}).
- $z_{EA}[n]$-ren tarte negatibo luzeena eta bere iraupena (v_{11} eta v_{12}).
- $z_{EA}[n]$ normalizatuaren laugarren ordenako polinomio-ereduaren koefizienteak v_{13}-v_{17}.

Ezaugarrien aukeraketa sekuentziala erabili zuten eta PE klase positibo gisa kontsideratuz, lortutako Se eta Sp balioak 90.0% eta 91.5% izan ziren 3 s erabiliz. Segmentuaren luzera handituz 10 s arte, Se 93.9% arte hobetzen zen Sp berdina mantenduz eta lortutako KAA 0.95 izan zen.

2010ean Cromie et aliik [103] beste proposamen bat egin zuten pultsua detektatzeko BI seinalean soilik oinarrituz. Jarraitutako metodologia desberdina izan zen, ikerketa bi fasetan banatuz. Lehen fasean, miokardioko perfusioa neurtzen zuten irudiak jaso zituzten OKBBGa jasan ez zuten gaixoetan, guztira ospitalera joandako 73 gaixo kontutan hartuz. Beraien helburua bihotzaren ezkerreko bentrikuluak ponpatutako odolaren bolumena eta BI seinalearen ezaugarri desberdinen arteko erlazioa bilatzea izan zen. Ikerketa horren ondorioen arabera, BI seinalearen lehen diferentziaren Fourierren transformatuan agertzen den maximoak (1.5 Hz eta 4.5 Hz artean) erlazioa dauka aipatutako bolumenarekin. Bigarren fasean zehar beraz, pultsu detektore bat garatu zuten horretan oinarrituta. Horretarako, BBGa jasan zuten 132 gaixo eta BBGa jasan ez zuten 97 gaixo erabili zituzten arauetan oinarritutako algoritmo bat sortzeko. Gaixoen erdiak algoritmoa diseinatzeko erabili zituzten eta beste erdia algoritmoa ebaluatzeko. Lortutako Se eta Sp 81.1% eta 97.1% izan ziren, 12 s-ko tarteak hartuz, egungo gidek gomendatzen dutena baina 2 s gehiago [24].

2013an Ruiz et aliik [104] metodo berritzaile bat proposatu zuten zirkulazio-osagaia iragazteko BI seinaletik abiatuta (s_{icc}). Beraien arabera, s_{icc} denboran aldakorra den Fourier serie gisa hurbildu daiteke, hots:

$$s_{\text{icc}}[t_j] = \sum_{k=1}^{K} a_k[t_j]\cos(2\pi k f[t_j]\cdot t_j) + b_k[t_j]\sin(2\pi k f[t_j]\cdot t_j) \quad (2.6)$$

non K harmoniko kopurua den, $a_k[t_j]$ eta $b_k[t_j]$ denboran aldakorrak diren Fourier koefizienteak diren eta $f[t_j]$ taupaden maiztasuna Hz-tan. Kasu horretan, ikerlariak K-ren balioa erabaki dezake eta $f[t_j]$ EKG seinaletik abiatuz estimatu daiteke. Beraz, ezezagunak $a_k[t_j]$ eta $b_k[t_j]$ dira. R uneak automatikoki detektatzen ziren KDA komertzial baten detektorea erabiliz, $K = 3$ ezarri zuten, eta BI seinalea 0.65-0.7 Hz tartean iragazi zuten zarata murrizteko. $a_k[t_j]$ eta $b_k[t_j]$ iragazki moldakorretan oinarritutako algoritmo bat erabiliz estimatu ziren (LMS, *least mean squares*). Guztira 165 PE eta 234 PGAE segmentu erabili zituzten, erdia algoritmoa garatzeko eta beste erdia ebaluatzeko. Lortutako s_{icc}-ren eta aurreneko diferentziaren piko-piko anplitudeak, batezbesteko potentziak eta batezbesteko azalerak kalkulatu zituzten. Ezaugarri guztiak banaka ebaluatu zituzten eta 0.96tik gorako KAA balioak erreportatu zituzten.

2016ean Alonso et aliik [7] pultsu-detektore automatiko bat garatu zuten s_{icc} eta EKG seinaleetan oinarrituta. Kasu horretan $a_k[t_j]$ eta $b_k[t_j]$ RLS (*recursive least squares*) algoritmoa erabiliz estimatu zituzten eta guztira 6 ezaugarri kalkulatu:

- s_{icc}-ren aurreneko diferentziaren (Δs_{icc}) batezbesteko azalera:

$$v_1 = \frac{1}{N} \sum_i |\Delta s_{\mathrm{icc}}[i]| \tag{2.7}$$

  non N lagin kopurua den.

- Batezbesteko RR tartea (v_2).
- Taupada bakoitzak s_{icc} seinalean sortutako anplitudeen desbideratze estandarra (v_3).
- Taupaden batezbesteko anplitudea (v_4).
- s_{icc}-ren batezbesteko azalera:

$$v_5 = \frac{1}{N} \sum_i |s_{\mathrm{icc}}[i]| \tag{2.8}$$

- Taupadek EKG seinalean sortzen dituzten anplitudeen desbideratze estandarra (v_6).

Ezaugarri horiek erabiliz erregresio logistikoan oinarritutako sailkatzaile bat entrenatu zuten. Guztira 1091 segmentu (385 gaixo) erabili zituzten, 5 s-ko iraupen minimo batekin. Ebaluaziorako datuetan lortutako Se eta Sp 92.3% eta 91.9% izan ziren, hurrenez hurren.

2018an Ruiz et aliik [105] metodo sinple bat proposatu zuten PE eta PGAE erritmoak bereizteko 3 s-ko segmentuak erabiliz. Segmentu bakoitza bi erditan banatzen da eta ezaugarri bakoitzaren balio minimoa hartzen da bi leihoen artean. Hots, $i = \{0, 1\}$ izanik ezaugarriak ondoko eran kalkulatu zituzten:

$$P_i = \frac{2}{N} \sum_{k=i \cdot N/2+1}^{(i+1) \cdot N/2} z^2[k], \quad v_1 = \min(P_0, P_1) \tag{2.9}$$

$$P_{ci} = \frac{2}{N} \sum_{k=i \cdot N/2+1}^{(i+1) \cdot N/2} |x[k]| \cdot |z[k]|, \quad v_2 = \min(P_{c0}, P_{c1}) \tag{2.10}$$

non N segmentuaren lagin kopurua den, $z[k]$ aurreprozesatutako BI seinalea eta $x[k]$ EKG seinalea. Egileek BI seinalea aurreprozesatu zuten zirkulazio osagaia hobeto antzemateko baina ez dira zehaztasun gehiago azaltzen iragazkiaren inguruan. Guztira, 167 gaixo erabili zituzten eta ezaugarriak zuhaitz-sailkatzaile bat erabiliz konbinatu zituzten. Ebaluaziorako datu-partizioan lortutako Se eta Sp 98.3% eta 98.4% izan ziren, hurrenez hurren.

Aipatutako ikerketa guztiek EKG edo/eta BI seinaleetan oinarritutako ezaugarriak erabiltzen zituzten sailkatzaileak diseinatzeko. Hala ere, etiketatuta dauden instantziak lortzeko ere bi seinale horiek erabiltzen zituzten kasu gehienetan, eta horrek alborapen bat sortu dezake prozeduran. Algoritmoaren fidagarritasuna bermatzeko, instantziak etiketatzeko erabili diren seinaleak ez lirateke sailkatzailea entrenatzeko erabili beharko.

2.2.2 Kapnografia BZIa detektatzeko

Azken urteetan hainbat ikerketek sustatu dute kapnografiaren erabilera pultsua detektatzeko BBGan. Are eta gehiago, egungo gidek EKG eta kapnografiaren erabilera gomendatzen dute BZIa lortu dela baieztatzeko [24]. 1987an jada ikerketa batek erakutsi zuen nola $EtCO_2$ balioak igo egiten ziren gaixoak BZI berreskuratzen duenean [106].

2013an Davis et aliik [107] 145 gaixo eta 588 bular-sakaden etenaldi aztertu zituzten (94 pultsuarekin) bihotz-maiztasuna eta $EtCO_2$ balioa aztertzeko pultsua dagoen eta ez dagoen kasuetan. Haien ustez, etenaldiaren aurretik bihotz-maiztasuna $> 40\,\text{min}^{-1}$ eta $EtCO_2 > 20\,\text{mmHg}$ izateak BZIren adierazle izan daiteke. Sakadak geratu ondoren $EtCO_2 < 20\,\text{mmHg}$-ra jaisten bada eta jaitsiera $> 10\,\text{mmHg}$ bada, sakadak berriro hasi behar dira. Protokolo hori 389 paziente erabiliz ebaluatu zuten eta lortutako Se eta Sp %98 eta %99 izan ziren. Ikerketa horrek frogatu zuen bi seinaleak erabiltzeak BZI detekzio algoritmoak indartu ditzakeela.

Pokorná et aliik [52] 2015ean garatutako ikerketaren arabera, batbateko $EtCO_2$ igoera batek BZI adierazi dezake. Guztira 108 gaixo aztertu zituzten (59 BZIdunak) eta $EtCO_2$ 10 mmHg baino gehiago igotzen zenean zer gertatzen zen aztertu zuten. Lortutako Se eta Sp %80 eta %40 izan ziren. Atalase-balio horrek BZI detektatzeko gaitasun ona duen arren, pultsu falta detektatzeko ez da nahikoa. Hala ere, 2016ean Lui et aliik [108] antzeko ikerketa bat garatu zuten 178 gaixo erabiliz. Analisi berdinaren bidez lortutako Se eta Sp %33 eta %97 izan ziren, emaitza oso desberdinak aurrekoarekin alderatuta. Autoreen arabera arrazoi posibleak ikerketaren diseinuan dauden desberdintasunak izan daitezke, bai gaixoak kontutan hartzeko irizpideengatik, bai OKBBGen ezaugarrien desberdintasunengatik. Beste atalase-balio batzuk ere frogatu zituzten, 20 mmHg-ko atalase balioa erabiliz lortutako Se eta Sp %20 eta %98 izan ziren.

Kapnografia soilik erabiliz guztiz automatikoa den metodo bat garatzen aurrenak Brinkrolf et aliik [109] izan ziren 2018an. Denborazko serieen aldakortasunak detektatzen zituzten literaturako algoritmo bat erabiliz (*slope comparing adaptive repeated median algorithm*). Kontutan 169 kasu hartuta (77 BZIdunak), joera positiboa zuten puntuen portzentaia handiagoa zela sumatu zuten BZIdun gaixoetan, atalase-balio optimoak emandako Se eta Sp %73.9 eta %58.4 izan ziren.

2.3 PGAE desberdinen ezaugarritzea

Urte asko pasa dira PGAE erritmoetan bihotzaren aktibitate mekanikoak maila desberdinak eduki ditzakeela ezaguna denetik. Horrela, BPGAE eta SPGAE desberdindu ziren, bakoitza aktibitate mekaniko maila desberdinekin, eta horri lotutako pronostiko eta aplikatu beharreko terapia desberdinekin [82, 84].

Hainbat ikerketen arabera SPGAEk pronostiko hobea dauka [84, 110, 111, 112, 113], zeinak BPGAEk ez bezala, miokardioaren aktibitate minimo bat erakusten baitu (nahiz eta nahikoa ez izan pultsua nabarmentzeko). Aktibitate hori aortaren presioa monitorizatuz edo ultrasoinuen teknologia erabiliz ikus daiteke [81, 114, 115]. Bestalde, EKGaren uhin formari dagokionez, QRS eta QR tarte laburragoak erakusten ditu SPGAE erritmoak BPGAEkin alderatuz [81].

SPGAE erritmoak leheneratzeko metodoak egon arren, horiek detektatzeko ultrasoinuen teknologia behar da, baina irudi horiek hartzea OKBBGan ez da ohikoa. 2019an J.H. Paxton eta B.J. O'Neil ikertzaileek BPGAE/SPGAE/PE erritmoen arteko diskriminatzaileen beharra azaleratu zuten arren [116], egun ez dago metodo automatikorik OKBBGan erabilgarriak direnak.

2.4 Bigarren geldialdia

Gaixo askok BZI lortu arren, bigarren geldialdi bat jasaten dute ospitalera iritsi aurretik, *re-arrest* (RA) moduan ere ezagutzen dena. Ikerketa desberdinen arabera, RAren intzidentzia tasa %24-43 tartean dago, eta gaixoen pronostikoak nabarmen egiten du okerrera [95, 96, 99, 98, 97]. RA eragiten duten faktoreei buruz gutxi jakin arren, garbi dago BBGaren bilakaeran faktore kaltegarria dela [97].

Literaturan hainbat esfortzu egin dira BBGa aurresateko [117, 118], baina ikerketa bakarra dago RA aurresaten saiatu zena, Salcido et aliik [119] garatutako ikerketa. Hainbat metrika kalkulatu zituzten BEAn oinarrituta 30 s, 1 min, 3 min and 5 min-ko leihoak erabiliz BZI hasieratik. RArekin erlazionatu zuten metrika bakarra RR tarteen desbideratze estandarra izan zen.

3 HIPOTESIA ETA HELBURUAK

Egun hainbat zailtasun daude zirkulazio-egoera identifikatzeko OKBBGan zehar. Tesi honen hipotesi nagusia ondokoa da: seinaleen prozesatzearen eta ikasketa automatikoaren bidez ekarpen esanguratsuak egin daitezkeela algoritmo automatikoak garatuz zirkulazio-egoera ezaugarritzen laguntzeko. Oro har, ondoko helburuak definitu ziren:

- **1. helburua: EKG seinalea soilik erabiliz PGAE eta PE erritmoak bereizten dituzten algoritmoen garapena.** Literaturan hainbat algoritmo proposatu dira pultsudun eta pultsurik gabeko erritmoak bereizteko EKG eta BI seinaleak erabiliz. Algoritmo horiek anplitude erresoluzio ona duten BI seinaleak eskatzen dituzte, KDA askok ez dutena. Are gehiago, BI seinalea askotan ez dago eskuragarri, baina EKG seinalea bai. Horregatik, PGAE eta PE erritmoak EKG seinalea soilik erabiliz bereizteak algoritmoaren erabilera unibertsala bermatuko luke.
- **2. helburua: iturri anitzeko algoritmoak aztertzea zirkulazio-egoera ebaluatzeko EKG, BI eta kapnografia seinaleak erabiliz.** Helburu hori honako azpi-helburutan banatzen da:
  - Kapnografiaren fase desberdinak automatikoki detektatzeko algoritmoen garapena OKBBGan zehar. Iturri anitzeko algoritmoetan kapnografia gehitzeko, horren fase desberdinen segmentazio automatiko ona gauzatu behar da lehendabizi. Horrela, $EtCO_2$ mailak ere automatikoki kalkulatu daitezke.

  - Kapnografiak eduki ahal duen balioa aztertzea PGAE eta PE erritmoak bereizteko.
  - Sailkatzaile bitarretatik harantzago joatea BPGAE, SPGAE eta PE erritmoen artean bereizteko gai diren algoritmoak garatuz. Aurreneko algoritmoa litzateke hiru klaseen arteko bereizketa egiteko gai dena.
- **3. helburua: RA aurresaten duen algoritmo baten garapena.** EKG seinalearen gaitasuna aztertu eta metodo automatiko bat proposatu RA aurresateko.

Helburu guztiak betetzeko benetako OKBBG kasuak erabili dira eta anotazioa gauzatzeko erabilitako informazio iturriak independenteak izan dira, ahal izan den neurrian.

4 EMAITZAK

Kapitulu honetan 3. kapituluan azaldutako helburuei lotutako emaitzak laburbiltzen dira. Egindako lan gehienak konferentzietan azaldu dira lehendabizi [120, 121, 122, 123, 124, 125, 126], eta gehiago landu direnean aldizkari zientifikoetan argitaratu dira [8, 2, 3, 4, 5, 6]. Aldizkarietan argitaratutako lanak laburbiltzen dira atal honetan, eta lan guztiak zehaztasun gehiagorekin aztertu daitezke A eranskinean.

4.1 Lehen helburuari lotutako emaitzak

EKG seinalean soilik oinarritzen diren pultsu detektore automatikoen abantaila nagusia horien erabilera unibertsala da. KDA edo monitore/desfibriladoreek ia beti jasotzen duten seinalea da EKGa. Tesi honen garapenean zehar, bi hurbilketa gauzatu dira. Alde batetik, eskuz hainbat ezaugarri diseinatu ziren sailkatzaile klasikoak erabiltzeko ondoren. Ezaugarri horiek diseinatzeko, problema zehatzari buruzko aurreko ezagutza beharrezkoa da. Beste alde batetik, ikasketa sakonean oinarritutako algoritmoak aztertu ziren. Horiek EKG seinalea hartzen dute sarrera gisa eta ezaugarrien diseinua entrenamendu prozesuan zehar gauzatzen da. Soluzio bakoitza aldizkari desberdin batean argitaratu da, $J1_1$ eta $J1_2$ argitalpenetan alegia. Gainera, tarteko emaitzak konferentzia nazional batean [121] eta bi nazioarteko konferentzietan [120, 122] aurkeztu ziren.

4.1.1 J1$_1$: ECG-based pulse detection during cardiac arrest using random forest classifier

Lan hau gauzatzeko erabilitako datu-basea benetako OKBBG episodioak erabiliz sortu zen, denak *Tualatin Valley Fire & Rescue* agentziak (Tigard, OR, EEBB) jasotakoak 2010-2014 artean. Erabilitako monitore/desfibriladorea *Philips HeartStart MRx* izan zen, zeinak EKG seinalea jasotzen duen desfibrilazio-txaplatak erabiliz. Datu-baseari buruzko zehaztasun gehiago [7] erreferentzian daude azalduta.

Guztira 4 s-ko 1177 segmentu erabili ziren, 191 paziente desberdinetatik erautsitakoak. OKBBGan adituak diren hiru pertsona desberdinek segmentu bakoitza PGAE edo PE gisa anotatu zuten, beraien arteko *kappa* akordio indizea 0.92 izanik. Berrikuste prozesuan gaixoaren informazio klinikoa, BZI unea eta azken pronostikoa gehienbat, eta kapnografia erabili zituzten. Zehaztasunak [7] erreferentzian daude azalduta.

EKG seinalea ($x[n]$) aurreprozesatu egin zen lehendabizi zarata murrizteko, eta R uneak kalkulatu ziren ondoren; EKG segmentu bakoitzeko 9 ezaugarri kalkulatu ziren. QRS detekziorako, Hamilton-Tompkins detektorean oinarritutako algoritmo bat garatu zen [127]. Horrek EKG seinalea aurreprozesatzen du lehen diferentzia kalkulatuz eta 125 ms-ko leihoa erabiliz batezbesteko mugikorra kalkulatzen du $d_2[n]$ deritzon seinalea lortzeko. 4.1. irudian lan honetan erabilitako PGAE eta PE segmentuen adibideak erakusten dira, baita detektatutako R uneak ere. Kalkulatutako ezaugarriak (v_1-v_9) ondokoak izan ziren:

- Batezbesteko RR tartea (v_1).
- SL mediana (v_2), Risdal et aliik [1] proposatutako antzeko metodo bat erabiliz.
- QRSen anplitudearen mediana, beraien iraupenarekiko normalizatuta (v_3).
- Lehen diferentziaren, $|x[n] - x[n-1]|$, batezbestekoa eta desbideratze estandarra (v_4 and v_5).
- $d_2[n]$-ren kurtosia (v_6).

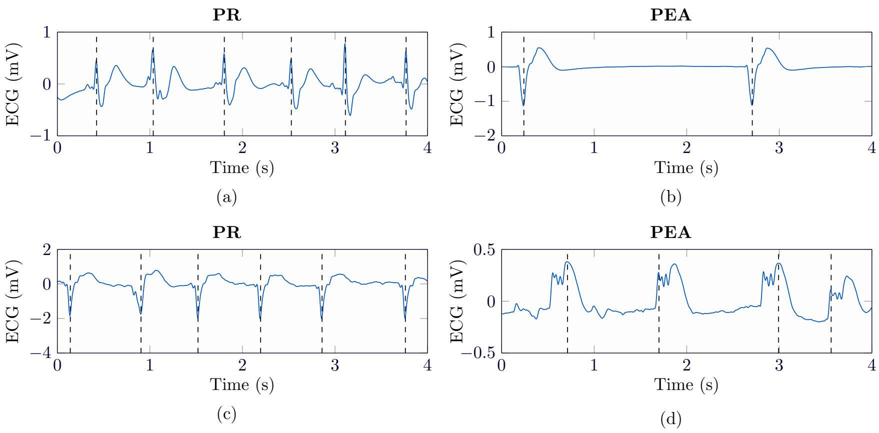

4.1. Irudia. $J1_1$ lanean erabilitako EKG (ECG) segmentuen adibideak. PE (PR) segmentuek bihotz-maiztasun azkarragoa dute oro har PGAE (PEA) segmentuekin alderatuta, baita QRS estuagoak ere. Detektatutako R uneak lerro beltzen bidez adierazten dira. Irudiaren iturria: [2].

- *Amplitude spectrum area* (AMSA), osagai espektralen batura beraien maiztasunarekin bidertuta (v_7).
- $x[n]$ seinalearen energia 17.5 Hz-tik gora (v_8).
- $x[n]$-ren entropia (v_9).

Ezaugarri horiek RF sailkatzaile bat erabiliz konbinatu ziren eta ebaluazioa gauzatzeko *leave-one-patient-out cross-validation* (LOPOCV) estrategia aplikatu zen. Banaketa estatistikoak estimatzeko *bootstrap* prozedura erabili zen.

Ezaugarrien aukeraketa aplikatu arren, emaitza hoberenak 9 ezaugarriak erabiliz lortu ziren, Se, Sp, BPP eta BPN %88.4, %89.7, %94.6 eta %79.1 izanik. Sailkatzaile desberdinak probatu ziren baina RF izan zen hoberena, 4.1. taulan egiaztatu daiteken moduan.

Azkenik, proposatutako metodoa Risdal et aliik [1] eta Alonso et aliik [7] proposatutako metodoekin alderatu zen. Metodoak inplementatzeko, EKG seinalean soilik oinarritutako ezaugarriak hartu ziren kontutan eta erabilitako sailkatzaileak lan originaletan proposatutako berdinak ziren. Emaitzak 4.2. taulan adierazten dira. Proposatutako metodoak artearen egoerak baino emaitza hobeak

4.1. Taula. Sailkatzaile desberdinen bidez lortutako emaitzak: *Logistic Regression* (LR), *Linear Discriminant Analysis* (LDA), *Quadratic Discriminant Analysis* (QDA), *k-Nearest Neighbours* (k-NN), *Support Vector Machine* (SVM), *Extreme Learning Machine* (ELM) eta *Random Forest* (RF). Emaitzak batezbestekoa (desbideratze estandarra) gisa daude azalduta.

Sailkatzailea	Se (%)	Sp (%)	Zehaztasuna (%)
LR	86.5 (1.8)	90.7 (1.6)	88.5 (1.2)
LDA	87.2 (1.9)	87.6 (1.7)	87.4 (1.4)
QDA	79.5 (2.8)	92.8 (1.4)	83.8 (1.9)
k-NN	83.7 (2.1)	91.1 (1.7)	86.1 (1.4)
SVM	83.9 (1.9)	90.0 (1.6)	86.5 (1.3)
ELM	90.1 (1.7)	82.6 (2.3)	86.3 (1.4)
RF	88.4 (1.8)	89.7 (1.4)	88.9 (1.2)

4.2. Taula. Errendimendu-metrikak Risdal et aliik [1] eta Alonso et aliik [7] proposatutako EKG ezaugarriak soilik erabiliz. Sailkatzaileak lan originaletako berdinak dira. Erabilitako errendimendu metrikak Se, Sp eta ZO izan ziren.

	# ezaugarri	Se (%)	Sp (%)	ZO (%)
Risdal et aliik [1]	7	87.3	80.9	85.2
Alonso et aliik [7]	3	85.9	79.0	83.7
Proposed reduced method	3	87.2	87.1	87.2
Proposed method	9	88.4	89.7	89.1

ematen ditu, baita 3 ezaugarri hoberenak (v_8, v_9 and v_1) soilik erabilitakoan ere.

Lan hau publikatu zenean, aurrenekoa izan zen EKG seinalea soilik erabiliz PGEA eta PE erritmoak bereizten zituena. Lortutako ZO %90-tik gertu zegoen, zeinak frogatzen duen soluzio sinple bat integratu daitekeela edozein desfibriladore komertzialetan.

4.1.2 J1$_2$: Deep Neural Networks for ECG-Based Pulse Detection during Out-of-Hospital Cardiac Arrest

Lan honetan beste algoritmo bat proposatzen da PGAE eta PE erritmoak automatikoki bereizteko EKG seinalea soilik erabiliz, oraingoan ikasketa sakonean oinarrituta. OKBBG episodioak Dallasen (TX, EEBB) jasotakoak dira *Philips HeartStart MRx* gailua erabiliz. Guztira 5 s-ko 3915 segmentu erabili ziren (2372 PE eta 1542 PGAE), 279 gaixo desberdinetatik erautsitakoak. Hiru adituk errebisatu zituzten segmentu guztiak eskuragarri zeuden seinaleak (EKG, BI eta kapnografia) eta informazio klinikoa erabiliz. Irizpideak oso kontserbadoreak izan ziren: PGAE segmentuak BZI gabeko gaixoetatik soilik erautsi ziren, eta PE segmentuak BZIdun gaixoetatik. Hau da, BZIdun gaixoetatik ez zen PGAE segmenturik erautsi.

Bi datu-partizio sortu ziren, bata modeloak entrenatzeko eta bestea ebaluatzeko (%80/%20). Entrenamendurako datuak beste 4 azpi-partiziotan banatu ziren hiper-parametroen optimizazioa gauzatzeko ebaluazio gurutzatua erabiliz.

Bi sare-arkitektura diseinatu ziren, S_1 eta S_2 (4.2 irudia): guztiz konboluzionala den sare bat eta sare konboluzionala GRU (*gated recurrent unit*) geruza bat gehituz, hurrenez hurren. Bi soluzioak ikasketa automatiko tradizionalarekin alderatzen dira. Horretarako, J1$_1$ publikazioan proposatutako ezaugarriak erautsi ziren eta hiru sailkatzaile frogatu: EBM, KLR (*kernel logistic regression*) eta RF. Emaitzak 4.3. taulan agertzen dira. Oro har, ikasketa sakonean oinarritutako algoritmoak ZO hobea eskaini zuten.

Ikasketa sakonean oinarritutako algoritmoek erautsitako ezaugarriak ere aztertu ziren. Horretarako, sailkatzeaz arduratzen den geruzaren aurreko ezaugarriak erautsi ziren eta RF, EBM eta KLR sailkatzaileak entrenatu eta ebaluatu. Emaitzak 4.3. irudian ageri dira. Bi arkitekturek erautsitako ezaugarriak (v_{D_1} eta v_{D_2}) eskuz diseinatutako ezaugarriak baino hobeak dira PGAE eta PE erritmoak bereizteko.

Azkenik, sarearen errendimendua aztertu zen horrek eskaintzen zuen ziurgabetasunaren arabera. Ziurgabetasuna *Monte-Carlo dropout*

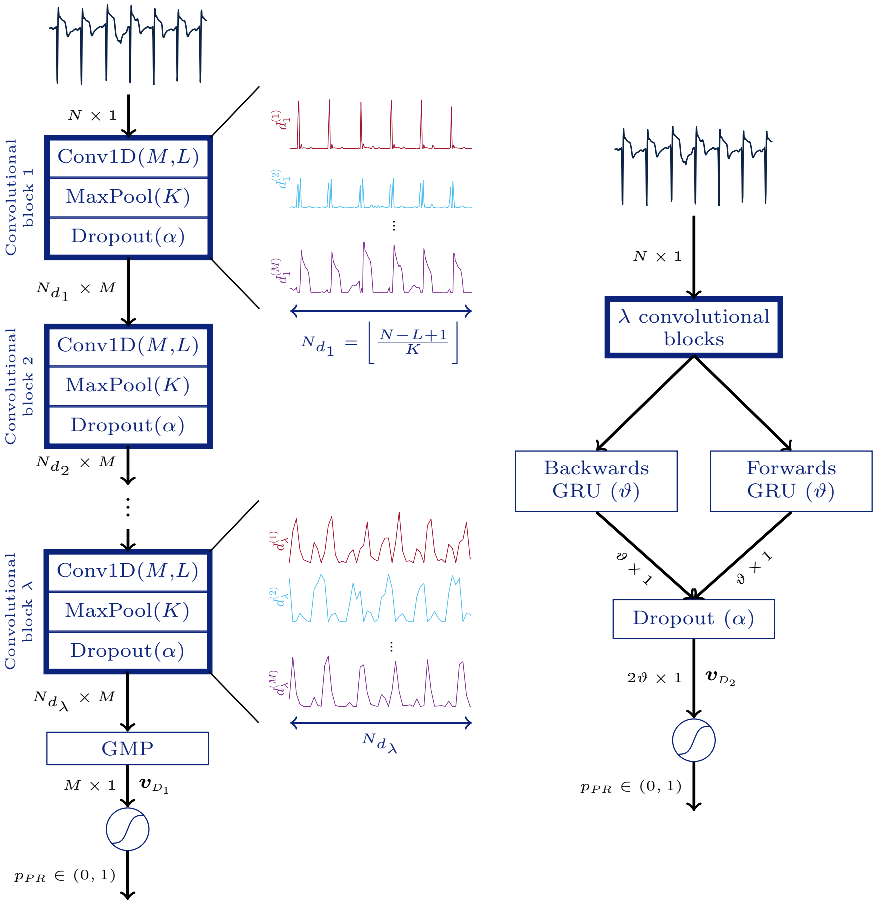

(a) S_1 (b) S_2

4.2. Irudia. Ikasketa sakonean oinarrituz proposatutako arkitekturak. Guztiz konboluzionala den sarea (S_1): N lagineko EKG seinalea erabiliz elikatzen da, λ etapa konboluzionalek osatzen dute, GMP (*global maximum pooling layer*) geruza bat erabiliz azken ezaugarriak erausteko eta guztiz konektaturiko azken geruza bat sailkapena egiteko. Azken geruzak segmentua PE izateko *probabilitatea* kalkulatzen du, p_{PR}. Hurrengo soluzioak berriz (S_2), BGRU (GRU bidirekzionala) geruza bat gehitzen du. Iturria: [3].

metodoa erabiliz estimatu zen eta entrenamendu-multzoa erabiliz, sareak erantzuna kasuen ehuneko zehatz batean emateko diseinatu zen. Emaitzak 4.4. taulan agertzen dira, non ikus daitekeen kasuen ZO hobetu egiten dela mugako kasuetan sailkapen-emaitza ez bada ematen.

4.3. Taula. Ikasketa automatiko tradizionalean eta ikasketa sakonean oinarrituta dauden algoritmoen emaitzen laburpena.

	Se (%)	Sp (%)	ZO (%)
Ikasketa automatiko tradizionala			
RF	96.0	87.4	91.7
EBM	97.6	86.2	91.9
KLR	97.5	86.2	91.8
Ikasketa sakona			
S_1	94.1	92.9	**93.5**
S_2	95.5	91.6	**93.5**

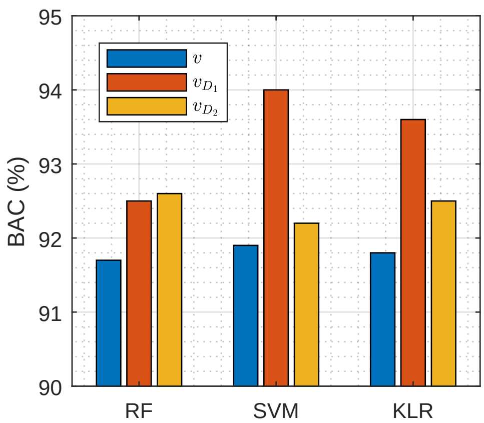

4.3. Irudia. RF, SVM (EBM) eta KLR sailkatzaileek eskainitako errendimendu-metrikak eskuz diseinatutako ezaugarriak erabiliz (v), S_1 arkitekturak eskainitako ezaugarriak erabiliz (v_{D_1}) eta S_2 arkitekturak eskainitako ezaugarriak erabiliz (v_{D_2}). Emaitzak ZO (BAC ingelesez) errendimendu-metrika gisa erabiliz ematen dira.

Ikasketa sakonean oinarritutako pultsu detekziorako argitaratutako lehen soluzioa izan zen hau. Hori posiblea izan zen Dallas-eko kolaboratzaileek konpartitutako datu-bolumen handiari esker, beharrezkoak izan zirenak ikasketa sakoneko algoritmoak diseinatzeko. Emaitzek argi erakusten dute teknika berritzaile horretan oinarritutako algoritmoek emaitza hobeak eskaintzen dituztela eta giza-begiak erautsi ezin dituen ezaugarriak erautsi ditzaketela sare neuronal hauek.

4.4. Taula. S_1 arkitekturaren emaitzak ziurgabetasun-maila desberdinentzat. Emaitzak ebaluazio-multzoarentzat ematen dira. Entrenamendu-multzoan eta ebaluazio-multzoan baztertzen diren kasuen ehunekoa ere taulan ikus daiteke.

Entrenamendu-multzoko %	Ebaluazio-multzoko %	Se (%)	Sp (%)	ZO (%)
80	78.5	100	95.2	97.6
90	89.6	96.6	93.2	94.9
95	95.4	97.1	92.2	94.6
97.5	98.1	96.3	92.1	94.2
100	100	94.1	92.9	93.5

Hurrengo helburura pasa aurretik, sare neuronal bat diseinatu zen BI seinalea soilik erabiliz PGAE eta PE erritmoak bereizteko [122]. Entrenamendu- eta ebaluazio-multzo berdinak erabiliz, lortutako Se, Sp eta ZO %94.2, %89.3 eta %91.8 izan ziren, hurrenez hurren. Oro har, EKG seinalea erabiliz errendimendu hobea lortzen da.

4.2 Bigarren helburuari lotutako emaitzak

Bigarren helburua iturri anitzeko metodoen garapena da zirkulazio-maila desberdinak ezaugarritzeko. Kasurik sinpleena bi klaseetako kasua da, PGAE eta PE bereizteko, eta espezifikoagoa da hiru klasetako sailkapena, BPGAE, SPGAE eta PE erritmoen arteko diskriminazioa. Hiru klaseetako problema datu-base berezi bati esker garatu ahal izan da, odol-presioaren uhin forma jarraitua duen datu-basea, non hiru klaseen anotazioa gauzatu ahal izan den. Iturri anitzeko algoritmoak diseinatzeko EKG, BI eta kapnografia seinaleak erabili dira. Kapnografiatik ezaugarriak erautsi ahal izateko, kapnografiaren segmentazioa beharrezkoa da. Hala nola, $EtCO_2$ mailak automatikoki kalkulatzeko. Azken soluzioak $J2_1$, $J2_2$ eta $J2_3$ publikazioetan agertzen dira, eta tarteko emaitzak kongresu ezberdinetan [123, 128, 129, 126].

4.2.1 $J2_1$: Feasibility of the capnogram to monitor ventilation rate during cardiopulmonary resuscitation

Lan honetan kapnografia seinalea segmentatzeko algoritmo sinple bat proposatu zen. OKBBGan zehar, bular-sakadek kapnografiaren uhin-forma aldatzen dute eta aireztapen bakoitzaren unea kalkulatzea zailagoa da. BBBaren kalitate ona beharrezkoa da gainera gaixoaren biziraupen-probabilitatea handitzeko, aireztapen-maiztasun egokia mantenduz beste faktore batzuekin batera. Kontutan hartu behar da, egun hiperbentilazioa oso ohikoa da OKBBGan zehar [130, 131, 132, 133, 134, 135, 136]. Aireztapen bakoitza detektatzeak kapnografiaren uhin-forma erabiliz aireztapen-maiztasunaren kalkulua ahalbidetzen du, baita $EtCO_2$ mailen kalkulu automatikoa ere. $EtCO_2$ mailen kalkulu automatikoa beharrezkoa izango denez hurrengo lanetan, kapnografian aireztapenak detektatzeko algoritmo bat garatzea da tesiaren bigarren helburuaren aurreneko pausua.

Bi datu-base erabili ziren lan honetan, ospitalez kanpoko datu-basea (OKDa) eta ospitale barruko datu-basea (OBDa). Aurreneko datu-basean BI seinalea eta kapnografia zeuden eskuragarri aireztapen bakoitzaren unea ezagutzeko, bigarrenean berriz gaixoak botatako gasen fluxuei loturiko hainbat seinale zeuden, kapnografia seinalearen desberdinak, erreferentzia independentetzat erabili zirenak aireztapenak anotatzeko. Bi datu-baseen estatistikak 4.5. taulan ageri dira.

Kapnografia aurreprozesatzeko 10 Hz-tako behe-paseko iragazki bat erabili zen eta 5 mmHg edo txikiagoak ziren balioak zerora jarri ziren. Ondoren, lehen diferentzia erabiliz piko positiboen eta negatiboen uneak detektatu ziren, horiek baitira aireztapen potentzialak. Azkenik, aireztapen potentzialak eta benetako aireztapenak honako 5 ezaugarri erabiliz bereizi ziren:

4.5. Taula. OKD eta OBD datu-baseen ezaugarriak.

Parametroa	**OKD**	**OBD**
Episodio kopurua	62	21
Iraupen totala (min)	2545	2335
Aireztapen kopurua (% BBBarekin)	16899 (38)	29841 (8)
Aireztapen-maiztasuna (min^{-1})	9.9 (8.7-13.1)	14.3 (12.6-18.2)
Minutuak hiperbentilazioarekin (%)	10 (2-35)	14 (0-88)

- Oinarriaren iraupena, D_{insp}.
- Batezbesteko CO_2 oinarrian, A_{insp}.
- Batezbesteko CO_2 balioa arnasa botatzen duen bitartean, A_{exp}.
- Arnasa botatzen hasten denean kapnografiaren aurreneko segundoaren kurbaren azpiko azalera, S_{exp}.
- CO_2-aren igoera erlatiboa:

$$A_r = \frac{A_{exp} - A_{insp}}{A_{exp}} \tag{4.1}$$

Ezaugarri guztiak 4.4. irudian erakusten dira. Bi ezaugarriekin atalase finkoak erabili ziren, D_{insp} eta bi aireztapenen arteko denbora tarteak. Beste ezaugarrien atalase balioak moldakorrak ziren, eta azkeneko p aireztapenak erabiliz kalkulatu ziren:

$$Th_k = \frac{w}{p} \sum_{n=k-p}^{k} x_n \tag{4.2}$$

non $w \in [0, 1]$ entrenamendu prozesuan ezartzen zen eta x_n lehen aipatutako ezaugarriak diren n. aireztapenarentzat. Aireztapen potentzial batek atalase-balio guztiak gainditzen zituenean, benetako aireztapen gisa sailkatzen zen.

OKDa bi multzotan banatu zen, entrenamendu-multzoa eta ebaluazio-multzoa. OBD osoa, berriz, algoritmoa ebaluatzeko erabili zen. Algoritmoa ebaluatzeko Se eta BPP kalkulatu ziren gaixo bakoitzarentzat eta banaketak aztertu ziren.

Se eta BPP metriken medianak %99.1 eta %97.0 izan ziren OKDa ebaluazio-multzoan (%99.0 eta %97.6 bular-sakadak dauden tarteetan). OBD, berriz, Se eta BPP metriken medianak %100 izan ziren (%99.8 eta %98.3 bular-sakadak zeuden tarteetan). Emaitza horiek frogatzen dute aireztapenen detekzio automatikoa posiblea dela OKBBGan zehar kapnografia erabiliz.

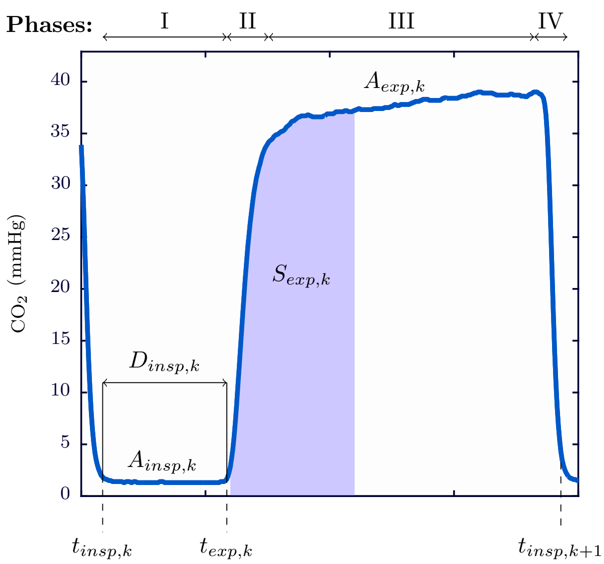

4.4. Irudia. Aireztapen batek kapnografia seinalean sortzen duen uhin forma, bere lau faseak eta algoritmoak erabilitako ezaugarriak.

4.2.2 J2$_2$: Capnography: A support tool for the detection of return of spontaneous circulation in out-of-hospital cardiac arrest

Lan honetan kapnografia seinaleak PGAE/PE diskriminatzaileei gehitzen dien informazioa aztertzen da, bigarren helburuaren lehenengo azpi-helburua betez.

Datuen iturria Dallas-en kokatzen da 2012 eta 2016 artean. Guztira 1561 episodio jaso ziren Philips HeartStart MRx gailua erabiliz. Informazio klinikoari eta eskuragarri zeuden seinaleei esker, BZI tarteak berrikusi ziren. Episodioak barne hartzeko irizpideak aplikatu ondoren, guztira 426 OKBBG episodio erabili ziren (117 BZIdunak). BZI unea erabiliz (t_R), PGAE/PE segmentuen datu-basea automatikoki sortu zen. Lehendabizi, bular-sakadak automatikoki detektatu ziren SS erabiliz edo BI seinalea erabiliz [56, 137], eta 3.2 s baino luzeagoak ziren etenaldiak aztertu ziren. KDA komertzial baten algoritmoa erabiliz erritmo organizatuak (PGAE edo PE) soilik hartu ziren [138]. Azkenik, t_R unean oinarrituta segmentu bakoitza PGAE edo PE gisa anotatu zen. 4.5. irudian EKG, BI eta kapnografia

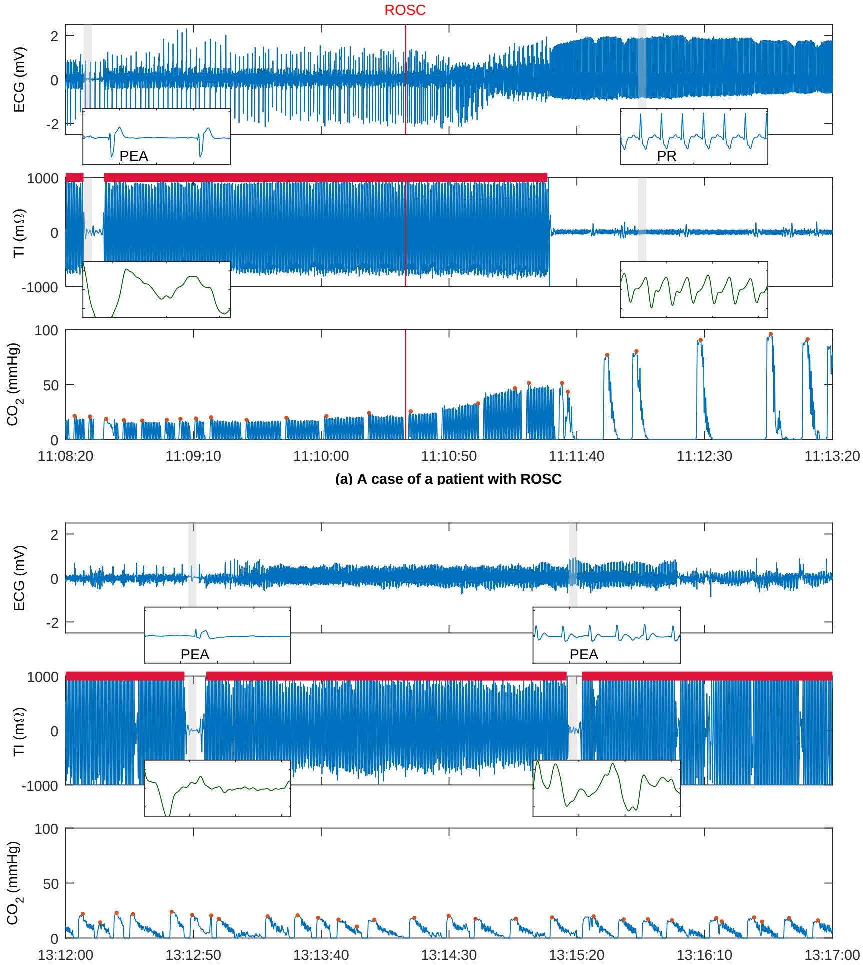

(a) A case of a patient with ROSC

(b) A case of a patient without ROSC

4.5. Irudia. EKG (ECG), BI (TI) eta kapnografia seinaleak BZIdun gaixo batentzat (a) eta BZI gabeko gaixo batentzat (b). Tokiko sorosleak apuntatutako BZI unea (ROSC) marra gorri bertikal batekin azaltzen da lehen adibidean. Aztertutako leihoak grisez markatzen dira eta handiago erakusten dira, PGAE (PEA) eta PE (PR) erritmoak. Sakada tarteak BI seinalearen gainean adierazten dira. Aireztapenak automatikoki detektatzen dira eta lortutako $EtCO_2$ mailak puntu gorriz adierazten dira kapnografia seinalean. Irudiaren iturria: [4].

seinaleak ageri dira BZIdun eta BZI gabeko gaixoen adibideak erakutsiz. Aukeratutako leihoak PGAE gisa anotatzen dira t_R baino lehen badaude edo BZI gabeko gaixo batetik erautsi badira, t_R baino beranduago aztertzen diren leihoak berriz PE gisa anotatzen dira.

Aurreko ikerketan ohartu ginen QRS uneak detektatzea PGAE segmentu motzetan oso zaila dela [2], eta egungo soluzioak ez direla bideragarriak. Horregatik, lan honetan erabilitako ezaugarriek ez dute QRS detekziorik behar. Guztira 10 ezaugarri erautsi ziren: 6 EKG seinalean oinarrituta, 2 BI seinalean oinarrituta, 1 EKG eta BI seinaleetan oinarrituta, eta 1 kapnografia seinalean oinarrituta. Artearen egoeran oinarrituta zeuden ezaugarri gehienak. Azken ezaugarria kalkulatzeko kapnografia segmentatu zen lehen azaldutako algoritmoa erabiliz [8] eta azken minutuko $EtCO_2$ mediana kalkulatu zen. Ezaugarri guztiak RF sailkatzaile bat erabiliz konbinatu ziren eta 10-multzotako ebaluazio gurutzatua erabili zen.

Emaitzak 4.6. taulan agertzen dira, non erraz antzematen den kapnografia seinalea gehitzeak modeloen errendimendua hobetzen duela, abiapuntuko hipotesia baieztatuz. Emaitzak bi era desberdinetara kalkulatu ziren: episodio osoak kontsideratuz eta BZIdun gaixoengatik erautsitako PGAE segmentuak baztertuz. Benetako eszenarioa lehenengo kasuistikan agertzen dena da, bigarrenak emaitza hobeak ematen dituen arren. Emaitzetan desberdintasun hori ikustean PGAE erritmo desberdinak daudela ondorioztatu zen, eta hurrengo ikerketa horren harira egin zen. RF sailkatzaileak itzulitako PE *probabilitatea* ere handitzen joaten zela ikusi zen t_R unea gerturatzen zein heinean. Honako bi ondorio atera daitezke:

- t_R unea ez da oso zehatza eta anotazioetan dagoen zaratak emaitzak okertzen ditu.
- Beranduago PE erritmo bat aurkezten duten gaixoetatik erautsitako PGAE erritmoak eta pultsurik gabeko gaixoetatik erautsitako PGAE erritmoak ezaugarri desberdinak dituzte.

Analisi sakonago bat gauzatu zen fenomeno horren inguruan, artikuloaren eranskinean [4]. Gainera, tarteko emaitzak nazioarteko konferentzia batean ere azaldu ziren [129]. Aurkikuntza garrantzitsua izan zen hori, ohikoa baita BZIdun gaixoetatik erautsitako PGAE

4.6. Taula. Sailkatzaile desberdinen emaitzak datu-base osoa kontutan hartzen denean eta BZIdun gaixoetatik erautsitako PGAE erritmoak baztertzen direnean.

	Datu-base guztia			BZIdun PGAEak baztertuz		
	KAA	Se	Sp	KAA	Se	Sp
$EtCO_2$	0.76	72.3	67.8	0.79	83.7	64.6
EKG	0.88	84.2	78.2	0.93	81.7	90.8
EKG+BI	0.90	86.7	81.6	0.94	88.4	87.0
EKG+$EtCO_2$	0.91	86.3	81.5	0.95	91.8	84.2
EKG+BI+$EtCO_2$	0.92	83.9	86.0	0.96	87.8	91.3

erritmoak baztertzea, eta emaitza hobeak ematen dituen arren, planteatzen den eszenarioa ez da errealista.

Lan honetan argitaratutako emaitzak aurreko lanetan argitaratutako emaitzak baino okerragoak ziren [1, 7, 2, 3]. Gehienbat datu-basearengatik gertatzen da hau, automatikoki sortzeak zarata sartzen duelako. Are gehiago, aurreko lan batean proposatutako algoritmoa lan honetan aplikatzean [2], lortutako Se eta Sp %78.8 eta %84.1 izan ziren (lan originalean baino askoz baxuagoak).

Azkenik, OKBBG episodio osoak automatikoki aztertzeko algoritmo baten bideragarritasuna aztertu zen. Horretarako, eredurik hoberena erabili zen (hiru seinaleetan oinarritutakoa) eta arau erraz bat ezarri zen: hiru analisi-segmentutatik bi PE gisa detektatzen badira, gaixoa BZIduna da. Lortutako emaitzak oso onak izan ziren, Se eta Sp %96.6 eta %94.5 izanik.

Beranduago, EKGan eta BIan oinarritutako algoritmo berdina datu-base independente eta handiago batean frogatu zen eta emaitzak kongresu batean azaldu ziren [126]. Guztira 893 kasu hartu ziren kontutan (261 BZIdunak), eta lortutako Se eta Sp %91.2 eta %94.3 izan ziren. Emaitza horiek frogatzen dute posiblea dela algoritmo hori erabiltzea OKBBG episodioak automatikoki aztertzeko.

4.2.3 $J2_3$: Multimodal algorithms for the classification of circulation states during out-of-hospital cardiac arrest

Ikerketa lan honek galdera garrantzitsu bati erantzuten dio: posiblea da BPGAE, SPGAE eta PE erritmoak bereiztea OKBBGan ohikoak diren seinaleak erabiliz?

Lan hau gauzatzeko datu-base berezi bat erabili zen, odol-presioaren uhin-formari begiratuz posiblea izan zen segmentuak hiru klaseetan banatzea anotazio prozesuan. Gainera, garatutako algoritmoek EKG, BI eta kapnografia seinaleekin egiten dute lan, beraz, anotazio prozesua guztiz independentea da algoritmoarekiko. Datuak Norvegiatik datoz, 2015 eta 2017 artean jasota Lifepak 15 (Stryker Ltd.) gailua erabiliz. Guztira 60 gaixo erabili ziren, 2506 segmentu (1463 PE, 364 SPGAE eta 679 BPGAE). Bi ingeniari biomedikuk eta mediku batek segmentu guztiak anotatu zituzten informazio klinikoa eta hainbat seinale (odol-presioa eta burmuineko oximetria) erabiliz. BPGAEan zehar, odol-presioaren uhin-forma laua da. SPGAE eta PE erritmoetan zehar fluktuazioak antzeman daitezke, bihotzaren aktibitate mekanikoak sortzen baititu presio-diferentzia horiek. Hala ere, PE erritmoetan zehar agertzen diren balioak handiagoak dira presio sistolikoarentzat (Sys), diastolikoarentzat (Dias) eta pultsu-presioarentzat (PP). Uhin-formen adibide bana agertzen da 4.6. irudian, $EtCO_2$ mailak ere erakusten dira. Odol-presioari lotutako neurri desberdinak berriz, 4.7. taulan agertzen dira.

Proposatutako algoritmoak EKG, BI eta kapnografia seinaleak erabiltzen ditu ezaugarrien erauzketarako, eta ondoren RF

4.7. Taula. Presio sistolikoaren (Sys), presio diastolikoaren (Dias) eta pultsu-presioaren (PP) banaketak erritmo-mota bakoitzeko

	BPGAE	SPGAE	PE
Sys (mmHg)	32.5 (24.6-41.7)	40.4 (35.0-49.1)	95.5 (68.9-148.7)
Dias (mmHg)	27.2 (19.5-36.4)	28.1 (25.9-33.7)	51.1 (40.0-75.9)
PP (mmHg)	4.1 (0.0-6.8)	11.3 (8.0-16.4)	45.4 (29.4-68.1)

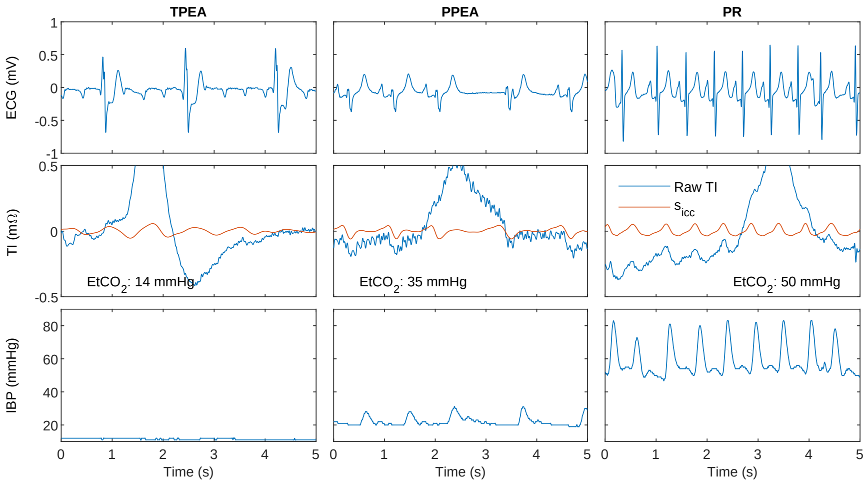

4.6. Irudia. Erabilitako BPGAE (TPEA), SPGAE (PPEA) eta PE (PR) erritmoen adibideak. Bakoitzarentzat EKG (ECG), BI (TI) eta odol-presioaren (IBP) uhin-formak erakusten dira. BI seinaletik erautsitako zirkulazio osagaia ere erakusten da (s_{icc}), eta azken minutuko $EtCO_2$ mediana. Irudiaren iturria: [5].

sailkatzaile bat erabiliz ezaugarrien aukeraketa eta sailkatzea egiten da. Lehendabizi, zirkulazio osagaia iragazteko metodoa hobetzen saiatu ginen. Zirkulazio osagaia Fourier serie gisa adieraziz (2.6 ekuazioa), $a_k[t_j]$ and $b_k[t_j]$ Kalman iragazki bat erabiliz estimatu ziren (adibideak 4.6. irudian). Ondoren, 172 ezaugarri erautsi ziren (37 artearen egoeratik hartuta).

Ezaugarrien aukeraketa EKG eta BI seinaleetatik erautsitako ezaugarrientzat egin zen, azken minutuko $EtCO_2$ balioen mediana eskuz gehitu zen gero ($MEtCO_2$). Ezaugarriak aukeratzeko metodoak ez dira optimoak gaur egun eta baliteke bestela $EtCO_2$ balioa kanpoan geratzea, baina aurretiko ezagutzagatik badakigu $EtCO_2$ balioek informazioa dutela gaixoaren zirkulazio-egoerari buruz. Ezaugarri aukeraketa prozesuan, N_f ezaugarri aukeratzen dira eta eredua berriro entrenatzen da ezaugarri hauek erabiliz. Ereduak ebaluatzeko 5-multzotako ebaluazio-gurutzatua gauzatu zen 100 aldiz. Emaitzen laburpena 4.8. taulan agertzen da, erabilitako seinaleak desberdinak direnean eta N_f balio desberdinentzat. Seinale eta ezaugarri kopurua handituz lorturiko emaitzak hobeak izan ziren, ZO= %69 izanik hiru seinaleak erabiliz eta $N_f = 40$.

4.8. Taula. Errendimendu-metrikak hiru klasetako sailkatzailearentzat, emaitzak mediana (75.pertzentila-25.pertzentila tartea) gisa adierazten dira.

Seinaleak	N_f	Se_{BPGAE}	Se_{SPGAE}	Se_{PE}	ZO	$F_{1,BPGAE}$	$F_{1,SPGAE}$	$F_{1,PE}$	F_{1m}
EKG, BI, CO_2	10*	70.3 (4.8)	50.4 (5.5)	78.4 (2.9)	66.2 (2.8)	67.9 (4.0)	41.1 (4.4)	69.0 (2.7)	59.2 (2.4)
EKG, BI, CO_2	20*	73.1 (3.7)	50.9 (4.6)	81.2 (2.4)	68.6 (2.4)	69.3 (2.4)	43.3 (3.3)	70.7 (2.5)	61.2 (1.8)
EKG, BI, CO_2	30*	74.4 (3.6)	50.2 (4.2)	82.3 (1.9)	68.8 (2.1)	69.3 (2.9)	44.3 (2.9)	71.1 (2.0)	61.5 (1.6)
EKG, BI, CO_2	40*	74.9 (3.7)	49.6 (3.7)	83.2 (1.5)	69.0 (2.1)	69.7 (2.8)	45.1 (3.0)	70.7 (1.7)	61.7 (1.5)
EKG	30	57.5 (4.5)	37.2 (5.5)	80.9 (2.7)	58.6 (2.6)	57.1 (2.8)	35.7 (4.4)	68.9 (1.9)	53.8 (2.2)
EKG, BI	30	71.8 (3.4)	47.7 (5.6)	81.5 (2.1)	66.9 (2.6)	65.8 (2.5)	42.9 (4.1)	70.8 (2.3)	59.8 (2.1)

* Azken eredua $N_f + 1$ ezaugarriz osatuta dago ($MEtCO_2$ barne)

Lan honen beste puntu garrantzitsu bat bi klaseetako algoritmoen ebaluazioa izan zen, BPGAE eta SPGAE elkartuz PGAE klasea sortzeko. Izan ere, artearen egoeran lehen aldiz anotazio-prozesua algoritmoarekiko guztiz independentea izan baitzen. Emaitzak 4.9. taulan agertzen dira. Ikus daiteken moduan, proposatutako algoritmoak errendimendu-metrika hobeak eskaini zituen. Bi gako zeuden emaitzak hobetzeko: Kalman iragazkiaren erabilera eta ezaugarrien erauzketa. Gainera, artearen egoeran proposatutako algoritmoak gure datu-basean frogatzean, lortutako emaitzak baxuagoak izan ziren oro har.

4.9. Taula. Errendimendu-metrikak bi klasetako sailkatzailearentzat, emaitzak mediana (75.pertzentila-25.pertzentila tartea) gisa adierazten dira.

	Seinaleak	N_f	Se_{PGAE}	Se_{PE}	ZO	$F_{1,PGAE}$	$F_{1,PE}$	F_{1m}	KAA
Risdal et al. [1]	EKG, BI	17	78.8 (2.7)	78.0 (3.1)	78.3 (2.2)	74.0 (1.8)	64.9 (2.0)	69.4 (1.7)	0.84 (0.02)
Risdal et al. [1]	EKG, BI	12	80.1 (3.2)	77.6 (2.2)	78.6 (2.2)	74.6 (2.3)	65.1 (2.0)	69.7 (1.8)	0.84 (0.02)
Alonso et al. [7]	EKG, BI	6	68.8 (1.7)	77.3 (1.4)	73.1 (1.4)	67.7 (1.3)	65.7 (1.9)	66.7 (1.4)	0.84 (0.02)
Elola et al. [2]	EKG	9	77.9 (2.2)	80.2 (2.6)	78.9 (1.6)	74.6 (1.2)	67.9 (1.8)	71.2 (1.5)	0.84 (0.01)
Elola et al. [4]	EKG, BI, CO_2	10	79.9 (2.2)	81.1 (2.2)	80.4 (1.9)	77.0 (2.0)	79.4 (2.0)	73.0 (1.7)	0.87 (0.01)
Gure proposamena	EKG, BI, CO_2	10*	83.1 (3.0)	79.8 (2.8)	81.5 (1.8)	78.8 (2.5)	70.0 (2.9)	74.5 (1.9)	0.87 (0.02)
Gure proposamena	EKG, BI, CO_2	20*	84.5 (2.5)	80.3 (2.3)	82.4 (1.7)	80.1 (1.7)	70.3 (2.5)	75.3 (1.5)	0.88 (0.01)
Gure proposamena	EKG, BI, CO_2	30*	85.6 (2.4)	81.3 (2.0)	83.2 (1.9)	80.6 (1.7)	70.4 (2.5)	75.6 (1.8)	0.89 (0.01)
Gure proposamena	EKG, BI, CO_2	40*	86.0 (2.1)	81.8 (2.1)	83.9 (1.7)	81.2 (1.7)	71.0 (2.6)	76.2 (1.8)	0.89 (0.01)
Gure proposamena	EKG	30	76.4 (2.6)	80.4 (4.0)	78.4 (2.2)	74.4 (1.8)	68.5 (2.1)	71.4 (1.6)	0.85 (0.01)
Gure proposamena	EKG, BI	30	85.9 (2.2)	80.5 (2.3)	83.1 (1.8)	80.6 (1.5)	70.3 (2.7)	75.5 (1.8)	0.88 (0.01)

* Azken eredua $N_f + 1$ ezaugarriz osatuta dago ($MEtCO_2$ barne)

4.3 Hirugarren helburuari lotutako emaitzak

Tesiaren azkenengo helburuari dagokionez, nazioarteko aldizkari batean argitalpen bat ($J3_1$) eta bi konferentzia [125, 124] argitaratu dira.

4.3.1 J3$_1$: Towards the Prediction of Rearrest during Out-of-Hospital Cardiac Arrest

Lan honen helburua RA aurresatea izan zen, hots, OKBBGan BZI lortu ondoren gaixoak bigarren geldialdi bat jasango duen ala ez aurresatea ospitalera iritsi aurretik. Erabilitako datuak Dallas-etik datoz, denak Philips HeartStart MRx gailua erabiliz lortutakoak. Guztira 162 gaixo erabili ziren (55 RAdunak) eta anotazioa informazio klinikoa eta eskuragarri zeuden seinaleak erabiliz gauzatu zen. 4.7. irudiak RAdun gaixo baten adibidea erakusten du. BZI unea eta RA unea anotatu ziren t_{RA} kalkulatzeko. Algoritmoak EKG seinalea soilik erabiliz egiten du lan, BZI ondoren t_w segundotako leiho bat erabiliz. RA gabeko gaixoak eta $t_{RA} >$ 12 min zuten gaixoak RA gabekoak gisa kontsideratu ziren (noRA). Besteak, aldiz, RAdunak. Normalean gaixoak BZI lortzen duenean ospitalera eramaten da, eta beharrezko denbora 12 minutu baino baxuagoa da, horregatik ezarri zen 12 minutuko denbora tartea.

4.10. taulak erautsitako 21 ezaugarriak laburbiltzen ditu, 17 BEAn oinarrituta eta beste 4 EKG seinalearen uhin forman. Ezaugarriak konbinatzeko RF sailkatzaile bat erabili zen, ezaugarrien aukeraketa egiteko beste artikulu batean jarraitutako prozedura jarraituz [5].

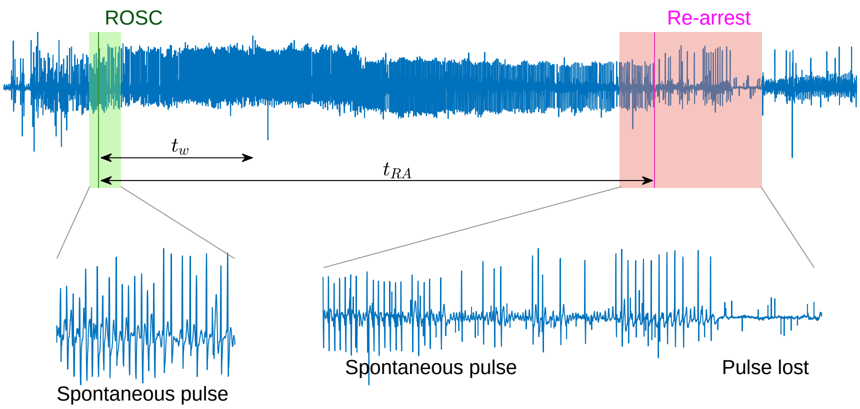

4.7. Irudia. OKBBG gaixo bat RA batekin. Gaixoak BZI (ROSC) lortzen du baina RA bat jasaten du beranduago, PE erritmoa PGAE bihurtzen da eta AS ondoren. Aztertutako segmentua t_w-dun EKG leihoa da, BZI ondoren segituan hartuta. Irudiaren iturria: [6].

Algoritmoa ebaluatzeko, 5-multzotako ebaluazio-gurutzatua egin zen 100 aldiz.

4.10. Taula. Erabilitako ezaugarrien laburpena [6].

Denboraren eremuko BEA ezaugarriak	**BEA ezaugarri ez-linealak**
v_1 : Batezbesteko RR tartea	v_{14} : SD1^2
v_2 : RR tarteen desbideratze estandarra	v_{15} : SD2^2
v_3 : RMSSD	v_{16} : SD1^2/SD2^2
v_4 : Aldakortasun koefizientea	v_{17} : Lagin entropia
v_5 : nNN50	**EKG uhin-forman oinarritutako ezaugarriak**
v_6 : RR tarteen kuartilarteko tartea	v_{18} : Maiztasun zentrala
Maiztasunaren eremuko BEA ezaugarriak	v_{19} : Seinalearen anplitudea
v_7 : LF potentzia absolutua	v_{20} : QRS potentzia erlatiboa
v_8 : LF potentzia erlatiboa	v_{21} : QRS zabaleraren desbideratze estandarra
v_9 : HF potentzia absolutua	
v_{10} : HF potentzia erlatiboa	
v_{11} : LF/HF potentzia	
v_{12} : LF maiztasun pikoa	
v_{13} : HF maiztasun pikoa	

Hasteko, ezaugarri bakoitza banaka ebaluatu zen. Horretarako, erregresio logistikoan oinarritutako sailkatzaile bat entrenatu eta ebaluatu zen ezaugarri bakarra erabiliz. 4.11. taulan ezaugarrien banaketak agertzen dira bi taldeentzat t_w balio desberdinentzat. Taulan 10 ezaugarri hoberenak soilik ageri dira. Oro har, RAdun gaixoek RR tarte aldakorragoak eta erregularragoak azaldu zituzten.

4.11. Taula. Erabilitako 10 ezaugarri hoberenen banaketak mediana (25.pertzentila-75.pertzentila) gisa adierazita, eta errendimendu-metriken mediana ezaugarri bakarra erabiltzean. Emaitzak t_w desberdinentzat adierazten dira.

$t_w = 1$ min					$t_w = 2$ min				
Ezaugarria	**NoRA**	**RA**	**KAA**	**PRKAA**	**Ezaugarria**	**NoRA**	**RA**	**KAA**	**PRKAA**
v_{15}	0.01 (0.02)	0.03 (0.10)	65.0	50.3	v_2	0.08 (0.12)	0.21 (0.37)	66.2	50.1
v_2	0.07 (0.10)	0.15 (0.25)	64.9	50.2	v_4	0.16 (0.19)	0.29 (0.40)	65.7	49.4
v_7	0.00 (0.00)	0.00 (0.01)	63.3	49.4	v_6	0.06 (0.11)	0.14 (0.26)	63.4	48.7
v_4	0.14 (0.17)	0.23 (0.24)	64.2	48.9	v_{17}	0.31 (0.45)	0.18 (0.27)	65.5	47.4
v_9	0.00 (0.00)	0.01 (0.03)	62.4	47.8	v_3	0.57 (0.23)	0.71 (0.49)	63.3	48.4
v_{14}	0.05 (0.06)	0.09 (0.18)	61.9	47.8	v_{14}	0.05 (0.09)	0.11 (0.20)	64.0	47.7
v_{17}	0.35 (0.51)	0.20 (0.30)	65.1	45.9	v_{15}	0.01 (0.02)	0.05 (0.22)	61.7	47.0
v_3	0.56 (0.26)	0.68 (0.45)	60.3	48.2	v_{20}	0.38 (0.20)	0.28 (0.22)	64.5	45.4
v_1	0.55 (0.24)	0.63 (0.38)	59.3	46.8	v_5	216 (81)	180 (104)	61.6	46.6
v_5	106 (45)	93 (54)	59.4	45.4	v_7	0.00 (0.00)	0.01 (0.03)	60.7	46.4

Ezaugarri guztiak konbinatzean RF sailkatzaileak emandako emaitzak 4.12. taulan adierazten dira. BEAn oinarrituta ez dauden ezaugarriak gehitzean emaitzak hobetzen ditu, baita t_w balioa handitzeak ere. Algoritmorik hoberenak emandako Se eta Sp %67.3 izan ziren, EKG seinaleak RAri buruzko informazioa duela frogatuz.

4.12. Taula. Proposatutako algoritmoaren errendimendu-metrikak mediana (25.pertzentila-75.pertzentila) gisa adierazita ezaugarri-familia desberdinak erabiliz eta t_w balio desberdinak erabiliz.

	t_w	Se (%)	Sp (%)	BPP (%)	F_1 (%)	KAA	PRKAA
BEA ezaugarriak	1 min	57.3 (11.8)	75.7 (14.5)	54.5 (9.8)	55.8 (2.8)	65.4 (2.3)	51.2 (2.9)
	2 min	61.8 (6.4)	72.9 (6.1)	54.4 (4.6)	57.6 (2.0)	67.3 (2.0)	50.7 (2.7)
Ezaugarri guztiak	1 min	63.6 (15.5)	69.2 (20.6)	51.5 (10.0)	55.4 (3.1)	66.2 (2.2)	52.0 (2.6)
	2 min	67.3 (9.1)	67.3 (10.3)	51.4 (5.3)	57.9 (1.7)	69.2 (1.6)	53.1 (3.0)

Lan honek proposatu zuen RA aurresateko lehen algoritmo automatikoa. Frogatzen da EKG seinaleak informazioa daukala RAri buruz, baina analisi sakonagoak beharrezkoak dira ondorioak sendotzeko.

5 ONDORIOAK

Kapitulu honetan tesiaren ekarpen nagusiak laburbiltzen dira. Hasteko, aurkikuntza garrantzitsuenak errepasatzen dira, ondoren finantziazio-iturriak aipatzen dira, lortutako publikazioen zerrenda ematen da eta dokumentua etorkizuneko ikerketa-lerroekin bukatzen da.

5.1 Tesiaren ekarpen nagusiak

Tesi honen helburu nagusia zirkulazio-egoera desberdinen identifikazio automatikorako metodoen garapena zen OKBBGan zehar. Ekarpen zientifiko nagusiak laburbiltzen dira ondoren:

- *EKG seinalea soilik erabiliz PGAE eta PE erritmoen diskriminazioa*. Ikasketa automatikoan oinarritutako teknika desberdinak proposatu dira [2, 3].
- *$EtCO_2$ mailen analisia PGAE/PE erritmoak bereizteko.* Kapnografiak sailkatzaile horiei gehitzen dioten balioa aztertu da, $EtCO_2$ mailak ezaugarri gisa erabiltzeak emaitzak hobetzen dituela frogatuz EKG eta BI seinaleetan oinarrituta dauden algoritmoekin alderatuta [4].
- *OKBBG episodioen ondorengo analisia.* Egindako lan batean sortutako datu-basea guztiz automatikoa zen eta lortutako emaitzak onargarriak izan ziren hala ere. Gainera, OKBBG episodioak automatikoki BZIdunak edo BZI gabekoak gisa sailkateko metodoak garatu dira [4, 126].

- *BPGAE/SPGAE/PE diskriminazioa.* Lehen aldiz, OKBBGan zehar erabilgarriak diren algoritmoak garatu dira zirkulazio-maila desberdinak bereizteko [5].
- *RAren aurresatea.* Tesi honen azken ekarpen garrantzitsua RA aurresateko algoritmoen garapena izan da[6].

5.2 Finantziazioa

Finantziazio-iturri nagusia Eusko Jaurlaritzak doktoretza egiteko emandako diru-laguntza izan da (P1). Hala ere, beste ikerketa-proiektu batzuk ere garrantzitsuak izan dira tesia garatzeko (P2, P3, P4, P5, P6 and P7).

P1 *Ayuda para la formación de personal investigador.*
Basque Government Department of Education, Universities and Research
Ref: PRE_2017_1_0112, PRE_2018_2_0260, PRE_2019_2_0100, PRE_2020_2_0209
2017 - 2020

P2 *BioRes (Biomedical Engineering and Resuscitation)*
Basque Government Department of Education, Universities and Research
Ref: IT1229-19
Urtarrila 2019 - Abendua 2022
Finantziazioa: 97000 €

P3 *BioRes (Biomedical Engineering and Resuscitation)*
University of the Basque Country
Ref: GIU17/31
Otsaila 2018 - Otsaila 2021
Finantziazioa: 15000 €

P4 *Determinación de valores de oximetría cerebral para la predicción de los resultados de intervención en pacientes en parada cardiorrespiratoria.*
Health department of the Basque Government
Ref: SAN19/01, SAN18/10, SAN17/12

Urtarrila 2017 - Abendua 2019
Finantziazioa: 48172 €

P5 *Procesado multimodal de señal y aprendizaje automático para la mejora del tratamiento de la parada cardiorrespiratoria extrahospitalaria.*
Spanish ministry of Economy and Competitiveness
Ref: RTI2018-101475-BI00
Urtarrila 2017 – Abendua 2019
Finantziazioa: 96000 €

P6 *Hacia la monitorización de la resucitación cardiopulmonar orientada a la respuesta del paciente.*
University of the Basque Country
Urtarrila 2017 – Abendua 2018
Finantziazioa: 11392 €

P7 *Hacia la monitorización inteligente en el entorno de la resucitación cardiopulmonar.*
University of the Basque Country
Urtarrila 2016 – Abendua 2018
Finantziazioa: 99825 €

5.3 Argitalpenak

Tesiaren garapenean, hainbat argitalpen zientifiko burutu dira, zeinak 5.3.1 eta 5.3.2 ataletan dauden zerrendatuta:

- Bi artikulu aldizkari zientifikoetan (A2 eta A3) eta hiru komunikazio konferentzietan (C3, C4 eta C6) tesiaren aurreneko helburuari lotuta.
- Bigarren helburuari dagokionez, lau artikulu zientifiko (A1, A4 eta A6) eta lau komunikazio konferentzietan (C1, C2, C7 eta C9).
- Azken helburuari dagokionez, artikulu zientifiko bat (A5) eta bi komunikazio konferentzietan (C5 eta C5).

5.3.1 Artikuluak

A1 *Feasibility of the capnogram to monitor ventilation rate during cardiopulmonary resuscitation.*
Elisabete Aramendi, Andoni Elola, Erik Alonso, Unai Irusta, Mohamud Daya, James K. Rusell, Pia Hubner, Fritz Sterz
Resuscitation 2017 (IF: 5.863, 1/26)

A2 *ECG-based pulse detection during cardiac arrest using random forest classifier.*
Andoni Elola, Elisabete Aramendi, Unai Irusta, Javier Del Ser, Erik Alonso, Mohamud Daya
Medical and Biological Engineering and Computing 2018 (IF: 2.039, 23/59)

A3 *Deep neural networks for ECG-based pulse detection during out-of-hospital cardiac arrest.*
Andoni Elola, Elisabete Aramendi, Unai Irusta, Artzai Picón, Erik Alonso, Pamela Owens, Ahamed Idris
Entropy 2019 (IF:2.494, 33/85)

A4 *Capnography: A support tool for the detection of return of spontaneous circulation in out-of-hospital cardiac arrest.*
Andoni Elola, Elisabete Aramendi, Unai Irusta, Erik Alonso, Yuanzheng Lu, Mary Chang, Pamela Owens, Ahamed Idris
Resuscitation 2019 (IF:4.215, 2/31)

A5 *Towards the Prediction of Rearrest during Out-of-Hospital Cardiac Arrest.*
Andoni Elola, Elisabete Aramendi, Enrique Rueda, Unai Irusta, Henry Wang, Ahamed Idris
Entropy 2020 (IF:2.494, 33/85)

A6 *Multimodal algorithms for the classification of circulation states during out-of-hospital cardiac arrest.*
Andoni Elola, Elisabete Aramendi, Unai Irusta, Per Olav Berve, Lars Wik
IEEE Transactions on Biomedical Engineering 2020 (IF: 4.424, 14/87)

5.3.2 Konferentziak

C1 *Potencial de la señal de capnografía para la detección de pulso durante la resucitación cardiopulmonar.*
Andoni Elola, Elisabete Aramendi, Unai Irusta, Inés Álvarez, Erik Alonso
CASEIB (Congreso Anual de la Sociedad Española de Ingeniería Biomédica) 2017

C2 *ECG characteristics of pulseless electrical activity associated with return of spontaneous circulation in out-of-hospital cardiac arrest.*
Andoni Elola, Elisabete Aramendi, Unai Irusta, Erik Alonso, Pamela Owens, Mary Chang, Ahamed Idris
ERC conference 2018

C3 *Deep learning for pulse detection in out-of-hospital cardiac arrest using the ECG.*
Andoni Elola, Elisabete Aramendi, Unai Irusta, Artzai Picón, Erik Alonso, Pamela Owens, Ahamed Idris
Computing in Cardiology Conference 2018

C4 *Arquitecturas de aprendizaje profundo para la detección de pulso en la parada cardiaca extrahospitalaria utilizando el ECG.*
Andoni Elola, Elisabete Aramendi, Unai Irusta, Artzai Picón, Erik Alonso
CASEIB (Congreso Anual de la Sociedad Española de Ingeniería Biomédica) 2018

C5 *Anaálisis de la Variabilidad del Ritmo Cardiaco para la Prediccioón de la Parada Cardiaca Extrahospitalaria Recurrente.*
Andoni Elola, Enrique Rueda, Naroa Amezaga, Elisabete Aramendi, Unai Irusta
CASEIB (Congreso Anual de la Sociedad Española de Ingeniería Biomédica) 2019

C6 *Convolutional Recurrent Neural Networks to Characterize the Circulation Component in the Thoracic Impedance during Out-of-Hospital Cardiac Arrest.*
Andoni Elola, Elisabete Aramendi, Unai Irusta, Artzai Picón, Erik Alonso, Iraia Isasi, Ahamed Idris

EMBC (Annual International Conference of the IEEE Engineering in Medicine and Biology Society) 2019

C7 *Using the Thoracic Impedance to Predict Measures From Invasive Arterial Blood Pressure in Out-Of-Hospital Cardiac Arrest.*
Andoni Elola, Elisabete Aramendi, Unai Irusta, Per Olav Berve, Fredrik Arnwald, Lars Wik, Fred Chapman
AHA ReSS (American Heart Association's Resuscitation Science Symposium) 2019

C8 *Machine Learning Techniques to Predict Cardiac Re-Arrest in Out-Of-Hospital Setting.*
Andoni Elola, Elisabete Aramendi, Unai Irusta, Naroa Amezaga, Jon Urteaga, Pamela Owens, Ahamed Idris
AHA ReSS (American Heart Association's Resuscitation Science Symposium) 2019

C9 *Automated Detection of Patients with Return of Spontaneous Circulation in the Retrospective Analysis of Resuscitation Episodes.*
Andoni Elola, Elisabete Aramendi, Unai Irusta, Henry Wang, Ahamed Idris
AHA ReSS (American Heart Association's Resuscitation Science Symposium) 2020

5.4 Etorkizuneko ikerketa-lerroak

Tesi honetan zehar gaixoaren egoera hemodinamikoaren monitorizazioa lantzen da eta hainbat aurrerapauso ematen dira. Hala ere, galdera berriak sortu dira, etorkizunean erantzuna beharko dutenak:

- Ikasketa sakonean oinarritutako algoritmoek gaitasuna dutela frogatu da PGAE eta PE erritmoak bereizteko EKG seinalea edo BI seinalea erabiliz [3, 122]. Hala ere, bi seinaleak batera ez dira frogatu PGAE eta PE diskriminatzeko, edo are eta gehiago, BPGAE, SPGAE eta PE diskriminatzeko.
- Frogatu den moduan, egunerokotasunean OKBBGan zehar jasotzen diren seinaleak erabiliz posiblea da PGAE egoera desberdinak bereiztea. Odol-presioaren seinalea erabiliz

gauzatu dira esperimentu horiek, baina beste anotazio-iturri batzuk erabiliz emaitzak konprobatu behar dira.

- Tesi honetan garatutako algoritmo guztiek sakaden etenaldietan egiten dute lan. Etenaldi horiek minimizatzeko asmoz, soroslea sakadak ematen ari den bitartean funtzionatzen duten algoritmoen garapena beharrezkoa da. Erronka handiagoa da hori, sakadek artefakto handiak sortzen baitituzte EKG eta BI seinaleetan.
- EKG seinalea erabiliz neurri batean RA aurresan daitekeela frogatu da. Hala ere, seinale gehiago erabiliz (BI edo kapnografia, adibidez) emaitza horiek hobetu daitezke. Gainera, datu gehiagorekin ikasketa sakonean oinarritutako algoritmoak garatzea posiblea da, agian emaitzak are eta gehiago hobetuz.

BIBLIOGRAFIA

[1] M. Risdal, S. O. Aase, J. Kramer-Johansen, and T. Eftesol, "Automatic identification of return of spontaneous circulation during cardiopulmonary resuscitation," *IEEE Transactions on Biomedical Engineering*, vol. 55, no. 1, pp. 60–68, 2007.

[2] A. Elola, E. Aramendi, U. Irusta, J. Del Ser, E. Alonso, and M. Daya, "ECG-based pulse detection during cardiac arrest using random forest classifier," *Medical & biological engineering & computing*, vol. 57, no. 2, pp. 453–462, 2019.

[3] A. Elola, E. Aramendi, U. Irusta, A. Picón, E. Alonso, P. Owens *et al.*, "Deep neural networks for ECG-based pulse detection during out-of-hospital cardiac arrest," *Entropy*, vol. 21, no. 3, p. 305, 2019.

[4] A. Elola, E. Aramendi, U. Irusta, E. Alonso, Y. Lu, M. P. Chang *et al.*, "Capnography: A support tool for the detection of return of spontaneous circulation in out-of-hospital cardiac arrest," *Resuscitation*, vol. 142, pp. 153–161, 2019.

[5] A. Elola, E. Aramendi, U. Irusta, P. O. Berve, and L. Wik, "Multimodal algorithms for the classification of circulation states during out-of-hospital cardiac arrest," *IEEE Transactions on Biomedical Engineering*, 2020.

[6] A. Elola, E. Aramendi, E. Rueda, U. Irusta, H. Wang, and A. Idris, "Towards the prediction of rearrest during out-of-hospital cardiac arrest," *Entropy*, vol. 22, no. 7, p. 758, 2020.

[7] E. Alonso, E. Aramendi, M. Daya, U. Irusta, B. Chicote, J. K. Russell *et al.*, "Circulation detection using the electrocardiogram and the thoracic impedance acquired by defibrillation pads," *Resuscitation*, vol. 99, pp. 56–62, 2016.

[8] E. Aramendi, A. Elola, E. Alonso, U. Irusta, M. Daya, J. K. Russell *et al.*, "Feasibility of the capnogram to monitor ventilation rate during cardiopulmonary resuscitation," *Resuscitation*, vol. 110, pp. 162–168, 2017.

[9] R. Cummins, D. Chamberlain, N. Abramson, M. Allen, P. Baskett, L. Becker *et al.*, "A statement for health professionals from a task force of the american heart association, the european resuscitation council, the heart and stroke foundation of canada, and the australian resuscitation council. Recommended guidelines for uniform reporting of data from out-of-hospital cardiac arrest: the utstein style," *Circulation*, vol. 84, no. 2, pp. 960–975, 1991.

[10] Z.-J. Zheng, J. B. Croft, W. H. Giles, and G. A. Mensah, "Sudden cardiac death in the united states, 1989 to 1998," *Circulation*, vol. 104, no. 18, pp. 2158–2163, 2001.

[11] D. P. Zipes and H. J. Wellens, "Sudden cardiac death," in *Professor Hein JJ Wellens*. Springer, 2000, pp. 621–645.

[12] S. S. Chugh, J. Jui, K. Gunson, E. C. Stecker, B. T. John, B. Thompson *et al.*, "Current burden of sudden cardiac death: multiple source surveillance versus retrospective death certificate-based review in a large us community," *Journal of the American College of Cardiology*, vol. 44, no. 6, pp. 1268–1275, 2004.

[13] J. J. de Vreede-Swagemakers, A. P. Gorgels, W. I. Dubois-Arbouw, J. W. Van Ree, M. J. Daemen, L. G. Houben *et al.*, "Out-of-hospital cardiac arrest in the 1990s: a population-based study in the Maastricht area on incidence, characteristics and survival," *Journal of the American College of Cardiology*, vol. 30, no. 6, pp. 1500–1505, 1997.

[14] S. S. Chugh, K. Reinier, C. Teodorescu, A. Evanado, E. Kehr, M. Al Samara *et al.*, "Epidemiology of sudden cardiac death: clinical and research implications," *Progress in cardiovascular diseases*, vol. 51, no. 3, pp. 213–228, 2008.

[15] M. Luu, W. G. Stevenson, L. W. Stevenson, K. Baron, and J. Walden, "Diverse mechanisms of unexpected cardiac arrest in advanced heart failure." *Circulation*, vol. 80, no. 6, pp. 1675–1680, 1989.

[16] L. A. Cobb, C. E. Fahrenbruch, M. Olsufka, and M. K. Copass, "Changing incidence of out-of-hospital ventricular fibrillation, 1980-2000," *Jama*, vol. 288, no. 23, pp. 3008–3013, 2002.

[17] C. Atwood, M. S. Eisenberg, J. Herlitz, and T. D. Rea, "Incidence of EMS-treated out-of-hospital cardiac arrest in europe," *Resuscitation*,

vol. 67, no. 1, pp. 75–80, 2005.

[18] S. Sans, H. Kesteloot, D. o. Kromhout, and T. Force, “The burden of cardiovascular diseases mortality in europe: Task force of the european society of cardiology on cardiovascular mortality and morbidity statistics in europe,” *European heart journal*, vol. 18, no. 8, pp. 1231–1248, 1997.

[19] J.-A. Álvarez-Fernández and R. J. Gazmuri, “Mortalidad evitable por parada cardíaca extrahospitalaria,” *Medicina Clínica*, vol. 130, no. 18, pp. 710–714, 2008.

[20] J. Cosin, “Muerte súbita extrahospitalaria en España,” in *Muerte súbita cardíaca*. Doyma Barcelona, 1991, pp. 13–21.

[21] K. Ibarguren, J. M. Unanue, D. Alonso, I. Vaqueriza, U. Irusta, E. Aramendi *et al.*, “Difference in survival from pre-hospital cardiac arrest between cities and villages in the Basque Autonomous Community,” *Resuscitation*, vol. 96, p. 114, 2015.

[22] E. J. Benjamin, S. S. Virani, C. W. Callaway, A. M. Chamberlain, A. R. Chang, S. Cheng *et al.*, “Heart disease and stroke statistics—2018 update: a report from the american heart association,” *Circulation*, 2018.

[23] G. D. Perkins, A. J. Handley, R. W. Koster, M. Castrén, M. A. Smyth, T. Olasveengen *et al.*, “European resuscitation council guidelines for resuscitation 2015: Section 2. adult basic life support and automated external defibrillation,” *Resuscitation*, vol. 95, pp. 81–99, 2015.

[24] J. Soar, J. P. Nolan, B. W. Böttiger, G. D. Perkins, C. Lott, P. Carli *et al.*, “European resuscitation council guidelines for resuscitation 2015: Section 3. adult advanced life support,” *Resuscitation*, vol. 95, pp. 100–147, 2015.

[25] J. Kramer-Johansen, D. P. Edelson, H. Losert, K. Köhler, and B. S. Abella, “Uniform reporting of measured quality of cardiopulmonary resuscitation (CPR),” *Resuscitation*, vol. 74, no. 3, pp. 406–417, 2007.

[26] R. O. Cummins, J. P. Ornato, W. H. Thies, and P. E. Pepe, “Improving survival from sudden cardiac arrest: the"chain of survival"concept.” *Circulation*, vol. 83, no. 5, pp. 1832–1847, 1991.

[27] A. J. Handley, R. Koster, K. Monsieurs, G. D. Perkins, S. Davies, and L. Bossaert, “European resuscitation council guidelines for resuscitation 2005: Section 2. adult basic life support and use of automated external defibrillators,” *Resuscitation*, vol. 67, pp. S7–S23, 2005.

[28] C. Sasson, M. A. Rogers, J. Dahl, and A. L. Kellermann, "Predictors of survival from out-of-hospital cardiac arrest: a systematic review and meta-analysis," *Circulation: Cardiovascular Quality and Outcomes*, vol. 3, no. 1, pp. 63–81, 2010.

[29] R. M. Sutton, B. French, A.Ñishisaki, D. E. Niles, M. R. Maltese, L. Boyle *et al.*, "American heart association cardiopulmonary resuscitation quality targets are associated with improved arterial blood pressure during pediatric cardiac arrest," *Resuscitation*, vol. 84, no. 2, pp. 168–172, 2013.

[30] J. Herlitz, L. Svensson, S. Holmberg, K.-A. Ängquist, and M. Young, "Efficacy of bystander CPR: intervention by lay people and by health care professionals," *Resuscitation*, vol. 66, no. 3, pp. 291–295, 2005.

[31] M. Holmberg, S. Holmberg, and J. Herlitz, "Effect of bystander cardiopulmonary resuscitation in out-of-hospital cardiac arrest patients in sweden," *Resuscitation*, vol. 47, no. 1, pp. 59–70, 2000.

[32] M. L. Selby, J. A. Kautz, T. J. Moore, W. R. Gombeski Jr, A. G. Ramirez, E. J. Farge *et al.*, "Indicators of response to a mass media CPR recruitment campaign." *American journal of public health*, vol. 72, no. 9, pp. 1039–1042, 1982.

[33] M. S. Eisenberg, L. Bergner, and A. Hallstrom, "Cardiac resuscitation in the community: importance of rapid provision and implications for program planning," *Jama*, vol. 241, no. 18, pp. 1905–1907, 1979.

[34] T. D. Valenzuela, D. J. Roe, G.Ñichol, L. L. Clark, D. W. Spaite, and R. G. Hardman, "Outcomes of rapid defibrillation by security officers after cardiac arrest in casinos," *New England Journal of Medicine*, vol. 343, no. 17, pp. 1206–1209, 2000.

[35] R. D. White, T. J. Bunch, and D. G. Hankins, "Evolution of a community-wide early defibrillation programme: experience over 13 years using police/fire personnel and paramedics as responders," *Resuscitation*, vol. 65, no. 3, pp. 279–283, 2005.

[36] M. L. Weisfeldt, R. E. Kerber, R. P. McGoldrick, A. J. Moss, G.Ñichol, J. P. Ornato *et al.*, "Public access defibrillation: a statement for healthcare professionals from the american heart association task force on automatic external defibrillation," *Circulation*, vol. 92, no. 9, pp. 2763–2763, 1995.

[37] P. S. Chan, H. M. Krumholz, G.Ñichol, B. K. Nallamothu, and A. H. A. N. R. of Cardiopulmonary Resuscitation Investigators, "Delayed time to defibrillation after in-hospital cardiac arrest," *New England*

Journal of Medicine, vol. 358, no. 1, pp. 9–17, 2008.

[38] T. D. Valenzuela, D. J. Roe, S. Cretin, D. W. Spaite, and M. P. Larsen, "Estimating effectiveness of cardiac arrest interventions: a logistic regression survival model," *Circulation*, vol. 96, no. 10, pp. 3308–3313, 1997.

[39] K. Sunde, M. Pytte, D. Jacobsen, A. Mangschau, L. P. Jensen, C. Smedsrud *et al.*, "Implementation of a standardised treatment protocol for post resuscitation care after out-of-hospital cardiac arrest," *Resuscitation*, vol. 73, no. 1, pp. 29–39, 2007.

[40] J. P. Nolan, J. Soar, A. Cariou, T. Cronberg, V. R. Moulaert, C. D. Deakin *et al.*, "European resuscitation council and european society of intensive care medicine guidelines for post-resuscitation care 2015: Section 5 of the european resuscitation council guidelines for resuscitation 2015," *Resuscitation*, vol. 95, pp. 202–222, 2015.

[41] W. Kubicek, D. Witsoe, R. Patterson, and A. From, "Development and evaluation of an impedance cardiographic system to measure cardiac output and other cardiac parameters," *Houston, National Aeronautics and Space Administration*, p. 468, 1969.

[42] S. Caffrey, "Feasibility of public access to defibrillation," *Current opinion in critical care*, vol. 8, no. 3, pp. 195–198, 2002.

[43] P. A. D. T. Investigators, "Public-access defibrillation and survival after out-of-hospital cardiac arrest," *New England Journal of Medicine*, vol. 351, no. 7, pp. 637–646, 2004.

[44] M. L. Weisfeldt, C. M. Sitlani, J. P. Ornato, T. Rea, T. P. Aufderheide, D. Davis *et al.*, "Survival after application of automatic external defibrillators before arrival of the emergency medical system: evaluation in the resuscitation outcomes consortium population of 21 million," *Journal of the American College of Cardiology*, vol. 55, no. 16, pp. 1713–1720, 2010.

[45] T. Kitamura, T. Iwami, T. Kawamura, K.Ñagao, H. Tanaka, and A. Hiraide, "Nationwide public-access defibrillation in japan," *New England Journal of Medicine*, vol. 362, no. 11, pp. 994–1004, 2010.

[46] C. Pantazopoulos, T. Xanthos, I. Pantazopoulos, A. Papalois, E. Kouskouni, and N. Iacovidou, "A review of carbon dioxide monitoring during adult cardiopulmonary resuscitation," *Heart, Lung and Circulation*, vol. 24, no. 11, pp. 1053–1061, 2015.

[47] J. L. Hamrick, J. T. Hamrick, J. K. Lee, B. H. Lee, R. C. Koehler, and D. H. Shaffner, "Efficacy of chest compressions directed by end-tidal

CO2 feedback in a pediatric resuscitation model of basic life support," *Journal of the American Heart Association*, vol. 3, no. 2, p. e000450, 2014.

[48] K. R. Sheak, D. J. Wiebe, M. Leary, S. Babaeizadeh, T. C. Yuen, D. Zive *et al.*, "Quantitative relationship between end-tidal carbon dioxide and CPR quality during both in-hospital and out-of-hospital cardiac arrest," *Resuscitation*, vol. 89, pp. 149–154, 2015.

[49] D. P. Edelson, J. Eilevstjønn, E. K. Weidman, E. Retzer, T. L. V. Hoek, and B. S. Abella, "Capnography and chest-wall impedance algorithms for ventilation detection during cardiopulmonary resuscitation," *Resuscitation*, vol. 81, no. 3, pp. 317–322, 2010.

[50] C. W. Callaway, J. Soar, M. Aibiki, B. W. Böttiger, S. C. Brooks, C. D. Deakin *et al.*, "Part 4: advanced life support: 2015 international consensus on cardiopulmonary resuscitation and emergency cardiovascular care science with treatment recommendations," *Circulation*, vol. 132, no. 16_suppl_1, pp. S84–S145, 2015.

[51] M. Kolar, M. Križmarić, P. Klemen, and Š. Grmec, "Partial pressure of end-tidal carbon dioxide successful predicts cardiopulmonary resuscitation in the field: a prospective observational study," *Critical care*, vol. 12, no. 5, p. R115, 2008.

[52] M. Pokorná, E.Ñečas, J. Kratochvíl, R. Skřipskỳ, M. Andrlík, and O. Franěk, "A sudden increase in partial pressure end-tidal carbon dioxide (PETCO2) at the moment of return of spontaneous circulation," *The Journal of emergency medicine*, vol. 38, no. 5, pp. 614–621, 2010.

[53] M. S. Bhende and A. E. Thompson, "Evaluation of an end-tidal CO2 detector during pediatric cardiopulmonary resuscitation," *Pediatrics*, vol. 95, no. 3, pp. 395–399, 1995.

[54] R. Sehra, K. Underwood, and P. Checchia, "End tidal CO2 is a quantitative measure of cardiac arrest," *Pacing and clinical electrophysiology*, vol. 26, no. 1p2, pp. 515–517, 2003.

[55] B. J. Bobrow, T. F. Vadeboncoeur, U. Stolz, A. E. Silver, J. M. Tobin, S. A. Crawford *et al.*, "The influence of scenario-based training and real-time audiovisual feedback on out-of-hospital cardiopulmonary resuscitation quality and survival from out-of-hospital cardiac arrest," *Annals of emergency medicine*, vol. 62, no. 1, pp. 47–56, 2013.

[56] U. Ayala, T. Eftestøl, E. Alonso, U. Irusta, E. Aramendi, S. Wali *et al.*, "Automatic detection of chest compressions for the assessment of CPR-quality parameters," *Resuscitation*, vol. 85, no. 7, pp. 957–963,

2014.

[57] R. O. Cummins, D. A. Chamberlain, N. S. Abramson, M. Allen, P. J. Baskett, L. Becker *et al.*, "Recommended guidelines for uniform reporting of data from out-of-hospital cardiac arrest: the Utstein Style," *Circulation*, vol. 84, no. 2, pp. 960–975, 1991.

[58] G. D. Perkins, I. G. Jacobs, V. M. Nadkarni, R. A. Berg, F. Bhanji, D. Biarent *et al.*, "Cardiac arrest and cardiopulmonary resuscitation outcome reports: update of the utstein resuscitation registry templates for out-of-hospital cardiac arrest," *Circulation*, vol. 132, no. 13, pp. 1286–1300, 2015.

[59] J. P. Nolan, R. A. Berg, L. W. Andersen, F. Bhanji, P. S. Chan, M. W. Donnino *et al.*, "Cardiac arrest and cardiopulmonary resuscitation outcome reports: update of the utstein resuscitation registry template for in-hospital cardiac arrest," *Circulation*, vol. 140, no. 18, pp. e746–e757, 2019.

[60] S. Viereck, T. P. Møller, A. K. Ersbøll, J. S. Bækgaard, A. Claesson, J. Hollenberg *et al.*, "Recognising out-of-hospital cardiac arrest during emergency calls increases bystander cardiopulmonary resuscitation and survival," *Resuscitation*, vol. 115, pp. 141–147, 2017.

[61] T. P. Møller, C. Andréll, S. Viereck, L. Todorova, H. Friberg, and F. K. Lippert, "Recognition of out-of-hospital cardiac arrest by medical dispatchers in emergency medical dispatch centres in two countries," *Resuscitation*, vol. 109, pp. 1–8, 2016.

[62] S. Y. Lee, Y. S. Ro, S. Do Shin, K. J. Song, K. J. Hong, J. H. Park *et al.*, "Recognition of out-of-hospital cardiac arrest during emergency calls and public awareness of cardiopulmonary resuscitation in communities: a multilevel analysis," *Resuscitation*, vol. 128, pp. 106–111, 2018.

[63] S.Ñ. Blomberg, F. Folke, A. K. Ersbøll, H. C. Christensen, C. Torp-Pedersen, M. R. Sayre *et al.*, "Machine learning as a supportive tool to recognize cardiac arrest in emergency calls," *Resuscitation*, vol. 138, pp. 322–329, 2019.

[64] B. Eberle, W. Dick, T. Schneider, G. Wisser, S. Doetsch, and I. Tzanova, "Checking the carotid pulse check: diagnostic accuracy of first responders in patients with and without a pulse," *Resuscitation*, vol. 33, no. 2, pp. 107–116, 1996.

[65] J. Bahr, H. Klingler, W. Panzer, H. Rode, and D. Kettler, "Skills of lay people in checking the carotid pulse," *Resuscitation*, vol. 35, no. 1, pp.

23–26, 1997.

[66] M. Liberman, A. Lavoie, D. Mulder, and J. Sampalis, "Cardiopulmonary resuscitation: errors made by pre-hospital emergency medical personnel," *Resuscitation*, vol. 42, no. 1, pp. 47–55, 1999.

[67] C. D. Deakin and J. L. Low, "Accuracy of the advanced trauma life support guidelines for predicting systolic blood pressure using carotid, femoral, and radial pulses: observational study," *Bmj*, vol. 321, no. 7262, pp. 673–674, 2000.

[68] P. Moule, "Checking the carotid pulse: diagnostic accuracy in students of the healthcare professions," *Resuscitation*, vol. 44, no. 3, pp. 195–201, 2000.

[69] W. F. Dick, B. Eberle, G. Wisser, and T. Schneider, "The carotid pulse check revisited: what if there is no pulse?" *Critical care medicine*, vol. 28, no. 11, pp. N183–N185, 2000.

[70] F. Lapostolle, P. Le Toumelin, J. M. Agostinucci, J. Catineau, and F. Adnet, "Basic cardiac life support providers checking the carotid pulse: performance, degree of conviction, and influencing factors," *Academic emergency medicine*, vol. 11, no. 8, pp. 878–880, 2004.

[71] J. Tibballs and P. Russell, "Reliability of pulse palpation by healthcare personnel to diagnose paediatric cardiac arrest," *Resuscitation*, vol. 80, no. 1, pp. 61–64, 2009.

[72] J. Tibballs and C. Weeranatna, "The influence of time on the accuracy of healthcare personnel to diagnose paediatric cardiac arrest by pulse palpation," *Resuscitation*, vol. 81, no. 6, pp. 671–675, 2010.

[73] M. Ruppert, M. W. Reith, J. H. Widmann, C. K. Lackner, R. Kerkmann, L. Schweiberer *et al.*, "Checking for breathing: evaluation of the diagnostic capability of emergency medical services personnel, physicians, medical students, and medical laypersons," *Annals of Emergency Medicine*, vol. 34, no. 6, pp. 720–729, 1999.

[74] J.Ñyman and M. Sihvonen, "Cardiopulmonary resuscitation skills in nurses and nursing students," *Resuscitation*, vol. 47, no. 2, pp. 179–184, 2000.

[75] D. Chamberlain, A. Smith, M. Woollard, M. Colquhoun, A. J. Handley, S. Leaves *et al.*, "Trials of teaching methods in basic life support (3): Comparison of simulated CPR performance after first training and at 6 months, with a note on the value of re-training," *Resuscitation*, vol. 53, no. 2, pp. 179–187, 2002.

[76] G. D. Perkins, B. Stephenson, J. Hulme, and K. G. Monsieurs, "Birmingham assessment of breathing study (BABS)," *Resuscitation*, vol. 64, no. 1, pp. 109–113, 2005.

[77] J. Breckwoldt, S. Schloesser, and H.-R. Arntz, "Perceptions of collapse and assessment of cardiac arrest by bystanders of out-of-hospital cardiac arrest (OOHCA)," *Resuscitation*, vol. 80, no. 10, pp. 1108–1113, 2009.

[78] E. C. Stecker, K. Reinier, A. Uy-Evanado, C. Teodorescu, H. Chugh, K. Gunson *et al.*, "Relationship between seizure episode and sudden cardiac arrest in patients with epilepsy: a community-based study," *Circulation: Arrhythmia and Electrophysiology*, vol. 6, no. 5, pp. 912–916, 2013.

[79] S. Zengin, H. Gümüşboğa, M. Sabak, Ş. H. Eren, G. Altunbas, and B. Al, "Comparison of manual pulse palpation, cardiac ultrasonography and doppler ultrasonography to check the pulse in cardiopulmonary arrest patients," *Resuscitation*, vol. 133, pp. 59–64, 2018.

[80] T. Aufderheide, N. Paradis, and H. Halperin, "Etiology, electrophysiology, and myocardial mechanics of pulseless electrical activity," *Cardiac arrest: the science and practice of resuscitation medicine*, vol. 22, p. 426, 2007.

[81] N. A. Paradis, G. B. Martin, M. G. Goetting, E. P. Rivers, M. Feingold, and R. M. Nowak, "Aortic pressure during human cardiac arrest: identification of pseudo-electromechanical dissociation," *Chest*, vol. 101, no. 1, pp. 123–128, 1992.

[82] G. Prosen, M. Križmarić, J. Završnik, and Š. Grmec, "Impact of modified treatment in echocardiographically confirmed pseudo-pulseless electrical activity in out-of-hospital cardiac arrest patients with constant end-tidal carbon dioxide pressure during compression pauses," *Journal of International Medical Research*, vol. 38, no. 4, pp. 1458–1467, 2010.

[83] R. J. Myerburg, H. Halperin, D. A. Egan, R. Boineau, S. S. Chugh, A. M. Gillis *et al.*, "Pulseless electric activity: definition, causes, mechanisms, management, and research priorities for the next decade: report from a national heart, lung, and blood institute workshop," *Circulation*, vol. 128, no. 23, pp. 2532–2541, 2013.

[84] U. A. P. Flato, E. F. Paiva, M. T. Carballo, A. M. Buehler, R. Marco, and A. Timerman, "Echocardiography for prognostication during the resuscitation of intensive care unit patients with non-shockable

rhythm cardiac arrest," *Resuscitation*, vol. 92, pp. 1–6, 2015.

[85] M. A. H. in't Veld, M. G. Allison, D. S. Bostick, K. R. Fisher, O. G. Goloubeva, M. D. Witting *et al.*, "Ultrasound use during cardiopulmonary resuscitation is associated with delays in chest compressions," *Resuscitation*, vol. 119, pp. 95–98, 2017.

[86] E. J. Clattenburg, P. Wroe, S. Brown, K. Gardner, L. Losonczy, A. Singh *et al.*, "Point-of-care ultrasound use in patients with cardiac arrest is associated prolonged cardiopulmonary resuscitation pauses: a prospective cohort study," *Resuscitation*, vol. 122, pp. 65–68, 2018.

[87] S. C. Brooks, N. Hassan, B. L. Bigham, and L. J. Morrison, "Mechanical versus manual chest compressions for cardiac arrest," *Cochrane database of systematic reviews*, no. 2, 2014.

[88] I. G. Jacobs, J. C. Finn, G. A. Jelinek, H. F. Oxer, and P. L. Thompson, "Effect of adrenaline on survival in out-of-hospital cardiac arrest: a randomised double-blind placebo-controlled trial," *Resuscitation*, vol. 82, no. 9, pp. 1138–1143, 2011.

[89] M. P. Chang, Y. Lu, B. Leroux, E. A. Ecenarro, P. Owens, H. E. Wang *et al.*, "Association of ventilation with outcomes from out-of-hospital cardiac arrest," *Resuscitation*, vol. 141, pp. 174–181, 2019.

[90] S. Sanchez, M. Miller, and S. Asha, "Assessing the validity of two-dimensional carotid ultrasound to detect the presence and absence of a pulse," *Resuscitation*, vol. 157, pp. 67–73, 2020.

[91] N. A. Cromie, J. D. Allen, C. Turner, J. M. Anderson, and A. A. J. Adgey, "The impedance cardiogram recorded through two electrocardiogram/defibrillator pads as a determinant of cardiac arrest during experimental studies*," *Critical Care Medicine*, vol. 36, no. 5, p. 1578, May 2008.

[92] R. W. Wijshoff, A. M. van Asten, W. H. Peeters, R. Bezemer, G. J. Noordergraaf, M. Mischi *et al.*, "Photoplethysmography-based algorithm for detection of cardiogenic output during cardiopulmonary resuscitation," *IEEE Transactions on Biomedical Engineering*, vol. 62, no. 3, pp. 909–921, 2014.

[93] E. Alonso, U. Irusta, E. Aramendi, and M. R. Daya, "A machine learning framework for pulse detection during out-of-hospital cardiac arrest," *IEEE Access*, vol. 8, pp. 161 031–161 041, 2020.

[94] C. F. Babbs, "We still need a real-time hemodynamic monitor for cpr," *Resuscitation*, 2013.

[95] E. Brooke Lerner, M. O'Connell, and R. G. Pirrallo, "Rearrest after prehospital resuscitation," *Prehospital Emergency Care*, vol. 15, no. 1, pp. 50–54, 2011.

[96] D. D. Salcido, M. L. Sundermann, A. C. Koller, and J. J. Menegazzi, "Incidence and outcomes of rearrest following out-of-hospital cardiac arrest," *Resuscitation*, vol. 86, pp. 19–24, 2015.

[97] D. D. Salcido, R. H. Schmicker, N. Kime, J. E. Buick, S. Cheskes, B. Grunau *et al.*, "Effects of intra-resuscitation antiarrhythmic administration on rearrest occurrence and intra-resuscitation ECG characteristics in the ROC ALPS trial," *Resuscitation*, vol. 129, pp. 6–12, 2018.

[98] A. Bhardwaj, D. J. Ikeda, A. V. Grossestreuer, K. R. Sheak, G. Delfin, T. Layden *et al.*, "Factors associated with re-arrest following initial resuscitation from cardiac arrest," *Resuscitation*, vol. 111, pp. 90–95, 2017.

[99] A. Vyas, P. S. Chan, P. Cram, B. K. Nallamothu, B. McNally, and S. Girotra, "Early coronary angiography and survival after out-of-hospital cardiac arrest," *Circulation: Cardiovascular Interventions*, vol. 8, no. 10, p. e002321, 2015.

[100] P. Johnston, Z. Imam, G. Dempsey, J. Anderson, and A. Adgey, "The transthoracic impedance cardiogram is a potential haemodynamic sensor for an automated external defibrillator," *European heart journal*, vol. 19, no. 12, pp. 1879–1888, 1998.

[101] H. Losert, M. Risdal, F. Sterz, J.Ñysæther, K. Köhler, T. Eftestøl *et al.*, "Thoracic-impedance changes measured via defibrillator pads can monitor signs of circulation," *Resuscitation*, vol. 73, no. 2, pp. 221–228, 2007.

[102] T. Kohama, S.Ñakamura, and H. Hoshino, "An efficient rr interval detection for ECG monitoring system," *IEICE Transactions on Information and Systems*, vol. 82, no. 10, pp. 1425–1432, 1999.

[103] N. A. Cromie, J. D. Allen, C.Ñavarro, C. Turner, J. M. Anderson, and A. A. J. Adgey, "Assessment of the impedance cardiogram recorded by an automated external defibrillator during clinical cardiac arrest," *Critical Care Medicine*, vol. 38, no. 2, pp. 510–517, 2010.

[104] J. Ruiz, E. Alonso, E. Aramendi, J. Kramer-Johansen, T. Eftestøl, U. Ayala *et al.*, "Reliable extraction of the circulation component in the thoracic impedance measured by defibrillation pads," *Resuscitation*, vol. 84, no. 10, pp. 1345–1352, 2013.

[105] J. M. Ruiz, S. R. de Gauna, D. M. González-Otero, P. Saiz, J. J. Gutiérrez, J. F. Veintemillas *et al.*, "Circulation assessment by automated external defibrillators during cardiopulmonary resuscitation," *Resuscitation*, vol. 128, pp. 158–163, 2018.

[106] A. R. Garnett, J. P. Ornato, E. R. Gonzalez, and E. B. Johnson, "End-tidal carbon dioxide monitoring during cardiopulmonary resuscitation," *JAMA*, vol. 257, no. 4, pp. 512–515, 1987.

[107] D. P. Davis, R. E. Sell, N. Wilkes, R. Sarno, R. D. Husa, E. M. Castillo *et al.*, "Electrical and mechanical recovery of cardiac function following out-of-hospital cardiac arrest," *Resuscitation*, vol. 84, no. 1, pp. 25–30, 2013.

[108] C. T. Lui, K. M. Poon, and K. L. Tsui, "Abrupt rise of end tidal carbon dioxide level was a specific but non-sensitive marker of return of spontaneous circulation in patient with out-of-hospital cardiac arrest," *Resuscitation*, vol. 104, pp. 53–58, 2016.

[109] P. Brinkrolf, M. Borowski, C. Metelmann, R.-P. Lukas, L. Pidde-Küllenberg, and A. Bohn, "Predicting ROSC in out-of-hospital cardiac arrest using expiratory carbon dioxide concentration: Is trend-detection instead of absolute threshold values the key?" *Resuscitation*, vol. 122, pp. 19–24, 2018.

[110] M. Blaivas and J. C. Fox, "Outcome in cardiac arrest patients found to have cardiac standstill on the bedside emergency department echocardiogram," *Academic Emergency Medicine*, vol. 8, no. 6, pp. 616–621, 2001.

[111] P. Salen, R. O'Connor, P. Sierzenski, B. Passarello, D. Pancu, S. Melanson *et al.*, "Can cardiac sonography and capnography be used independently and in combination to predict resuscitation outcomes?" *Academic Emergency Medicine*, vol. 8, no. 6, pp. 610–615, 2001.

[112] H. Cebicci, O. Salt, S. Gurbuz, S. Koyuncu, and O. Bol, "Benefit of cardiac sonography for estimating the early term survival of the cardiopulmonary arrest patients," *Hippokratia*, vol. 18, no. 2, p. 125, 2014.

[113] R. Gaspari, A. Weekes, S. Adhikari, V. E. Noble, J. T. Nomura, D. Theodoro *et al.*, "Emergency department point-of-care ultrasound in out-of-hospital and in-ed cardiac arrest," *Resuscitation*, vol. 109, pp. 33–39, 2016.

[114] P. Salen, L. Melniker, C. Chooljian, J. S. Rose, J. Alteveer, J. Reed *et al.*, "Does the presence or absence of sonographically identified cardiac

activity predict resuscitation outcomes of cardiac arrest patients?" *The American Journal of Emergency Medicine*, vol. 23, no. 4, pp. 459–462, 2005.

[115] F. Teran, A. J. Dean, C. Centeno, N. L. Panebianco, A. J. Zeidan, W. Chan *et al.*, "Evaluation of out-of-hospital cardiac arrest using transesophageal echocardiography in the emergency department," *Resuscitation*, vol. 137, pp. 140–147, 2019.

[116] J. H. Paxton and B. J. O'Neil, "When is PEA really ROSC?" *Resuscitation*, vol. 142, pp. 182–183, 2019.

[117] J. W. Waks, C. M. Sitlani, E. Z. Soliman, M. Kabir, E. Ghafoori, M. L. Biggs *et al.*, "Global electric heterogeneity risk score for prediction of sudden cardiac death in the general population: the atherosclerosis risk in communities (ARIC) and cardiovascular health (CHS) studies," *Circulation*, vol. 133, no. 23, pp. 2222–2234, 2016.

[118] J.-M. Kwon, Y. Lee, Y. Lee, S. Lee, and J. Park, "An algorithm based on deep learning for predicting in-hospital cardiac arrest," *Journal of the American Heart Association*, vol. 7, no. 13, p. e008678, 2018.

[119] D. Salcido, M. Sundermann, A. Koller, and J. Menegazzi, "Towards predicting the time and rhythm of rearrest after out-of-hospital cardiac arrest," *Resuscitation*, vol. 96, p. 10, 2015.

[120] A. Elola, E. Aramendi, U. Irusta, A. Picón, E. Alonso, P. Owens *et al.*, "Deep learning for pulse detection in out-of-hospital cardiac arrest using the ECG," in *2018 Computing in Cardiology Conference (CinC)*, vol. 45. IEEE, 2018, pp. 1–4.

[121] "Arquitecturas de aprendizaje profundo para la detección de pulso en la parada cardiaca extrahospitalaria utilizando el ECG, author=Elola Artano, Andoni and Aramendi Ecenarro, Elisabete and Irusta Zarandona, Unai and Picón Ruiz, Artzai and Alonso González, Erik, year=2018, publisher=Ediciones VISILAB."

[122] A. Elola, E. Aramendi, U. Irusta, A. Picón, E. Alonso, I. Isasi *et al.*, "Convolutional recurrent neural networks to characterize the circulation component in the thoracic impedance during out-of-hospital cardiac arrest," in *2019 41st Annual International Conference of the IEEE Engineering in Medicine and Biology Society (EMBC)*. IEEE, 2019, pp. 1921–1925.

[123] A. Elola, E. Aramendi, U. Irusta, P.-O. Berve, F. K. Arnwald, L. Wik *et al.*, "Using the thoracic impedance to predict measures from invasive arterial blood pressure in out-of-hospital cardiac arrest,"

vol. 140, no. Suppl_2. Am Heart Assoc, 2019, pp. A237–A237.

[124] A. Elola, E. Aramendi, U. Irusta, N. Amezaga, J. Urteaga, P. Owens *et al.*, "Machine learning techniques to predict cardiac re-arrest in out-of-hospital setting," *Circulation*, vol. 140, no. Suppl_2, pp. A127–A127, 2019.

[125] A. Elola Artano, E. Rueda Ballestero, N. Amezaga, E. Aramendi Ecenarro, and U. Irusta Zarandona, "Análisis de la variabilidad del ritmo cardiaco para la predicción de la parada cardiaca extrahospitalaria recurrente." Grupo de Técnicas Ópticas Aplicadas, Universidad de Cantabria, 2019.

[126] A. Elola, E. Aramendi, U. Irusta, H. E. Wang, and A. H. Idris, "Automated detection of patients with return of spontaneous circulation in the retrospective analysis of resuscitation episodes," *Circulation*, vol. 142, no. Suppl_4, pp. A308–A308, 2020.

[127] P. S. Hamilton and W. J. Tompkins, "Quantitative investigation of qrs detection rules using the mit/bih arrhythmia database," *IEEE transactions on biomedical engineering*, no. 12, pp. 1157–1165, 1986.

[128] A. Elola Artano, E. Aramendi Ecenarro, U. Irusta Zarandona, I. Álvarez Testillano, and E. Alonso González, "Potencial de la señal de capnografía para la detección de pulso durante la resucitación cardiopulmonar," 2018.

[129] A. Elola, E. Aramendi, U. Irusta, E. Alonso, P. Owens, M. Chang *et al.*, "ECG characteristics of pulseless electrical activity associated with return of spontaneous circulation in out-of-hospital cardiac arrest," vol. 130. Elsevier, 2018, p. e54.

[130] B. S. Abella, J. P. Alvarado, H. Myklebust, D. P. Edelson, A. Barry, N. O'Hearn *et al.*, "Quality of cardiopulmonary resuscitation during in-hospital cardiac arrest," *JAMA*, vol. 293, no. 3, pp. 305–310, Jan. 2005.

[131] A. D. McInnes, R. M. Sutton, A. Orioles, A.Ñishisaki, D.Ñiles, B. S. Abella *et al.*, "The first quantitative report of ventilation rate during in-hospital resuscitation of older children and adolescents," *Resuscitation*, vol. 82, no. 8, pp. 1025–1029, Aug. 2011.

[132] F. S. Stecher, J.-A. Olsen, R. E. Stickney, and L. Wik, "Transthoracic impedance used to evaluate performance of cardiopulmonary resuscitation during out of hospital cardiac arrest," *Resuscitation*, vol. 79, no. 3, pp. 432–437, Dec. 2008.

[133] T. P. Aufderheide, G. Sigurdsson, R. G. Pirrallo, D. Yannopoulos, S. McKnite, C. von Briesen *et al.*, "Hyperventilation-induced hypotension during cardiopulmonary resuscitation," *Circulation*, vol. 109, no. 16, pp. 1960–1965, Apr. 2004.

[134] T. P. Aufderheide and K. G. Lurie, "Death by hyperventilation: a common and life-threatening problem during cardiopulmonary resuscitation," *Critical Care Medicine*, vol. 32, no. 9 Suppl, pp. S345–351, Sep. 2004.

[135] S. O. Park, D. H. Shin, K. J. Baek, D. Y. Hong, E. J. Kim, S. C. Kim *et al.*, "A clinical observational study analysing the factors associated with hyperventilation during actual cardiopulmonary resuscitation in the emergency department," *Resuscitation*, vol. 84, no. 3, pp. 298–303, Mar. 2013.

[136] J. F. O'Neill and C. D. Deakin, "Do we hyperventilate cardiac arrest patients?" *Resuscitation*, vol. 73, no. 1, pp. 82–85, Apr. 2007.

[137] E. Alonso, J. Ruiz, E. Aramendi, D. González-Otero, S. R. de Gauna, U. Ayala *et al.*, "Reliability and accuracy of the thoracic impedance signal for measuring cardiopulmonary resuscitation quality metrics," *Resuscitation*, vol. 88, pp. 28–34, 2015.

[138] U. Irusta, J. Ruiz, E. Aramendi, S. R. de Gauna, U. Ayala, and E. Alonso, "A high-temporal resolution algorithm to discriminate shockable from nonshockable rhythms in adults and children," *Resuscitation*, vol. 83, no. 9, pp. 1090–1097, 2012.

A | ARGITARATUTAKO EDO ONARTUTAKO LANAK

A.1 Lehenengo helburuari lotutako argitalpenak

A.1.1 Lehenengo helburuari lotutako aurreneko argitalpena nazioarteko aldizkarian

A.1. Taula. Lehenengo helburuari lotutako aurreneko argitalpena nazioarteko aldizkarian.

	Argitalpena nazioarteko aldizkarian
Erreferentzia	Andoni Elola, Elisabete Aramendi, Unai Irusta, Javier Del Ser, Erik Alonso, Mohamud Daya, "ECG-based pulse detection during cardiac arrest using random forest classifier", *Medical & Biological Engineering and Computing 2018*, vol.57, pp. 453-462.
Kalitate adierazleak	• **Argitalpen mota**: JCRen indexatutako aldizkari artikulua • **Kuartila**: Q2 (23/59) (*Web of Science* 2018) • **Inpaktu faktorea**: 2.039

Medical & Biological Engineering & Computing (2019) 57:453–462
https://doi.org/10.1007/s11517-018-1892-2

ORIGINAL ARTICLE

ECG-based pulse detection during cardiac arrest using random forest classifier

Andoni Elola[1] · Elisabete Aramendi[1] · Unai Irusta[1] · Javier Del Ser[1,2,3] · Erik Alonso[4] · Mohamud Daya[5]

Received: 28 May 2018 / Accepted: 29 August 2018 / Published online: 13 September 2018

Abstract

Sudden cardiac arrest is one of the leading causes of death in the industrialized world. Pulse detection is essential for the recognition of the arrest and the recognition of return of spontaneous circulation during therapy, and it is therefore crucial for the survival of the patient. This paper introduces the first method based exclusively on the ECG for the automatic detection of pulse during cardiopulmonary resuscitation. Random forest classifier is used to efficiently combine up to nine features from the time, frequency, slope, and regularity analysis of the ECG. Data from 191 cardiac arrest patients was used, and 1177 ECG segments were processed, 796 with pulse and 381 without pulse. A leave-one-patient out cross validation approach was used to train and test the algorithm. The statistical distributions of sensitivity (SE) and specificity (SP) for pulse detection were estimated using 500 patient-wise bootstrap partitions. The mean (std) SE/SP for nine-feature classifier was 88.4 (1.8) %/89.7 (1.4) %, respectively. The designed algorithm only requires 4-s-long ECG segments and could be integrated in any commercial automated external defibrillator. The method permits to detect the presence of pulse accurately, minimizing interruptions in cardiopulmonary resuscitation therapy, and could contribute to improve survival from cardiac arrest.

Keywords Pulse detection · Cardiac arrest · Random forest · Pulseless electrical activity · Pulsed rhythm

1 Introduction

Early intervention is key for the survival of out-of-hospital cardiac arrest (OHCA) patients. Survival rates decrease by 7–10% every minute defibrillation is delayed [19], although the decrease can be ameliorated if cardiopulmonary resuscitation (CPR) is provided [34]. The automated external defibrillator (AED) has universalized access to electrical therapy in OHCA scenarios. Besides therapy, two key factors can contribute to improve survival: recognition of the arrest (absence of pulse) and recognition of return of spontaneous circulation (effective pulse) during therapy [30, 37]. Both factors require efficient methods to detect pulse in the arrested patient.

The defibrillation therapy is combined with cardiopulmonary resuscitation treatment, based on chest compressions and ventilations, to treat a patient in OHCA. As a response, the patient will transient through different cardiac rhythms, evolving from rhythms with no perfusion to the return of spontaneous circulation in a successful outcome. In hemodynamically stable patients beats are effective and associated with a perfusing rhythm. In contrast, the main challenge of detecting pulse during cardiopulmonary resuscitation relies on discriminating organized ECG with pulsed rhythm (PR) from organized ECG with electrical function dissociated from the mechanical function. In the latter, the cardiac contractions may not be effective for adequate blood pumping and no clinical pulse is palpable, which is classified as pulseless electrical activity (PEA).

Electronic supplementary material The online version of this article (https://doi.org/10.1007/s11517-018-1892-2) contains supplementary material, which is available to authorized users.

✉ Andoni Elola
andoni.elola@ehu.eus

1 Communications Engineering Department, University of the Basque Country UPV/EHU, Alameda Urquijo S/N, 48013, Bilbao, Spain

2 OPTIMA (Optimization, Modeling and Analytics) Research Area, TECNALIA, Parque Tecnologico, Edificio 700, 48160, Derio, Spain

3 Data Science Group, Basque Center for Applied Mathematics (BCAM), Alameda de Mazarredo 14, 48009 Bilbao, Spain

4 Department of Applied Mathematics, University of the Basque Country UPV/EHU, Rafael Moreno “Pitxitxi”, 3 48013 Bilbao, Spain

5 Department of Emergency Medicine, Oregon Health & Science University, Portland, OR, 97239-3098 USA

The latest Resuscitation Guidelines of the European Resuscitation Council stress the need of accurate pulse detection methods in the context of cardiac arrest to improve survival rates [32]. Pulse detection remains a challenge for both lay rescuers and healthcare professionals [10, 23, 33], and although many studies recently published in reputed scientific journals addressed automatic solutions [1, 6, 28, 35, 36], pulse detection during cardiac arrest is still a truly unsolved problem [3]. When advanced monitoring is feasible, other signals such as capnography, pulsioximetry, or even cerebral oximetry can be used to effectively detect pulse. The AED, which is designed to be used by non-clinical staff, only records the ECG and the thoracic impedance signals acquired by the defibrillation pads. Conceiving a method that can detect pulse once the AED has detected the presence of a rhythm with QRS complexes would permit introducing pulse detection functionally in AEDs.

Methods based on the processing of the ECG signal acquired by the defibrillation pads of AEDs have been used to design shock advice algorithms [12, 16], classify cardiac arrest rhythms [26], predict rhythm transitions [2], or predict shock outcome [7, 22]. Nevertheless, cardiac arrest rhythms are far from the typical rhythms of hemodynamically stable subjects; rapid rhythm transitions, aberrant QRS complexes, and non stationary signals are characteristic of cardiac arrest rhythms with discernible QRS complexes. All those aspects make very challenging a proper characterization of the ECG during cardiac arrest for automatic decision algorithms.

Most computer methods for pulse detection during cardiac arrest are based on information derived from the thoracic impedance, because effective heartbeats produce measurable fluctuations in the impedance waveform [25]. In fact, Losert et al. defined a set of nine characteristic impedance features and combined them in a neural network classifier to detect effective circulation [20]. Cromie et al. and Navarro et al. used spectral analysis of the derivative of the impedance to recognize cardiac arrest in animals [9] and humans [8, 21]. The first pulse detection method to apply ECG-based QRS detection to extract ECG and impedance features was described by Risdal et al. and used neural networks in the classification stage [28]. Ruiz et al. and Alonso et al. followed on this idea and developed adaptive filters to estimate the circulatory component in the impedance using QRS detections from the ECG [1, 31], and Alonso et al. designed a full ECG- and impedance-based pulse detector using a logistic regression classifier [1].

Unfortunately, for many AEDs, the integration of such algorithms is unfeasible. Currently, most AEDs only measure the impedance at well-defined instants to ensure the defibrillation pads are well attached and to adjust the energy of the defibrillation discharge. The circulatory component in the impedance has very small amplitudes (less than 100 mΩ) [1], and its characterization requires high amplitude resolutions and continuous recordings with sampling frequencies above 20 Hz. These characteristics are not present in the impedance circuitry of most current AEDs. Although some computer methods use a combination of ECG and impedance to detect pulse [1, 28], the potential of an ECG-only solution is still unexplored. Since ECG recording is a prerequisite for rhythm analysis, availability of such a solution would mean that computer-based pulse detection could be incorporated to any AED.

In this paper, we propose a pulse detector based exclusively on the ECG, for universal use in AEDs. New ECG features for pulse detection are implemented, in combination with features proposed by other authors. All features are then fed to a state-of-the-art random forest (RF) classifier to obtain an accurate pulse detection method.

2 Methods

2.1 Data materials

The dataset used in this study was a subset of a large OHCA registry maintained by the Tualatin Valley Fire & Rescue (Tigard, OR, USA). Biomedical signals were recorded from patients in OHCA using the Philips HeartStart MRx monitor/defibrillator. The digitized ECG was acquired with a sampling frequency of $f_s = 250$ Hz, with a resolution of 1.03 µV per least significant bit, and a bandwidth of 0–50 Hz. ECG segments corresponding to organized rhythms, free of artefacts, and with a minimum duration of 5 s were extracted from the original episodes. Three expert reviewers made the extraction and labeled the segments as PEA or PR with an inter-rater agreement, Kappa score, of $\kappa = 0.92$. The annotation criteria were based on the capnogram and on extensive clinical information available from pre-hospital records. Further details on the annotation process and the criteria can be found in Alonso et al. [1]. A total of 191 OHCA patients were included and 1177 ECG segments were extracted, 381 PEA with a median (IQR, inter-quartile range) duration of 9.6 (7.0–13.6) s and 796 PR with a median duration of 7.9 (6.4–10.9) s. In this study, we only considered the first 4 s of those segments. Figure 1 shows two characteristic PEA and PR examples, and as observed in the figure, heart rates are higher in PR and QRS complexes are wider and more aberrant in PEA.

2.2 Signal processing and feature extraction

ECG signal segments were processed to extract D classification features, resulting in a binary-labeled dataset $\{\mathbf{V}_k, y_k\}_{k=1}^{K}$, with $\mathbf{V}_k = [v_{1k}, v_{2k}, \ldots, v_{Dk}]$ the feature vector of the kth ECG segment, and y_k={PEA:0, PR:1} its

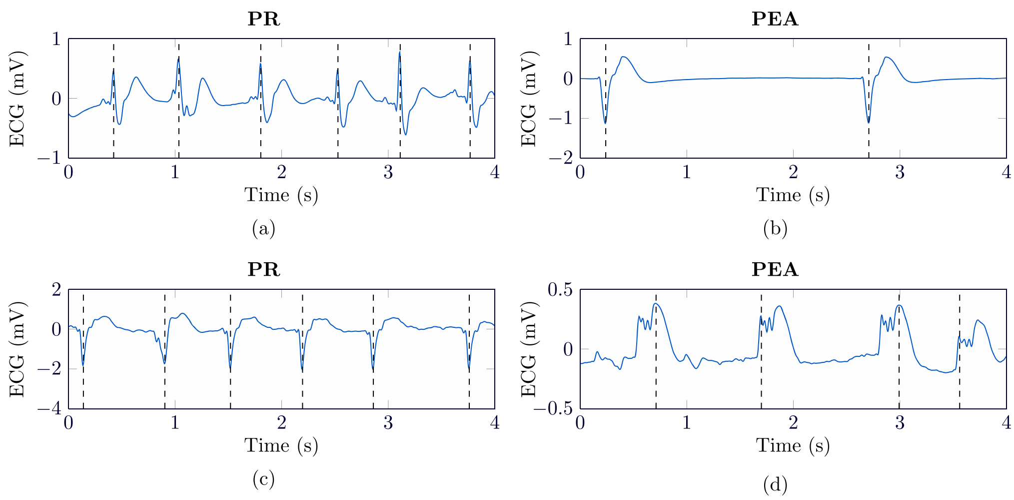

Fig. 1 Examples of ECG segments used in the study. PR segments (left) have higher rates and narrower QRS complexes than PEA segments (right). Black dashed lines depict automatically detected R instants

binary label, K is the number of ECG segments in the dataset. In this paper, the ECG is denoted by $x[n]$ and N is its length in samples. The time instants of the jth QRS complex of the segment are denoted as q_j (onset), r_j (peak), and s_j (offset).

The ECG segments were processed with a typical AED bandpass filter (0.5–30 Hz) to remove baseline oscillations and high-frequency noise. This bandwidth reproduces the effect of the defibrillation pads used to acquire the ECG, which have much larger surfaces (around 100 cm^2) than standard ECG leads. Although restrictive, the use of such ECG bandwidths is inevitable in AEDs and still permits the development of very accurate diagnostic algorithms, as it has been widely reported [1, 12, 27, 28]. For the detection of QRS complexes, an algorithm based on a peak detector was used, inspired by the detector proposed by Hamilton and Tompinks [14]. First, the squared first difference of the signal was computed as follows:

$$d_1[n] = (x[n] - x[n-1])^2, \tag{1}$$

and then $d_2[n]$ was obtained by filtering $d_1[n]$ with a moving averaging filter of 125 ms. Peaks were detected on $d_2[n]$ using an amplitude threshold and a refractory period of 300 ms. The amplitude threshold was set to 50% of the 98th amplitude percentile of the 4-s ECG segment. Each r_j was located at the highest/lowest peak near to the marks. For the detection of the onset and offset instants of each QRS complex, a threshold-based detector was used in slope and amplitude. Detected R instants are depicted in Fig. 1 with black dashed lines.

The features proposed to discriminate PEA from PR quantify heart rate, amplitude, and QRS complex characteristics distinctive of effective heartbeats. Features were grouped into those derived from detected QRS complexes, the slope domain, the spectral analysis, and the complexity of the ECG. Visualization of the intermediate signals and the behavior of each feature can be found in Supplementary Materials.

QRS-based features

The first three features, $[v_1–v_3]$, were computed on the basis of the detected QRS instants. Features v_1 and v_3 quantify the rates and amplitudes, which are higher and more stable in PRs, because they correspond to a later dynamic state in the transition to return of spontaneous circulation. Feature v_2 is associated with the duration and morphology of QRS complexes and is larger in PEA since PEA presents more aberrant QRS complexes [24]. For each ECG segment, inter-beat intervals were computed as $rr_j = r_{j+1} - r_j$ for $j = 1, .., L - 1$, where L is the number of QRS complexes detected in the segment. The first feature was:

$$v_1(\mathrm{s}) = \overline{rr_j}, \tag{2}$$

where $\overline{rr_j}$ stands for the mean rr interval.

Risdal et al. [28] proposed the signal length (sl) based on the real cepstrum of the QRS complex for PEA/PR classification based on QRS morphology. We modified Risdal et al.'s method and computed the real cepstrum of beat j in a 0.3-s interval centered around the r_j instant, and then normalized it by the maximum ECG excursion in the interval. The normalized cepstrum $C_j[n]$ was then used to compute the signal length of beat j, feature v_2, as follows:

$$sl_j = \frac{\sum_n w[n] \cdot C_j^2[n]}{\sum_n C_j^2[n]}, \tag{3}$$

$$v_2 = \widetilde{sl_j}, \tag{4}$$

where $\widetilde{sl_j}$ stands for the median of sl_j, and $w[n]$ is a non-decreasing weighting function in the shape of a Tuckey window.

Feature v_3 was the median amplitude of the QRS complexes (A_j) in the Q-S interval, normalized by QRS complex duration ($qs_j = s_j - q_j$):

$$A_j = \frac{\max\{x[n]\} - \min\{x[n]\}}{qs_j}, \quad q_j < n \cdot T_s < s_j, \quad (5)$$

$$v_3\left(\frac{\text{mV}}{\text{s}}\right) = \widetilde{A}_j, \quad (6)$$

where $T_s = 1/f_s$.

Slope domain features

Larger slopes in the ECG are associated with shorter and better conduction pathways characteristic of PR. PEA is frequently associated with dysfunctional conduction, which produces wider and more aberrant QRS complexes, and therefore smaller slopes. Features v_4–v_6 were computed based on the first difference of the signal ($x_\Delta[n] = x[n] - x[n-1]$) and $d_2[n]$ (obtained for QRS detection). Features v_4 and v_5 were the mean and standard deviation of $|x_\Delta[n]|$, respectively. The last feature of the slope domain was the kurtosis of $d_2[n]$, v_6.

Spectral features

Spectral features quantify how energy is distributed in the harmonic components of the heart rate. The waveform of PR is linked to higher rates and more periodic signals (more harmonics) in contrast to slower, more aberrant and irregular waveform typical in PEA. Feature v_7 was the amplitude spectrum area (AMSA), the sum of the spectral amplitudes of the ECG weighted by their frequency [29]. AMSA was computed as described in [29] based on the spectral amplitudes $A_i(f_i)$ at frequency f_i using a $N_F = 4096$ point FFT of the Tuckey windowed ECG segment:

$$v_7(\text{mV} \cdot \text{Hz}) = \sum_i A_i \cdot f_i, \quad 2 < f_i(\text{Hz}) < 30. \quad (7)$$

Feature v_8 was the energy of the ECG segment at frequencies higher than 17.5 Hz, in line with Jekova et al. [17] that limits the bandwidth for organized rhythms:

$$v_8(\text{mV}^2 \cdot \text{Hz}) = \frac{f_s}{2N_F} \sum_i A_i^2, \quad 17.5 < f_i < 30. \quad (8)$$

Measure of signal regularity

Fuzzy entropy (FuzzEn), v_9, as defined in [7] was proposed to quantify the regularity of the signal. When applied to our data, it shows lower values for PEA indicating a more predictable waveform. This is caused by the very low rates of PEA with very long intervals with isoelectric content between beats. PR have more beats and much less isoelectric content presenting a less predictable waveform and larger values of FuzzEn. To compute v_9, the ECG was resampled to 100 Hz and $m = 2$ was used, with an exponential function of width $r = 1$ and gradient $n = 0.1$.

2.3 RF classifier

Features were fed to a RF classifier, because these classifiers present good accuracy, controlled output variance, and low probability to overfit [5]. The learning method relies on the *bagging* concept, by which T weak learners (in this case, decision trees) are trained over subsets drawn with replacement from the training set and their outputs voted to produce a predictive estimate of the model. This procedure has been shown to decrease the variance of the model without increasing its bias, as the weak tree learners are fed with different training sets that consequently decorrelate their structure and provide diversity to the ensemble. A T-sized random forest model is grown as follows:

1. For every tree $t \in \{1, \ldots, T\}$, a bootstrap of M' instances is drawn uniformly at random with replacement from the original set of M training instances. These instances will constitute the training set for growing tree t. In this study, $M' = 2/3M$ and $T = 150$ were used.
2. During training, only $D' < D$ features are considered at each node of every tree. The best split at the node is decided using $D' = \lfloor\sqrt{D}\rfloor$ features selected at random from the D available features [13].
3. Every new test instance (ECG segment) is run down all T trees of the forest producing T predictions for the test instance. The RF classifier aggregates those predictions through voting to produce the classifier's prediction.

A byproduct of training RF ensembles is $w(d) \in [0, 1]$, a quantitative measure of the relative predictive *importance* of feature d. To compute the importance of feature d, the values of the feature are permuted among the training data, and the average variation of the out of bag error is computed. If the errors are large, the feature is important for classification. The process is repeated for all features, and $w(d)$ is obtained normalizing by the largest average variation to produce $0 < w(d) \leq 1$. In this work, $w(d)$ was used to rank and select features.

2.4 Statistical analysis and performance metrics

The RF classifier was evaluated in terms of typical measures for two class problems: sensitivity (Se; for PR), specificity (Sp; for PEA), accuracy (Acc), and positive and negative predictive values (PPV and NPV, respectively). A leave-one-patient out cross validation (LOPOCV) procedure was used to obtain the predicted labels for each patient. The statistical distributions of the performance metrics were

Table 1 Median values (25–75 percentiles) of every feature for the PEA and PR segments

Feature	PEA	PR	AUC
v_1	1.36 (0.99–1.83)	0.61 (0.51–0.79)	0.89
v_2	0.83 (0.50–1.00)	0.38 (0.31–0.49)	0.83
v_3	6.52 (4.10–10.11)	16.24 (11.51–21.26)	0.85
v_4	0.78 (0.50–1.16)$\times 10^{-2}$	2.28 (1.77–3.11)$\times 10^{-2}$	0.91
v_5	1.85 (1.14–2.63)$\times 10^{-2}$	4.80 (3.60–6.30)$\times 10^{-2}$	0.90
v_6	2.56 (2.09–3.28)	1.43 (1.16–1.87)	0.85
v_7	13.22 (7.85–19.47)	36.08 (26.69–46.92)	0.89
v_8	7.45 (2.57–31.48)	197.21 (68.38–390.77)	0.92
v_9	0.19 (0.15–0.27)	0.36 (0.27–0.43)	0.81

The median values were significantly different for all features ($p < 0.05$, Mann-Whitney U test). The last column shows the AUC for each individual feature, calculated using the whole dataset

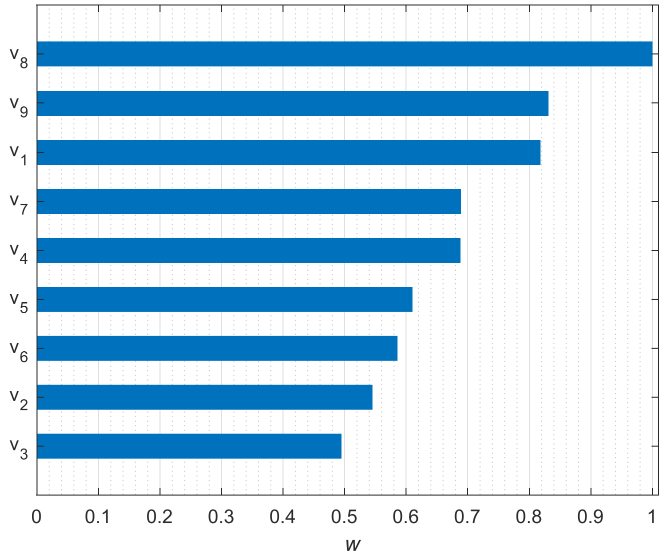

Fig. 2 Feature ranking in the RF models according to the 90th percentile of normalized feature importance ($w(d)$) among 191 folds. The most important features were v_8, v_9, and v_1

estimated using bootstrapping. Five hundred patient-wise bootstrap subsets were created by randomly selecting 2/3 of the patients without replacement.

Several experiments were conducted to characterize the RF classifier. First a RF classifier based on all the computed features (v_1–v_9) was designed. Then, features were ranked according to importance $w(d)$ and RF classifiers with different feature subsets were trained. The feature subsets were constructed by sequentially adding features ranked by importance for each training set, thus avoiding leakage between the training and test sets in the LOPOCV.

Finally, the performance of the proposed RF classifier was compared to a set of state-of-the-art classifiers.

3 Results

All features showed significant differences between PR and PEA segments. Their median (IQR) values for all the PEA and PR segments of the dataset are compared in Table 1. The table also shows the results of the receiver operating characteristic (ROC) curve analysis considering each feature individually. Data are reported in terms of area under the curve (AUC), to measure the feature's discriminative power. For all the features, the AUC values were higher than 0.8, and three of them (v_4, v_5, and v_8) showed an AUC higher than 0.9.

Figure 2 shows how features were ranked in the RF models that included all features ($D = 9$). Specifically, it shows the 90th percentile of $w(d)$ over 191 folds. The figure shows that the most important features were v_8, v_9, and v_1. It also indicates how features were subsequently added in most cases.

The analysis of the RF training showed that in more than 90% of the folds, v_8, v_9, and v_1 were the most important features. The first one was computed in the frequency domain, and presents higher values for PR, reflecting that the power content of the high frequencies is larger for PRs than for PEAs. This feature includes the effect of both, the higher heart rate and the narrower QRS complexes of PR, which imply broader spectra. The heart rate, quantified by v_1, shows a good AUC, but it was not of the highest importance in the RF. Other features contribute to correctly classify high-rate PEA and low-rate PR, as shown by the cases (c) and (d) in Fig. 4. The selection of FuzzEn (v_9) shows that regularity is also important for pulse detection; although entropy features have been applied to other ECG applications [7], it is the first time that FuzzEn is used for pulse detection. In our study, the PEA showed more isoelectric content than PR. In PR, more beats and more variability of the ECG within the 4-s observation interval are shown; this was quantified as less regular by FuzzEn. Panel b of Fig. 1 shows a PEA with two equal beats and a long isoelectric line ($v_9 = 0.08$). However, the PR of panel a with six beats showed more variability between beats in amplitude, waveform, and inter-beat interval ($v_9 = 0.37$). Consequently, FuzzEn as measured by feature v_9 is lower for PEA class. Our results indicate that a multi-domain approach is needed to capture all the subtle ECG waveform variations that differentiate PR from PEA. Features strongly dependent on accurate QRS detection and precise R-peak location, such as v_2 and v_3, are strongly affected by the difficulties of such detections on PEA rhythms, as evidenced by the example (d) in Fig. 1. This partly explains

Table 2 Bootstrapped estimates of the performance metrics for the RF classifiers using different numbers of features. Results are shown as mean (std)

Features	Se	Sp	PPV	NPV	Acc
2:$\{v_8, v_9\}$	83.3 (2.1)	83.9 (1.8)	91.5 (1.3)	70.6 (3.9)	83.5 (1.5)
3:$\{\ldots, v_1\}$	87.2 (1.8)	87.1 (1.7)	93.4 (1.1)	76.4 (3.1)	87.2 (1.3)
4:$\{\ldots, v_7\}$	86.5 (1.8)	87.5 (1.7)	93.5 (1.1)	75.5 (3.3)	86.8 (1.3)
5:$\{\ldots, v_4\}$	86.5 (1.8)	86.9 (1.8)	93.2 (1.2)	75.4 (3.4)	86.6 (1.4)
6:$\{\ldots, v_5\}$	86.4 (1.8)	88.0 (1.8)	93.8 (1.1)	75.5 (3.1)	86.9 (1.3)
7:$\{\ldots, v_6\}$	87.3 (1.8)	88.5 (1.9)	94.1 (1.2)	76.7 (3.1)	87.7 (1.3)
8:$\{\ldots, v_2\}$	88.4 (1.8)	88.7 (1.5)	94.1 (1.0)	78.7 (3.1)	88.5 (1.3)
9:$\{\ldots, v_3\}$	88.4 (1.8)	89.7 (1.4)	94.6 (0.9)	79.1 (2.9)	88.9 (1.2)

why those features were ranked low in importance by the RF classifier.

To better understand the correlation between features, the correlation matrix, $|\mathbf{R}|$, is next given. As shown in $|\mathbf{R}|$, the three most important features (v_8, v_9, and v_1) show low correlation between them ($r = 0.15$–0.3), and they were selected by the RF classifier in most of the cases as shown in Fig. 2. Features v_3, v_4, v_5, and v_7 showed high discriminative power (AUC > 0.85), but they correlate with feature v_8 ($r = 0.68$-0.81) so they were not so important for the RF classifier. Finally, v_2 and v_6 were the least important and the latest showed a correlation coefficient of $r = 0.75$ with v_1. Nevertheless, all the features are required to obtain the best performance (88.9%) that was achieved with $D = 9$, as shown in Table 2.

$$
\begin{array}{c}
 \\ v_1 \\ v_2 \\ v_3 \\ v_4 \\ v_5 \\ v_6 \\ v_7 \\ v_8 \\ v_9
\end{array}
\begin{array}{c}
\begin{array}{ccccccccc} v_1 & v_2 & v_3 & v_4 & v_5 & v_6 & v_7 & v_8 & v_9 \end{array} \\
\begin{pmatrix}
1 & .55 & .35 & .28 & .24 & .74 & .2 & .15 & .30 \\
 & 1 & .55 & .33 & .36 & .62 & .37 & .26 & .42 \\
 & & 1 & .74 & .88 & .44 & .86 & .79 & .19 \\
 & & & 1 & .93 & .56 & .87 & .68 & .39 \\
 & & & & 1 & .44 & .96 & .81 & .22 \\
 & & & & & 1 & .36 & .29 & .57 \\
 & & & & & & 1 & .81 & .21 \\
 & & & & & & & 1 & .15 \\
 & & & & & & & & 1
\end{pmatrix}
\end{array}
$$

The bootstrapped estimates of the performance metrics for the RF classifiers based on different numbers of features are reported in Table 2. Our results show that the highest accuracy (88.9%) was obtained for the full feature set. A solution based on fewer features might be acceptable, for instance, the accuracy was 86.8% using only three features. Reducing the number of features may be a requirement if the algorithm needs to be implemented in a hardware platform with very limited processing power.

In addition, Fig. 3 shows the mean out-of-bag classification errors among 191 folds for different design parameters of the RF classifier, i.e., the number of bagged trees (T) and the number of features per node (D'). The figure shows that our preliminary design choices were good and that errors stabilize for $T > 100$ and for $D' \approx \sqrt{D}$. As shown in the figure, these parameters were not critical in the design of the classifier and were therefore not optimized.

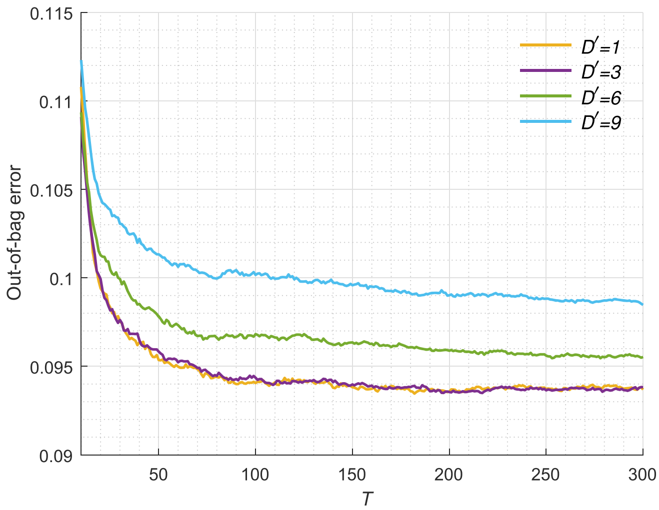

Fig. 3 Mean out-of-bag error for different design parameters: number of trees (T) and number of features per node (D')

Figure 4 depicts six ECG segment examples to illustrate the algorithm's performance. The figure shows that the algorithm correctly identifies pulse, under very different rate and QRS morphology conditions. A few borderline cases were missclassified, as the cases c and f. Panel c shows a PR with quite short RR interval and low v_1, but wide QRS complexes which result in low values of v_8, since the high-frequency content of the ECG is smaller than expected for a PR. Instead, the narrow QRS complexes of the PEA shown in panel f lead to higher frequency components which produce a v_8 value above what is typical for PEA. The importance of v_8 in the RF classifier explains those missclassifications.

Finally, the proposed nine-feature classifier (RF algorithm) was compared to the following classifiers: logistic regression (LR), linear discriminant analysis (LDA), quadratic discriminant analysis (QDA), k-nearest neighbors (k-NN), support vector machine (SVM), and extreme learning machine (ELM) [13, 15]. Table 3 shows the bootstrap estimates for Se, Sp, and Acc. The best results were achieved for RF, followed by a LR classifier.

4 Discussion

This study is framed in the context of cardiopulmonary resuscitation where detecting the presence of pulse implies discriminating between PR and PEA rhythms. As a response to CPR, the patient transients through different cardiac

Fig. 4 Examples of successful and unsuccessful classifications for the algorithm. PR segments are shown in the left and PEA segments in the right. There are important differences in rates and QRS durations among all the examples within each class

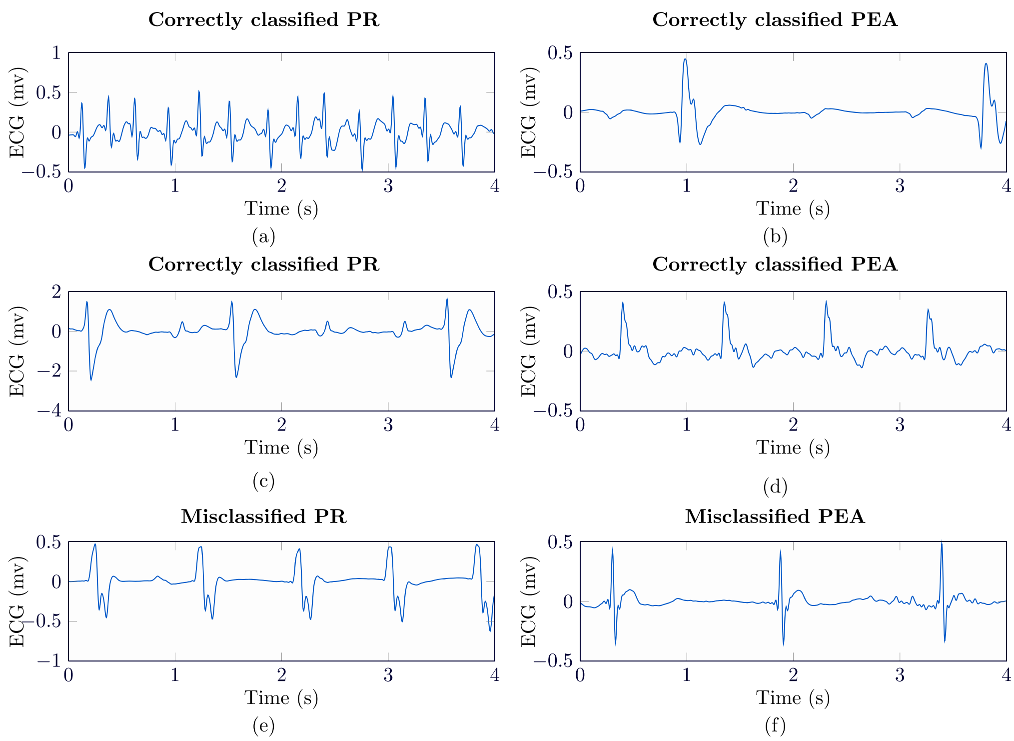

rhythms, and manual pulse detection to discriminate when spontaneous circulation was restored has been proven inaccurate [4, 10, 18, 23, 33]. The non-invasive detection of pulse in cardiac arrest is a challenging technical problem, and there is a clear need for accurate computer-based methods using the signals acquired by defibrillators. This study introduces, to the best of our knowledge, the first computer-based pulse detector for cardiac arrest patients using exclusively the ECG. It could be integrated in any current commercial defibrillator and could be run whenever an organized rhythm is detected by the defibrillator.

One of the components of the algorithm is the QRS complex detector. We have observed that the detection of the QRS instants is a challenging issue mainly in the more

Table 3 Bootstrapped estimates of the performance metrics for different classifiers: logistic regression (LR), linear discriminant analysis (LDA), quadratic discriminant analysis (QDA), *k*-nearest neighbors (*k*-NN), support vector machine (SVM), extreme learning machine (ELM), and random forest (RF). Results are shown as mean (std)

Classifier	Se (%)	Sp (%)	Acc (%)
LR	86.5 (1.8)	90.7 (1.6)	88.5 (1.2)
LDA	87.2 (1.9)	87.6 (1.7)	87.4 (1.4)
QDA	79.5 (2.8)	92.8 (1.4)	83.8 (1.9)
k-NN	83.7 (2.1)	91.1 (1.7)	86.1 (1.4)
SVM	83.9 (1.9)	90.0 (1.6)	86.5 (1.3)
ELM	90.1 (1.7)	82.6 (2.3)	86.3 (1.4)
RF	88.4 (1.8)	89.7 (1.4)	88.9 (1.2)

unstable PEA rhythms. When evaluated with our dataset the QRS detector proposed by Hamilton and Tompkins [14] showed a Se/PPV of 91.23%/82.42%, well below the 99.69%/99.77% provided by that algorithm with the organized rhythms of the MIT-BIH database. Applying the Hamilton-Tompkins detector to our PEA segments, the PPV dropped to 68.90%. So we modified the QRS detector to provide an overall SE/PPV of 89.56%/89.35% with 4-s segments. A more accurate QRS detector, adjusted to the unstable organized rhythms observed during cardiac arrest, increases the accuracy of ECG based methods for pulse detection. Accurate QRS detection is a challenging issue still unaddressed for cardiac arrest rhythms.

The overall results for the RF classifier were obtained applying LOPOCV. The scores estimated using LOPOCV (Se/Sp of 88.4%/89.7%) are in our opinion the best unbiased estimates of the performance of the algorithm for new patients. We tested other patient-wise partitions on the data, such as training/test validation, but scores were strongly affected by the selected random partition, accuracies ranged from 79.3 up to 95.5%. Over 100 repetitions, mean Acc was 89.1%, similar to the Acc obtained with LOPOCV.

No methods based exclusively on the ECG have been proposed so far, but Risdal et al. [28] and Alonso et al. [1] integrated ECG features, combined with impedance features, in their algorithms. These two methods were reproduced considering the three ECG features and the logistic classifier proposed by Alonso et al., and the six ECG features and the neural network classifier proposed by Risdal et al. in an effort to make a direct comparison of

Table 4 Performance of the ECG features proposed in [1, 28] with replicated classifiers in terms of sensitivity, specificity, and balanced accuracy

	No. features	SE (%)	SP (%)	BAC (%)
Risdal et al. [28]	7	87.3	80.9	85.2
Alonso et al. [1]	3	85.9	79.0	83.7
Proposed reduced method	3	87.2	87.1	87.2
Proposed method	9	88.4	89.7	89.1

performance. The overall performance is reported in Table 4 in terms of SE, SP, and BAC (balanced accuracy; mean value of Se and Sp). It can be observed that our solution outperformed the others 4/5 points of BAC, with an increase of 1/3 and 9/10 points of Se and Sp, respectively. Our simplest solution with the best three features also showed better results, with an increase of 2/3 points of BAC with respect to the other methods.

Although the accuracy of our method is high, Se and Sp are close to 90%; its performance is marginally worse than that of previous methods based on a combination of the impedance and the ECG [1, 28]. Risdal et al. and Alonso et al. obtained SE/SP scores close to 91/90% and 92/92% respectively. However, those studies used a training/test validation scheme and results for SE/SP were not statistically characterized, so it is difficult to assess what part of the results is due to the data partition used. Using the same dataset, the performance of our algorithm was only 3 points lower than the best result reported to date, but it added three relevant improvements to previous approaches based on the ECG and TI [1, 28]. On the one hand, Alonso et al. used manual QRS annotations, and in our study, the QRS detection was automatic, which is important if the algorithm is to be implemented in an equipment. On the other hand, our solution only requires 4-s ECG segments. Integrating adaptive algorithms, as proposed in [1, 31], requires transients of 2–5 s, which increase the time interval for the analysis. Keeping the analysis interval short is very important since longer interruptions in the resuscitation therapy may compromise patient survival [11]. Finally, and the most important, our algorithm is based only on the ECG and is therefore applicable to all defibrillators without the need for the onerous adaptations of the TI circuitry.

In addition, our method could easily be integrated into ECG-based retrospective (off-line) resuscitation rhythm classifiers for the annotation of large databases of OHCA cases. Such algorithms have attracted interest lately [26, 27]; they are a prerequisite to analyze large volumes of data (thousands of cases over 30 min long) with the objective of assessing treatment decisions that improve therapy and survival. One of the most important weaknesses of these algorithms is the low sensitivity for PEA and PR detection, under 70% when all rhythms are considered or below 75% for the PEA/PR decisions [26]. The features, feature ranking, and classifiers described in this paper could contribute to overcome one of the most important limitations of such algorithms, closing the gap between automated algorithm classification and expert reviewer's accuracy.

5 Conclusions

A computer method to detect pulse during cardiac arrest using only the ECG is introduced. Our method can be incorporated to any AED and would contribute to the early recognition of the arrest and to the recognition of return of spontaneous circulation during therapy. The SE and SP of the algorithm were close to 90% with ECG segments as short as 4 s.

Funding information This work has been partially supported by the Spanish Ministerio de Economía y Competitividad, jointly with the Fondo Europeo de Desarrollo Regional (FEDER), project TEC2015-64678-R, by the University of the Basque Country via the Ayudas a Grupos de Investigación GIU17/031 and the unit UFI11/16, and by the Basque Government through the Emaitek programme and the grant PRE_2017_1_0112.

Compliance with Ethical Standards

Ethical approval The CPR process files used in this study were collected as part of an effort to develop an airway check algorithm using the capnography signal. Since these raw data files have no identifying information, the Institutional Review Board at the Oregon Health & Science University determined that the proposed activity is not human subject research because the proposed activity does not meet the definition of human subject per 45 CFR 46.102(f).

References

1. Alonso E, Aramendi E, Daya M, Irusta U, Chicote B, Russell JK, Tereshchenko LG (2016) Circulation detection using the electrocardiogram and the thoracic impedance acquired by defibrillation pads. Resuscitation 99:56–62
2. Alonso E, Eftestøl T, Aramendi E, Kramer-Johansen J, Skogvoll E, Nordseth T (2014) Beyond ventricular fibrillation analysis: Comprehensive waveform analysis for all cardiac rhythms occurring during resuscitation. Resuscitation 85(11):1541–1548
3. Babbs CF (2013) We still need a real-time hemodynamic monitor for cpr. Resuscitation
4. Berg RA, Hemphill R, Abella BS, Aufderheide TP, Cave DM, Hazinski MF, Lerner EB, Rea TD, Sayre MR, Swor RA (2010) Part 5: Adult basic life support 2010 American Heart Association guidelines for cardiopulmonary resuscitation and emergency cardiovascular care. Circulation 122(18 suppl 3):S685–S705
5. Breiman L (2001) Random forests. Mach Learn 45(1):5–32
6. Brinkrolf P, Borowski M, Metelmann C, Lukas R-P, Pidde-Küllenberg L, Bohn A (2018) Predicting ROSC in out-of-hospital cardiac arrest using expiratory carbon dioxide concentration: Is trend-detection instead of absolute threshold values the key? Resuscitation 122:19–24

7. Chicote B, Irusta U, Alcaraz R, Rieta JJ, Aramendi E, Isasi I, Alonso D, Ibarguren K (2016) Application of entropy-based features to predict defibrillation outcome in cardiac arrest. Entropy 18(9):313
8. Cromie NA, Allen JD, Navarro C, Turner C, Anderson JM, Adgey AAJ (2010) Assessment of the impedance cardiogram recorded by an automated external defibrillator during clinical cardiac arrest. Crit Care Med 38(2):510–517
9. Cromie NA, Allen JD, Turner C, Anderson JM, Adgey AAJ (2008) The impedance cardiogram recorded through two electrocardiogram/defibrillator pads as a determinant of cardiac arrest during experimental studies. Crit Care Med 36(5):1578–1584
10. Eberle B, Dick W, Schneider T, Wisser G, Doetsch S, Tzanova I (1996) Checking the carotid pulse check: diagnostic accuracy of first responders in patients with and without a pulse. Resuscitation 33(2):107–116
11. Edelson DP, Abella BS, Kramer-Johansen J, Wik L, Myklebust H, Barry AM, Merchant RM, Hoek TLV, Steen PA, Becker LB (2006) Effects of compression depth and pre-shock pauses predict defibrillation failure during cardiac arrest. Resuscitation 71(2):137–145
12. Figuera C, Irusta U, Morgado E, Aramendi E, Ayala U, Wik L, Kramer-Johansen J, Eftestøl T, Alonso-Atienza F (2016) Machine learning techniques for the detection of shockable rhythms in automated external defibrillators. PloS one 11(7):e0159654
13. Friedman J, Hastie T, Tibshirani R (2001) The elements of statistical learning, vol 1. Springer series in statistics Springer, Berlin
14. Hamilton PS, Tompkins WJ (1986) Quantitative investigation of QRS detection rules using the MIT/BIH arrhythmia database. IEEE Trans Biomed Eng BME 33(12):1157–1165
15. Huang G-B, Zhu Q-Y, Siew C-K (2006) Extreme learning machine: theory and applications. Neurocomputing 70(1-3):489–501
16. Irusta U, Ruiz J, Aramendi E, de Gauna SR, Ayala U, Alonso E (2012) A high-temporal resolution algorithm to discriminate shockable from nonshockable rhythms in adults and children. Resuscitation 83(9):1090–1097
17. Jekova I, Krasteva V (2004) Real time detection of ventricular fibrillation and tachycardia. Physiol Meas 25(5):1167
18. Koster RW, Baubin MA, Bossaert LL, Caballero A, Cassan P, Castrén M, Granja C, Handley AJ, Monsieurs KG, Perkins GD et al (2010) European resuscitation council guidelines for resuscitation 2010 section 2. Adult basic life support and use of automated external defibrillators. Resuscitation 81(10):1277–1292
19. Larsen MP, Eisenberg MS, Cummins RO, Hallstrom AP (1993) Predicting survival from out-of-hospital cardiac arrest: a graphic model. Ann Emerg Med 22(11):1652–1658
20. Losert H, Risdal M, Sterz F, Nysæther J, Köhler K, Eftestøl T, Wandaller C, Myklebust H, Uray T, Aase SO et al (2007) Thoracic-impedance changes measured via defibrillator pads can monitor signs of circulation. Resuscitation 73(2):221–228
21. Navarro C, Cromie NA, Turner C, Escalona OJ, Anderson JM (2011) Detection of cardiac arrest using a simplified frequency analysis of the impedance cardiogram recorded from defibrillator pads. In: 2011 annual international conference of the IEEE engineering in medicine and biology society, EMBC, pp 1709–1712. IEEE
22. Neurauter A, Eftestøl T, Kramer-Johansen J, Abella BS, Sunde K, Wenzel V, Lindner KH, Eilevstjønn J, Myklebust H, Steen PA et al (2007) Prediction of countershock success using single features from multiple ventricular fibrillation frequency bands and feature combinations using neural networks. Resuscitation 73(2):253–263
23. Nyman J, Sihvonen M (2000) Cardiopulmonary resuscitation skills in nurses and nursing students. Resuscitation 47(2):179–184
24. Paradis NA, Halperin HR, Kern KB, Wenzel V, Chamberlain DA (2007) Cardiac arrest: the science and practice of resuscitation medicine. Cambridge University Press, Cambridge
25. Pellis T, Bisera J, Tang W, Weil MH (2002) Expanding automatic external defibrillators to include automated detection of cardiac, respiratory, and cardiorespiratory arrest. Critical care medicine 30(4):S176–S178
26. Rad AB, Eftestol T, Engan K, Irusta U, Kvaloy JT, Kramer-Johansen J, Wik L, Katsaggelos AK (2017) Ecg-based classification of resuscitation cardiac rhythms for retrospective data analysis. IEEE Transactions on Biomedical Engineering
27. Rad AB, Engan K, Katsaggelos AK, Kvaløy JT, Wik L, Kramer-Johansen J, Irusta U, Eftestøl T (2016) Automatic cardiac rhythm interpretation during resuscitation. Resuscitation 102:44–50
28. Risdal M, Aase SO, Kramer-Johansen J, Eftesol T (2008) Automatic identification of return of spontaneous circulation during cardiopulmonary resuscitation. IEEE Trans Biomed Eng 55(1):60–68
29. Ristagno G, Li Y, Fumagalli F, Finzi A, Quan W (2013) Amplitude spectrum area to guide resuscitation—a retrospective analysis during out-of-hospital cardiopulmonary resuscitation in 609 patients with ventricular fibrillation cardiac arrest. Resuscitation 84(12):1697–1703
30. Rittenberger JC, Menegazzi JJ, Callaway CW (2007) Association of delay to first intervention with return of spontaneous circulation in a swine model of cardiac arrest. Resuscitation 73(1):154–160
31. Ruiz J, Alonso E, Aramendi E, Kramer-Johansen J, Eftestøl T, Ayala U, González-Otero D (2013) Reliable extraction of the circulation component in the thoracic impedance measured by defibrillation pads. Resuscitation 84(10):1345–1352
32. Soar J, Nolan JP, Böttiger BW, Perkins GD, Lott C, Carli P, Pellis T, Sandroni C, Skrifvars MB, Smith GB et al (2015) European resuscitation council guidelines for resuscitation 2015: section 3. adult advanced life support. Resuscitation 95:100–147
33. Tibballs J, Russell P (2009) Reliability of pulse palpation by healthcare personnel to diagnose paediatric cardiac arrest. Resuscitation 80(1):61–64
34. Valenzuela TD, Roe DJ, Cretin S, Spaite DW, Larsen MP (1997) Estimating effectiveness of cardiac arrest interventions a logistic regression survival model. Circulation 96(10):3308–3313
35. Wei L, Chen G, Yang Z, Yu T, Quan W, Li Y (2017) Detection of spontaneous pulse using the acceleration signals acquired from cpr feedback sensor in a porcine model of cardiac arrest. PloS one 12(12):e0189217
36. Wijshoff RW, van der Sar T, Peeters WH, Bezemer R, Aelen P, Paulussen IW, Ordelman SC, Venema A, van Berkom PF, Aarts RM et al (2013) Detection of a spontaneous pulse in photoplethysmograms during automated cardiopulmonary resuscitation in a porcine model. Resuscitation 84(11):1625–1632
37. Xiong Y, Zhan H, Lu Y, Guan K, Okoro N, Mitchell D, Dwyer M, Leatham A, Salazar G, Liao X et al (2017) Out-of-hospital cardiac arrest without return of spontaneous circulation in the field: Who are the survivors? Resuscitation 112:28–33

Andoni Elola was born in Donostia in 1992. He received his bachelors and masters degrees in the years 2015 and 2017, both from the University of the Basque Country where he is currently working on his PhD degree. His research is focused on applications of biomedical signal processing and advance machine learning techniques applied to improve therapy during cardiac arrest. He has made contributions to automatic pulse detection and ventilation detection during cardiopulmonary resuscitation.

Elisabete Aramendi Ph.D. in Telecommunications Engineering, joined the Telecommunication Engineering Department of the University of the Basque Country in 1994. She is Associate Professor since 2002 lecturing on advanced statistical signal processing. Her research is centered in the application of signal processing techniques in bioengineering, focused on topics related to resuscitation and treatment of cardiac arrest. In that field, she has published over 20 papers in SCI-IF, several book chapters, and more than 80 contributions to scientific conferences. She is also inventor in four patents for defibrillation monitors and diagnosis aid systems. She has conducted research stays at several universities and medical centers.

Unai Irusta was Born in Bilbao in 1973. He received the M.Sc. degree in Telecommunications engineering with honors in 1998 from the University of the Basque Country, where he has taught as assistant professor since 2003 and as associate professor since 2011. His field of expertise is biomedical signal processing, machine learning, and data management applied to improve treatment of cardiac arrest. In this field, he has published over 25 papers in SCI-IF journals and over 60 contributions to scientific conferences.

Javier Del Ser received his first PhD in Telecommunication Engineering (Cum Laude) from the University of Navarra, Spain, in 2006, and a second PhD in Computational Intelligence (Summa Cum Laude, Extraordinary Prize) from the University of Alcala, Spain, in 2013. Currently, he is a principal researcher in data analytics and optimization at TECNALIA (Spain), a visiting fellow at the Basque Centre for Applied Mathematics (BCAM), and a lecturer at the University of the Basque Country (UPV/EHU). His research interests gravitate on the use of descriptive, prescriptive and predictive algorithms for data mining and optimization in a diverse range of application fields such as Energy, Transport, Telecommunications, Health, and Industry, among others. In these fields, he has published more than 220 scientific articles, co-supervised 6 Ph.D. theses (plus another 7 ongoing), edited 5 books, and co-authored 6 patents. He is a senior member of the IEEE and a recipient of the Bizkaia Talent prize for his research career.

Erik Alonso was born in Basauri, Spain, in 1987. He received the BEng, MSc and PhD degrees from The University of the Basque Country (UPV/EHU)in 2010, 2011 and 2014, respectively. He is currently an associate professor with the Department of Applied Mathematics, University of the Basque Country (UPV/EHU). His research interests include biomedical signal processing and machine learning applied to data from cardiac arrest episodes.

Mohamud Daya was born in Nairobi, Kenya in 1959. He received his BSc (Biochemistry) and MD from the University of British Columbia in 1980 and 1984, respectively. He subsequently received an MSc degree (Infection and Health in the Tropics) from the London School of Tropical Medicine and Hygiene in 1998. He is currently a professor in the Department of Emergency Medicine at the Oregon Health & Science University (OHSU) and Emergency Medical Services (EMS) Medical Director in Oregon. His research interests include computer-based decision support in out-of-hospital medical emergencies care sudden cardiac arrest.

Supplementary materials: Comparative analysis of the ECG-features for PR/PEA

In an effort to better understand the real information extracted by each feature and its discriminative power, two examples (PR and PEA) were selected from the dataset and processed in detail. Fig. 1 showsthe PR segment on the left and PEA segment on the right. From top to bottom, the ECG and the intermediate signals used to compute the v_1-v_9 features, are depicted. The features for both cases are given in Table 1.

The PR rhythms are associated with higher rates, higher peak-to-peak amplitudes and narrower QRS complexes than PEA cases. The first three features are based on that evidence. Top panel of Fig. 1 shows the ECG waveform with the instants of the QRS complexes marked. The median RR interval is shorter for the PR which leads to a lower v_1. The median signal length per beat, v_2, was computed using the normalized cepstrum, $C_j[n]$ (shown in the third panel of the figure for the second beat, $C_2[n]$). It can be observed that values are more concentrated around zero for the PR case, leading to lower v_2 values. The third feature, v_3, is the relation between the peak-to-peak amplitude and the width of the QRS. For each complex the onset (pink dashed lines) and offset (red dashed lines) are computed, as shown for the QRS complex zoomed in the second panel. PR segments present narrower and usually higher amplitude QRS complexes, resulting in a higher value of v_3.

The next three features were based on the first difference of the signal ($x_\Delta[n]$) and $d_2[n]$. The first difference for the PR, shown in the fourth panel, shows higher slopes and higher variance which provides higher mean and standard deviation values (v_4 and v_5 respectively). The fifth panel shows the probability density function of $d_2[n]$, which is more concentrated around zero for the PEA, leading to higher kurtosis.

Features v_7 and v_8 are spectral characteristics, based on the FFT of the signal shown in the last panel of Fig. 1. PR rhythms usually show higher amplitudes and higher harmonic content, so AMSA (v_7), which is the sum of the spectral amplitudes weighted by their frequency, will be higher for PR. Frequencies above 17.5 Hz are shaded in red, as feature v_9 is the power of the signal in that frequency band. It can be seen that the PR exhibits important harmonic components in that band, in contrast to the PEA spectrum more concentrated in lower frequencies.

The last feature, v_9, quantifies the fuzzy entropy, and it is lower for the PEA case due to the longer isoelectric lines.

Feature	**PR**	**PEA**
v_1	0.35	1.47
v_2	0.44	0.67
v_3	23.7	0.82
v_4	$3.97 \cdot 10^{-2}$	$0.10 \cdot 10^{-2}$
v_5	$7.77 \cdot 10^{-2}$	$0.02 \cdot 10^{-2}$
v_6	0.65	2.38
v_7	42.87	1.54
v_8	594.17	0.08
v_9	0.35	0.19

Table 1 Values of nine features for PR/PEA examples shown in Fig. 1.

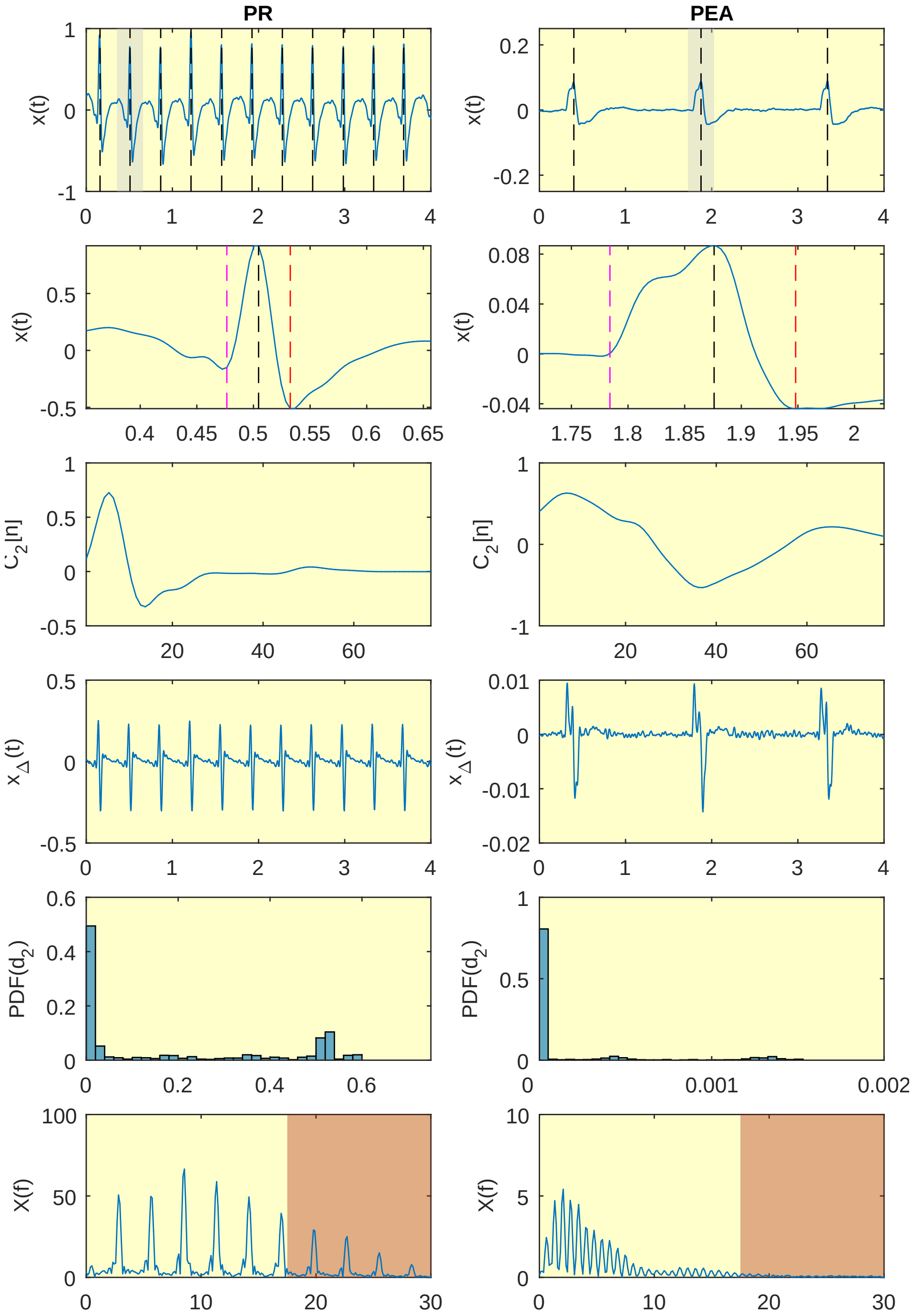

Fig. 1 Two examples associated to PR (left) and PEA (right) are shown with the intermediate signals used to compute the ECG features.

A.1.2 Lehenengo helburuari lotutako aurreneko argitalpena nazioarteko konferentzian

A.2. Taula. Lehenengo helburuari lotutako aurreneko argitalpena nazioarteko konferentzian.

	Argitalpena nazioarteko konferentzian
Erreferentzia	Andoni Elola, Elisabete Aramendi, Unai Irusta, Artzai Picón, Erik Alonso, Iraia Isasi, Ahamed Idris, "Deep Learning for Pulse Detection in Out-of-Hospital Cardiac Arrest Using the ECG", *Computing in Cardiology*, 2018, vol. 45, pp. 1-4.
Kalitate adierazleak	• **Argitalpen mota**: SJRen indexatutako nazioarteko konferentzia • **Inpaktu faktorea**: 0.202

Deep Learning for Pulse Detection in Out-of-Hospital Cardiac Arrest Using the ECG

Andoni Elola[1], Elisabete Aramendi[1], Unai Irusta[1], Artzai Picón[2], Erik Alonso[1], Pamela Owens[3], Ahamed Idris[3]

[1] University of the Basque Country, Bilbao, Bizkaia, Spain
[2] TECNALIA, Derio, Bizkaia, Spain
[3]University of Texas Southwestern Medical Center, Dallas, Texas, USA

Abstract

Pulse detection during out-of-hospital cardiac arrest is necessary to identify cardiac arrest and detect return of spontaneous circulation. Currently, carotid pulse checking and checking for signs of life are the most widespread procedures for pulse detection, but both have been proven inaccurate and time consuming. Automatic methods that could be integrated in Automated External Defibrillators (AEDs) are needed. In this study we propose a deep neural network classifier to detect pulse using exclusively the ECG. We extracted 3914 segments of 4 s from 279 patients, all of them with an organized rhythm. They were annotated as pulsed rhythm or pulseless rhythm based on clinical information. A total of 2372 pulsed rhythms and 1542 pulseless rhythms were included in the study. To train and test the model 3038 (223 patients) and 876 segments (56 patients) were used, respectively. The model was evaluated in terms of Sensitivity (Se) and Specificity (Sp) for pulse detection. The network showed a Se/Sp of 89.4%/97.2% during training process and 91.7%/92.5% for the test set.

1. Introduction

Sudden cardiac death is one of the leading causes of death in the industrialized world. Despite progress in different fields, survival rates in the out-of-hospital settings remain low, around 10%. The detection of pulse is crucial for the recognition of both, cardiac arrest and the Return of Spontaneous Circulation (ROSC) [1].

Palpation of carotid has been long used to detect pulse, but it has been proven to be inaccurate and time consuming [2,3]. Current Resuscitation guidelines [1] recommend looking for signs of life in the patient, which has not been proven to be more accurate [4].

Several automatic methods have been proposed using the ECG and the thoracic impedance recorded by the defibrillation pads [5–7]. Availability and low resolution of the impedance signal compromise the applicability of those methods. A more universal approach, usable in any Automated External Defibrillator (AED), is to use only the ECG to detect pulse. This paper presents a new approach based on a deep neural network.

Deep learning techniques showed good accuracies in physiological signal classification tasks [8]. In this paper we propose a novel deep network to classify an organized ECG into pulsed rhythm (PR) or pulseless electrical activity (PEA).

2. Materials

The data used for this study were a subset of a large Out-of-Hospital Cardiac Arrest (OHCA) database recorded by the DFW center for resuscitation research (UTSW, Dallas). All episodes were recorded using the Philips HeartStart MRx device, including ECG with a sampling frequency of 250 Hz and a resolution of 1.03 μV per least significant bit.

A total of 1015 episodes containing concurrent ECG and impedance recordings were considered and separated into two groups (ROSC/no-ROSC) using the ROSC and time of ROSC (t_{rosc}) annotations made by the clinicians in the scene. ROSC episodes had no chest compressions or shocks after t_{rosc}. In the no-ROSC group, we discarded patients transported to hospital and episodes with sustained organized rhythms once chest compressions were suspended, because such actions are associated with patients in ROSC.

Five second segments presenting an organized rhythm were automatically extracted during intervals without chest compression artifacts [9]. These segments were labelled as PR and PEA for classification. PR segments were extracted in the ROSC episodes after t_{rosc} with a minimum interval between segments of 30 s. PEA segments were extracted in the no-ROSC group with a minimum interval between segments of 1 s.

 ISSN: 2325-887X DOI: 10.22489/CinC.2018.093

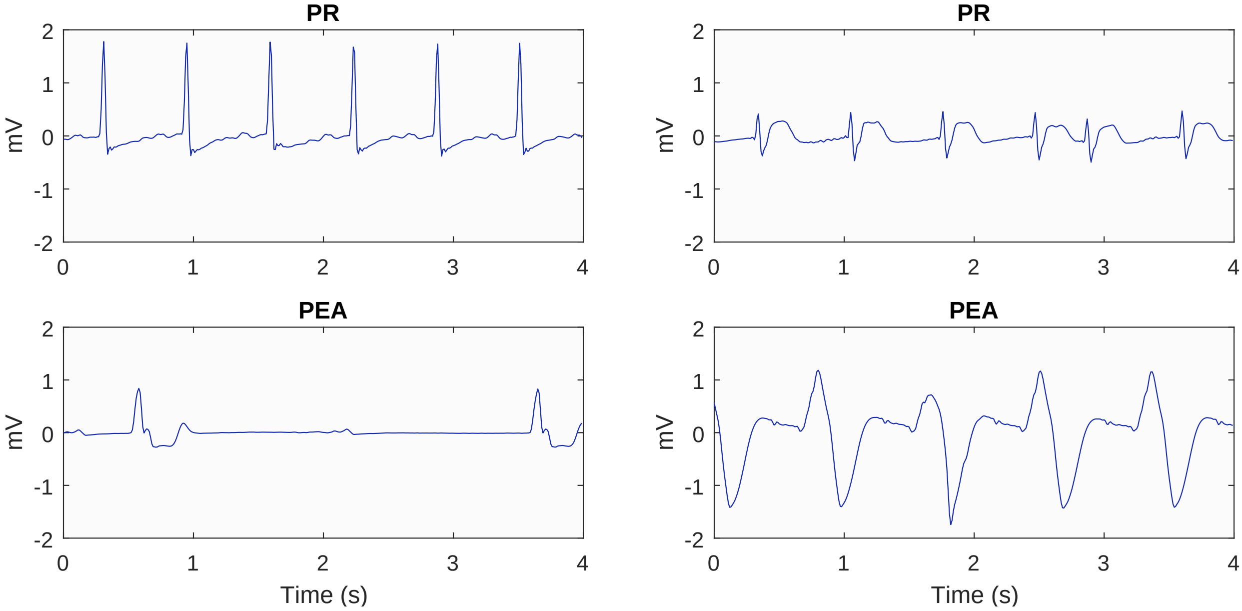

Figure 1. Pulsed rhythm (PR) and Pulseless Electrical Activity (PEA) examples.

The final dataset contained 279 episodes (134 ROSC/145 no-ROSC), and a total of 3914 segments, 2372 PR and 1542 PEA. Figure 1 shows examples of PR and PEA segments, and shows that narrower QRS complexes and higher heart rates are associated with PR. Data were divided in patient-wise training and test sets. The first one is composed by 3038 segments from 223 patients (1871 PR and 1167 PEA) and the second one by 876 segments from 56 patients (501 PR and 375 PEA).

3. Methods

ECG data were downsampled to 100 Hz and bandpass filtered between 0.5-30 Hz. The analysis window was 4 s, so 400 samples were input to the deep neural network classifier. The network was implemented using Keras with Tensorflow backend [10, 11].

3.1. Network design

Figure 2 shows the overall scheme of the deep neural network applied in this proposal. A total of 4 layers constitute the final solution (in blue) and the extra layers were used to train the model (in red).

The first layer adds gaussian noise (mean zero and $\sigma = 0.03$) to the input signal to avoid overfitting in the training process.

The second layer is a convolutional layer, which applies temporal convolution to the input data. The n-th sample of the ℓ-th filtered signal is obtained following the next equation:

$$x_\ell[n] = f\left(\sum_{i=0}^{m-1} w_{i\ell} x[n-i] + b_{i\ell}\right) \quad (1)$$

where $f(\bullet)$ is the linear rectifier and $m = 3$ was taken. A total of 6 filters ($\ell = 1, \ldots, 6$) were applied, and the weigths, w_{il}, and the biases, b_{il}, were optimized in the training process.

The third layer, the pooling layer, downsamples the filtered signals by a ratio of 3 and a maximum criteria.

The fourth layer was a recurrent layer, used to exhibit the temporal behaviour of the data. Gate Recurrent Unit (GRU) is a simpler version of Long Short-Term Memory (LSTM), which was designed to learn long-term dependencies [12], but its accuracy is similar [13]. In our solution two GRU layers were applied, backwards and forwards, of 10 units each.

The final stage, includes a single neuron as classification stage with the sigmoid as activation function. The output, y, is the likelihood of the segment being PR.

In the training process we adopted some methods to avoid overfitting. Besides adding gaussian noise, dropout layers were added between third and fourth layer and between the last two layers. These kind of layers drops out units under a certain probability [14], shown between layers in Figure 2. According to [14], when using dropout probabilities it is specially useful to constrain the norm of the weight vector at each layer, i.e. the layers are optimized under the constraint $||\boldsymbol{w}|| < \gamma$. In our solution $\gamma = 2$ and the constraint was applied to convolutional and recurrent

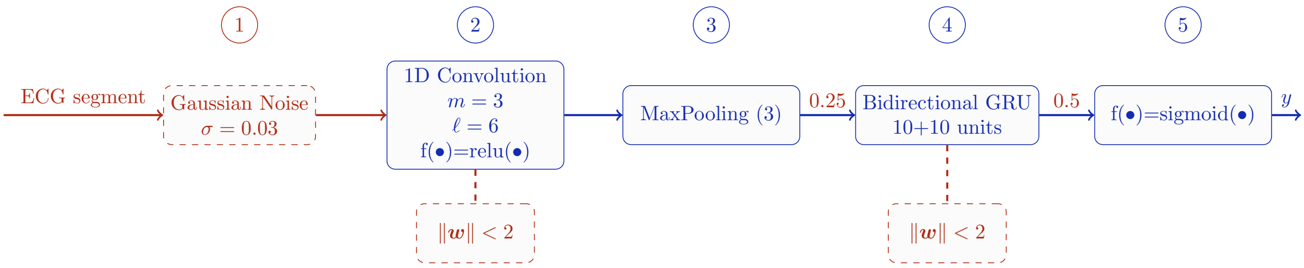

Figure 2. Overall architecture of the deep learning solution

layers. All weights were initialized using Xavier normal distribution and we used binary cross-entropy as loss function to optimize the network. All patients were weighted equally to compute the loss function and we used the RMSprop optimizer. Finally, training data were shuffled at the beginning of each epoch to change the batches. The batch size was set to 4 and the number of epochs was 200.

3.2. Performance metrics

The unweighted accuracy (UAcc) of the network proposed was evaluated for the training and the test set at each epoch in order to analyse the convergence of the network.

The overall performance of the method was given in terms of Sensitivity (Se), proportion of correctly classified PRs; Specificity (Sp), proportion of correctly classified PEAs and Balanced Accuracy (BAC), the mean value of Se and Sp. To compute the performance metrics each patient was weighted equally.

4. Results

Figure 3 shows the unweighted accuracy of the network at each epoch for the training and testing sets. UAcc converges for epoch 100 with a difference below 4% in the end between training and test sets.

At the final epoch, the network showed a Se/Sp of 89.4%/97.2% for the training set and 91.7%/92.5% for the test set. A BAC reduction of 1.2% was measured for the test set.

5. Discussion and conclusions

Pulse detection remains challenging during OHCA for both experts and laypeople, so there is a clear need of accurate automatic methods. This is, for the best of our knowledge, the first study that proposes using a deep learning approach to detect pulse using only the ECG signal. This allows the universal use of the algorithm, as recording the ECG signal is necessary to analyse the patient's rhythm.

Our solution is based only in 4 layers, and several regularization techniques (adding gaussian noise, constraining the weights and dropout) were used to avoid overfitting.

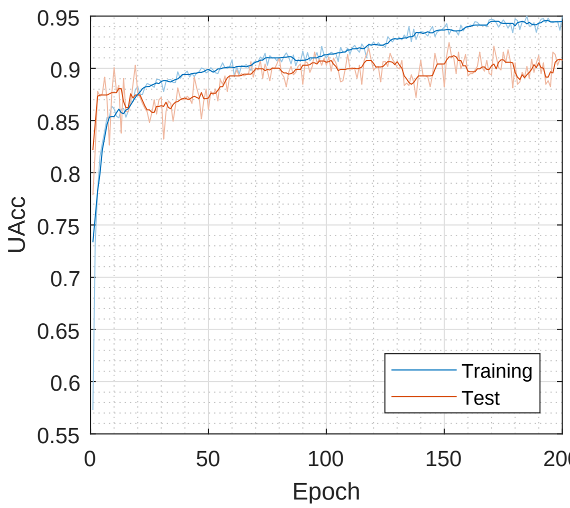

Figure 3. Unweighted accuracy of the network at each epoch of the training process.

Figure 3 shows the UAcc of the training and test sets per epoch. UAcc of the training set improves along epochs, but the test set's UAcc does not improve from epoch 100 to the end. However, it does not fall, showing that the adopted regularization techniques were good enough. We also trained and tested the network without regularization techniques, and achieved a Se/Sp of 98.7%/97.0% during training, but 94.6%/87.8% for the test set. The difference in BAC is 6.7 points, well above from 1.2 points achieved using regularization techniques. Further adjustment of the regularization parameters, using data augmentation and more data could further reduce the gap between training and test performances.

The algorithm showed a Se/Sp of 91.7%/92.5% respectively. Those scores are similar to other solutions that require both ECG and impedance [5, 6]. Our solution based exclusively on the ECG permits the universal use of the algorithm in any AED.

Acknowledgements

This work has been partially supported by the Spanish Ministerio de Economía y Competitividad, jointly with the Fondo Europeo de Desarrollo Regional (FEDER), through project TEC2015-64678-R, by the University of the Basque Country via the Ayudas a Grupos de Investigación GIU17/031 and the unit UFI11/16, and by the Basque Government through the grant PRE_2017_1_0112.

References

[1] Soar J, Nolan JP, Böttiger BW, Perkins GD, Lott C, Carli P, Pellis T, Sandroni C, Skrifvars MB, Smith GB, et al. European resuscitation council guidelines for resuscitation 2015: section 3. adult advanced life support. Resuscitation 2015; 95:100–147.

[2] Eberle B, Dick W, Schneider T, Wisser G, Doetsch S, Tzanova I. Checking the carotid pulse check: diagnostic accuracy of first responders in patients with and without a pulse. Resuscitation 1996;33(2):107–116.

[3] Tibballs J, Russell P. Reliability of pulse palpation by healthcare personnel to diagnose paediatric cardiac arrest. Resuscitation 2009;80(1):61–64.

[4] Ruppert M, Reith MW, Widmann JH, Lackner CK, Kerkmann R, Schweiberer L, Peter K. Checking for breathing: evaluation of the diagnostic capability of emergency medical services personnel, physicians, medical students, and medical laypersons. Annals of Emergency Medicine 1999; 34(6):720–729.

[5] Risdal M, Aase SO, Kramer-Johansen J, Eftesol T. Automatic identification of return of spontaneous circulation during cardiopulmonary resuscitation. IEEE Transactions on Biomedical Engineering 2008;55(1):60–68.

[6] Alonso E, Aramendi E, Daya M, Irusta U, Chicote B, Russell JK, Tereshchenko LG. Circulation detection using the electrocardiogram and the thoracic impedance acquired by defibrillation pads. Resuscitation 2016;99:56–62.

[7] Ruiz JM, de Gauna SR, González-Otero DM, Saiz P, Gutiérrez JJ, Veintemillas JF, Bastida JM, Alonso D. Circulation assessment by automated external defibrillators during cardiopulmonary resuscitation. Resuscitation 2018; 128:158–163.

[8] Faust O, Hagiwara Y, Hong TJ, Lih OS, Acharya UR. Deep learning for healthcare applications based on physiological signals: a review. Computer Methods and Programs in Biomedicine 2018;.

[9] Alonso E, Ruiz J, Aramendi E, González-Otero D, de Gauna SR, Ayala U, Russell JK, Daya M. Reliability and accuracy of the thoracic impedance signal for measuring cardiopulmonary resuscitation quality metrics. Resuscitation 2015;88:28–34.

[10] Chollet F, et al. Keras. `https://keras.io`, 2015.

[11] Abadi M, Agarwal A, Barham P, Brevdo E, Chen Z, Citro C, Corrado GS, Davis A, Dean J, Devin M, Ghemawat S, Goodfellow I, Harp A, Irving G, Isard M, Jia Y, Jozefowicz R, Kaiser L, Kudlur M, Levenberg J, Mané D, Monga R, Moore S, Murray D, Olah C, Schuster M, Shlens J, Steiner B, Sutskever I, Talwar K, Tucker P, Vanhoucke V, Vasudevan V, Viégas F, Vinyals O, Warden P, Wattenberg M, Wicke M, Yu Y, Zheng X. TensorFlow: Large-scale machine learning on heterogeneous systems, 2015. URL `https://www.tensorflow.org/`. Software available from tensorflow.org.

[12] Hochreiter S, Schmidhuber J. Long short-term memory. Neural computation 1997;9(8):1735–1780.

[13] Chung J, Gulcehre C, Cho K, Bengio Y. Empirical evaluation of gated recurrent neural networks on sequence modeling. arXiv preprint arXiv14123555 2014;.

[14] Srivastava N, Hinton G, Krizhevsky A, Sutskever I, Salakhutdinov R. Dropout: A simple way to prevent neural networks from overfitting. The Journal of Machine Learning Research 2014;15(1):1929–1958.

Address for correspondence:

Andoni Elola
Engineering school of Bilbao
andoni.elola@ehu.eus

A.1.3 Lehenengo helburuari lotutako bigarren argitalpena nazioarteko aldizkarian

A.3. Taula. Lehenengo helburuari lotutako bigarren argitalpena nazioarteko aldizkarian.

	Argitalpena nazioarteko aldizkarian
Erreferentzia	Andoni Elola, Elisabete Aramendi, Unai Irusta, Artzai Picón, Erik Alonso, Pamela Owens, Ahamed Idris, "Deep neural networks for ECG-based pulse detection during out-of-hospital cardiac arrest", *Entropy 2019*, vol. 21, no. 3, p. 305.
Kalitate adierazleak	• **Argitalpen mota**: JCRen indexatutako aldizkari artikulua • **Kuartila**: Q2 (33/85) (*Web of Science* 2019) • **Inpaktu faktorea**: 2.494

entropy

Article

Deep Neural Networks for ECG-Based Pulse Detection during Out-of-Hospital Cardiac Arrest

Andoni Elola [1,*], Elisabete Aramendi [1], Unai Irusta [1], Artzai Picón [2,3], Erik Alonso [4], Pamela Owens [5] and Ahamed Idris [5]

[1] Department of Communications Engineering, University of the Basque Country, 48013 Bilbao, Spain; elisabete.aramendi@ehu.eus (E.A.); unai.irusta@ehu.eus (U.I.)
[2] Computer Vision, TECNALIA Research & Innovation, 48160 Derio, Spain; artzai.picon@ehu.eus
[3] Department of Engineering Systems and Automatics, University of the Basque Country, 48013 Bilbao, Spain
[4] Department of Applied Mathematics, University of the Basque Country, 48013 Bilbao, Spain; erik.alonso@ehu.eus
[5] Department of Emergency Medicine, University of Texas Southwestern Medical Center, Dallas, TX 75390, USA; Pamela.Owens@utsouthwestern.edu (P.O.); Ahamed.Idris@utsouthwestern.edu (A.I.)
* Correspondence: andoni.elola@ehu.eus; Tel.: +34-946-01-39-56

Received: 8 March 2019; Accepted: 19 March 2019; Published: 21 March 2019

Abstract: The automatic detection of pulse during out-of-hospital cardiac arrest (OHCA) is necessary for the early recognition of the arrest and the detection of return of spontaneous circulation (end of the arrest). The only signal available in every single defibrillator and valid for the detection of pulse is the electrocardiogram (ECG). In this study we propose two deep neural network (DNN) architectures to detect pulse using short ECG segments (5 s), i.e., to classify the rhythm into pulseless electrical activity (PEA) or pulse-generating rhythm (PR). A total of 3914 5-s ECG segments, 2372 PR and 1542 PEA, were extracted from 279 OHCA episodes. Data were partitioned patient-wise into training (80%) and test (20%) sets. The first DNN architecture was a fully convolutional neural network, and the second architecture added a recurrent layer to learn temporal dependencies. Both DNN architectures were tuned using Bayesian optimization, and the results for the test set were compared to state-of-the art PR/PEA discrimination algorithms based on machine learning and hand crafted features. The PR/PEA classifiers were evaluated in terms of sensitivity (Se) for PR, specificity (Sp) for PEA, and the balanced accuracy (BAC), the average of Se and Sp. The Se/Sp/BAC of the DNN architectures were 94.1%/92.9%/93.5% for the first one, and 95.5%/91.6%/93.5% for the second one. Both architectures improved the performance of state of the art methods by more than 1.5 points in BAC.

Keywords: pulse detection; ECG; pulseless electrical activity; out-of-hospital cardiac arrest; convolutional neural network; deep learning; Bayesian optimization

1. Introduction

Out-of-hospital cardiac arrest (OHCA) remains a major public health problem, with 350,000–700,000 individuals per year affected in Europe and survival rates below 10% [1,2]. Early recognition of OHCA is key for survival [3] as it allows a rapid activation of the emergency system and facilitates bystander cardiopulmonary resuscitation (CPR). Bystanders should apply an automated external defibrillator (AED), designed to be used with minimal training and to guide the rescuer until the arrival of medical personnel [4]. The main goal of OHCA treatment is to achieve return of spontaneous circulation (ROSC), so that post-resuscitation care can be initiated and the patient can be transported to hospital. Early recognition and post-resuscitation care are two key factors for the survival of the patient, and both these factors require the accurate detection of presence/absence of pulse.

Nowadays, healthcare professionals check for pulse by manual palpation of the carotid artery or by looking for signs of life. However, carotid pulse palpation has been proven inaccurate (specificity 55%) and time consuming (median delays of 24 s) for both bystanders and healthcare personnel [5–9]. Consequently, current resuscitation guidelines recommend the assessment of carotid pulse together with looking for signs of life only for experienced people [10]. Checking for signs of life alone has not been proven to be more accurate. In fact, healthcare personnel show difficulties when discriminating between normal (pulse present) and agonal (absence of pulse) breathing [11,12]. More modern approaches use ultrasound to visually assess the mechanical activity of the heart and detect pulse-generating rhythms accurately [13]. Unfortunately, the required equipment is not available during bystander CPR and very rarely for medical personnel in the out-of-hospital setting. Besides, some studies suggest that the use of ultrasound lengthens the duration of chest compression pauses [14,15], decreasing the probability of survival of the patient. Automatic accurate pulse detectors are still needed to assist the rescuer in monitoring the hemodynamic state of the patient [16].

Cardiac arrest rhythms are grouped into the following 4 categories [10]: ventricular fibrillation (VF), ventricular tachycardia (VT), asystole (AS), and pulseless electrical activity (PEA). When ROSC is achieved the patient shows a pulse-generating rhythm (PR). VF and VT need a defibrillation, and a vast number of algorithms have been proposed to detect them [17–20]. Among non-shockable rhythms, AS is defined as the absence of electrical and mechanical activity of the heart. PEA shows an organized electrical activity of the heart but no clinically palpable pulse, i.e., the mechanical activity is not efficient enough to maintain the consciousness of the patient [21]. AS rhythms can be discriminated using features that are sensitive to amplitude [22], so the most challenging scenario for pulse detection is the discrimination between PR and PEA rhythms. A precise PR/PEA discrimination would allow an earlier recognition of the arrest, and also the identification of ROSC when treating the OHCA patient.

In the last two decades many efforts have been dedicated to automated methods for PR/PEA discrimination based on several non-invasive biomedical signals monitored by defibrillators. The thoracic impedance (TI) shows small fluctuations ($\approx$40 mΩ) with each effective heartbeat [23–25], so it has been proposed for pulse detection alone [26,27] or in combination with the ECG [28,29]. However, many commercial defibrillators do not have enough amplitude resolution to detect TI fluctuations produced by effective heartbeats, and the methods have not been proven to be reliable during ventilations because of the TI fluctuations produced by air insufflation [29]. Other signals such as the photoplethysmogram [30,31], capnogram [32], or acceleration [33] have been also included in algorithms for PR/PEA discrimination, but these signals are not commonly available in all monitor/defibrillators. Instead, the ECG acquired using the defibrillation pads is available in all defibrillators, and algorithms based exclusively on the ECG could be of universal use, and easy to integrate in any device.

The main objective of this study was to develop a pulse detection algorithm based exclusively on the ECG acquired by defibrillation pads. Previously a machine learning technique was proposed using a random forest (RF) classifier based on hand-crafted features [34]. Alternatively, deep neural networks (DNN) have shown superior performance in classification problems with large datasets in many fields [35–38]. DNN solutions have no need of feature engineering as the signals are directly fed to the network which does the exploratory data analysis. Convolutional neural networks (CNN) have been successfully used for heartbeat arrhythmia classification [39–41] or the detection of myocardial affections [42,43], and recurrent neural networks (RNN) have been proven accurate for diagnostic applications when time dependencies in the signal are important [44,45]. This work proposes and compares various DNN solutions for PR/PEA classification. The manuscript is organized as follows: Section 2 describes the data used in this study; in Section 3 the proposed DNN solutions are described; classical machine learning based approaches are described in Section 4 and used for comparison;

Section 5 describes the optimization process of the models and the evaluation methods applied; and in Sections 6 and 7 the results are presented and discussed.

2. Data Collection

The data of the study were a subset of a large OHCA episode collection gathered by the DFW centre for resuscitation research (UTSW, Dallas). Every episode was recorded using the Philips HeartStart MRx device, which acquires the ECG signal through defibrillation pads with a sampling frequency of 250 Hz and a resolution of 1.03 μV per least significant bit.

There were a total of 1561 episodes of which 1015 contained concurrent ECG and TI signals. The TI signal was necessary to identify ECG intervals free of artefacts due to chest compressions provided to the patient during CPR. Episodes were separated in ROSC and no-ROSC groups based on the instant of ROSC annotated by the clinicians on scene. PEA rhythms were extracted from no-ROSC patients. PR rhythms were extracted after the instant of ROSC for patients who showed sustained ROSC.

ECG segments of 5 s were automatically extracted during intervals without chest compressions. Chest compressions were automatically detected in the TI using the algorithm proposed in [46], or in the compression depth signal of the monitor [47]. Then, organized rhythms (PR or PEA) were automatically identified using an offline version of a commercial shock advise algorithm [17]. Three biomedical engineers reviewed the segments to check they contained visible QRS complexes with a minimum rate of 12 bpm. Every segment was annotated as PEA or PR based on the clinical annotations. Consecutive ECG segments were extracted using a minimum separation between segments of 1 s for PEA and 30 s for PR. PEA is more variable than PR, and occurs during the arrest. During PEA, CPR is given to the patient and intervals without compressions are not frequent. After ROSC is identified (PR segments) chest compressions are interrupted, and long intervals of artefact-free ECG are available. A longer separation between PR segments was considered to increase the variability.

A total of 3914 segments (2372 PR and 1542 PEA) from 279 patients (134 with ROSC and 145 without ROSC) comprised the dataset. Patient-wise training and test sets were created ($\approx$ 80%/20% of the patients). The training set contained 3038 segments (1871 PR) from 223 patients (105 with ROSC). The test set contained 876 segments (501 PR) from 56 patients (29 with ROSC).

Figure 1 shows examples of three PR segments (panel a) and three PEA segments (panel b). PR usually shows higher rates, narrower QRS complexes, less heart rate variability and higher frequency content (steeper QRS complexes) than PEA. However, PR in cardiac arrest often shows irregular beats as in the last two examples of Figure 1a. PEA rhythms may show more aberrant QRS complexes, absence of P waves, or more ectopic heartbeats compared to PR.

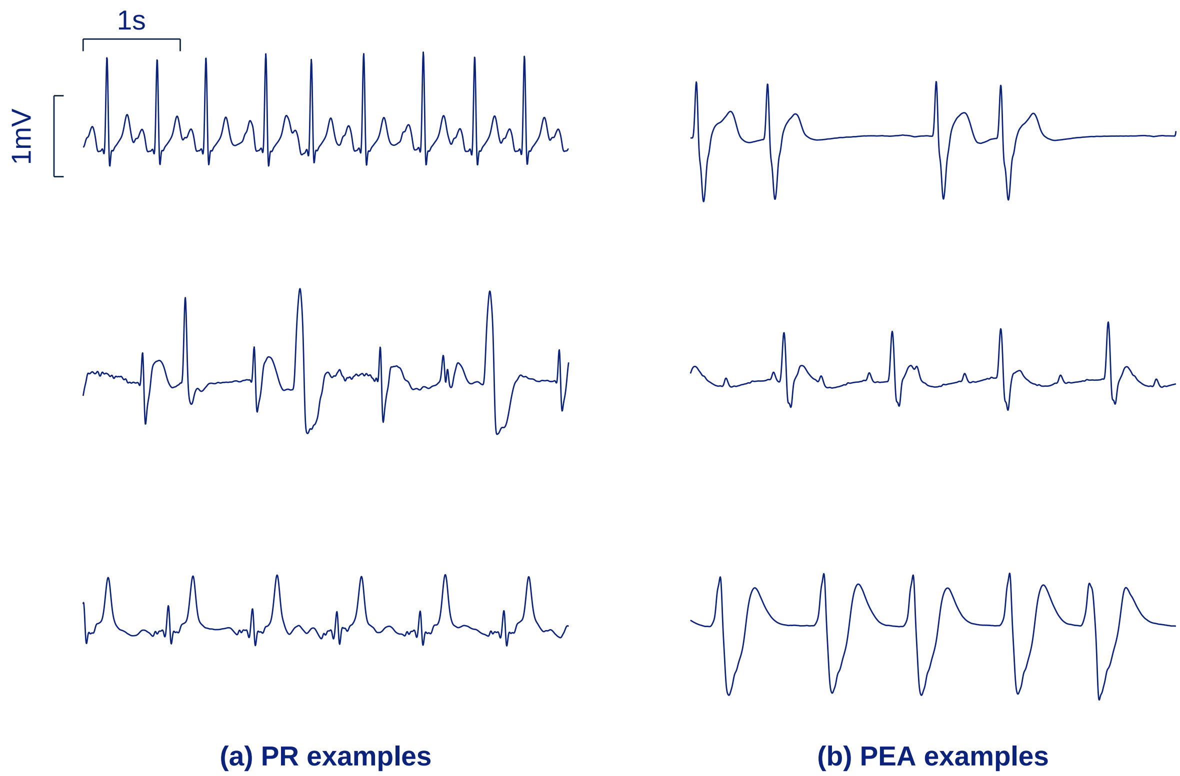

Figure 1. Segments of 5 s corresponding to pulsed rhythm (PR) (**a**) and pulseless electrical activity (PEA) (**b**) from the study dataset.

3. Proposed DNN Architectures

Two DNN architectures were implemented for the binary classification of ECG into PR/PEA. The 5 s ECG segments were first bandpass filtered using the typical AED bandwidth (0.5–30 Hz). The filtered ECG was downsampled to 100 Hz to obtain $s[n]$, a signal of $N = 500$ samples, that was fed to the DNN networks. The output of the networks was $p_{PR} \in (0, 1)$, the likelihood that a 5 s segment corresponds to a PR segment. The first solution we propose is a fully convolutional neural network, and the second solution integrates recurrent layers.

3.1. First Architecture: Fully Convolutional Neural Network

Panel a of Figure 2 shows the overall architecture of the first solution (S_1). It consists of λ convolutional blocks, each one composed of a convolutional, a maximum pooling and a dropout layer.

Convolutional layers apply temporal convolution to the input signal. M different convolution kernels of size L allows obtaining M representations of the signal. The $\ell = 1, \ldots, M$-th output for the input signal $s[n]$ is calculated as follows:

$$c_1^{(\ell)}[n] = \phi\left(\sum_{i=0}^{L-1} w_i^{(\ell)} s[n-i] + b_i^{(\ell)}\right) \tag{1}$$

where w and b are the weights and biases, respectively, of the convolution kernel (adjusted during training) and $\phi(\cdot)$ is an activation function. The linear rectifier was adopted as activation function, i.e., $\phi(\cdot) = \max\{0, \cdot\}$. Since no padding was applied to $s[n]$ the length of $c_1^{(\ell)}[n]$ was $N_{c_1} = N - L + 1$ (the first $L - 1$ samples were discarded). The outputs of the first convolutional layer are fed into a max-pooling layer, which downsamples each input signal by applying the maximum operation with a pool size $K = 2$ to non-overlapping signal segments:

$$p_1^{(\ell)}[n] = \max\{c_1^{(\ell)}[k]\}_{k=(n-1)K+1}^{n\cdot K} \quad \text{for} \quad n = 1, \ldots, \left\lfloor \frac{N_{c_1}}{K} \right\rfloor \tag{2}$$

The next step is to apply the dropout operation, which is only present during training and it is a common technique to avoid overfitting. It consists in dropping out some units under a certain probability α at each training step in a mini-batch. When some units are removed different networks are created at each step, so it can be seen as an ensemble technique. Let us denote the outputs of this layer as $d_1^{(\ell)}[n]$, which will have the same size as $p_1^{(\ell)}[n]$. Note that once the network is trained $d_1^{(\ell)}[n] = p_1^{(\ell)}[n]$.

Pooling layers remove redundant information and reduce the computational cost of the upper layers. The convolution operation of the network permits learning time-invariant features. We added more convolutional blocks with the same number of kernels M of size L. The outputs of the second convolutional layer are given by the following equation:

$$c_2^{(\ell)}[n] = \phi\left(\sum_{j=1}^{M}\sum_{i=0}^{L-1} w_{ij}^{(\ell)} d_1^{(j)}[n-i] + b_{ij}^{(\ell)}\right) \tag{3}$$

These outputs are fed into another max-pooling and dropout layers to obtain $d_2^{(\ell)}[n]$, with M different representations of N_{d_2} samples. The above equations can be easily adapted to obtain the outputs of the i-th convolutional block ($c_i^{(\ell)}$, $p_i^{(\ell)}$ and $d_i^{(\ell)}$) for $i = 1, \ldots, \lambda$, where λ is the number of convolutional blocks.

The next layer is another pooling layer, namely a global maximum pooling layer. Having M different representations of the signal the maximum value of each representation is adopted to obtain a feature vector of M elements, i.e.,

$$\boldsymbol{v}_{D_1} = \max\{d_\lambda^{(\ell)}[n]\}_n \quad \text{for} \quad \ell = 1, \ldots, M \tag{4}$$

Finally, a fully connected layer was used as classification stage. This layer is composed of a single neuron with sigmoid activation function to produce p_{PR}:

$$p_{PR} = \frac{1}{1 + e^{-(\boldsymbol{w}\cdot\boldsymbol{v}_{\mathrm{D}_1} + \boldsymbol{b})}} \tag{5}$$

According to [48], it is especially useful to train some layers of the network under the constraint $||\boldsymbol{w}|| < \gamma$ when using dropout. This additional constraint during the training process reduces overfitting, so every convolutional layer was trained with $\gamma = 3.5$.

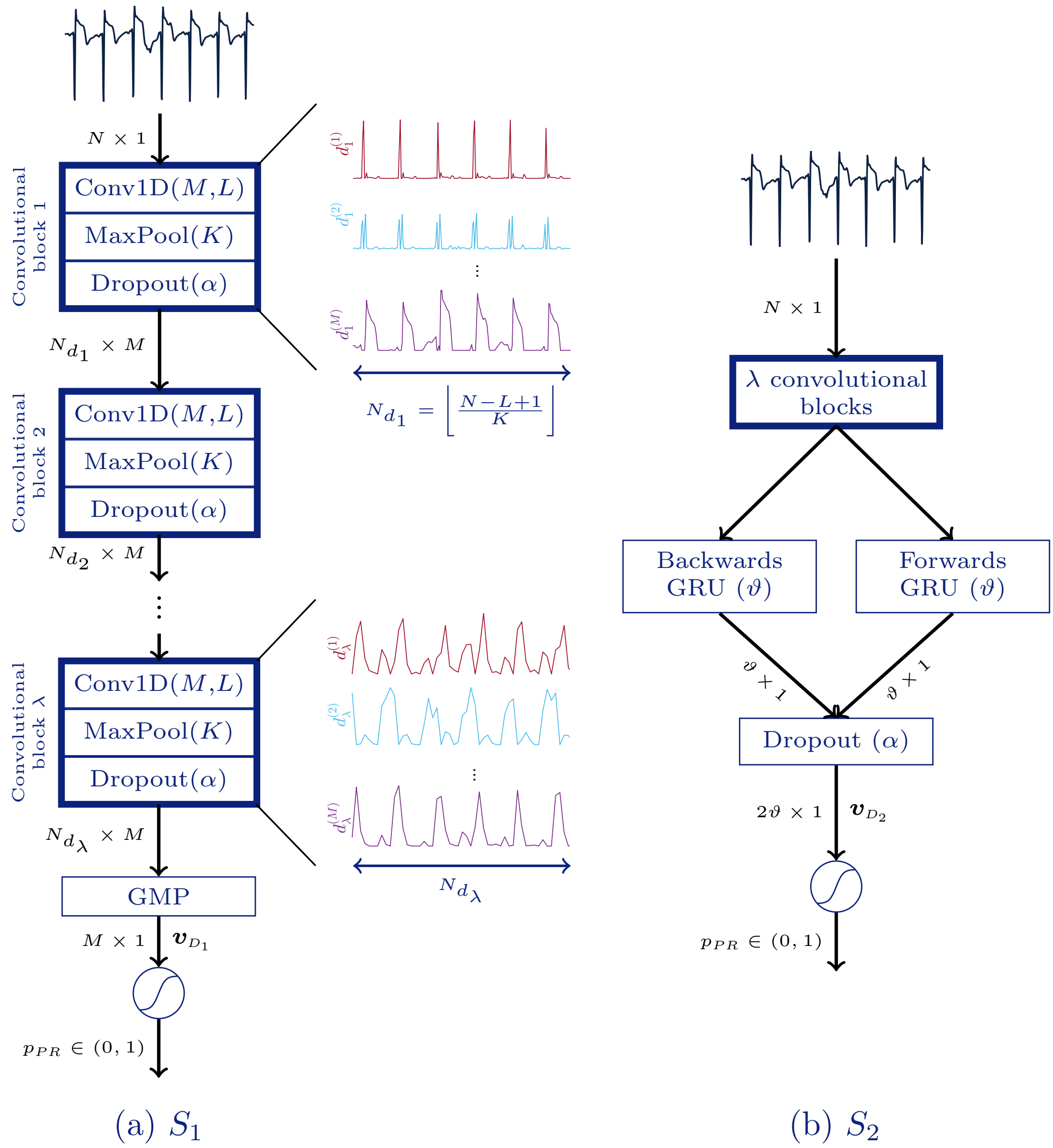

Figure 2. Architectures of the proposed deep neural networks. The fully convolutional solution (S_1), (**a**), is fed with an electrocardiogram (ECG) segment of N samples and includes up to λ convolutional blocks, a global maximum pooling layer (GMP), and a final fully connected layer which provides final likelihood of PR, p_{PR}. The S_2 solution, (**b**), includes up to λ convolutional blocks, a bidirectional gated recurrent unit (BGRU), an extra dropout layer, and a fully connected layer.

3.2. Second Architecture: CNN Combined with a Recurrent Layer

PEA and PR segments show different temporal behaviour. For instance, the time evolution for PR segments is known to be more regular than for PEA segments. These kind of temporal dynamics can be learned by a RNN. So the second solution proposed in this study (S_2) combines CNN and a bidirectional gated recurrent unit (BGRU), as shown in panel b of Figure 2.

GRU [49] is a simplified version of the well-known long short-term memory (LSTM) [50] with a similar performance [49]. These layers resolve long-term dependencies and avoid vanishing gradient problems. BGRU was inserted between the last convolutional block and the classification stage, removing the global maximum pooling layer. BGRU is composed of two GRU layers, one forward and the other one backward, so more sophisticated temporal features can be extracted by exploiting past and future information at time step n. Finally, both outputs were concatenated. A single GRU calculates hidden states $\boldsymbol{h}_n$ at time step $n = 1, \ldots, N_{d_\lambda}$ based on the past state. Given $\mathbf{D} = [d_\lambda^{(1)}, \ldots, d_\lambda^{(M)}]$, the equations of the forwards GRU are described as follows:

$$\boldsymbol{z}_n = \sigma(\mathbf{W}_z\mathbf{D} + \mathbf{U}_z\boldsymbol{h}_{n-1} + \boldsymbol{b}_z) \tag{6}$$

$$\boldsymbol{r}_n = \sigma(\mathbf{W}_r\mathbf{D} + \mathbf{U}_r\boldsymbol{h}_{n-1} + \boldsymbol{b}_r) \tag{7}$$

$$\boldsymbol{h}'_n = \tanh(\mathbf{WD} + \boldsymbol{r}_n \odot \mathbf{U}\boldsymbol{h}_{n-1} + \boldsymbol{b}) \tag{8}$$

$$\boldsymbol{h}_n = \boldsymbol{z}_n \odot \boldsymbol{h}_{n-1} + (1 - \boldsymbol{z}_n) \odot \boldsymbol{h}'_n \tag{9}$$

where $\mathbf{W}$ and $\mathbf{U}$ are weight matrices, $\boldsymbol{b}$ is the bias vector, $\sigma(\bullet)$ stands for sigmoid function, and $\odot$ is the Hadamard product. In the equations above $\boldsymbol{z}_n$ and $\boldsymbol{r}_n$ correspond to the update and reset gates, respectively. The backwards GRU works in the same way but the temporal representations of the input are flipped. The hidden state at the last time step, $\boldsymbol{h}_{n=N_{d_\lambda}}$, is fed in to the next layer. Having ϑ units for each direction, a total of 2ϑ features, $\boldsymbol{v}_{\mathrm{D}_2} = [v_{\mathrm{D}_2}^{(1)}, \ldots, v_{\mathrm{D}_2}^{(2\vartheta)}]$, are fed to the last classification layer after applying dropout. The convolutional and recurrent layers were trained under the constraint $||\boldsymbol{w}|| < \gamma$.

Another kind of dropout in RNN is recurrent dropout [51], which affects the connections between recurrent units instead of the inputs/outputs of the layer. A recurrent dropout fraction of 0.15 was used to train the final model.

This architecture is optimized simultaneously to obtain the optimal representations of the signal (convolutional layers) and obtain the optimal temporal features (BGRU) for an artificial neural network classifier (fully connected layer).

3.3. Training Process

The weights and biases of every layer were optimized using the adaptive moment estimation (ADAM) optimizer [52]. ADAM is a stochastic gradient descent algorithm with adaptive learning rate. According to [52], good default settings are a learning rate of 0.001 and exponential decay rates of 0.9 and 0.999.

The training data were fed into the DNN in batches of 8 during 75 epochs. At the beginning of each epoch training data were shuffled, so the mini-batches at each epoch were different. Additionally, zero-mean Gaussian noise with standard deviation of 10^{-4} was added to the signal, and its amplitude was modified by $\pm 2\%$ (uniformly distributed) at each mini-batch. This process enriches the generalization of the model, as the input data for each epoch differs slightly.

The cost function to minimize was the binary cross-entropy:

$$\mathcal{L}(p) = \sum_i \eta_i \left[y_i^{(true)} \ln(p_{PR_i}) + (1 - y_i^{(true)}) \ln(1 - p_{PR_i}) \right] \tag{10}$$

where $y^{(true)} = \{0 : \mathrm{PEA}, 1 : \mathrm{PR}\}$ are the manual annotations and η_i are the sample weights. As patients contribute with different number of segments, every patient was weighted equally to train the DNN, so the sum of η_i within the same patient is equal to 1.

Every experiment was carried out using Keras framework [53] with Tensorflow backend [54]. The DNNs were trained on an NVIDIA GeForce GTX 1080 Ti.

3.4. Uncertainty Estimation

The network's output, p_{PR}, represents the likelihood of PR, but it is not an indicator of the prediction confidence of the model. The uncertainty of the DNN decision can be estimated using dropout and data augmentation also during the test phase, a procedure known as Monte–Carlo dropout [55]. For each segment of the test set the prediction is repeated N times but adding two random effects: dropout in the DNN network, and the addition of white noise to the ECG. This produces N values of p_{PR}, and the variance of those values is interpreted as the uncertainty of the prediction. In our experiments N was set to 100. The decisions in the test set with an uncertainty above an acceptable threshold were discarded, and in those cases feedback would not be given to the rescuer. The threshold of uncertainty is determined in the training set. The uncertainty of each training instance is computed and the threshold is determined as the uncertainty for which a proportion of feedbacks will be given. In our experiments we tested a proportion of feedbacks from 100% to 80%.

4. Baseline Approaches

Machine learning solutions based on well-known ECG features were implemented and compared with S_1 and S_2. A total of nine hand-crafted features proposed in [34], $\boldsymbol{v} = [v^{(1)}, \ldots, v^{(9)}]$, were computed. They quantify the PR/PEA differences in terms of QRS complex rate and narrowness, slope steepness, spectral energy distribution, and regularity of the signal (fuzzy entropy).

Three classifiers were optimized and trained:

- **RF:** Introduced in [56], RF constructs many weak learners, each trained with a certain proportion of the training data, φ. Each subset is generated by resampling with replacement. Each weak learner is a tree, and only ψ features are considered (drawn randomly from an uniform distribution) at each node. The final decision is made by majority voting. We set the number of trees to 300, and optimized the hyper-parameters φ and ψ.
- **Support vector machine (SVM):** Given a feature vector $\boldsymbol{v}$, the SVM makes the prediction using the following formula [57]:
$$y^{(pred)} = \text{sign}\Big(b + \sum_{i=1}^{N_s} w_i K(\boldsymbol{v}, \boldsymbol{v_i})\Big) \tag{11}$$
where b is the intercept term and N_s is the number of support vectors (w_i is non-zero only for these vectors). Here $K(\cdot,\cdot)$ denotes the kernel function, which for a Gaussian kernel with γ_s width is:
$$K(\boldsymbol{v}, \boldsymbol{v_i}) = \exp(-\gamma_s ||\boldsymbol{v} - \boldsymbol{v_i}||^2) \tag{12}$$
The hyper-parameters soft margin C and γ_s were optimized for the SVM.
- **Kernel logistic regression (KLR):** This is a version of the well-known logistic regression by applying a kernel-trick [57,58]. The prediction is made using Equation (11), and the kernel of Equation (12). The hyper-parameters to optimize were the regularization-term λ_l and γ_s.

5. Evaluation Setup and Optimization Process

5.1. Evaluation Setup

The performance of the models was evaluated in terms of sensitivity (Se, probability of correctly identifying PR), specificity (Sp, probability of correctly identifying PEA), and balanced accuracy (BAC, arithmetic mean between Se and Sp). The balanced error rate (BER) was defined as $1 - \text{BAC}$. As patients have different numbers of segments, every patient was weighted equally to compute the performance metrics.

5.2. Hyper-Parameter Optimization Process

The hyper-parameters of every model were optimized using Bayesian optimization (BO) [59]. BO is a probabilistic model based approach that attempts to minimize an objective function associated with a real-valued metric, and the variables to optimize can be discrete or continuous. Recent studies report that BO is more efficient than grid search, random search, or manual tuning since it requires less time and the overall performance on the test set is better [60].

BO approximates the objective function to a surrogate function that is cheaper to evaluate. At each iteration a candidate solution is tested to update the surrogate using the past information. With more iterations the approximation of the surrogate is better. BO algorithm variants differ on how this surrogate is constructed. In this study we considered tree-structured parzen estimators (BO-TPE, to optimize S_1 and S_2) and Gaussian processes (BO-GP, to optimize RF, SVM, and KLR) [60,61].

The training data were divided patient-wise into 4 folds, and the cross-validated BER was the objective function to minimize. The search space for all models is shown in Table 1.

Table 1. Search space of Bayesian optimization (BO) for all models. Here $\mathcal{U}(\min, \max)$ denotes a uniform distribution between min and max values.

Model	Hyper-Parameters
RF	$\vartheta = \mathcal{U}(0.5, 1)$ $\psi = \{1, \ldots, 9\}$
SVM	$C = \mathcal{U}(0.001, 10{,}000)$ $\gamma_s = \mathcal{U}(0.001, 10{,}000)$
KLR	$\lambda_l = \mathcal{U}(0.0001, 0.2)$ $\gamma_s = \mathcal{U}(0.0001, 15)$
S_1	$\lambda = \{1,2,3,4,5\}$ $M = \{8,16,24\}$ $L = \{5,6,7,8\}$ $\alpha = \mathcal{U}(0.05, 0.5)$
S_2	$\lambda = \{1,2,3,4,5\}$ $M = \{8,16,24\}$ $L = \{5,6,7,8\}$ $\alpha = \mathcal{U}(0.05, 0.5)$ $\vartheta = \{4,5,6,7,8\}$

6. Results

The results of the BO-TPE algorithm applied for S_1 are shown in Figure 3. For each hyper-parameter the values of the cross-validated BER are given, continuous for α and median (10–90 percentiles) for the other discrete hyper-parameters. The distributions of the values selected by the optimizing algorithm are also shown (as histogram for α). The number of convolutional blocks, λ, and the dropout rate, α, turned out very determinant. Values of $\alpha > 0.3$ rapidly increased the BER, and including up to $\lambda = 4$ blocks was the most selected option by the optimization algorithm. The values of M and L in the selected range had small effect on the performance of the classifier.

Figure 4 shows the results of BO-TPE for S_2. Increasing λ overfitted the model rapidly and BER was minimum for $\lambda = 2$; less convolutional blocks did not provide detailed enough features and increasing λ overfitted the model. Another influential hyper-parameter was α, which showed minimum BER values around 0.4. The hyper-parameters M, L, and ϑ had little effect on BER.

Figure 5 shows the results of the BO-GP algorithm applied to tune the hyper-parameters of the KLR, SVM, and RF models. The cross-validated BER is color-coded (KLR and SVM) or depicted in the vertical axis (RF). Each point shows a single hyper-parameter combination tested by the BO-GP. In the case of KLR, both hyper-parameters were important, but low values of λ_l especially yielded lower BER values. For the SVM, low values of C and high values of γ_s produced the worst results, but the selection in the range of values was not as critical as in the KLR solution. Lastly, for RF $\psi = 1$ was the best option, particularly for $0.5 < \varphi < 0.6$, although the fine tuning of φ was not critical.

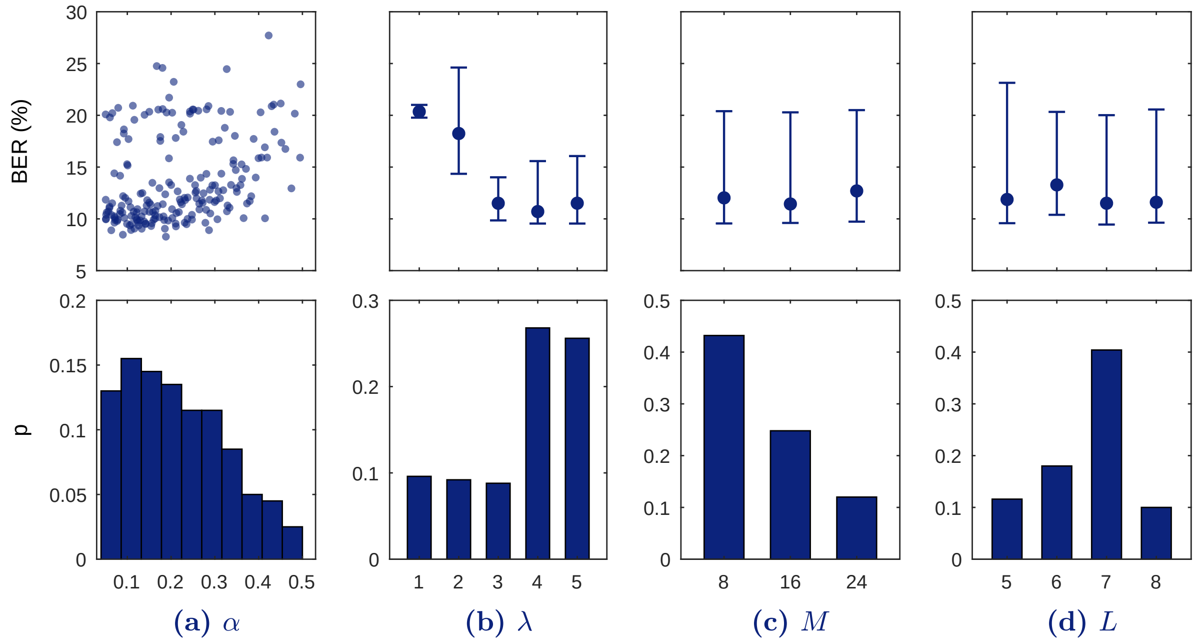

Figure 3. Results of the Bayesian optimization with tree-structured parzen estimators (BO-TPE) optimization algorithm for every hyper-parameter range in S_1. In the top row balanced error rate (BER) is shown for each continuous value (**a**) or for each discrete value as median and 10–90 percentiles (**b**–**d**). The bottom figures show the probability of selection of the hyper-parameter values in the BO-TPE algorithm.

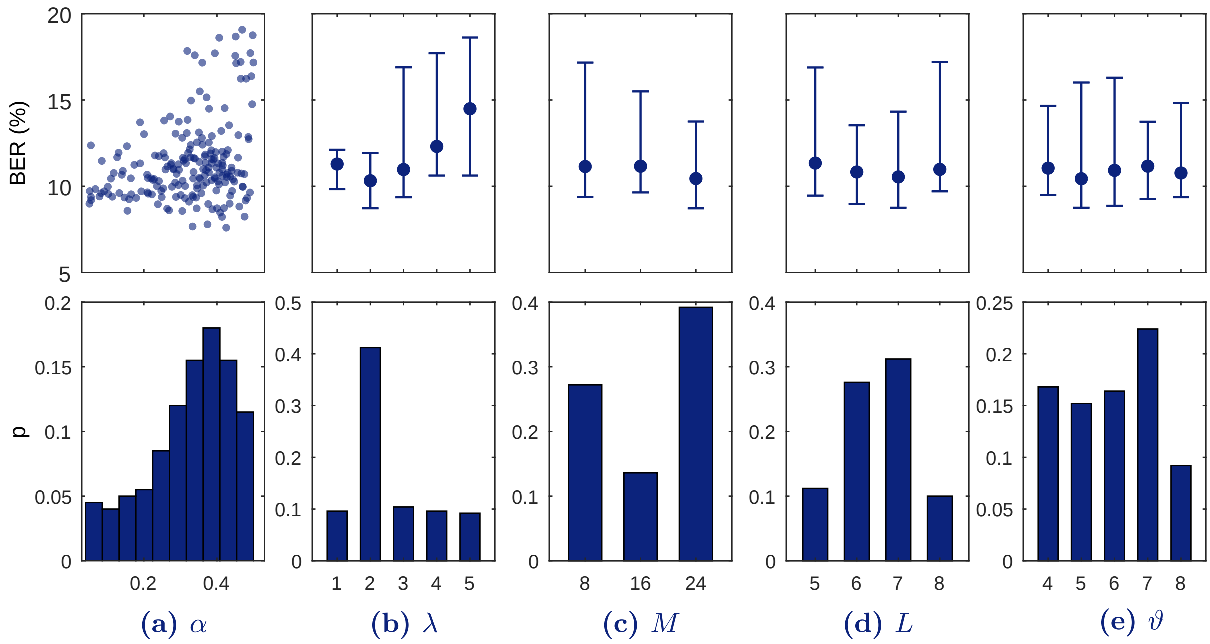

Figure 4. Results of the BO-TPE optimization algorithm for every hyper-parameter range in S_2. On the top BER is shown for each continuous value (**a**) or for each discrete value as median and 10–90 percentiles (**b**–**e**). The bottom figures show the probability of selection of the hyper-parameter values in the BO-TPE algorithm.

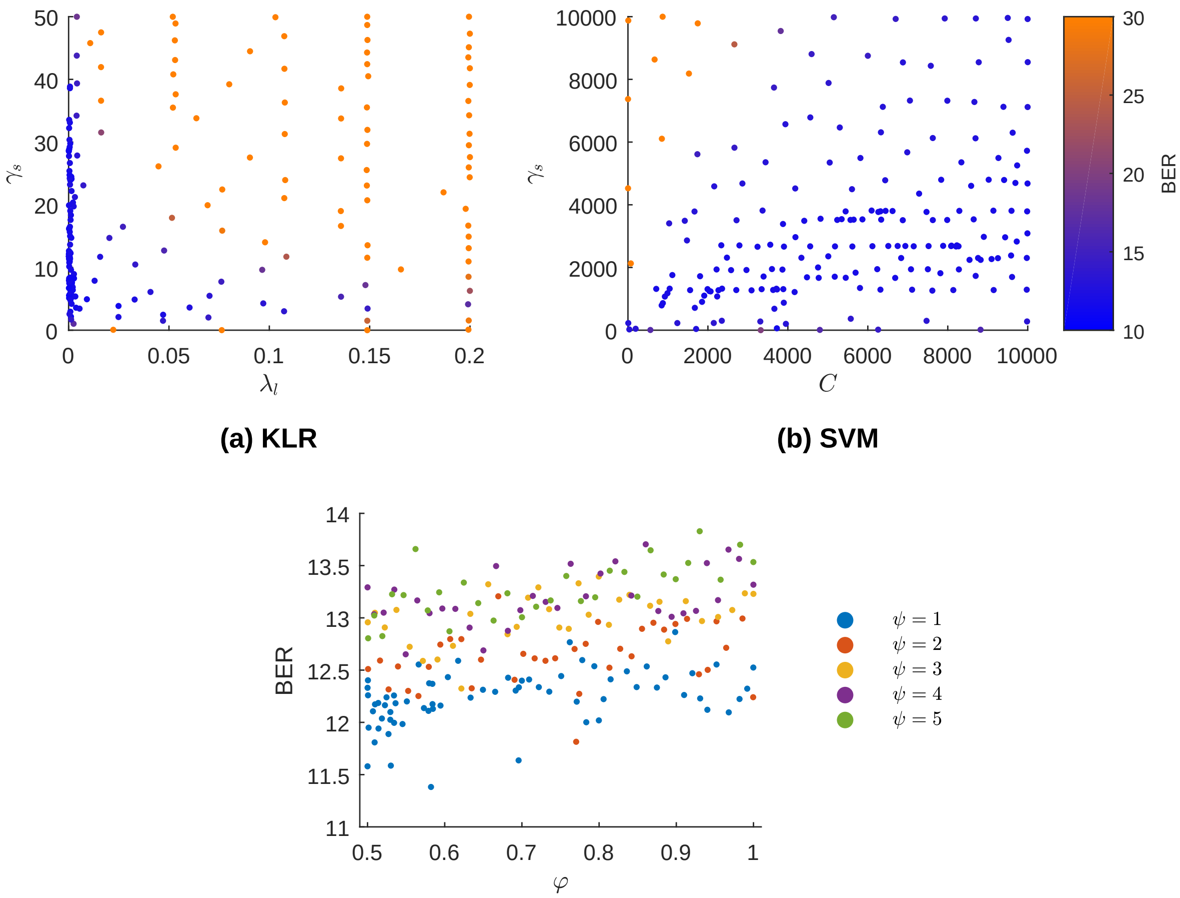

(a) KLR **(b) SVM** **(c) RF**

Figure 5. Bayesian optimization with Gaussian processes (BO-GP) results for three different machine learning models. The BER is color-coded in (**a**,**b**) (kernel logistic regression (KLR) and support vector machine (SVM) classifiers) and each point represents the selected solution of the BO-GP in some iteration. In (**c**) (random forest (RF) classifier), discrete values of ψ are color-coded and BER plotted for a range of values for φ.

Table 2 shows the overall test results of the baseline models and the deep learners in terms of Se, Sp, and BAC, and the set of selected hyper-parameters tuned during the optimization process. There were no differences between the RF, SVM, and KLR models, and any of the deep learning solutions outperformed the baseline models by nearly two percentage points of BAC. Although there was no difference in performance between S_1 and S_2, the training process of S_1 is simpler with less trainable parameters than S_2 (1441 vs. 4777).

In Table 3 the computation time of the different models is compared. The mean time required to classify the 5 s segment is given, separately for the baseline classifiers in terms of required time for feature extraction (t_1) and classification (t_2). Processing times were calculated on a single core of an Intel Xeon 3.6 GHz. As shown in Table 3 the fully convolutional solution, S_1, was by far the fastest one followed by the baseline models.

Table 2. Summary of the performance of the deep learners and baseline models with the test set and the optimal hyper-parameters chosen by the Bayesian optimization with Gaussian processes (BO-GP) and Bayesian optimization with tree-structured parzen estimators (BO-TPE) algorithms with 5-s electrocardiogram (ECG) segments. DNN models outperformed baseline models in terms of BAC.

	Se (%)	Sp (%)	BAC (%)	Hyper-Parameters
Baseline models				
RF	96.0	87.4	91.7	$\{\varphi, \psi\} = \{0.58, 1\}$
SVM	97.6	86.2	91.9	$\{C, \gamma_s\} = \{2038, 1246\}$
KLR	97.5	86.2	91.8	$\{\lambda_l, \gamma_s\} = \{0.0013, 7\}$
DNN models				
S_1	94.1	92.9	**93.5**	$\{\lambda, M, L, \alpha\} = \{4, 8, 7, 0.2\}$
S_2	95.5	91.6	**93.5**	$\{\lambda, M, L, \alpha, \vartheta\} = \{2, 24, 6, 0.4, 6\}$

Table 3. Computation time to classify a 5-s segment for the baseline and deep neural network (DNN) models. The fastest model was S_1.

	t_1 (ms)	t_2 (ms)	Total (ms)
Baseline models			
RF	63.5	0.28	63.8
SVM	63.5	0.35	63.9
KLR	63.5	0.25	63.8
DNN models			
S_1	-	-	**1.6**
S_2	-	-	101.1

Comparative analyses were performed between the 9 hand-crafted features of the baseline models ($\boldsymbol{v}$) and the features learnt by DNN solutions S_1 and S_2 ($\boldsymbol{v}_{D_1}$ and $\boldsymbol{v}_{D_2}$ respectively). The area under the curve (AUC) for $\boldsymbol{v}$ ranged between 0.88 and 0.94, showing that they had been wisely selected in different domains as described in [34]; but the $M = 8$ features ($\boldsymbol{v}_{D_1}$) that S_1 extracted reported high discriminative values from 0.61 to 0.97, showing that the deep architecture found some very selective features. Next, feature sets from the deep learners $\boldsymbol{v}_{D_1}$ and $\boldsymbol{v}_{D_2}$ were fed into the baseline classifiers to compare their performance with that of the original $\boldsymbol{v}$. The BO-GP optimization procedure was repeated for the RF, SVM, and KLR classifiers and results for the test set are depicted in Figure 6. Training the classifiers with $\boldsymbol{v}_{D_1}$ and $\boldsymbol{v}_{D_2}$ yielded higher BAC values than those obtained with the pre-designed $\boldsymbol{v}$ features. This experiment shows that features defined by the neural networks integrate information not considered by the hand-crafted features, and that they can be successfully used with other classifiers.

The duration of the ECG segment fed into any of the solutions is critical when using a pulse detection algorithm during OHCA treatment. During CPR the ECG signal is strongly affected by chest compression artefacts and electrical defibrillation attempts. For any diagnosis based on the ECG, intervals free of artefact must be used, i.e., extracted either during pauses for rhythm analysis or during chest compression pauses. The segment length used in this study is below the typical interruption for a rhythm analysis, which is between 5.2–26.3 s [62]. However, decreasing the length of the analysis segment would contribute to shorter interruptions in compressions for pulse detection. Reducing hands-off intervals that compromise oxygen delivery to the vital organs increases survival rates [63,64]. Consequently, the solutions of this proposal were tested for different segment durations, from 5 s down to 2 s. The models that were trained for 5-s ECG segments were used, features were extracted using the first seconds of the segment, and those features were fed into the baseline models. The DNN models were fed with the same first seconds of the ECG segments used for feature calculation (note that S_1 and S_2 can work with any segment duration at the input). As shown in Figure 7 the best performance for the baseline models was obtained for segment lengths of 5 s. The DNN models outperformed the best baseline models for any segment length, including segments as short as 2 s.

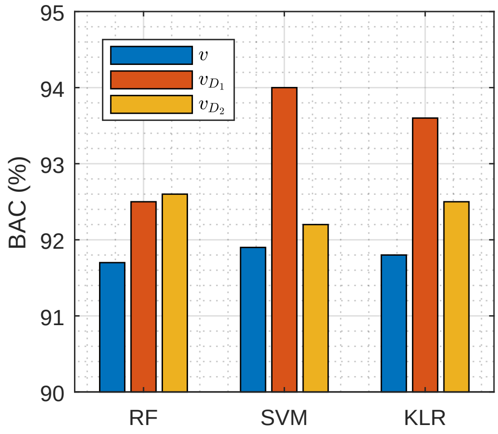

Figure 6. Performance of RF, SVM, and KLR classifiers with hand-crafted features (v), and features extracted by the deep learning architectures S_1 and S_2 (v_{D_1} and v_{D_2} respectively).

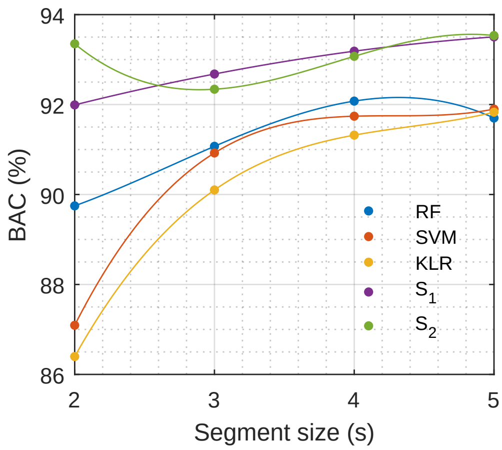

Figure 7. Performance of different models in terms of balanced accuracy (BAC) depending on the duration of the input ECG segment.

A last evaluation of S_1 was performed to assess the influence of the degree of uncertainty in the decision of the model. Table 4 shows the performance of the model if the system was designed to give feedback only in a percentage of the analyses, those in which the uncertainty of the decision was lowest. Different percentage thresholds were tested in the training set, from 100% (always give feedback) to 80% (give feedback when the uncertainty is low). Assuming no feedback in 5% of the cases increased the BAC by one percentage point, and the BAC increased up to 97.6% if the system was designed to discard the 20% of the analyses with largest uncertainty.

Table 4. Performance of S_1 with different degrees of uncertainty. Scores are given for the test set and the percentage of feedback in the test set are reported. The threshold for feedback was set in the training set.

Training Percentage	Testing Percentage	Se (%)	Sp (%)	BAC (%)
80	78.5	100	95.2	97.6
90	89.6	96.6	93.2	94.9
95	95.4	97.1	92.2	94.6
97.5	98.1	96.3	92.1	94.2
100	100	94.1	92.9	93.5

7. Discussion and Conclusions

Pulse detection during OHCA is still an unsolved problem, and there is a need for automatic methods to assist the rescuer (bystander or medical personnel) to decide whether the patient has pulse or not [10]. Non-invasive pulse detection is still a challenging problem [16], and no solutions are currently integrated in monitors/defibrillators. To the best of our knowledge, this is the first study that uses DNN models to discriminate between PR and PEA rhythms using exclusively the ECG.

The two DNN models proposed in this study outperformed the best PR/PEA discriminators based exclusively on the ECG published to date. A RF classifier based on hand-crafted features was proposed in [34] and reported Se/Sp of 88.4%/89.7% for a smaller dataset. A DNN model using a single convolutional layer followed by a recurrent layer was introduced in a conference paper [65], but the Se/Sp/BAC were 91.7%/92.5%/92.1% on the dataset used for this study, that is the BAC was 1.5 percentage points below the current solution. Other DNN solutions were tested in another conference paper [66], where we reported BAC values of 91.2% and 92.6% for preliminary versions of S_1 and S_2. Performance was improved in this study adding a general DNN architecture with multiple convolutional layers, a Bayesian optimization procedure which provided insights into the critical hyper-parameters of the networks (see Figures 3 and 4), and a better data augmentation procedure. All these factors contributed to an improved BAC of 93.5% for S_1 and S_2, an increase of nearly 2 points from a baseline BAC around 92%, i.e., achieving 20% of the available margin for improvement (8 points) on our initial architectures. Furthermore, we also introduced a new usage framework in which the algorithm was able to automatically assess the uncertainty of the decision, and improved feedback by only reporting decisions with low uncertainties.

There was no difference in terms of BAC between S_1 and S_2. The second solution is more complex and should be able to capture more sophisticated features of the signal. However, the number of trainable parameters was 1441 in S_1 and 4777 in S_2. Increasing the number of trainable parameters makes the DNN model prone to overfitting, the model "memorizes" the training data loosing generalization capacity and shows poorer performance with unseen data [67,68]. In fact, S_2 showed higher accuracies during training than S_1 (98.5% vs. 96.6%). Besides, training was computationally more costly for S_2, optimizing S_1 required $\approx$ 37 h and optimizing $S_2 \approx$ 82 h. However, it is possible that with larger datasets S_2 could generalize better and provide a more accurate model, but OHCA datasets with pulse annotations are costly.

DNN architectures are capable of automatically learning the discrimination features. Our results show that the features learned by S_1 and S_2 produced more accurate PR/PEA classifiers than hand-crafted features when fed to the classical machine learning models (see Figure 6). The DNN architectures were able to capture some important ECG characteristics for the identification of pulse that are not accounted for in the hand-crafted features proposed in the literature. In particular, the most discriminative features were those learned by S_1, which when fed to an SVM classifier boosted the BAC from 92% for hand-crafted features to above 94%.

One of the salient features of the proposed DNN solutions is that they are based solely on the ECG. The ECG is available in all defibrillators/monitors used to treat OHCA patients, so it could be integrated into any equipment. PR/PEA discrimination algorithms that use the ECG and TI have also been proposed [28,29], the TI adds relevant information because effective heartbeats may produce small fluctuations in the TI [23,24]. The BACs of ECG/TI-based PR/PEA discriminators using classical machine learning approaches were around 92% for smaller datasets [28,29]. Defibrillators measure the impedance to check that pads are properly attached to the patient's chest, that is the reason why the TI signal is not recorded with mΩ amplitude resolution in many devices. In any case, multi-modal deep learning solutions could be explored to increase the accuracy by designing DNN solutions that use both the ECG and TI signals. Moreover, S_1 extracted significant features, so it could be used as a feature extractor and those features could be combined with features derived from the TI, and other surrogate measures of the hemodynamic state of the patient.

Another critical factor of automatic PR/PEA discrimination algorithms is the ECG segment length needed for an accurate decision. PR/PEA discrimination algorithms need an ECG without chest compression artefacts, this means that compressions have to be interrupted for pulse detection. Pauses in chest compressions compromise the survival of the patient [63,64]. Therefore, current guidelines recommend interruptions of less than 10 s for pulse checks [4,10], but in practice these interruptions are longer than 10 s in more than 50% of cases [14,15]. Our DNN models were very accurate for a segment length of 5 s. Moreover, the length of the segment could be shortened down to 2 s without compromising the BAC of our models (see Figure 7). Consequently, our automatic algorithm could be used to reliably detect pulse during OHCA with interruptions as short as 2–3 seconds, and could be used to avoid the excessively long pauses in chest compressions for pulse detection observed during OHCA treatment.

Measuring the uncertainty of the prediction may be useful when misclassifying an input has a considerable cost, for instance a false pulse indication may unnecessarily interrupt a life saving therapy like CPR. Many efforts have been made to estimate the uncertainty in DNN models, but it is still a challenging problem [69–73]. In this work the uncertainty of the decision was measured using a method known as Monte–Carlo dropout [55], and we found that only giving feedback when the uncertainty was low considerably increased the BAC. For instance, giving a feedback in the 95% of the cases improved the BAC by more than 1 point, and only giving feedback in 80% of cases increased the BAC by over 4 points. During OHCA treatment CPR should be continued until a reliable pulse detection is identified by the algorithm, and the pauses in compressions for the potential feedbacks (reliable or unreliable) will be short, since our algorithms only require ECG segments of 2–3 s. Further work should be done to improve the estimate of the uncertainty of the decision, so that BACs of 97% could be obtained by discarding less than 20% of the potential feedbacks.

In conclusion, this study introduces the use of deep neural networks to discriminate between pulseless and pulsatile rhythms during OHCA using only the ECG. The proposed DNN models outperformed hand-crafted feature-based machine learning solutions, and were able to accurately detect pulse with ECG segments as short as 2–3 s. Moreover, a first attempt at a quantification of the uncertainty of the decision was also introduced to improve the reliability of the feedback given to the rescuer. The proposed solution is based exclusively on the ECG and could be integrated into any monitor/defibrillator.

Author Contributions: A.E. and E.A. (Elisabete Aramendi) conceived and designed the study. A.E. programmed the experiments and obtained the results. A.E., E.A. (Elisabete Aramendi) and U.I. participated in the curation and annotation of datasets. E.A. (Elisabete Aramendi), U.I., A.P. and E.A. (Erik Alonso). helped with the interpretation of the experiments. A.I. and P.O. provided the datasets from the defibrillators, and helped with the interpretation of the biomedical signals and the clinical information. All authors contributed to the writing of the manuscript.

Funding: This work was supported by: The Spanish Ministerio de Economía y Competitividad, TEC2015-64678-R, jointly with the Fondo Europeo de Desarrollo Regional (FEDER), UPV/EHU via GIU17/031 and the Basque Government through the grant PRE_2018_2_0260.

Conflicts of Interest: A.I. receives research grants from the US National Institutes of Health (NIH) and serves as an unpaid volunteer on the American Heart Association National Emergency Cardiovascular Care Committee and the HeartSine, Inc. Clinical Advisory Board.

Abbreviations

The following abbreviations are used in this manuscript:

ADAM	Adaptive moment estimation
AED	Automated external defibrillator
AS	Asystole
AUC	Area under the curve
BAC	Balanced accuracy
BER	Balanced error rate

BO	Bayesian optimization
BO-GP	Bayesian optimization with Gaussian processes
BO-TPE	Bayesian optimization with tree-structured parzen estimators
CNN	Convolutional neural network
CPR	Cardiopulmonary resuscitation
DNN	Deep neural network
ECG	Electrocardiogram
BGRU	Bidirectional gated recurrent unit
KLR	Kernel logistic regression
OHCA	Out-of-hospital cardiac arrest
PEA	Pulseless electrical activity
PR	Pulsed rhythm
RF	Random forest
RNN	Recurrent neural network
ROSC	Return of Spontaneous Circulation
Se	Sensitivity
Sp	Specificity
SVM	Support vector machine
TI	Thoracic impedance
VF	Ventricular fibrillation
VT	Ventricular tachycardia

References

1. Gräsner, J.T.; Bossaert, L. Epidemiology and management of cardiac arrest: What registries are revealing. *Best Pract. Res. Clin. Anaesthesiol.* **2013**, *27*, 293–306. [CrossRef] [PubMed]
2. Berdowski, J.; Berg, R.A.; Tijssen, J.G.; Koster, R.W. Global incidences of out-of-hospital cardiac arrest and survival rates: Systematic review of 67 prospective studies. *Resuscitation* **2010**, *81*, 1479–1487. [CrossRef] [PubMed]
3. Deakin, C.D. The chain of survival: Not all links are equal. *Resuscitation* **2018**, *126*, 80–82. [CrossRef] [PubMed]
4. Perkins, G.D.; Handley, A.J.; Koster, R.W.; Castrén, M.; Smyth, M.A.; Olasveengen, T.; Monsieurs, K.G.; Raffay, V.; Gräsner, J.T.; Wenzel, V.; et al. European Resuscitation Council Guidelines for Resuscitation 2015: Section 2. Adult basic life support and automated external defibrillation. *Resuscitation* **2015**, *95*, 81–99. [CrossRef] [PubMed]
5. Bahr, J.; Klingler, H.; Panzer, W.; Rode, H.; Kettler, D. Skills of lay people in checking the carotid pulse. *Resuscitation* **1997**, *35*, 23–26. [CrossRef]
6. Eberle, B.; Dick, W.; Schneider, T.; Wisser, G.; Doetsch, S.; Tzanova, I. Checking the carotid pulse check: Diagnostic accuracy of first responders in patients with and without a pulse. *Resuscitation* **1996**, *33*, 107–116. [CrossRef]
7. Ochoa, F.J.; Ramalle-Gomara, E.; Carpintero, J.; Garcıa, A.; Saralegui, I. Competence of health professionals to check the carotid pulse. *Resuscitation* **1998**, *37*, 173–175. [CrossRef]
8. Lapostolle, F.; Le Toumelin, P.; Agostinucci, J.M.; Catineau, J.; Adnet, F. Basic cardiac life support providers checking the carotid pulse: Performance, degree of conviction, and influencing factors. *Acad. Emerg. Med.* **2004**, *11*, 878–880. [CrossRef]
9. Tibballs, J.; Russell, P. Reliability of pulse palpation by healthcare personnel to diagnose paediatric cardiac arrest. *Resuscitation* **2009**, *80*, 61–64. [CrossRef] [PubMed]
10. Soar, J.; Nolan, J.; Böttiger, B.; Perkins, G.; Lott, C.; Carli, P.; Pellis, T.; Sandroni, C.; Skrifvars, M.; Smith, G.; et al. Section 3. Adult advanced life support: European Resuscitation Council Guidelines for Resuscitation 2015. *Resuscitation* **2015**, *95*, 100–147. [CrossRef]
11. Ruppert, M.; Reith, M.W.; Widmann, J.H.; Lackner, C.K.; Kerkmann, R.; Schweiberer, L.; Peter, K. Checking for breathing: Evaluation of the diagnostic capability of emergency medical services personnel, physicians, medical students, and medical laypersons. *Ann. Emerg. Med.* **1999**, *34*, 720–729. [CrossRef]
12. Perkins, G.D.; Stephenson, B.; Hulme, J.; Monsieurs, K.G. Birmingham assessment of breathing study (BABS). *Resuscitation* **2005**, *64*, 109–113. [CrossRef]

13. Zengin, S.; Gümüşboğa, H.; Sabak, M.; Eren, Ş.H.; Altunbas, G.; Al, B. Comparison of manual pulse palpation, cardiac ultrasonography and Doppler ultrasonography to check the pulse in cardiopulmonary arrest patients. *Resuscitation* **2018**, *133*, 59–64. [CrossRef] [PubMed]
14. Clattenburg, E.J.; Wroe, P.; Brown, S.; Gardner, K.; Losonczy, L.; Singh, A.; Nagdev, A. Point-of-care ultrasound use in patients with cardiac arrest is associated prolonged cardiopulmonary resuscitation pauses: A prospective cohort study. *Resuscitation* **2018**, *122*, 65–68. [CrossRef]
15. in't Veld, M.A.H.; Allison, M.G.; Bostick, D.S.; Fisher, K.R.; Goloubeva, O.G.; Witting, M.D.; Winters, M.E. Ultrasound use during cardiopulmonary resuscitation is associated with delays in chest compressions. *Resuscitation* **2017**, *119*, 95–98. [CrossRef] [PubMed]
16. Babbs, C.F. We still need a real-time hemodynamic monitor for CPR. *Resuscitation* **2013**, *84*, 1297–1298. [CrossRef]
17. Irusta, U.; Ruiz, J.; Aramendi, E.; de Gauna, S.R.; Ayala, U.; Alonso, E. A high-temporal resolution algorithm to discriminate shockable from nonshockable rhythms in adults and children. *Resuscitation* **2012**, *83*, 1090–1097. [CrossRef] [PubMed]
18. Figuera, C.; Irusta, U.; Morgado, E.; Aramendi, E.; Ayala, U.; Wik, L.; Kramer-Johansen, J.; Eftestøl, T.; Alonso-Atienza, F. Machine learning techniques for the detection of shockable rhythms in automated external defibrillators. *PLoS ONE* **2016**, *11*, e0159654. [CrossRef]
19. Li, Q.; Rajagopalan, C.; Clifford, G.D. Ventricular fibrillation and tachycardia classification using a machine learning approach. *IEEE Trans. Biomed. Eng.* **2014**, *61*, 1607–1613. [PubMed]
20. Jekova, I.; Krasteva, V. Real time detection of ventricular fibrillation and tachycardia. *Physiol. Meas.* **2004**, *25*, 1167. [CrossRef] [PubMed]
21. Myerburg, R.J.; Halperin, H.; Egan, D.A.; Boineau, R.; Chugh, S.S.; Gillis, A.M.; Goldhaber, J.I.; Lathrop, D.A.; Liu, P.; Niemann, J.T.; et al. Pulseless electric activity: Definition, causes, mechanisms, management, and research priorities for the next decade: Report from a National Heart, Lung, and Blood Institute workshop. *Circulation* **2013**, *128*, 2532–2541. [CrossRef] [PubMed]
22. Ayala, U.; Irusta, U.; Ruiz, J.; Eftestøl, T.; Kramer-Johansen, J.; Alonso-Atienza, F.; Alonso, E.; González-Otero, D. A reliable method for rhythm analysis during cardiopulmonary resuscitation. *BioMed Res. Int.* **2014**, *2014*, 872470. [CrossRef] [PubMed]
23. Johnston, P.; Imam, Z.; Dempsey, G.; Anderson, J.; Adgey, A. The transthoracic impedance cardiogram is a potential haemodynamic sensor for an automated external defibrillator. *Eur. Heart J.* **1998**, *19*, 1879–1888. [CrossRef]
24. Pellis, T.; Bisera, J.; Tang, W.; Weil, M.H. Expanding automatic external defibrillators to include automated detection of cardiac, respiratory, and cardiorespiratory arrest. *Crit. Care Med.* **2002**, *30*, S176–S178. [CrossRef] [PubMed]
25. Losert, H.; Risdal, M.; Sterz, F.; Nysæther, J.; Köhler, K.; Eftestøl, T.; Wandaller, C.; Myklebust, H.; Uray, T.; Aase, S.O.; et al. Thoracic-impedance changes measured via defibrillator pads can monitor signs of circulation. *Resuscitation* **2007**, *73*, 221–228. [CrossRef]
26. Cromie, N.A.; Allen, J.D.; Turner, C.; Anderson, J.M.; Adgey, A.A.J. The impedance cardiogram recorded through two electrocardiogram/defibrillator pads as a determinant of cardiac arrest during experimental studies. *Crit. Care Med.* **2008**, *36*, 1578–1584. [CrossRef]
27. Cromie, N.A.; Allen, J.D.; Navarro, C.; Turner, C.; Anderson, J.M.; Adgey, A.A.J. Assessment of the impedance cardiogram recorded by an automated external defibrillator during clinical cardiac arrest. *Crit. Care Med.* **2010**, *38*, 510–517. [CrossRef]
28. Risdal, M.; Aase, S.O.; Kramer-Johansen, J.; Eftesol, T. Automatic identification of return of spontaneous circulation during cardiopulmonary resuscitation. *IEEE Trans. Biomed. Eng.* **2008**, *55*, 60–68. [CrossRef]
29. Alonso, E.; Aramendi, E.; Daya, M.; Irusta, U.; Chicote, B.; Russell, J.K.; Tereshchenko, L.G. Circulation detection using the electrocardiogram and the thoracic impedance acquired by defibrillation pads. *Resuscitation* **2016**, *99*, 56–62. [CrossRef]
30. Lee, Y.; Shin, H.; Choi, H.J.; Kim, C. Can pulse check by the photoplethysmography sensor on a smart watch replace carotid artery palpation during cardiopulmonary resuscitation in cardiac arrest patients? a prospective observational diagnostic accuracy study. *BMJ Open* **2019**, *9*. [CrossRef]

31. Wijshoff, R.W.; van Asten, A.M.; Peeters, W.H.; Bezemer, R.; Noordergraaf, G.J.; Mischi, M.; Aarts, R.M. Photoplethysmography-based algorithm for detection of cardiogenic output during cardiopulmonary resuscitation. *IEEE Trans. Biomed. Eng.* **2015**, *62*, 909–921. [CrossRef] [PubMed]
32. Brinkrolf, P.; Borowski, M.; Metelmann, C.; Lukas, R.P.; Pidde-Küllenberg, L.; Bohn, A. Predicting ROSC in out-of-hospital cardiac arrest using expiratory carbon dioxide concentration: Is trend-detection instead of absolute threshold values the key? *Resuscitation* **2018**, *122*, 19–24. [CrossRef]
33. Wei, L.; Chen, G.; Yang, Z.; Yu, T.; Quan, W.; Li, Y. Detection of spontaneous pulse using the acceleration signals acquired from CPR feedback sensor in a porcine model of cardiac arrest. *PLoS ONE* **2017**, *12*, e0189217. [CrossRef] [PubMed]
34. Elola, A.; Aramendi, E.; Irusta, U.; Del Ser, J.; Alonso, E.; Daya, M. ECG-based pulse detection during cardiac arrest using random forest classifier. *Med. Biol. Eng. Comput.* **2019**, *57*, 453–462. [CrossRef] [PubMed]
35. Faust, O.; Hagiwara, Y.; Hong, T.J.; Lih, O.S.; Acharya, U.R. Deep learning for healthcare applications based on physiological signals: A review. *Comput. Methods Programs Biomed.* **2018**, *161*, 1–13. [CrossRef]
36. Shen, S.; Yang, H.; Li, J.; Xu, G.; Sheng, M. Auditory Inspired Convolutional Neural Networks for Ship Type Classification with Raw Hydrophone Data. *Entropy* **2018**, *20*, 990. [CrossRef]
37. Almgren, K.; Krishna, M.; Aljanobi, F.; Lee, J. AD or Non-AD: A Deep Learning Approach to Detect Advertisements from Magazines. *Entropy* **2018**, *20*, 982. [CrossRef]
38. Cohen, I.; David, E.O.; Netanyahu, N.S. Supervised and Unsupervised End-to-End Deep Learning for Gene Ontology Classification of Neural In Situ Hybridization Images. *Entropy* **2019**, *21*, 221. [CrossRef]
39. Al Rahhal, M.M.; Bazi, Y.; Al Zuair, M.; Othman, E.; BenJdira, B. Convolutional neural networks for electrocardiogram classification. *J. Med. Biol. Eng.* **2018**, *38*, 1014–1025. [CrossRef]
40. Kiranyaz, S.; Ince, T.; Gabbouj, M. Real-time patient-specific ECG classification by 1-D convolutional neural networks. *IEEE Trans. Biomed. Eng.* **2016**, *63*, 664–675. [CrossRef]
41. Acharya, U.R.; Fujita, H.; Lih, O.S.; Hagiwara, Y.; Tan, J.H.; Adam, M. Automated detection of arrhythmias using different intervals of tachycardia ECG segments with convolutional neural network. *Inf. Sci.* **2017**, *405*, 81–90. [CrossRef]
42. Xia, Y.; Wulan, N.; Wang, K.; Zhang, H. Detecting atrial fibrillation by deep convolutional neural networks. *Comput. Biol. Med.* **2018**, *93*, 84–92. [CrossRef]
43. Acharya, U.R.; Fujita, H.; Oh, S.L.; Hagiwara, Y.; Tan, J.H.; Adam, M. Application of deep convolutional neural network for automated detection of myocardial infarction using ECG signals. *Inf. Sci.* **2017**, *415*, 190–198. [CrossRef]
44. Lipton, Z.C.; Kale, D.C.; Elkan, C.; Wetzel, R. Learning to diagnose with LSTM recurrent neural networks. *arXiv* **2015**, arXiv:1511.03677.
45. Chauhan, S.; Vig, L. Anomaly detection in ECG time signals via deep long short-term memory networks. In Proceedings of the 2015 IEEE International Conference on Data Science and Advanced Analytics (DSAA), Paris, France, 19–21 October 2015; pp. 1–7.
46. Alonso, E.; Ruiz, J.; Aramendi, E.; González-Otero, D.; de Gauna, S.R.; Ayala, U.; Russell, J.K.; Daya, M. Reliability and accuracy of the thoracic impedance signal for measuring cardiopulmonary resuscitation quality metrics. *Resuscitation* **2015**, *88*, 28–34. [CrossRef]
47. Ayala, U.; Eftestøl, T.; Alonso, E.; Irusta, U.; Aramendi, E.; Wali, S.; Kramer-Johansen, J. Automatic detection of chest compressions for the assessment of CPR-quality parameters. *Resuscitation* **2014**, *85*, 957–963. [CrossRef]
48. Srivastava, N.; Hinton, G.; Krizhevsky, A.; Sutskever, I.; Salakhutdinov, R. Dropout: A simple way to prevent neural networks from overfitting. *J. Mach. Learn. Res.* **2014**, *15*, 1929–1958.
49. Chung, J.; Gulcehre, C.; Cho, K.; Bengio, Y. Empirical evaluation of gated recurrent neural networks on sequence modeling. *arXiv* **2014**, arXiv:1412.3555.
50. Hochreiter, S.; Schmidhuber, J. Long short-term memory. *Neural Comput.* **1997**, *9*, 1735–1780. [CrossRef]
51. Gal, Y.; Ghahramani, Z. A theoretically grounded application of dropout in recurrent neural networks. *Adv. Neural Inf. Process. Syst.* **2016**, 1019–1027.
52. Kingma, D.P.; Ba, J. Adam: A method for stochastic optimization. *arXiv* **2014**, arXiv:1412.6980.
53. Chollet, F. Keras-Team/keras. Available online: https://github.com/fchollet/keras (accessed on 20 March 2019).

54. Abadi, M.; Agarwal, A.; Barham, P.; Brevdo, E.; Chen, Z.; Citro, C.; Corrado, G.S.; Davis, A.; Dean, J.; Devin, M.; et al. TensorFlow: Large-Scale Machine Learning on Heterogeneous Systems. 2015. Available online: tensorflow.org (accessed on 20 March 2019).
55. Gal, Y.; Ghahramani, Z. Dropout as a bayesian approximation: Representing model uncertainty in deep learning. In Proceedings of the International Conference on Machine Learning, New York, NY, USA, 19–24 June 2016; pp. 1050–1059.
56. Breiman, L. Random forests. *Mach. Learn.* **2001**, *45*, 5–32. [CrossRef]
57. Hastie, T.; Tibshirani, R.; Friedman, J. *The Elements of Statistical Learning*; Springer Series in Statistics; Springer: New York, NY, USA, 2001.
58. Zhu, J.; Hastie, T. Kernel logistic regression and the import vector machine. In Proceedings of the Advances in Neural Information Processing Systems, Vancouver, BC, Canada, 3–8 December 2001; pp. 1081–1088.
59. Snoek, J.; Larochelle, H.; Adams, R.P. Practical bayesian optimization of machine learning algorithms. In Proceedings of the Advances in Neural Information Processing Systems, Lake Tahoe, NV, USA, 3–6 December 2012; pp. 2951–2959.
60. Bergstra, J.; Yamins, D.; Cox, D.D. Making a Science of Model Search: Hyperparameter Optimization in Hundreds of Dimensions for Vision Architectures. In Proceedings of the 30th International Conference on International Conference on Machine Learning—Volume 28, Atlanta, GA, USA, 16–21 June 2013; pp. I-115–I-123.
61. Bergstra, J.S.; Bardenet, R.; Bengio, Y.; Kégl, B. Algorithms for hyper-parameter optimization. In Proceedings of the Advances in Neural Information Processing Systems, Granada, Spain, 12–15 December 2011; pp. 2546–2554.
62. Snyder, D.; Morgan, C. Wide variation in cardiopulmonary resuscitation interruption intervals among commercially available automated external defibrillators may affect survival despite high defibrillation efficacy. *Crit. Care Med.* **2004**, *32*, S421–S424. [CrossRef]
63. Kern, K.B.; Hilwig, R.W.; Berg, R.A.; Sanders, A.B.; Ewy, G.A. Importance of continuous chest compressions during cardiopulmonary resuscitation: Improved outcome during a simulated single lay-rescuer scenario. *Circulation* **2002**, *105*, 645–649. [CrossRef]
64. Vaillancourt, C.; Everson-Stewart, S.; Christenson, J.; Andrusiek, D.; Powell, J.; Nichol, G.; Cheskes, S.; Aufderheide, T.P.; Berg, R.; Stiell, I.G.; et al. The impact of increased chest compression fraction on return of spontaneous circulation for out-of-hospital cardiac arrest patients not in ventricular fibrillation. *Resuscitation* **2011**, *82*, 1501–1507. [CrossRef]
65. Elola, A.; Aramendi, E.; Irusta, U.; Picón, A.; Alonso, E.; Owens, P.; Idris, A. Deep Learning for Pulse Detection in Out-of-Hospital Cardiac Arrest Using the ECG. In Proceedings of the 2018 Computing in Cardiology Conference (CinC), Maastricht, The Netherlands, 23–26 September 2018.
66. Elola Artano, A.; Aramendi Ecenarro, E.; Irusta Zarandona, U.; Picón Ruiz, A.; Alonso González, E. Arquitecturas de aprendizaje profundo para la detección de pulso en la parada cardiaca extrahospitalaria utilizando el ECG. In Proceedings of the Libro de Actas del XXXVI Congreso Anual de la Sociedad Española de Ingeniería Biomédica, Ciudad Real, Spain, 21–23 November 2018; pp. 375–378.
67. Zhang, C.; Bengio, S.; Hardt, M.; Recht, B.; Vinyals, O. Understanding deep learning requires rethinking generalization. *arXiv* **2016**, arXiv:1611.03530.
68. Arpit, D.; Jastrzębski, S.; Ballas, N.; Krueger, D.; Bengio, E.; Kanwal, M.S.; Maharaj, T.; Fischer, A.; Courville, A.; Bengio, Y.; et al. A closer look at memorization in deep networks. In Proceedings of the 34th International Conference on Machine Learning—Volume 70, Sydney, Australia, 6–11 August 2017; pp. 233–242.
69. Hafner, D.; Tran, D.; Irpan, A.; Lillicrap, T.; Davidson, J. Reliable uncertainty estimates in deep neural networks using noise contrastive priors. *arXiv* **2018**, arXiv:1807.09289.
70. Harang, R.; Rudd, E.M. Principled Uncertainty Estimation for Deep Neural Networks. *arXiv* **2018**, arXiv:1810.12278.
71. Lakshminarayanan, B.; Pritzel, A.; Blundell, C. Simple and scalable predictive uncertainty estimation using deep ensembles. In Proceedings of the Advances in Neural Information Processing Systems, Long Beach, CA, USA, 4–9 December 2017; pp. 6402–6413.

72. McDermott, P.L.; Wikle, C.K. Bayesian recurrent neural network models for forecasting and quantifying uncertainty in spatial-temporal data. *Entropy* **2019**, *21*, 184. [CrossRef]
73. Shadman Roodposhti, M.; Aryal, J.; Lucieer, A.; Bryan, B.A. Uncertainty Assessment of Hyperspectral Image Classification: Deep Learning vs. Random Forest. *Entropy* **2019**, *21*, 78. [CrossRef]

A.1.4 Lehenengo helburuari lotutako bigarren argitalpena nazioarteko konferentzian

A.4. Taula. Lehenengo helburuari lotutako bigarren argitalpena nazioarteko konferentzian.

	Argitalpena nazioarteko konferentzian
Erreferentzia	Andoni Elola, Elisabete Aramendi, Unai Irusta, Artzai Picón, Erik Alonso, Iraia Isasi, Ahamed Idris, "Convolutional Recurrent Neural Networks to Characterize the Circulation Component in the Thoracic Impedance during Out-of-Hospital Cardiac Arrest", *41st Annual International Conference of the IEEE Engineering in Medicine and Biology Society (EMBC)*, 2019, pp. 1921-1925.
Kalitate adierazleak	• **Argitalpen mota**: SJRen indexatutako nazioarteko konferentzia • **Inpaktu faktorea**: 0.281

Convolutional Recurrent Neural Networks to Characterize the Circulation Component in the Thoracic Impedance during Out-of-Hospital Cardiac Arrest

Andoni Elola[1], Elisabete Aramendi[1], Unai Irusta[1], Artzai Picón[1,2], Erik Alonso[1], Iraia Isasi[1] and Ahamed Idris[3]

Abstract— **Pulse detection during out-of-hospital cardiac arrest remains challenging for both novel and expert rescuers because current methods are inaccurate and time-consuming. There is still a need to develop automatic methods for pulse detection, where the most challenging scenario is the discrimination between pulsed rhythms (PR, pulse) and pulseless electrical activity (PEA, no pulse). Thoracic impedance (TI) acquired through defibrillation pads has been proven useful for detecting pulse as it shows small fluctuations with every heart beat. In this study we analyse the use of deep learning techniques to detect pulse using only the TI signal. The proposed neural network, composed by convolutional and recurrent layers, outperformed state of the art methods, and achieved a balanced accuracy of 90% for segments as short as 3 s.**

I. INTRODUCTION

Out-of-hospital cardiac arrest (OHCA) remains a major public health problem, with survival rates around 10% [1]. The four links of the chain of survival [2] comprise early detection of cardiac arrest, cardiopulmonary resuscitation, early defibrillation and post resuscitation care. Detecting the presence of pulse is key for two tasks: cardiac arrest recognition and detection of return of spontaneous circulation. The first task consists of discriminating between cardiac arrest and other collapse states, so cardiopulmonary resuscitation efforts can be initiated earlier. The second task allows an earlier start of post-resuscitation care and transport to hospital. Today, pulse is detected by carotid pulse checks or looking for signs of life, but both methods have been proven inaccurate and time consuming [3], [4]. Furthermore, it has been reported that chest compression pauses for manual pulse checks exceed the maximum time interval of 10 s recommended by the guidelines in more than 50% of the cases [5]. That is why there is still a need for automatic methods to assist the rescuer in the detection of pulse, and the scientific community has made many efforts in the last years to develop algorithms to identify rhythms with pulse [6], [7].

In OHCA there are three types of non-shockable rhythms [8]: pulse-generating rhythms (PR), pulseless electrical activity (PEA) and asystole. Asystole is defined as the absence of electrical activity of the heart. PR and PEA present an organized electrical activity of the heart (QRS complexes). However, PEA shows an electromechanical dissociation, the heart does not pump effectively and there is no spontaneous circulation (not palpable clinical pulse). Therefore, in a cardiac arrest scenario pulse detection consists in discriminating between PR and PEA, since asystole can be discriminated using power or amplitude measurements of the ECG [9].

Most of the commercially available automated external defibrillators (AEDs) record two signals: ECG and thoracic impedance (TI). TI is linked to the cardiac output and shows very small fluctuations with every effective heart beat [10]. Pulse detection methods have been proposed based on the characterization of that circulation component [11], [12], [13], [14]. Current methods show two main limitations. Firstly, the reliable extraction of circulation component requires accurate QRS detection [11], [12], which may be challenging in short PEA segments [15]. Secondly, the ventilations induce high amplitude fluctuations in the TI signal. Some of the referenced studies discarded segments containing ventilations, which is not practical in a real scenario. We therefore need new methods to characterize circulation in the TI signal.

Deep neural networks have shown great performance in many bio-signal classification tasks, even for pulse detection during OHCA using only the ECG [16]. In this study we propose a deep neural network to detect pulse using only the TI signal, and compare it with machine learning techniques based on a comprehensive set of features based on the available literature.

II. METHODS

A. Data Collection

The data used in this study were collected by the DFW center for resuscitation research (UTSW, Dallas). All episodes were recorded using the Philips HeartStart MRx monitor/defibrillator, which records the ECG signal with a sampling frequency (f_s) of 250 Hz. The TI signal was recorded through defibrillation pads by applying a sinusoidal

*This work was supported by: The Spanish Ministerio de Economía y Competitividad, TEC2015-64678-R, jointly with the Fondo Europeo de Desarrollo Regional (FEDER), UPV/EHU via GIU17/031 and the Basque Government through the grant pre-2018-2-0260

[1]Andoni Elola, Elisabete Aramendi, Unai Irusta, Artzai Picón, Erik Alonso and Iraia Isasi are with the University of the Basque Country UPV/EHU, Ingeniero Torres Quevedo Plaza, 1, 48013, Bilbao, Spain (e-mail: andoni.elola@ehu.eus)

[2]Artzai Picón is also with TECNALIA Research and Innovation, Derio, Bizkaia, Spain

[3]Ahamed Idris is with the University of Texas Southwestern Medical Center, Dallas, Texas, USA

excitation current (32 kHz, 3 mA peak-to-peak) and f_s = 200 Hz.

From the set of 1015 patients that fulfilled the criteria (details in [16]), a total of 3914 segments (2372 PR and 1542 PEA) of 5-s were extracted from 279 patients (134 recovered pulse). Data were divided patient-wise into training and test sets ($\approx$ 80/20%). The first set contained 3038 segments (1871 PR and 1167 PEA) from from 223 patients. The second set contained 876 segments (501 PR and 375 PEA) from 56 patients.

Figure 1 shows two PR (panels a and b) and two PEA examples (panels c and d). Each panel shows 4 s of concurrent ECG (top) and TI (bottom) signals. PR shows higher rates and narrower QRS complexes. Most importantly, for the PR cases components correlated with the ECG signal can be observed in the TI.

B. Deep Learning Approach

The TI signal was first preprocessed and then fed into a deep neural network, where the output of the network represents an indicator of pulse. This is a binary classification problem where $y_{true} = \{0 : \mathrm{PEA}, 1 : \mathrm{PR}\}$ is our gold standard (based on clinical annotations, details in [16]) and $y_{out} = \{0 : \mathrm{PEA}, 1 : \mathrm{PR}\}$ is the output of the network.

1) Signal preprocessing: The TI signal was downsampled to 100 Hz and filtered between 0.5 and 8 Hz using an order 4 Butterworth filter and zero-phase filtering in order to remove noise and enhance the circulation component. Then, it was clipped between $[-0.25, 0.25]\,\Omega$ and normalized by the same factor to avoid the saturation of the network and accelerate the training process. The network requires segments of 4 s.

2) Network architecture: The overall architecture of the proposed solution, shown in Figure 2, consists of convolutional layers, pooling layers and recurrent layers. The convolutional layers perform two different operations. First, temporal convolution is applied to the input signal using a convolutional kernel (kernel size $k = 7$) and 16 filters to obtain different representations of the input signal. The weights of the convolution kernel and biases are adjusted during training. The second step is to apply linear rectifier function (ReLU) to each output sample.

Convolutional layers are followed by max-pooling layers, which divide the signal in non-overlapping chunks of length $m = 3$ and take the maximum. This removes redundant information while reducing the computational cost of the upper layers. Two convolutional layers were applied, each one followed by a pooling layer. These blocks can learn time-invariant features, and stacking these blocks allows to learn more complex features. A total of 16 representations of the signal are obtained, $\mathbf{X} = [x_1, \ldots, x_{16}]^T$, each of $t = \{1, \ldots, 41\}$ samples (after 2 max-pooling stages).

To encode the sequential patterns output by the previous convolutional block, a bidirectional gated recurrent unit (BGRU) layer was adopted [17]. These kind of layers can exhibit the temporal behaviour of the input sequences and resolve long-term dependency and vanishing gradient problems. The GRU calculates hidden states $\boldsymbol{h}_t$ at time step $t = \{1, \ldots, 41\}$ based on the past states. Our solution applies two GRU layers, a forward and a backward layer (BGRU) with 5 units each, so more complex temporal features can be extracted. The hidden state at the last time step, $\boldsymbol{h}_{t=41}$, is fed into the next layer, a total of 10 features denoted as $\boldsymbol{v}_{\mathrm{D}}$.

The next layer is a dropout layer [18], which is available only during the training process. It is a common regularization technique to avoid overfitting, it drops out units under certain probability at each training step in a mini-batch. It can be seen as a ensemble method, because different networks are created when some units are removed. We set the probability of dropout to 0.2. When using dropout, training the network layers constraining to have a maximum norm γ is specially useful [18]. The convolutional layers and the BGRU were trained under this constraint with $\gamma = 3$.

Finally, a fully connected layer with a single neuron and the sigmoid activation function produces the desired output $p \in (0, 1)$, which can be interpreted as the likelihood of having PR, and can be used to classify the segment.

3) Online data augmentation: At each training epoch, a data transformation was applied, so the network updates its parameters with different data at each epoch. Since the segments of our dataset have a duration of 5 s and the network requires only 4-s input segments, the first step was to choose a 4-s random window within the 5 seconds. The second step was to vary the amplitude of the signal by $\pm 2\%$. We chose a small number for the amplitude variation because the TI amplitude contains information about pulse. Lastly, zero-mean gaussian noise was added to the signal with a standard deviation of 10^{-5}.

4) Training procedure: The parameters of the whole network were optimized using the adaptive moment estimation (ADAM) optimizer [19], a type of stochastic gradient descent algorithm with adaptive learning rate. An initial learning rate of 0.001 and exponential decay rates of 0.9 and 0.999 were adopted, good default settings according to [19]. The training data were fed into the convolutional recurrent neural network in batches of 8 during 75 epochs. Every patient was weighted equally to train the network. At the beginning of each epoch training data were shuffled to change the batches. The network was developed using Keras framework [20] with TensorFlow backend [21], and was trained on a NVIDIA GeForce GTX 1080 Ti.

5) Alternative architectures: The complete architecture, composed by two convolutional and one recurrent layers (2CRNN) as shown in Figure 2, was compared to a single convolutional and recurrent network (1CRNN) and to a fully convolutional network (CNN). The hyperparameters of both alternative architectures were the same as for 2CRNN. For the CNN, we applied a global maximum pooling layer after the convolutional stage, which takes the maximum value for each representation of the signal (a feature vector of size 16 is obtained).

C. Machine Learning Approach

We compared our deep learning solution against classical machine learning methods using the most discriminative TI

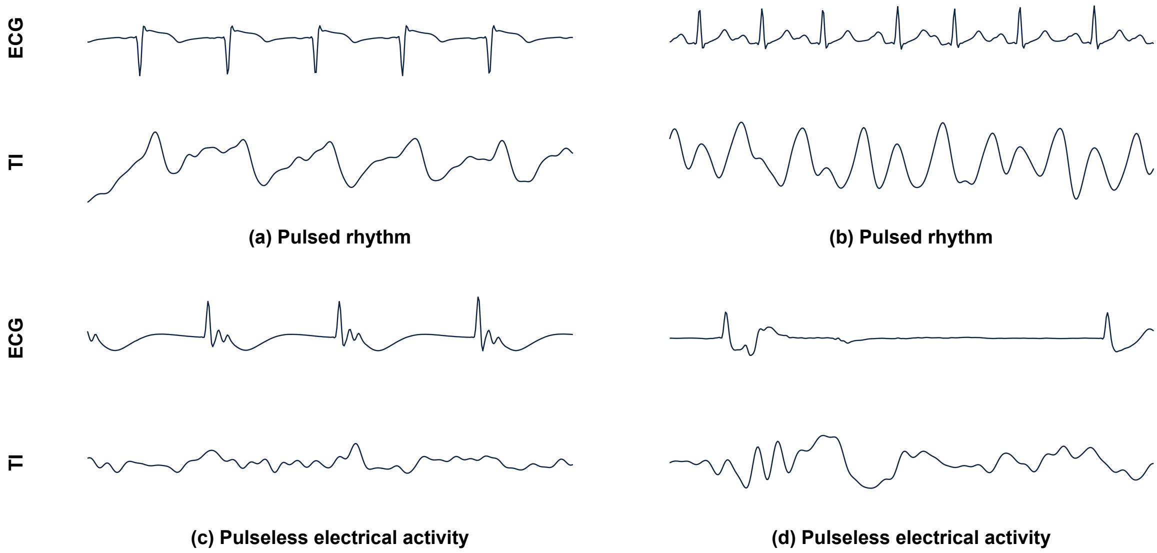

Fig. 1. PR (panels a and b) and PEA (panels c and d) examples. Each panel shows the ECG on the top and the TI signal in the bottom (4 s each). As shown in the examples the TI activity correlated to the ECG (QRS complexes) is larger for PR rhythms.

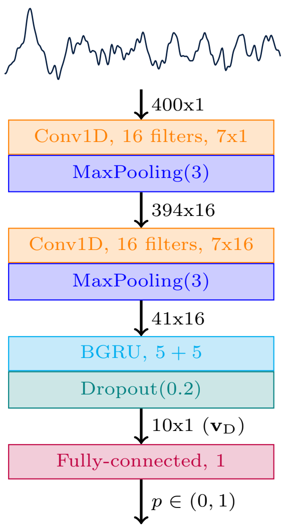

Fig. 2. General scheme of the proposed deep learning solution. The network is based on convolutional, pooling, dropout and recurrent layers.

features proposed in the literature [11], [12], [13]. This set of 15 features, $\boldsymbol{v} = [v_1, \ldots, v_{15}]$, were fed into three well known classification schemes in order to classify a segment as PR or PEA: support vector machine (SVM), Kernel Logistic Regression (KLR) and Random Forest (RF). The TI signal was first resampled to 250 Hz and then filtered between $[0.7, 8]$ Hz using an order 4 Butterworth filter and zero-phase filtering to obtain $z[n]$.

1) Feature extraction: The first three features were computed as proposed in [11] from the circulation component $z_{cc}[n]$ of the impedance segment $z[n]$. This component can be considered quasi-periodic in short intervals [11], so it can be expressed as a Fourier series, where the instantaneous frequency is calculated from QRS complex instants. Alonso et al. [11] estimated the coefficients using the recursive least squares algorithm and extracted three features from TI: the standard deviation of the peaks caused by each effective heartbeat (v_1), mean area (v_2) and mean area of $z_{cc}[n] - z_{cc}[n-1]$ (v_3). A modified version of Hamilton-Tompkins algorithm was used for QRS detection [15], and the forgetting factor was set to 0.9997.

Alternatively, Risdal et al. [12] proposed to apply ensemble average to the TI signal to obtain $z_{EA}(m)$, and extracted 10 features: amplitude range divided by its duration (v_4); the amplitude range of the first difference (v_5); area under the waveform once the minimum value has been subtracted (v_6); peak to peak amplitude of the longest negative flank (v_7); the duration of the longest negative flank (v_8); coefficients obtained fitting the waveform to 4th order polynomial ($v_9 - v_{13}$), once $z_{EA}(m)$ has been normalized to have a peak-to-peak amplitude of 1 and 1 s duration.

The last two features were adopted from [13] and were independent from QRS instants. The TI segment was divided in two halves, the minimum variance of both was v_{14} and the minimum mean cross-power v_{15}.

2) Feature selection: A classical approach called recursive feature elimination (RFE) was used for feature selection. Using patient-wise 10-fold cross-validation in the training set, we started training a Random Forest classifier with all features and the least important feature was eliminated at each iteration. The importance of the features was calculated as the increase in the out-of-bag error when the feature values were permuted, and the feature with the lowest median increase among 10-folds was removed at each iteration.

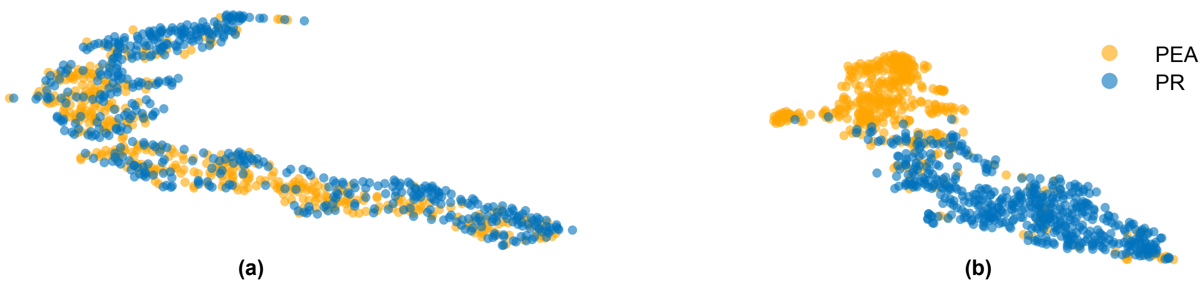

Fig. 3. t-SNE representation of $\boldsymbol{v}$ (panel a) and $\boldsymbol{v}_\mathrm{D}$ (panel b).

3) Classification: Three different classifiers were used: RF, KLR with gaussian kernel and SVM with gaussian kernel. The RF classifier was trained using 300 trees. The hyperparameters of the KLR (gaussian kernel width and regularization term) and SVM (gaussian kernel width and soft margin) were optimized in the training set using patient-wise 10-fold cross-validation and bayesian optimization with gaussian processes. The function to minimize was the cross-validated balanced error rate (BER) and the number of iterations was 30. These folds were also used to choose the number of features, N, for each classifier. Every patient was weighted equally to train each classifier.

D. Evaluation setup

The PR/PEA classifiers were evaluated in terms of sensitivity (Se, proportion of correctly detected PRs), specificity (Sp, proportion of correctly detected PEAs) and balanced accuracy (BAC, the arithmetic mean between Se and Sp) by comparing y_{true} and y_{out}. Different segments within the same patients may be correlated, so to compute performance metrics every patient was weighted equally.

III. Results

To compare the deep learning and the classical solutions, first the two feature vectors, $\boldsymbol{v}_\mathrm{D}$ and $\boldsymbol{v}$, were analysed. We applied a dimensionality reduction technique, the classical t-distributed stochastic neighbour embedding (t-SNE), to interpret the data in a lower dimension space. Figure 3 shows the t-SNE visualization of $\boldsymbol{v}$ (panel a) and $\boldsymbol{v}_\mathrm{D}$ (panel b) for the test subset. In the case of panel b ($\boldsymbol{v}_\mathrm{D}$) the clusters are more separated. However, some samples are mixed, hindering the correct classification of PR/PEA. We also analysed the Pearson correlation coefficients between $\boldsymbol{v}$ and $\boldsymbol{v}_\mathrm{D}$, which ranged between $[-0.25, 0.25]$.

Table I shows the Se, Sp and BAC for different algorithms. The optimal number of features was taken as $N = 8$ for the three machine learning classifiers. It can be observed that deep learning approaches outperform classical approaches by more than 2 points in terms of BAC. In fact, the best Se and Sp were also obtained using deep neural networks. Training a RF classifier with $\boldsymbol{v}_\mathrm{D}$ yielded a Se/Sp/BAC of 97.0/86.2/91.6 % for the test set, still above the RF trained with classical features.

TABLE I

Se, Sp and BAC values for different machine learning approaches and deep learning architectures.

	Se (%)	Sp (%)	BAC (%)
SVM	83.8	86.7	85.3
KLR	83.5	87.8	85.6
RF	95.3	84.2	89.7
CNN	94.3	86.4	90.3
1CRNN	**97.0**	85.1	91.1
2CRNN	94.2	**89.3**	**91.8**

The duration of the segment to discriminate PR/PEA rhythms is important, as it defines the duration of the interruption in chest compressions. We evaluated our trained neural network for different segment durations as shown in Figure 4. Note that our neural network architecture can work regardless to the segment duration, so despite training with 4-s segments, it can also work with different segment durations. It can be observed that 2CRNN network was superior to the other two networks for any segment duration, reaching a BAC of 90% for segments as short as 3 s.

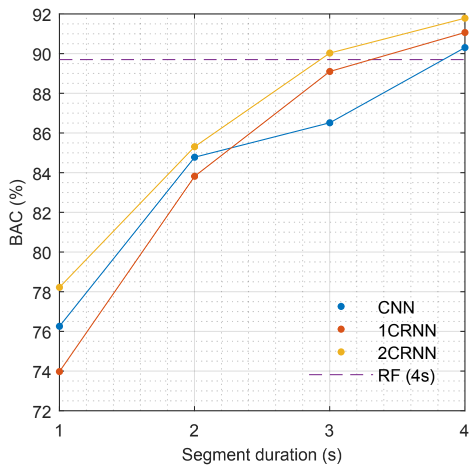

Fig. 4. Performance of the networks depending on the input segment duration.

IV. Discussion

Pulse detection remains challenging during OHCA for both laypeople and healthcare professionals. Despite the many proposals to discriminate between PR and PEA rhythms, we still need automated methods to assist the rescuer in the detection of pulse. To the best of our knowledge, this is the first study that analyses the power of deep neural networks to discriminate between PR/PEA segments using only the TI signal.

We tested three different neural network solutions with 4-s segments, and they outperformed the machine learning solution that included TI based features. All $\boldsymbol{v}$ features, except v_{14}, also required information of the ECG. Nonetheless, the neural network showed better performance using only the TI and the features extracted from the neural network were uncorrelated with the classical features. We might think that the neural network is able to extract discriminative information not included in the features proposed to date.

Keeping the duration of the TI segment as short as possible is important, as these algorithms need chest compression pauses to work correctly, and minimizing these pauses increases survival rates [22]. Accurate QRS detection need longer ECG segments, and adaptive filters also need a transient interval. Besides, fluctuations caused by ventilations hinder the detection of pulse according to previous studies [11], [13]. In [13], they proposed to make the automatic pulse checks during rhythm analysis pauses, where ventilations are not present. However, overcoming this limitation would allow the use of the algorithm at any moment. In this study we did not discard segments containing ventilations, so our network only needs 4 s segments free of chest compression artefacts.

The major limitation of the proposed method is the low specificity (below 90%). Wrongly classifying a PEA might involve stopping resuscitation therapy, reducing survival probabilities of the patient with no pulse.

Under the same training/test split, in [16] we reported a Se/Sp/BAC of 91.7/92.5/92.1% using only the ECG, which is slightly above the results reported in this study. Adding $\boldsymbol{v}_{\mathrm{D}}$ to the classical ECG features or combining ECG and TI in a single neural network might improve the performance and contribute to a better algorithm to be implemented in an AED or more advanced monitor/defibrillators.

References

[1] J. Berdowski, R. A. Berg, J. G. Tijssen, and R. W. Koster, "Global incidences of out-of-hospital cardiac arrest and survival rates: systematic review of 67 prospective studies," *Resuscitation*, vol. 81, no. 11, pp. 1479–1487, 2010.

[2] J. Nolan, J. Soar, and H. Eikeland, "The chain of survival," *Resuscitation*, vol. 71, no. 3, pp. 270–271, 2006.

[3] M. Ruppert, M. W. Reith, J. H. Widmann, C. K. Lackner, R. Kerkmann, L. Schweiberer, and K. Peter, "Checking for breathing: evaluation of the diagnostic capability of emergency medical services personnel, physicians, medical students, and medical laypersons," *Annals of Emergency Medicine*, vol. 34, no. 6, pp. 720–729, 1999.

[4] B. Eberle, W. Dick, T. Schneider, G. Wisser, S. Doetsch, and I. Tzanova, "Checking the carotid pulse check: diagnostic accuracy of first responders in patients with and without a pulse," *Resuscitation*, vol. 33, no. 2, pp. 107–116, 1996.

[5] E. J. Clattenburg, P. Wroe, S. Brown, K. Gardner, L. Losonczy, A. Singh, and A. Nagdev, "Point-of-care ultrasound use in patients with cardiac arrest is associated prolonged cardiopulmonary resuscitation pauses: a prospective cohort study," *Resuscitation*, vol. 122, pp. 65–68, 2018.

[6] L. Wei, G. Chen, Z. Yang, T. Yu, W. Quan, and Y. Li, "Detection of spontaneous pulse using the acceleration signals acquired from cpr feedback sensor in a porcine model of cardiac arrest," *PloS one*, vol. 12, no. 12, p. e0189217, 2017.

[7] R. W. Wijshoff, A. M. van Asten, W. H. Peeters, R. Bezemer, G. J. Noordergraaf, M. Mischi, and R. M. Aarts, "Photoplethysmography-based algorithm for detection of cardiogenic output during cardiopulmonary resuscitation," *IEEE Transactions on Biomedical Engineering*, vol. 62, no. 3, pp. 909–921, 2015.

[8] J. Soar, J. P. Nolan, B. W. Böttiger, G. D. Perkins, C. Lott, P. Carli, T. Pellis, C. Sandroni, M. B. Skrifvars, G. B. Smith, *et al.*, "European resuscitation council guidelines for resuscitation 2015: section 3. adult advanced life support," *Resuscitation*, vol. 95, pp. 100–147, 2015.

[9] U. Ayala, U. Irusta, J. Ruiz, T. Eftestøl, J. Kramer-Johansen, F. Alonso-Atienza, E. Alonso, and D. González-Otero, "A reliable method for rhythm analysis during cardiopulmonary resuscitation," *BioMed research international*, vol. 2014, 2014.

[10] H. Losert, M. Risdal, F. Sterz, J. Nysæther, K. Köhler, T. Eftestøl, C. Wandaller, H. Myklebust, T. Uray, S. O. Aase, *et al.*, "Thoracic-impedance changes measured via defibrillator pads can monitor signs of circulation," *Resuscitation*, vol. 73, no. 2, pp. 221–228, 2007.

[11] E. Alonso, E. Aramendi, M. Daya, U. Irusta, B. Chicote, J. K. Russell, and L. G. Tereshchenko, "Circulation detection using the electrocardiogram and the thoracic impedance acquired by defibrillation pads," *Resuscitation*, vol. 99, pp. 56–62, 2016.

[12] M. Risdal, S. O. Aase, J. Kramer-Johansen, and T. Eftesol, "Automatic identification of return of spontaneous circulation during cardiopulmonary resuscitation," *IEEE Transactions on Biomedical Engineering*, vol. 55, no. 1, pp. 60–68, 2008.

[13] J. M. Ruiz, S. R. de Gauna, D. M. González-Otero, P. Saiz, J. J. Gutiérrez, J. F. Veintemillas, J. M. Bastida, and D. Alonso, "Circulation assessment by automated external defibrillators during cardiopulmonary resuscitation," *Resuscitation*, vol. 128, pp. 158–163, 2018.

[14] N. A. Cromie, J. D. Allen, C. Navarro, C. Turner, J. M. Anderson, and A. A. J. Adgey, "Assessment of the impedance cardiogram recorded by an automated external defibrillator during clinical cardiac arrest," *Critical care medicine*, vol. 38, no. 2, pp. 510–517, 2010.

[15] A. Elola, E. Aramendi, U. Irusta, J. Del Ser, E. Alonso, and M. Daya, "Ecg-based pulse detection during cardiac arrest using random forest classifier," *Medical & biological engineering & computing*, vol. 57, no. 2, pp. 453–462, 2019.

[16] A. Elola, E. Aramendi, U. Irusta, A. Picón, E. Alonso, P. Owens, and A. Idris, "Deep learning for pulse detection in out-of-hospital cardiac arrest using the ecg," in *2018 Computing in Cardiology Conference (CinC)*, 2018.

[17] J. Chung, C. Gulcehre, K. Cho, and Y. Bengio, "Empirical evaluation of gated recurrent neural networks on sequence modeling," *arXiv preprint arXiv:1412.3555*, 2014.

[18] N. Srivastava, G. Hinton, A. Krizhevsky, I. Sutskever, and R. Salakhutdinov, "Dropout: A simple way to prevent neural networks from overfitting," *The Journal of Machine Learning Research*, vol. 15, no. 1, pp. 1929–1958, 2014.

[19] D. P. Kingma and J. Ba, "Adam: A method for stochastic optimization," *arXiv preprint arXiv:1412.6980*, 2014.

[20] F. Chollet *et al.*, "Keras," https://keras.io, 2015.

[21] M. Abadi, A. Agarwal, P. Barham, E. Brevdo, Z. Chen, C. Citro, G. S. Corrado, A. Davis, J. Dean, M. Devin, S. Ghemawat, I. Goodfellow, A. Harp, G. Irving, M. Isard, Y. Jia, R. Jozefowicz, L. Kaiser, M. Kudlur, J. Levenberg, D. Mané, R. Monga, S. Moore, D. Murray, C. Olah, M. Schuster, J. Shlens, B. Steiner, I. Sutskever, K. Talwar, P. Tucker, V. Vanhoucke, V. Vasudevan, F. Viégas, O. Vinyals, P. Warden, M. Wattenberg, M. Wicke, Y. Yu, and X. Zheng, "TensorFlow: Large-scale machine learning on heterogeneous systems," 2015, software available from tensorflow.org. [Online]. Available: https://www.tensorflow.org/

[22] C. Vaillancourt, S. Everson-Stewart, J. Christenson, D. Andrusiek, J. Powell, G. Nichol, S. Cheskes, T. P. Aufderheide, R. Berg, I. G. Stiell, *et al.*, "The impact of increased chest compression fraction on return of spontaneous circulation for out-of-hospital cardiac arrest patients not in ventricular fibrillation," *Resuscitation*, vol. 82, no. 12, pp. 1501–1507, 2011.

A.2 Bigarren helburuari lotutako argitalpenak

A.2.1 Bigarren helburuari lotutako aurreneko argitalpena nazioarteko aldizkarian

A.5. Taula. Bigarren helburuari lotutako aurreneko argitalpena nazioarteko aldizkarian.

	Argitalpena nazioarteko aldizkarian
Erreferentzia	Elisabete Aramendi, Andoni Elola, Erik Alonso, Unai Irusta, Mohamud Daya, James K. Rusell, Pia Hubner, Fritz Sterz, "Feasibility of the capnogram to monitor ventilation rate during cardiopulmonary resuscitation", *Resuscitation 2017*, vol. 110, pp. 162-168.
Kalitate adierazleak	• **Argitalpen mota**: JCRen indexatutako aldizkari artikulua • **Kuartila**: Q1 (1/26) (*Web of Science* 2017) • **Inpaktu faktorea**: 5.863

Resuscitation 110 (2017) 162–168

Contents lists available at ScienceDirect

Resuscitation

journal homepage: www.elsevier.com/locate/resuscitation

Clinical paper

Feasibility of the capnogram to monitor ventilation rate during cardiopulmonary resuscitation☆

Elisabete Aramendi[a,*], Andoni Elola[a], Erik Alonso[b], Unai Irusta[a], Mohamud Daya[c], James K. Russell[c], Pia Hubner[d], Fritz Sterz[d]

[a] Communications Engineering Department, University of the Basque Country UPV/EHU, Alameda Urquijo S/N, 48013 Bilbao, Spain
[b] Department of Applied Mathematics, University of the Basque Country UPV/EHU, Rafael Moreno "Pitxitxi", 3, 48013 Bilbao, Spain
[c] Department of Emergency Medicine, Oregon Health & Science University, 97239-3098 Portland, OR, United States
[d] Department of Emergency Medicine, Medical University of Vienna, 1090 Wien, Austria

ARTICLE INFO

Article history:
Received 5 May 2016
Received in revised form 27 July 2016
Accepted 9 August 2016

Keywords:
Capnography
Ventilation monitoring
Cardiopulmonary resuscitation
Hyperventilation

ABSTRACT

Aim: The rates of chest compressions (CCs) and ventilations are both important metrics to monitor the quality of cardiopulmonary resuscitation (CPR). Capnography permits monitoring ventilation, but the CCs provided during CPR corrupt the capnogram and compromise the accuracy of automatic ventilation detectors. The aim of this study was to evaluate the feasibility of an automatic algorithm based on the capnogram to detect ventilations and provide feedback on ventilation rate during CPR, specifically addressing intervals where CCs are delivered.
Methods: The dataset used to develop and test the algorithm contained in-hospital and out-of-hospital cardiac arrest episodes. The method relies on adaptive thresholding to detect ventilations in the first derivative of the capnogram. The performance of the detector was reported in terms of sensitivity (SE) and Positive Predictive Value (PPV). The overall performance was reported in terms of the rate error and errors in the hyperventilation alarms. Results were given separately for the intervals with CCs.
Results: A total of 83 episodes were considered, resulting in 4880 min and 46,740 ventilations (8741 during CCs). The method showed an overall SE/PPV above 99% and 97% respectively, even in intervals with CCs. The error for the ventilation rate was below 1.8 min^{-1} in any group, and >99% of the ventilation alarms were correctly detected.
Conclusion: A method to provide accurate feedback on ventilation rate using only the capnogram is proposed. Its accuracy was proven even in intervals where canpography signal was severely corrupted by CCs. This algorithm could be integrated into monitor/defibrillators to provide reliable feedback on ventilation rate during CPR.

1. Introduction

Quality of cardiopulmonary resuscitation (CPR) is a key factor in the outcome of cardiac arrest patients. Advanced life support (ALS) treatment of out-of-hospital cardiac arrest (OHCA) includes good-quality chest compressions (CCs) and a reliable airway management. The 2015 resuscitation guidelines recommend continuous chest compressions after intubation, ventilation rates of 10 min^{-1} and avoidance of hyperventilation.[1] Hyperventilation increases intrathoracic pressure, reshapes the oxygen dissociation curve (increasing oxygen affinity) and behaves as a cerebral vasoconstrictor.[2,3] It has also has been proven to lower coronary perfusion pressure and to contribute to hemodynamic deterioration in animal experiments.[4–8] All these factors decrease the probability of survival.[9,10] Nevertheless rescuers providing pre-hospital CPR often exceed the recommended ventilation rates. Several studies report rates ranging from moderate (14 min^{-1}) to severe (>20 min^{-1}) hyperventilation during long duration OHCA.[5–7,9–12]

CPR feedback systems, either standalone or incorporated into defibrillators, have been shown to improve adherence to guideline recommendations.[13,14] Feedback on CCs based on acceleration, force or thoracic impedance (TI) has been extensively studied;[11,15–17] but little attention has been given to feedback on ventilation rate during CPR. The TI channel, recorded through the defibrillation pads, has been explored to monitor ventilation

☆ A Spanish translated version of the abstract of this article appears as Appendix in the final online version at doi:10.1016/j.resuscitation.2016.08.033.

* Corresponding author.
E-mail address: elisabete.aramendi@ehu.es (E. Aramendi).

http://dx.doi.org/10.1016/j.resuscitation.2016.08.033
0300-9572/

rate.[11,18,19] However, an analysis of long resuscitation episodes showed that artefacts limit the reliability of TI for instantaneous feedback on ventilation rate.[17] Currently, no commercial system is available for feedback on ventilation rate using the TI.

The recently released resuscitation guidelines have placed an increased emphasis on the use of the capnogram during CPR to monitor, among other things, ventilation rate and to avoid hyperventilation.[1] During CPR compression artefacts often corrupt the capnogram compromising the accuracy of automatic algorithms for ventilation rate feedback.[20–22] Few such algorithms have been published,[23,24] and their performance during CPR has not been systematically evaluated and/or documented.

This study proposes an automatic algorithm for ventilation detection during CPR based on the typical waveform characteristics of the capnogram and on the use of adaptive thresholds to identify ventilations. The aim of the study is to analyse the feasibility of using the capnogram to provide an accurate automated feedback on ventilation rate and hyperventilation alarms during CPR.

2. Materials and methods

2.1. Data materials

Two datasets of episodes with signals from monitor/defibrillators were used in this study, an out-of-hospital dataset (OHD) and an in-hospital dataset (IHD). The OHD was recorded during cardiac arrest, with manual CPR (CCs and ventilations) provided in all episodes. The signals available to monitor ventilations were the TI and the capnogram. The IHD corresponded to patients who suffered cardiac arrest, some recorded during manual CPR (CCs and ventilations) and some recorded after cardiac arrest during postresucitation care (mechanical ventilation). They were monitored with the capnogram and the expired air flow.

The OHD was a subset of a large OHCA registry containing 623 episodes maintained by the Tualatin Valley Fire & Rescue (Tigard, Oregon, USA), an ALS first response agency. The episodes were collected using the HeartStart MRx monitor/defibrillator (Philips, Andover, MA) between 2006 and 2009. Ventilations in these episodes were provided manually with an endotracheal tube or laryngeal tube airway. Episodes with at least 20 minutes of concurrent and readable recordings of the compression depth (CD), the TI and the capnogram were included in this study, resulting in a dataset of 62 episodes. The CD signal from the Q-CPR assist pad by Philips was used to identify the intervals with CCs. The capnogram was acquired using Microstream (sidestream acquisition) with a sampling rate of 40/125 Hz and a resolution of 0.004 mmHg per bit. The instants of ventilations were marked in the TI ventilation channel,[11,17] first automatically and then manually reviewed by three experienced biomedical engineers. Reviewers used the capnogram to make a decision in unclear intervals. Fig. 1 shows examples of two episodes of the OHD, where ventilations are visible in both the TI ventilation channel (in black) and the capnogram, for an artefact free interval (panel a), and when CCs were provided (panel b).

The IHD was a subset of the APACHI study conducted by Philips Healthcare at the Medical University of Vienna between November 2012 and January 2014. The APACHI study recorded physiological signals (arterial blood pressure, electrocardiogram, photoplethysmogram, capnogram and airway flow and pressure) from multiple monitors during hemodynamic crisis in the emergency department of the Vienna General Hospital, under the direction of Drs. Sterz and Hubner. From a total of 50 patients enrolled in the trial, the 21 that suffered cardiac arrest and had concurrent recordings of capnogram and ventilatory flow were included. Six of the episodes were recorded during CPR and 15 after resuscitation. The mainstream capnogram was acquired by the NICO 7300 monitor using the

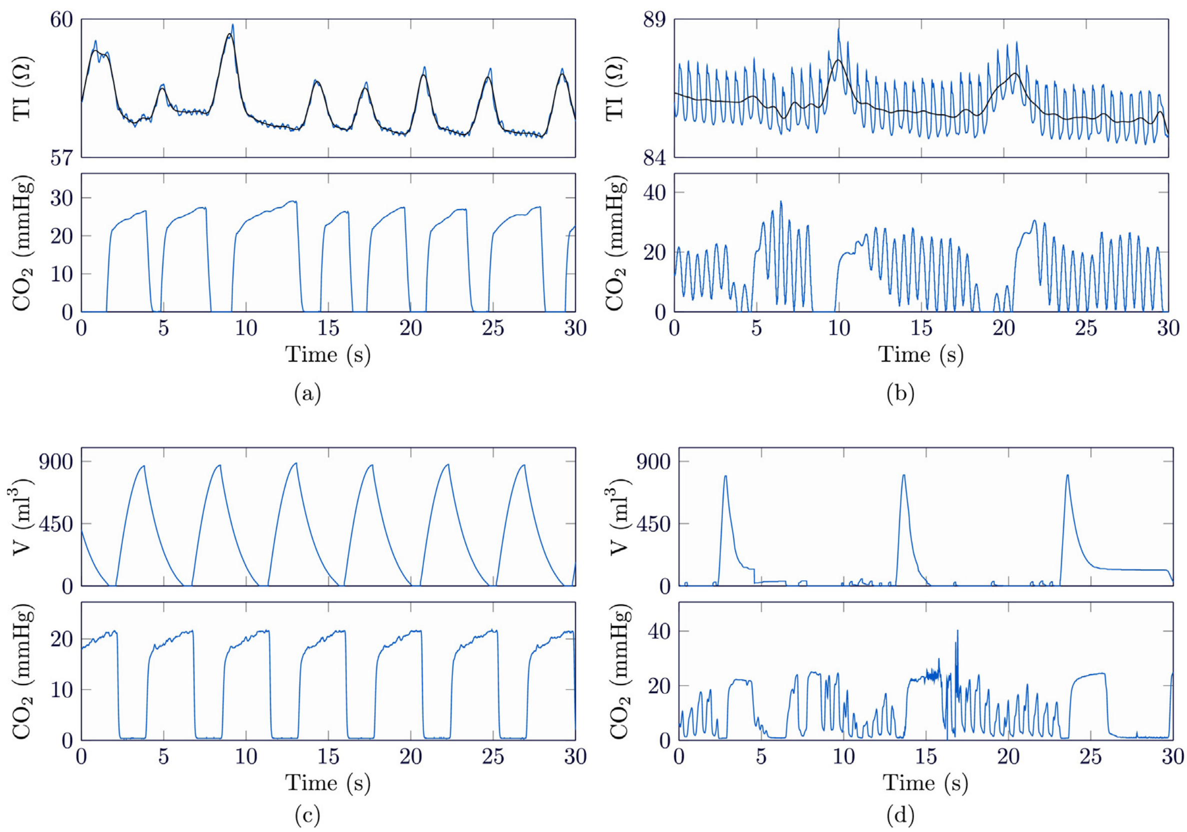

Fig. 1. Intervals from the out-of-hospital and in-hospital datasets, OHD and IHD, showing the capnogram and the Gold Standard (GS) to annotate ventilations. Panels a and b show OHD examples without and with chest compressions, with the impedance ventilation channel (GS) in black on top and the capnogram below. Panels c and d show IHD examples without and with CCs, with the air volume (GS) on top and the capnogram below.

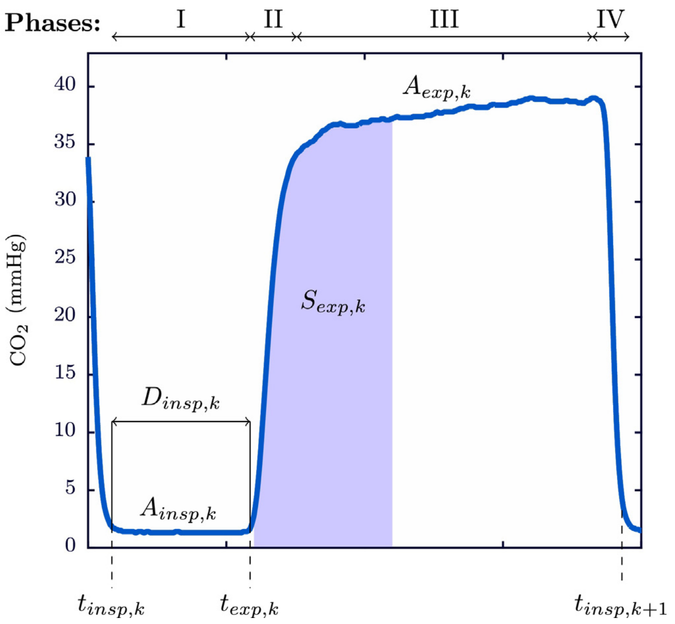

Fig. 2. The four phases of the normal capnogram and the features of the ventilation detector associated to potential ventilation number k. The time stamps $t_{insp,k}$ and $t_{exp,k}$ correspond to the inspiration and expiration times respectively.

Capnostat CO_2 sensor by Philips (−125/125 L/min, 4 mV/L/min, 100 Hz). The respiratory signals were acquired by the same monitor; the airflow and the air volume signals were used as gold standard (GS) to annotate the ventilations. Fig. 1 shows examples of two episodes of the IHD, where ventilations are visible in the air volume and the capnogram, for an artefact free interval (panel c) and when CCs were provided (panel d).

2.2. Ventilation detector

An automated algorithm that detects ventilations in the capnogram was developed based on the four basic phases of a normal capnogram shown in Fig. 2: the inspiration baseline (phase I), the expiration upstroke (phase II), the expiratory plateau (phase III) and the expiration downstroke (phase IV).

The capnogram was first low-pass filtered to remove spectral components above 10 Hz, and then a value of 5 mmHg was adopted as baseline. The inspiration (t_{insp}) and expiration (t_{exp}) times of potential ventilations were automatically detected from positive and negative peaks in the first difference of the signal. For every potential ventilation the five features shown in Fig. 2 were computed:

- Duration of the inspiration baseline, D_{insp}, in seconds.
- Mean CO_2 value of the inspiration baseline, A_{insp}, in mmHg.
- Mean CO_2 value of the expiratory plateau, A_{exp}, in mmHg.
- Area of the first second of the expiratory plateau, S_{exp}, in mmHg· s^{-1}.
- Relative CO_2 increase, $A_r = \frac{A_{exp} - A_{insp}}{A_{exp}}$.

The ventilation detector consists of a feature based decision algorithm which detects ventilations by comparing D_{insp} and the minimum distance between ventilations with a fixed threshold value (0.3 s and 1.5 s respectively) and features A_{exp}, S_{exp} and A_r with adaptive thresholds based on the last p ventilations as follows:

$$Th_k = \frac{w}{p} \cdot \sum_{n=k-p}^{k} x_n \tag{1}$$

Table 1
Characteristics of the out-of-hospital dataset (OHD) and the in-hospital dataset (IHD).

Parameter	OHD	IHD
Number of episodes	62	21
Total duration (min)	2545	2335
Total number of ventilations (% with CPR)	16,899 (38)	29,841 (8)
Instantaneous ventilation rate (min^{-1})	9.9 (8.7–13.1)	14.3 (12.6–18.2)
Minutes with hyperventilation per episode (%)	10 (2–35)	14 (0–88)

where Th_k is the adaptive threshold for kth potential ventilation, w is a weighting factor between 0 and 1, and x_n represents the value of the feature for ventilation n.

A more detailed technical description of the algorithm is supplied in the Appendix A, where signal processing techniques and ventilation detection criteria for the decision algorithm are supplied. Two illustrative examples are also included to provide intermediate results that clarify the implementation of the algorithm.

2.3. Instantaneous ventilation rate and hyperventilation alarm

The instants of ventilations detected in the capnogram were used to compute the ventilation rate and to report hyperventilation alarms when an established rate was exceeded. Both measures could be used to give real-time feedback to the rescuer. The instantaneous ventilation rate was computed every 15 s as the inverse of the median interval between ventilations in the previous minute. Hyperventilation was defined for rates exceeding 15 min^{-1}, following the criteria established by Kramer Johansen et al.[13]

2.4. Evaluation and statistical analysis

The episodes of the OHD were randomly allocated to training and test sets. The ventilation detector was developed with the training set of the OHD, and evaluated with OHD test set and the complete IHD. Results are given separately for intervals with and without CCs. All the results were reported as median (interquartile range, IQR), as data did not pass the Anderson-Darling normality test.

The performance of the ventilation detector was evaluated in terms of sensitivity (SE), the proportion of correctly detected ventilations, and Positive Predictive Value (PPV), the proportion of detected ventilations corresponding to real ventilations.

The Concordance Correlation Coefficient (CCC) was reported in order to quantify the agreement between the ventilation rate calculated from the GS and from the algorithm. The percentage of ventilation rate errors >2 min^{-1} per episode were reported. Bland-Altman plots were used to show the level of agreement (95% LOA) between the algorithm and the GS.

The performance of the hyperventilation detector was evaluated in terms of correctly detected hyperventilation alarms and the number of false hyperventilation alarms.

3. Results

Table 1 summarizes the main characteristics of the datasets. For the 62 episodes of the OHD the duration was 38 (34–46) min, the median ventilation rate per episode was 9.9 (8.7–13.1) min^{-1} and the hyperventilation fraction per episode was 10 (2–35)%. For the 21 episodes of the IHD the duration was 91 (50–141) min, the median ventilation rate per episode was 14.3 (12.6–18.2) min^{-1}

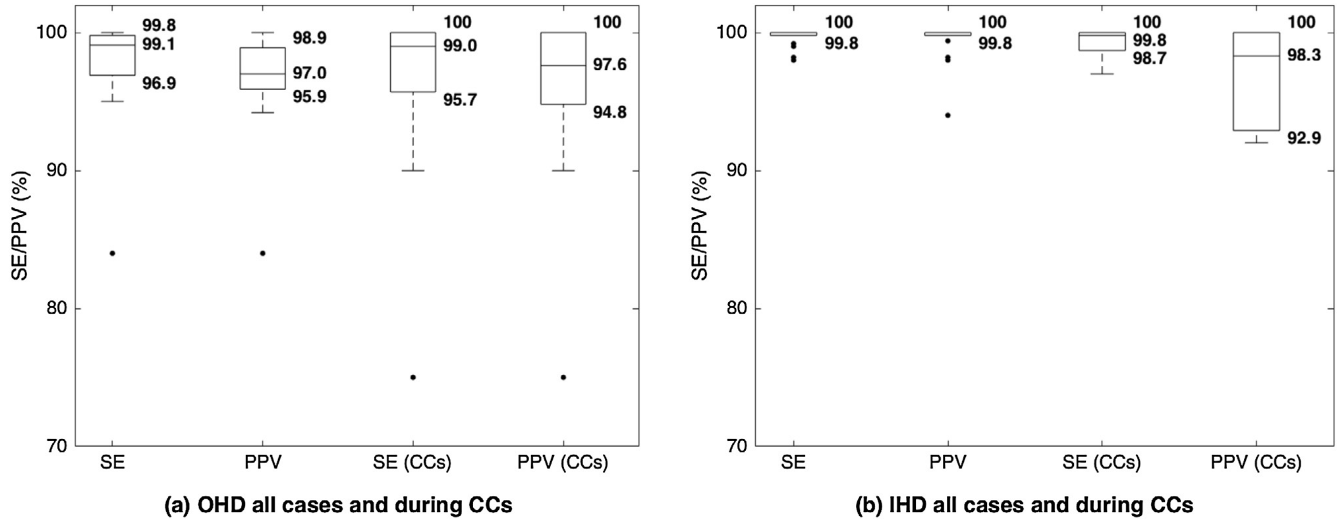

Fig. 3. Box plots showing the performance of the ventilation detector for the out-of-hospital dataset, OHD, in panel a, and for the in-hospital dataset, IHD, in panel b. Results are also given for the intervals with chest compressions (CCs).

with 14 (0–88)% of hyperventilation fraction. The OHD episodes were allocated randomly to training (37) and test sets (25). Fig. 3 shows the boxplot of the performance of the ventilation detector for both the OHD and IHD datasets. The SE was above 99% and the PPV above 97% overall. The boxplots show a slight deterioration for the intervals during CCs. The median SE and PPV decreased at most one point during CCs, and the lower quartile between 1 and 7 points.

Fig. 4 shows four examples where the dashed lines represent ventilations annotated in the GS and the red triangles represent the ventilations detected by the algorithm. Panels a and b show two examples of OHD where ventilations were missed due to too short inspiration intervals (panel a) and because of the 'shark fin' waveform of the capnogram (panel b). Panels c and d show intervals of the OHD and IHD, where the ventilations were correctly identified despite severe CC artefacts.

The concordance between the instantaneous ventilation rate obtained from the GS and from the algorithm was high (CCC > 0.98) for the two datasets, even during CCs. The proportion of errors larger than >2 min^{-1} were 0 (0–4.2)% per episode for the OHD and 0 (0–1.2)% for the IHD. Fig. 5 shows the Bland-Altman plots and the 95% LOA between the GS and the algorithm, which was in all cases smaller than 1.8 min^{-1}.

For the OHD, the algorithm correctly detected 841 of 860 alarms, and 26 of the 867 given alarms were false. For the IHD, the hyperventilation detector correctly reported 3563 of the 3566 hyperventilation alarms, and 12 of the 3575 given were false.

4. Discussion

This study proposes an automatic algorithm to detect ventilations using the capnogram, and thoroughly tests its accuracy for ventilation rate feedback during CPR, specifically addressing intervals in which CCs were delivered. The algorithm identifies the instants of ventilations based on adaptive thresholds to accommodate to the time-varying levels of CO_2, and avoids the rapidly changing artefacts added by the CCs. This algorithm would permit an accurate ventilation rate monitoring and a better control of hyperventilation both in- and out-of-hospital, where rates recommended by resuscitation guidelines are frequently exceeded.[5–7,9–12]

4.1. The dataset and the gold standard

The dataset used in this study includes both in-hospital and OHCA episodes, with a total of 46,740 ventilations (8741 during CCs). In the OHD impedance was used as gold standard, and annotations were reviewed with the capnogram, but only in unclear intervals (see panel a of Fig. 4). This procedure, which was a standard practice in previous studies because no better gold standard is available for the OHCA data,[23] might limit the validity of the results. In order to overcome this limitation an independent GS, not available in the OHCA setting, was introduced in the IHD, the airway flow signal which provides reliable information for ventilation monitoring.[1,23] In our IHD the airway flow and volume signals from the NICO respiratory monitor by Philips were used as GS. The number of episodes in our IHD is small, however this dataset contains the most reliable GS used to date to validate capnogram based ventilation detectors during cardiac arrest. The results obtained with this dataset confirmed the accuracy observed for the ventilation detection algorithm with the OHCA dataset.

The global SE/PPV of the detector were 0.7/2.8 points better for the IHD than for the OHD (Fig. 3), which may reflect various factors. On the one hand, the capnography technique was different in our two datasets, mainstream for the IHD and sidestream for the OHD.[25] In mainstream capnography the sensor is located directly in the way of the expired flow. In sidestream capnography a sample of the patient's expired gases is trasported to the sensor site using a 1–2 m long tube. This produces a delay in the capnogram with respect to the TI (4 s in our data) and the diffusion of the gases during transport lowers the slopes (dampening) of the capnogram.[26] This last effect might jeopardize the discrimination of ventilations in the OHD, as the algorithm is based on the detection of abrupt changes in the capnogram, and might partially explain the lower accuracy obtained for the OHD dataset. On the other hand, the OHD reflects more challenging scenarios in which ventilations were manual and CPR was delivered in most of the cases, while 15 of the 21 in-hospital cases were mechanically ventilated and/or had no CCs. However, when cases during CPR were considered the results were similar for the OHD and IHD (see Fig. 3 during CPR). This primarily is because during CPR both datasets reflected the effects of greater variability in ventilation patterns, CC artefacts and the intervention of multiple rescuers. The results for the IHD data with a reliable and independent GS confirm the observations on the larger OHD, and the

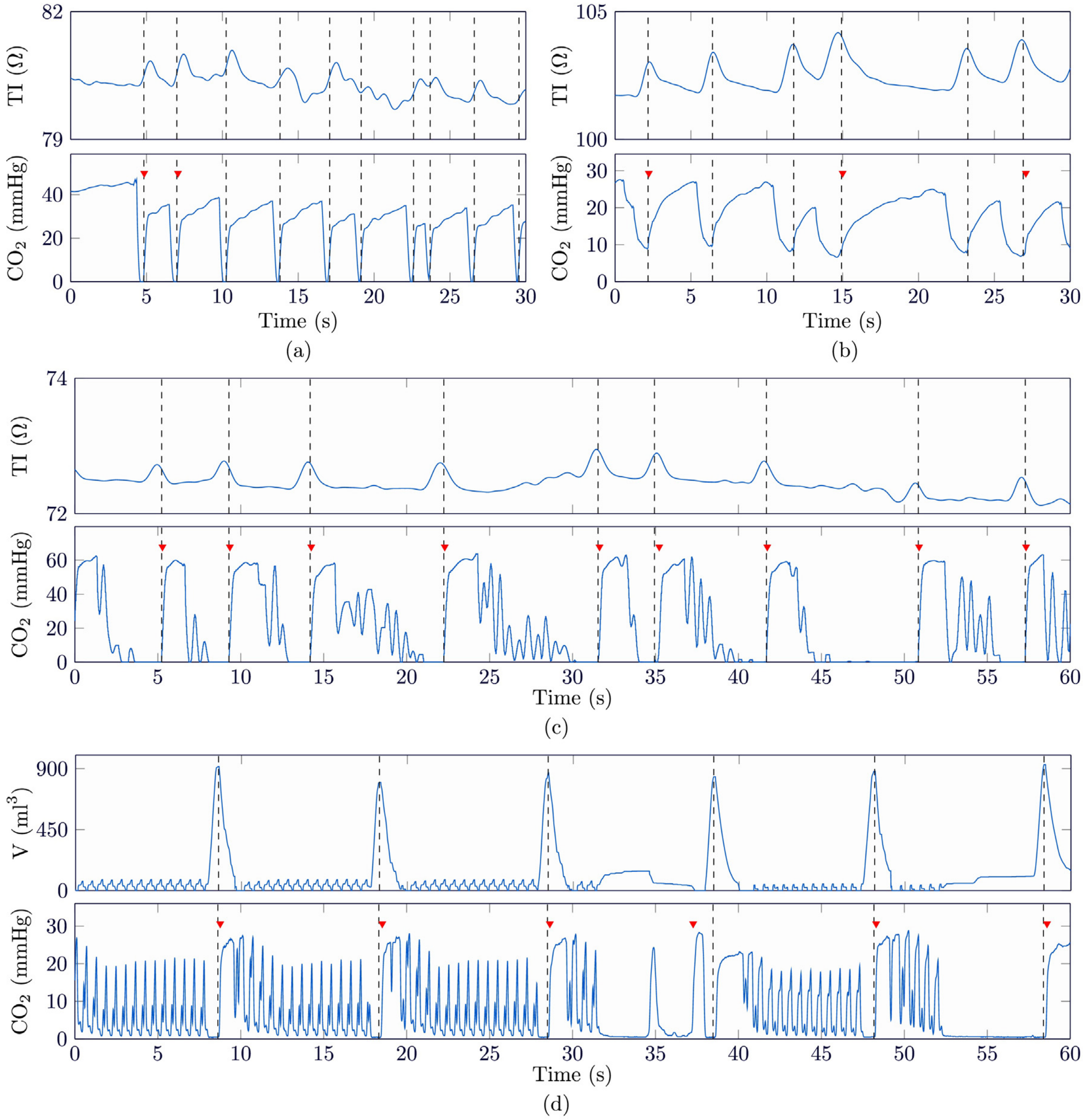

Fig. 4. Performance of the ventilation detection algorithm with four episodes. The examples of panels a, b and c correspond to episodes from the out-of-hospital dataset, and example of panel d to an episode from the in-hospital dataset. For every example the gold standard (GS) is shown (impedance ventilation signal or air flow volume signal). The GS annotations are shown with black dashed lines, and the detected ventilations with red triangles. (For interpretation of the references to color in this figure legend, the reader is referred to the web version of this article.)

accuracy of the algorithm with both mainstream and sidestream capnography.

4.2. The capnogram based ventilation detector

To date few capnogram based ventilation detectors applicable to OHCA data have been described. However, the universalization of the capnogram during ALS and the importance of adequate ventilation for the survival of the patient call for new and improved capnogram based ventilation feedback algorithms. Our method relies on an adaptive thresholding to classify possible ventilations detected in the first derivative (slope) of the capnogram. A preliminary version of the method was previously described.[27] Edelson et al. proposed an adaptive CPR artefact suppressing filter before detecting ventilations in the first derivative of the filtered signal and then used fixed detection thresholds.[23] Adaptive filtering requires additional CPR-assist pad signals, such as depth, acceleration and/or force signal. These signals need to be synchronized to the capnogram which is often recorded by a different device. Edelson et al. reported SE/PPV of 82/91% respectively for the ventilation detector, slightly below our results, and >80% of the rate errors below $\pm 2\,\text{min}^{-1}$, compared to the >90% of our algorithm. As it can be observed in Fig. 4 the error of our algorithm hardly increased for the intervals with CCs in the OHD, with LOAs close to $1.8\,\text{min}^{-1}$; the difference is higher in the IHD where the LOA is $1.5\,\text{min}^{-1}$ in the intervals with CCs, and $0.5\,\text{min}^{-1}$ for the complete dataset. This difference is attributable to the CC artefacts as well as to the mechanical ventilations of the IHD.

Panels c and d of Fig. 4 show two cases where the algorithm was effective in the presence of large CC artefacts. Panels a and b, are two exceptional cases that show the limitations of the algorithm. Panel a corresponds to a ventilation technique leading to baselines too short to be detected as true ventilations. Panel b shows a capnogram of a patient with airway obstruction, due to bronchospasm,

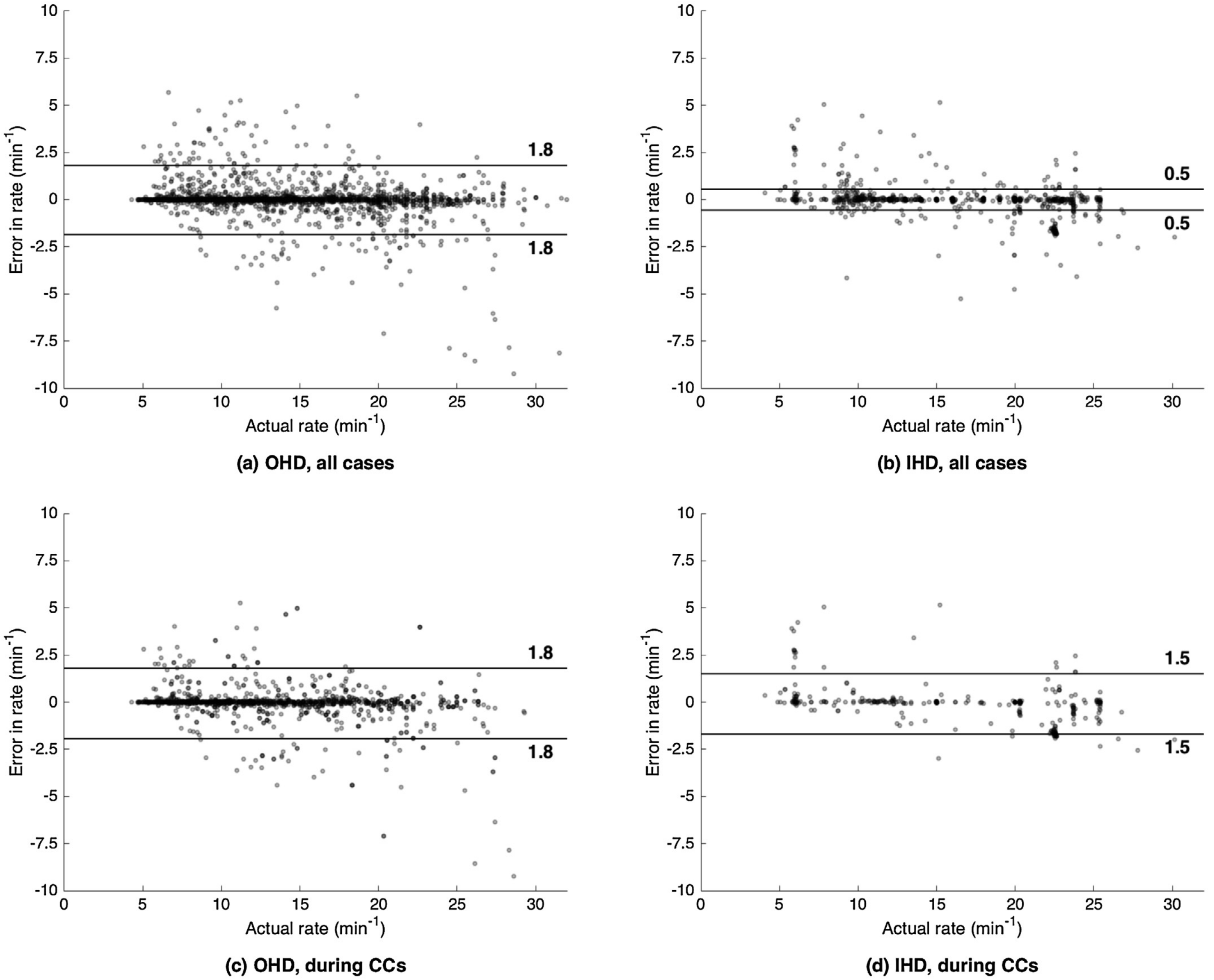

Fig. 5. Bland-Altman plots for the out-of-hospital and in-hospital datasets, OHD and IHD respectively, for all cases and for the intervals with chest compressions. The horizontal lines show the 95% level of agreement.

asthma or chronic obstructive pulmonary disease. In both cases the detector missed most of the ventilations of the interval.

The artefacts in the capnogram due to CCs were visually identified in previous studies[24,20] and are frequent in OHCA episodes, 73.3% of the cases in the study by Idris et al.[22] and 78.8% in our study (37.6% of the ventilations). The severity of the artefact has not been characterized yet and might vary with the position/depth of the CCs, the physiology of the patient, and probably with the technology used to acquire. It is known that the sidestream capnography shows artifacts and distortions that may appears as false disease waveforms,[26] and it might also show different susceptibility to CC artifacts compared to mainstream capnography. A thorough research is needed for a better understanding of the level, characteristics and differences of the CC artefact in both capnography sampling techniques.

4.3. Application scenarios

Monitoring ventilation rate to avoid hyperventilation is a challenge in OHCA scenarios where many feedback systems are available for CCs but not for ventilatory assistance. During BLS, the impedance measured through defibrillation pads has been proposed to monitor ventilations. Although impedance can be used for debriefing, it showed limited performance for monitoring instantaneous ventilation rate. Alonso et al. reported significant errors due to non ventilatory components of the impedance waveform,[17] an observation consistent with the manual annotations required in several studies on CPR quality.[11,28] For ALS, where advance airway management is integrated, the latest guidelines encourage the use of the capnogram to monitor CPR quality. Our results show that ventilation rate algorithms should be further evaluated with capnograms acquired during CCs before they are incorporated into feedback systems.

4.4. Limitations

The use of the algorithm is limited by the characteristics of the capnograms. As capnogram is dependent on the perfusion and metabolism of the patient, for very low levels (<5 mmHg in our algorithm), ventilations would not be detected. The IHD used to test the algorithm is limited by the number of episodes, 6 out of 21, which include CCs. Although few cases were available, the inclusion of this dataset enabled the validation of the algorithm with a robust and independent GS.

5. Conclusions

Our study proves that an accurate feedback on ventilation rate using only the capnogram is feasible, even in intervals where the capnogram signal is severely corrupted by CCs. Technology based on this type of algorithms could be integrated in monitor/defibrillators to provide reliable feedback on ventilation rate and alarms on hyperventilation during CPR.

Ethical approval

The CPR process files used in the OHD were collected as part of an effort to develop an airway check algorithm using the capnogram. Since these raw data files have no identifying information, the Institutional Review Board at the Oregon Health & Science University determined that the proposed activity is not human subject research because the proposed activity does not meet the definition of human subject per 45 CFR 46.102(f).

The files used in the IHD were collected as part of the investigation approved by the ethics committee of the Medical University in Vienna. Subjects resuscitated successfully signed written informed consent. For all others the Institutional Review Board waived the need for informed consent [https://ekmeduniwien.at/core/catalog/2012 (EK-Nr: 1574/2012)].

Conflict of interest statement

Mohamud Daya is an unpaid consultant for Philips Healthcare.

Acknowledgements

This work received financial support from the Ministerio de Economía y Competitividad of Spain and FEDER through the projects TEC2012-31928 and TEC2015-64678-R, and from the University of the Basque Country (UPV/EHU) through the unit UFI11/16. The Medical University of Vienna received support in the form of a grant and the equipment used from Philips Healthcare, Bothell, WA, USA.

Appendix A. Supplementary data

Supplementary data associated with this article can be found, in the online version, at http://dx.doi.org/10.1016/j.resuscitation.2016.08.033.

References

1. Soar J, Nolan JP, Böttiger BW, et al. European Resuscitation Council Guidelines for Resuscitation 2015. Resuscitation 2015;95:100–47.
2. Woodson RD. Physiological significance of oxygen dissociation curve shifts. Crit Care Med 1979;7:368–73.
3. Madden JA. The effect of carbon dioxide on cerebral arteries. Pharmacol Ther 1993;59:229–50.
4. Karlsson T, Stjernström EL, Stjernström H, Norln K, Wiklund L. Central and regional blood flow during hyperventilation. An experimental study in the pig. Acta Anaesthesiol Scand 1994;38:180–6.
5. Aufderheide TP, Sigurdsson G, Pirrallo RG, et al. Hyperventilation-induced hypotension during cardiopulmonary resuscitation. Circulation 2004;109:1960–5.
6. Aufderheide TP, Lurie KG. Death by hyperventilation: a common and life-threatening problem during cardiopulmonary resuscitation. Crit Care Med 2004;32(Suppl.):S345–351.
7. O'Neill JF, Deakin CD. Do we hyperventilate cardiac arrest patients? Resuscitation 2007;73:82–5.
8. Yannopoulos D, Tang W, Roussos C, Aufderheide TP, Idris AH, Lurie KG. Reducing ventilation frequency during cardiopulmonary resuscitation in a porcine model of cardiac arrest. Respir Care 2005;50:628–35.
9. Abella BS, Alvarado JP, Myklebust H, et al. Quality of cardiopulmonary resuscitation during in-hospital cardiac arrest. JAMA 2005;293:305–10.
10. McInnes AD, Sutton RM, Orioles A, et al. The first quantitative report of ventilation rate during in-hospital resuscitation of older children and adolescents. Resuscitation 2011;82:1025–9.
11. Stecher FS, Olsen J-A, Stickney RE, Wik L. Transthoracic impedance used to evaluate performance of cardiopulmonary resuscitation during out of hospital cardiac arrest. Resuscitation 2008;79:432–7.
12. Park SO, Shin DH, Baek KJ, et al. A clinical observational study analysing the factors associated with hyperventilation during actual cardiopulmonary resuscitation in the emergency department. Resuscitation 2013;84:298–303.
13. Kramer-Johansen J, Edelson DP, Losert H, Köhler K, Abella BS. Uniform reporting of measured quality of cardiopulmonary resuscitation (CPR). Resuscitation 2007;74:406–17.
14. Hostler D, Everson-Stewart S, Rea TD, et al. Effect of real-time feedback during cardiopulmonary resuscitation outside hospital: prospective, cluster-randomised trial. BMJ (Clinical research ed.) 2011;342:d512.
15. Aase SO, Myklebust H. Compression depth estimation for CPR quality assessment using DSP on accelerometer signals. IEEE Trans Biomed Eng 2002;49:263–8.
16. Ayala U, Eftestøl T, Alonso E, et al. Automatic detection of chest compressions for the assessment of CPR-quality parameters. Resuscitation 2014;85:957–63.
17. Alonso E, Ruiz J, Aramendi E, et al. Reliability and accuracy of the thoracic impedance signal for measuring cardiopulmonary resuscitation quality metrics. Resuscitation 2015;88:28–34.
18. Risdal M, Aase SO, Stavland M, Eftestøl T. Impedance-based ventilation detection during cardiopulmonary resuscitation. IEEE Trans Bio-Med Eng 2007;54:2237–45.
19. Losert H, Risdal M, Sterz F, et al. Thoracic impedance changes measured via defibrillator pads can monitor ventilation in critically ill patients and during cardiopulmonary resuscitation. Crit Care Med 2006;34:2399–405.
20. Daya MR, Idris AH, Helfenbein ED, Babaeizadeh S, Zhou S, Zive D. Abstract 237: assessment of airway placement during out-of-hospital cardiac arrest using an automated capnogram analysis algorithm. Circulation 2010;122(Suppl. 21):A237.
21. Daya M, Helfenbein E, Idris A, et al. Abstract 84: hyperventilation alert during out-of-hospital cardiopulmonary resuscitation using an automated capnogram analysis algorithm. Circulation 2011;124(Suppl.):A84.
22. Idris AH, Daya M, Owens P, et al. Abstract 83: high incidence of chest compression oscillations associated with capnography during out-of-hospital cardiopulmonary Resuscitation. Circulation 2010;122(Suppl.):A83.
23. Edelson DP, Eilevstjønn J, Weidman EK, Retzer E, Hoek TLV, Abella BS. Capnography and chest-wall impedance algorithms for ventilation detection during cardiopulmonary resuscitation. Resuscitation 2010;81:317–22.
24. Aramendi E, Alonso E, Russell JK, Daya M, Gonzlez-Otero D, Ayala U. Monitoring respiratory rate with capnography during cardiopulmonary resuscitation. Resuscitation 2014;85(Suppl. 1):S26–7.
25. Jaffe MB. Mainstream or sidestream capnography?, vol. 4. Respironics, Inc.; 2002. p. 5.
26. Pascucci RC, Schena JA, Thompson JE. Comparison of a sidestream and mainstream capnometer in infants. Crit Care Med 1989;17:560–2.
27. Elola A, Chicote B, Aramendi E, et al. A method to measure ventilation rate during cardiopulmonary resuscitation using the capnogram. In: Computing in Cardiology Conference (CinC), 2015. 2015. p. 1001–4.
28. Idris AH, Beadle S, Daya M, Zive D. Abstract P101: comparison of ventilation rate measured with thoracic bioimpedance and with capnography during out-of-hospital cardiopulmonary resuscitation. Circulation 2008;118(Suppl. 18):S_1467.

APPENDIX A: Algorithm for detecting the ventilations in the capnogram

This section describes in detail the algorithm proposed in the paper to detect ventilations in the capnogram. All the technical details and procedures to fully reproduce the algorithm are provided. The appendix is structured in four subsections describing: the signal preprocessing and detection of potential ventilations, feature computation, the decision algorithm and two illustrative examples.

A.1 Signal preprocessing and detection of potential ventilations

The capnogram was preprocessed, first applying low-pass order 4 butterworth filter to remove spectral components above 10 Hz. The filtered signal thus obtained is denoted as $CO_2[n]$ where n is the waveform sample index, which is related to time by $t = \frac{1}{f_s}$, being f_s the sampling rate. Finally, a 5 mmHg value was used as a baseline to compute the preprocessed signal $s[n]$ as follows:

$$s[n] = \begin{cases} CO_2[n] & \text{if } CO_2[n] \geq 5\,\text{mmHg} \\ 0 & \text{if } CO_2[n] < 5\,\text{mmHg} \end{cases}$$

Potential ventilations were identified in the slope of $s[n]$ computed as:

$$d[n] = f_s \cdot (s[n] - s[n-1]) \qquad (1)$$

and the expiration (t_{exp}) and inspiration (t_{insp}) times were identified for potential ventilation when $d[n] > 0.35 \cdot f_s\,\text{mmHg} \cdot \text{s}^{-1}$ (for t_{exp}) and $d[n] < -0.45 \cdot f_s\,\text{mmHg} \cdot \text{s}^{-1}$ (for t_{insp}).

Fig. 6 shows the preprocessed signal, $s[n]$, for two illustrative examples. The a case corresponds to the $0 - 30$ s interval of case b in Fig. 4, and case b corresponds to the $17 - 47$ s interval of case d in Fig. 4.

A.2 Feature computation

For each potential ventilation (k-th ventilation) a set of features was computed using the following formulas:

$$D_{insp,k} = t_{exp,k} - t_{insp,k} \qquad (2)$$

$$A_{exp,k} = \frac{1}{f_s \cdot (t_{insp,k+1} - t_{exp,k})} \sum_{n=t_{exp,k} \cdot f_s}^{t_{insp,k+1} \cdot f_s} s[n] \tag{3}$$

$$A_{insp,k} = \frac{1}{f_s \cdot (t_{exp,k} - t_{insp,k})} \sum_{n=t_{insp,k} \cdot f_s}^{t_{exp,k} \cdot f_s} s[n] \tag{4}$$

$$A_{r,k} = \frac{A_{exp,k} - A_{insp,k}}{A_{exp,k}} \tag{5}$$

$$S_{exp,k} = \frac{1}{f_s} \sum_{n=t_{exp,k} \cdot f_s}^{(t_{exp,k}+1) \cdot f_s} s[n] \tag{6}$$

The physical meaning and graphical representation of the features are shown in section 2.2 and Fig. 2 of the manuscript.

In addition the time elapse between the potential k-th ventilation and the last true ventilation detected was computed in seconds and denoted as $t_{ref,k}$.

A.3 Decision algorithm

Fig. 7 shows the decision algorithm applied to every k-th potential ventilation. The criteria included comparing the features with either fixed or adaptive thresholds. If all the criteria were met the j-th true ventilation was identified in the instant $t_j = t_{exp}$. The adaptive thresholds Th_1, Th_2 and Th_3 applied to A_{exp}, A_r and S_{exp} respectively, were initiated for $k = 1$ with $Th_{1,1} = 5$; $Th_{2,1} = 0.5$; $Th_{3,1} = 0$, and updated for the k-th potential ventilation using values of the features associated to previously detected ventilations. Formulas applied to the thresholds were:

$$Th_{1,k} = \frac{0.4}{5} \cdot \sum_{n=j-5}^{j-1} A_{exp,n} \tag{7}$$

$$Th_{2,k} = \frac{0.7}{5} \cdot \sum_{n=j-5}^{j-1} A_{r,n} \tag{8}$$

$$Th_{3,k} = \frac{0.4}{2} \cdot \sum_{n=j-2}^{j-1} S_{exp,n} \tag{9}$$

where $j-1$ denotes the last detected true ventilation prior to the k-th potential ventilation. For Th_2 a minimum value of 0.5 was set.

A.4 Illustrative examples

Fig. 6 shows the intermediate results of the algorithm applied to two illustrative examples: a corresponding to the interval of case in Fig. 4 b, and b corresponding to the $17-47\,$s interval of case in Fig. 4 d. The t_{exp} and t_{insp} instants of every potential ventilation that fulfilled the criterion of $D_{insp} > 0.3\,$s are plotted in dashed and in dotted lines respectively. The ventilations that met all the criteria of the algorithm to be a true ventilation are marked with a red triangle in the t_j instant.

In the first example, for the initial 6 ventilations the range of values for the A_{exp} was $17-22$, higher in all cases than Th_1, in the $7-8$ range; S_{exp} values, $14-17$, were higher than the threshold for Th_3 in the range of $6-9$ and $t_{ref} > 1.5$, fulfilling the criteria of the algorithm. The values for A_r were in the range of $0.37-0.55$ and only 3 of the potential ventilations fulfilled the criteria of $> Th_2 = 0.5$; they are marked with red triangles.

In the second example a total of 26 ventilations were detected as potential ventilations. The A_{exp} was $6-23$ (Th_1 in $8-9$ range); S_{exp} was $2-23$ (Th_3 in $7-9$ range) and A_r was $0.97-0.99$ ($Th_2 = 0.68-0.69$). Only potential ventilations 1, 13, 15 and 16, as numbered in Fig. 6, met the criteria. The application of $t_{ref} > 1.5$ criterion rejected ventilation 16 as shown with red triangles.

List of Figures

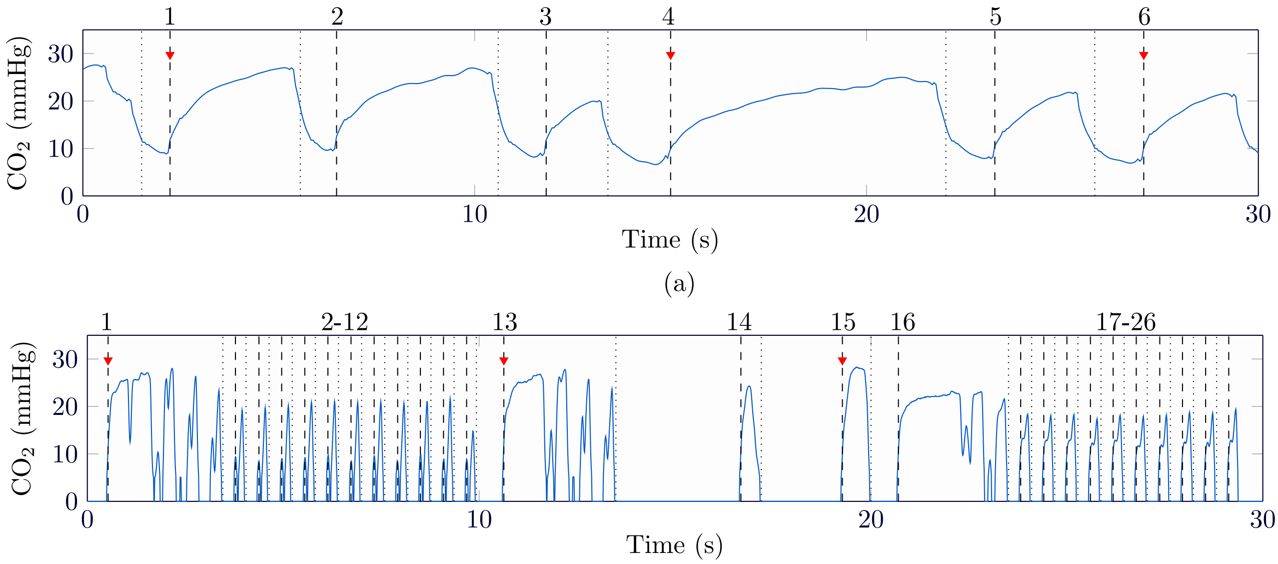

(a)

(b)

Figure 6: Examples of a failed case a and a successful case b, corresponding the $0 - 30\,\mathrm{s}$ interval of case b of Fig. 4 and the $17 - 47\,\mathrm{s}$ interval of case d of Fig. 4 respectively. The potential t_{exp} and t_{insp} are depicted with dashed and dotted lines respectively. The final ventilations are marked with red triangles.

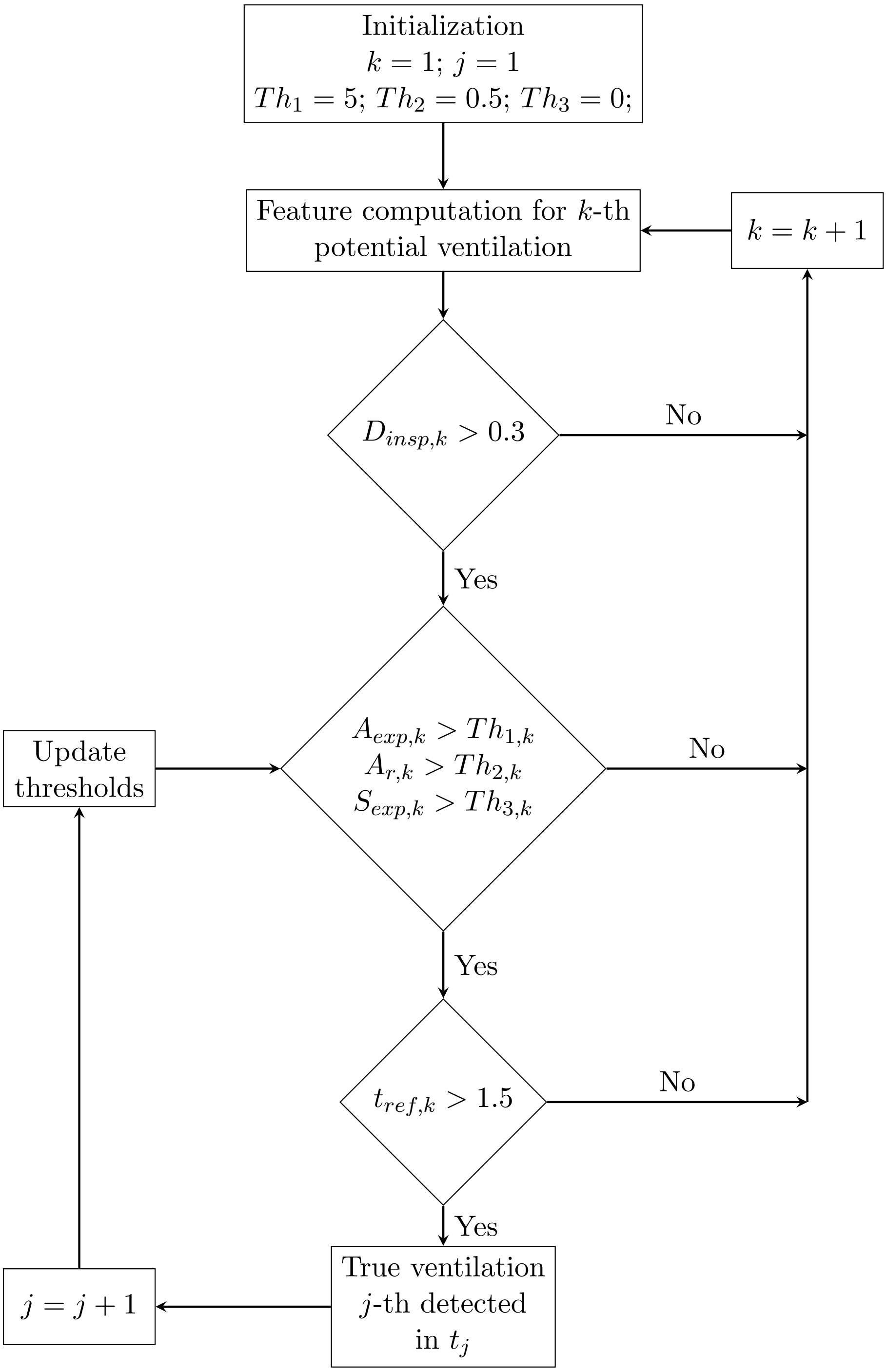

Figure 7: Block diagram of the decision algorithm

A.2.2 Bigarren helburuari lotutako aurreneko argitalpena nazioarteko aldizkarian

A.6. Taula. Bigarren helburuari lotutako aurreneko argitalpena nazioarteko aldizkarian.

	Argitalpena nazioarteko aldizkarian
Erreferentzia	Andoni Elola, Elisabete Aramendi, Unai Irusta, Erik Alonso, Yuanzheng Lu, Mary Chang, Pamela Owens, Ahamed Idris, "Capnography: A support tool for the detection of return of spontaneous circulation in out-of-hospital cardiac arrest", *Resuscitation 2019*, vol.142, pp. 153-161.
Kalitate adierazleak	• **Argitalpen mota**: JCRen indexatutako aldizkari artikulua • **Kuartila**: Q1 (2/31) (*Web of Science* 2019) • **Inpaktu faktorea**: 4.215

RESUSCITATION 142 (2019) 153–161

Available online at www.sciencedirect.com

Resuscitation

journal homepage: www.elsevier.com/locate/resuscitation

Clinical paper

Capnography: A support tool for the detection of return of spontaneous circulation in out-of-hospital cardiac arrest

Andoni Elola[a,*], Elisabete Aramendi[a], Unai Irusta[a], Erik Alonso[a], Yuanzheng Lu[b], Mary P. Chang[c], Pamela Owens[c], Ahamed H. Idris[c]

[a] Communications Engineering Department, University of the Basque Country UPV/EHU, 48013 Bilbao, Spain
[b] Emergency and Disaster Medicine Center, The Seventh Affiliated Hospital, Sun Yat-sen University, Shenzhen, China
[c] Department of Emergency Medicine, University of Texas SouthWestern Medical Center (UTSW), Dallas, United States

Abstract

Background: Automated detection of return of spontaneous circulation (ROSC) is still an unsolved problem during cardiac arrest. Current guidelines recommend the use of capnography, but most automatic methods are based on the analysis of the ECG and thoracic impedance (TI) signals. This study analysed the added value of $EtCO_2$ for discriminating pulsed (PR) and pulseless (PEA) rhythms and its potential to detect ROSC.

Materials and methods: A total of 426 out-of-hospital cardiac arrest cases, 117 with ROSC and 309 without ROSC, were analysed. First, $EtCO_2$ values were compared for ROSC and no ROSC cases. Second, 5098 artefact free 3-s long segments were automatically extracted and labelled as PR (3639) or PEA (1459) using the instant of ROSC annotated by the clinician on scene as gold standard. Machine learning classifiers were designed using features obtained from the ECG, TI and the $EtCO_2$ value. Third, the cases were retrospectively analysed using the classifier to discriminate cases with and without ROSC.

Results: $EtCO_2$ values increased significantly from 41 mmHg 3-min before ROSC to 57 mmHg 1-min after ROSC, and $EtCO_2$ was significantly larger for PR than for PEA, 46 mmHg/20 mmHg ($p < 0.05$). Adding $EtCO_2$ to the machine learning models increased their area under the curve (AUC) by over 2 percentage points. The combination of ECG, TI and $EtCO_2$ had an AUC for the detection of pulse of 0.92. Finally, the retrospective analysis showed a sensitivity and specificity of 96.6% and 94.5% for the detection of ROSC and no-ROSC cases, respectively.

Conclusion: Adding $EtCO_2$ improves the performance of automatic algorithms for pulse detection based on ECG and TI. These algorithms can be used to identify pulse on site, and to retrospectively identify cases with ROSC.

Keywords: Return of spontaneous circulation (ROSC), ROSC detection, Capnography, End-tidal CO_2 ($EtCO_2$), Electrocardiogram (ECG), Thoracic impedance

1 Introduction

The main goal of resuscitative efforts during out-of-hospital cardiac arrest (OHCA) is to achieve return of spontaneous circulation (ROSC). Those efforts include high quality cardiopulmonary resuscitation (CPR), during which chest compressions should be minimally interrupted for actions like rhythm analysis or pulse checks. Current pulse detection methods such as carotid pulse check, or checking for signs of life as recommended by the current guidelines, are both time consuming and inaccurate.[1–5] There is therefore a need for accurate and automated pulse detection methods[6] that can be used by

* Corresponding author.
E-mail address: andoni.elola@ehu.es (A. Elola).
https://doi.org/10.1016/j.resuscitation.2019.03.048
Received 10 December 2018; Received in revised form 27 February 2019; Accepted 18 March 2019

emergency medical personnel as a decision support tool to identify ROSC. Such methods would contribute to improve therapy, reduce and shorten pauses in chest compressions, and increase survival rates.[7,8]

Current guidelines support the use of capnography for early detection of ROSC.[9] Higher values of end tidal CO_2 ($EtCO_2$), and sudden increases in $EtCO_2$ have been linked to ROSC in OHCA.[10–13] Although some medical algorithms exist for the detection of ROSC using $EtCO_2$ values,[14] the only automatic method based on capnography was recently proposed.[15]

Most automatic methods for the detection of pulse in OHCA rest on the analysis of the ECG and the thoracic impedance (TI). The TI signal shows low amplitude fluctuations for every effective heartbeat,[16] so features characterizing the TI signal have been proposed alone,[17–19] or in combination with ECG features[20–22] for the detection of pulse. In this context, detection of pulse is framed as a classification problem with two types of organized rhythms: pulse-generating rhythms (PR) and pulseless electrical activity (PEA).

The purpose of this study was to evaluate the added value of capnography for the classification of PR/PEA during OHCA. First, $EtCO_2$ values were automatically detected in order to compare the values between patients with and without ROSC, and to analyse how $EtCO_2$ changed as the patient approached ROSC. Then, the added value of $EtCO_2$ for PR/PEA classification was evaluated by developing machine learning PR/PEA classifiers.

2 Materials

For this study we analysed 1561 OHCA episodes retrospectively, treated by the Dallas FortWorth Center for Resuscitation Research (UTSW, Dallas) using the Philips HeartStart MRx device between 2012 and 2016. The device files included the ECG and TI recorded through the defibrillation pads with sampling frequencies of 250 Hz/ 200 Hz respectively, and capnography recorded through sidestream acquisition with a sampling frequency of 125 Hz. The electronic files were linked to clinical annotations and ROSC was defined as palpable pulse in any vessel for any length of time. The first ROSC instant annotated by the rescuer on scene was the gold standard; based on that instant PR and PEA annotations were made automatically and patients with ROSC and without ROSC were classified.

The following patient inclusion/exclusion criteria were applied. Only episodes with TI, ECG and capnography were considered ($n = 835$). Cases where ROSC was suspected but not annotated by clinicians on site were excluded, which comprised patients transported to hospital ($n = 252$), or episodes with long periods (>2 min) without compressions presenting an organized rhythm with $EtCO_2$ above 25 mmHg ($n = 26$). Episodes with suspected intermittent ROSC were also excluded, these were episodes in which shocks or chest compressions (>2min) were delivered after the annotated onset of ROSC ($n = 76$). For our analysis of the ROSC cases, the capnogram had to be available at least 4 min before and 1 min after the onset of ROSC. If not, the case was excluded ($n = 55$). The final dataset contained 426 episodes, 117 with ROSC and 309 without ROSC. Fig. 1 shows a 3-min interval from two cases of the study dataset. In the ROSC case (top panel) $EtCO_2$ increases at ROSC onset, and after ROSC the heart rate increases and there is pulse related activity in the TI. In the no-ROSC case (bottom panel) $EtCO_2$ is always below 20 mmHg, and although the heart rate changes during PEA there is no pulse related activity in the TI.

3 Methods

Three analyses were conducted: $EtCO_2$ levels in episodes with and without ROSC, development and evaluation of a PR/PEA classifier using ECG/TI segments and $EtCO_2$ values, and a case study of the use of the classifier to retrospectively identify cases as ROSC/no-ROSC.

3.1 Analysis of $EtCO_2$ levels

Onset and offset of each ventilation were automatically delineated in the capnogram using a method introduced in a previous study.[23] For each ventilation, $EtCO_2$ was automatically calculated as the maximum CO_2 value during the alveolar plateau (see Fig. 1).

In ROSC cases, median $EtCO_2$ levels were computed every minute ($MEtCO_2$) in a 5 min interval around ROSC (4-min before to 1-min after). Similarly, for patients without ROSC, the $MEtCO_2$ values were computed for each one of the last 5 min of the episode. The $MEtCO_2$ value for the last minute of the episode corresponds to the last minute before the EOE, i.e. the instant when the monitor/ defibrillator was disconnected.

3.2 PR/PEA machine learning classifier

Following the classical scheme proposed in previous studies,[22,20,21] the detection of ROSC implies the discrimination between PR and PEA once an organized rhythm is identified by the shock advice algorithm. It is therefore a two class classification problem, for which, first, the dataset of PR/PEA segments was defined, and then a classifier was designed using features extracted from the ECG, TI and capnography signals.

3.2.1 PR/PEA segment dataset

PR and PEA segments of 3.2-s duration were extracted during intervals with no chest compression artefacts. Pauses in chest compressions were automatically detected using the compression depth signal from the CPR assist pad when available,[24] or the TI otherwise.[25] Segments with large ECG amplitude oscillations (>3.5 mV) were discarded as noisy, and then organized rhythms (PEA or PR) were detected during the pauses using an offline version of a rhythm analysis algorithm of a commercial automated external defibrillator (AED).[26] In ROSC cases, all segments before ROSC onset were labelled as PEA, and those after ROSC onset as PR (see Fig. 1, panel a). In no-ROSC cases, all segments were labelled as PEA (see Fig. 1, panel b). A minimum separation between consecutive segments of 20-s was enforced to foster ECG and TI waveform diversity in the segments.

3.2.2 Machine learning PR/PEA classifier

Nine PR/PEA classification features were computed from the most recently proposed algorithms, six ECG features introduced in Ref.[27] and three TI features.[22,17,28] These ECG and TI features are described in detail in Appendix A. The $MEtCO_2$, the median $EtCO_2$ in the minute before the analysis window (pause in chest compressions with organized ECG rhythm) was also added. The features were combined in a Random Forest (RF) classifier, a machine learning algorithm based on the aggregate vote of several independently designed uncorrelated decision trees.[29] RF classifiers

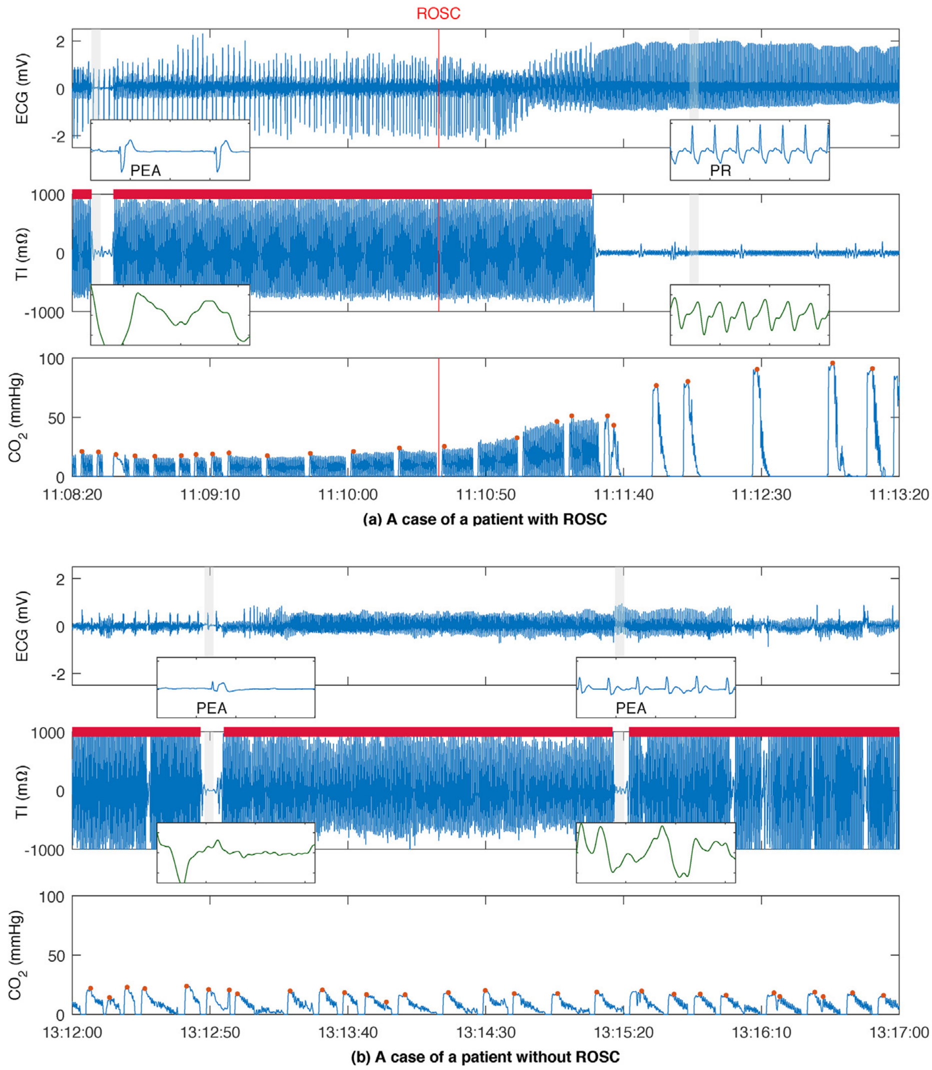

Fig. 1 – ECG, Thoracic Impedance (TI) and capnography signals for a patient with ROSC, panel (a), and without ROSC, panel (b). ROSC onset, as annotated by a clinician on site, is represented by a red line in the first example. The extracted 3.2-s segments are shaded in grey and the ECG and TI (green) are zoomed in. Chest compression intervals are depicted above TI signal. In the ROSC case a PEA and a PR segments were extracted in the depicted interval, and two PEA segments in the no-ROSC case. Ventilations were automatically detected in the CO_2 curve, and the automatically measured $EtCO_2$ value is highlighted with red dots. In the ROSC case after pulse recovery the ECG presents stable and normal QRS complexes and heart rate, and chest compressions are stopped so there is no activity in the impedance.

have shown excellent performance in many classification problems, including PR/PEA classification,[27] and are robust against annotation errors.

All patients were weighted equally to train the RF classifier and 300 trees were used. For each segment, the RF classifier computes the probability of being PR (p_{pr}), and segments were classified as PR for $p_{pr} > 0.5$ and as PEA otherwise. The classifier was trained and tested using a patient wise 10-fold cross-validation procedure.[30] For each of the 10 folds, the algorithm was optimized using 90% of the cases, and the accuracy results were obtained from the remaining 10% (test fold). This procedure guaranteed that the optimization of the classifier and the estimation of its accuracy were done on data from separate patients, and that the performance was assessed using all available data.

3.3 Case study: retrospective identification of patients with ROSC

Using the PR/PEA classifier, a simple method was developed to automatically identify patients with ROSC in a retrospective analysis of a set of OHCA episodes. This method may be used as an automated tool for post arrest debriefing or annotation. Complete episodes (until EOE) were processed and the case was labelled as ROSC if from any three consecutive segments at least two were identified as PR by the classifier.

Our ground truth was the ROSC instant annotated by clinicians on scene, which discriminated the group of patients with ROSC and patients without ROSC, and the detection of episodes with ROSC was evaluated using the test sets in the 10-fold cross validation procedure.

3.4 Statistical analysis

MEtCO$_2$ distributions did not pass the Kolmogorov–Smirnov normality test, and are reported as median and interquartile range (IQR). MEtCO$_2$ distributions at different times (within ROSC cases) or between ROSC/no-ROSC cases were compared using the Mann–Whitney *U* test. Differences were considered significant for $p < 0.05$.

PR/PEA classification was evaluated using Receiver Operating Characteristic (ROC) curves, and the area under the curve (AUC) was used as measure of performance.[31] The Youden index was used to define the optimal point in the ROC curve, which gives equal importance to the sensitivity (SE, for PR segments) and specificity (SP, for PEA segments).[32]

When the classifier was used as a retrospective tool to identify ROSC, SE and SP were defined as the proportion of correctly identified ROSC and no-ROSC cases, respectively.

4 Results

The mean (standard deviation) durations were 58 (23) min and 38 (11) min for the episodes with and without ROSC, respectively. The commercial AED algorithm detected 5098 segments with organized rhythms. A total of 3639 PR segments were extracted from episodes with ROSC, and 1459 PEA segments, 308 from episodes with ROSC and 1151 from episodes without ROSC. Some examples of the extracted ECG segments can be found in Figs. 1 and 4 . The median (IQR) ventilation rate per episode was 7.8 (5.7–10.5) min^{-1}.

The MEtCO$_2$ for ROSC cases were statistically significantly larger than for no-ROSC cases at all time-stamps (Fig. 2). Elevated EtCO$_2$ levels were observed in patients with ROSC, with an upward trend from 41 mmHg (at 3 min before ROSC) to 57 mmHg close to ROSC onset (see Fig. 2a).

Fig. 3 shows the ROC curves of the RF classifier for different features sets. The curves in panel (a) were calculated using the whole dataset, while the curves in panel (b) were calculated excluding the PEA segments extracted from patients with ROSC, that is the pre-ROSC PEA segments. The analysis of the ROC curves is shown in Table 1. The ROC curves showed that the AUC of the PR/PEA classifier increased as features from different sources were added. Including MEtCO$_2$ in the classifier increased the AUC for all feature combinations, thanks to the added uncorrelated information. Adding MEtCO$_2$ to an ECG-only and to an ECG+TI based classifiers increased their AUCs in 3 and 2-points, respectively. The best classifier combined all features and presented an AUC of 0.92 with a SE and SP of 84% and 86%, respectively (see Table 1). MEtCO$_2$ alone was also a good classifier (AUC around 0.76), the median MEtCO$_2$ values were 46 (32–64) mmHg for PR and 20 (8–38) mmHg for PEA segments ($p < 0.05$).

The accuracy of the classifiers increased when PEAs that transitioned to PR (episodes with ROSC) were not included. The accuracy increase was on average 4-points for all classifiers (see Table 1). Significant differences were observed between PEAs in ROSC and no-ROSC cases. The MEtCO$_2$ values of the PEA in the ROSC and no-ROSC cases were 31 (20–44) mmHg and 16 (7–35) mmHg ($p < 0.05$), respectively. The probabilities of being PR, p_{pr}, for the classifier with all features were also significantly different for these two subgroups of PEA, 0.09 (0.03–0.29) for the PEA from no-ROSC cases and 0.33 (0.11–0.58) for those of the ROSC cases ($p < 0.05$).

Fig. 4 shows the performance of the PR/PEA classifier with three consecutive segments in three patients. Each panel represents the 3 consecutive 3.2-s ECG and TI segments used for analysis, and the capnogram in the 1-min interval before the segment, which was used to compute MEtCO$_2$ (depicted as a dashed line). The text on top of each segment shows the true class followed by the class predicted by the classifier. The first example (panel a) shows a patient achieving ROSC transitioning from PEA to PR in which all segments were correctly classified. The first segment was taken 80 s prior to ROSC (PEA) and the other two after ROSC. It can be observed that heart rate, TI activity and MEtCO$_2$ (specially in PEA/PR transition) increase among consecutive segments. The second example (panel b) shows three correctly classified PEA segments in a patient without ROSC.

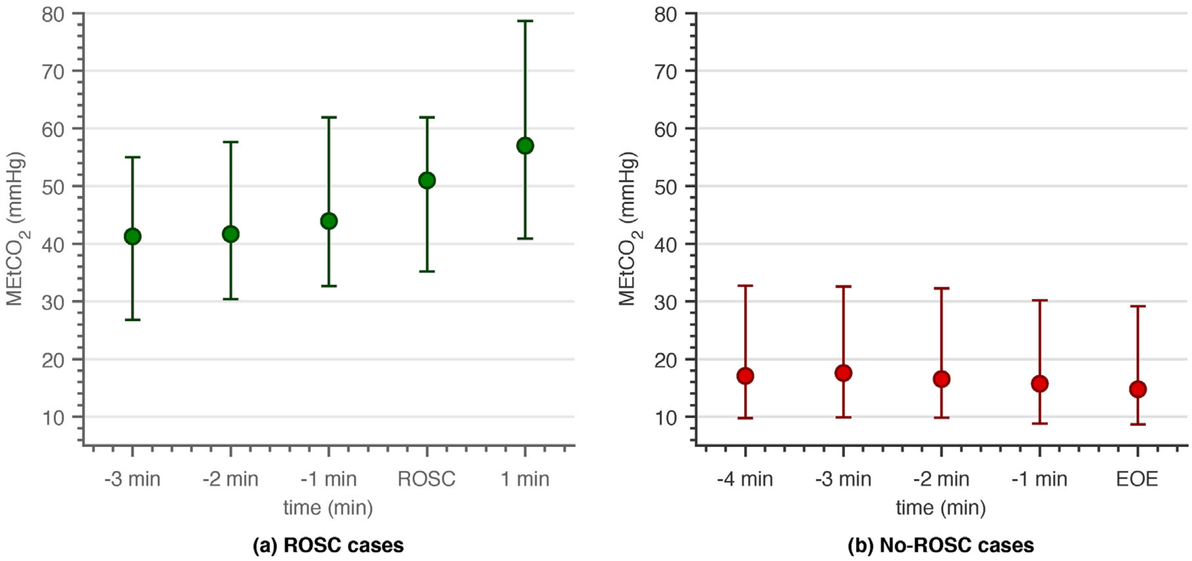

Fig. 2 – Median EtCO$_2$ (MEtCO$_2$) values and their interquartile ranges for cases with ROSC (left) and no-ROSC (right). For ROSC cases the interval around ROSC onset is analysed, in the no-ROSC cases the 5 min before the end of episode (EOE) are shown. MEtCO$_2$ was calculated as the median EtCO$_2$ value of all ventilations in a 1-min interval before the indicated time-stamp.

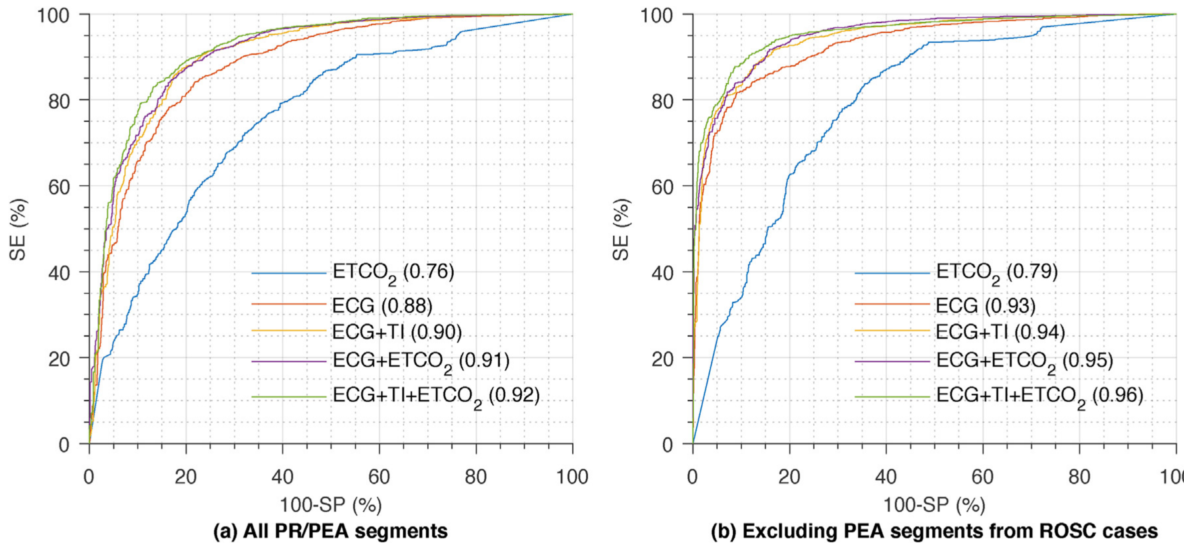

Fig. 3 – ROC curves of the RF classifier for different feature sets. Panel (a) shows results for the whole dataset, while panel (b) shows the curves after excluding the PEAs from episodes with ROSC. The AUC value for each classifier is shown between parentheses.

Table 1 – ROC curve analysis of the machine learning classifier when the whole PR/PEA dataset is considered and when the PEAs from ROSC cases were excluded. The SE and SP are given for the optimal point according to the Youden index.

	All PR/PEA segments			Excluding PEAs from ROSC		
	AUC	SE	SP	AUC	SE	SP
$EtCO_2$	0.76	72.3	67.8	0.79	83.7	64.6
ECG	0.88	84.2	78.2	0.93	81.7	90.8
ECG+TI	0.90	86.7	81.6	0.94	88.4	87.0
ECG+$EtCO_2$	0.91	86.3	81.5	0.95	91.8	84.2
ECG+TI+$EtCO_2$	0.92	83.9	86.0	0.96	87.8	91.3

Despite having a heart rate above 60 bpm, low $EtCO_2$ values and low circulation-related TI activity yielded the correct classification of the three segments and of the patient without ROSC. The third example, however, corresponds to a patient without ROSC incorrectly identified as patient with ROSC. Two of the segments were classified as PR because the ECG was regular with a heart rate above 60 bpm, the TI showed large fluctuations and $EtCO_2$ levels were above 30 mmHg.

When the PR/PEA classifier with all features was used as a retrospective tool to automatically identify episodes with and without ROSC, the SE and SP were 96.6% and 94.5%, respectively. Only 4 cases with ROSC were misidentified as no-ROSC, and 17 cases with no-ROSC were identified as ROSC cases.

5 Discussion

Detection of ROSC remains a challenge in OHCA, and there is still a need for a reliable monitoring of the hemodynamic state of the patient.[6] This study shows that $EtCO_2$ has great potential to support the rescuer in the identification of ROSC, both as a stand-alone marker but also in combination with the ECG and TI. This is, to the best of our knowledge, the first study that demonstrates that the addition of $EtCO_2$ improves PR/PEA classification based on the ECG or on the combination of ECG and TI.

The results shown in Fig. 2 and Table 1 reveal that a three-signal classifier provides better performance than two-signal solutions, which are better than a classifier based on a single signal. These results may help in the design of PR/PEA classification systems, and different solutions may be implemented depending on the availability or usability of the signals in a particular monitor/defibrillator.

For this study, we extracted PEA segments from patients with and without ROSC, and we relied on the ROSC onset annotations made by clinicians on site. We believe that is the most realistic (and challenging) scenario, although we observed differences in the characteristics of the PEA obtained from patients that ultimately recovered ROSC and those who did not. $MEtCO_2$ levels during PEA were significantly higher in patients that recovered ROSC, and the AUCs of the PR/PEA classifiers increased by over 4-points when PEAs from patients that recovered ROSC were not included. In fact, the SP for the PEAs of the patients that recovered ROSC was 61.2%, significantly lower than 91.2% obtained for the patients with no ROSC. There are two main reasons behind the differences in SP. First, the instant of ROSC annotated by clinician on scene and used as gold standard might show some delay depending on the rescuer. Second, there are differences between PEAs leading to PR (from ROSC patients) and PEAs not leading to PR (from patients without ROSC). Rhythms from first group are more likely to be pseudo-PEAs since they present a better prognosis, and they show different ECG

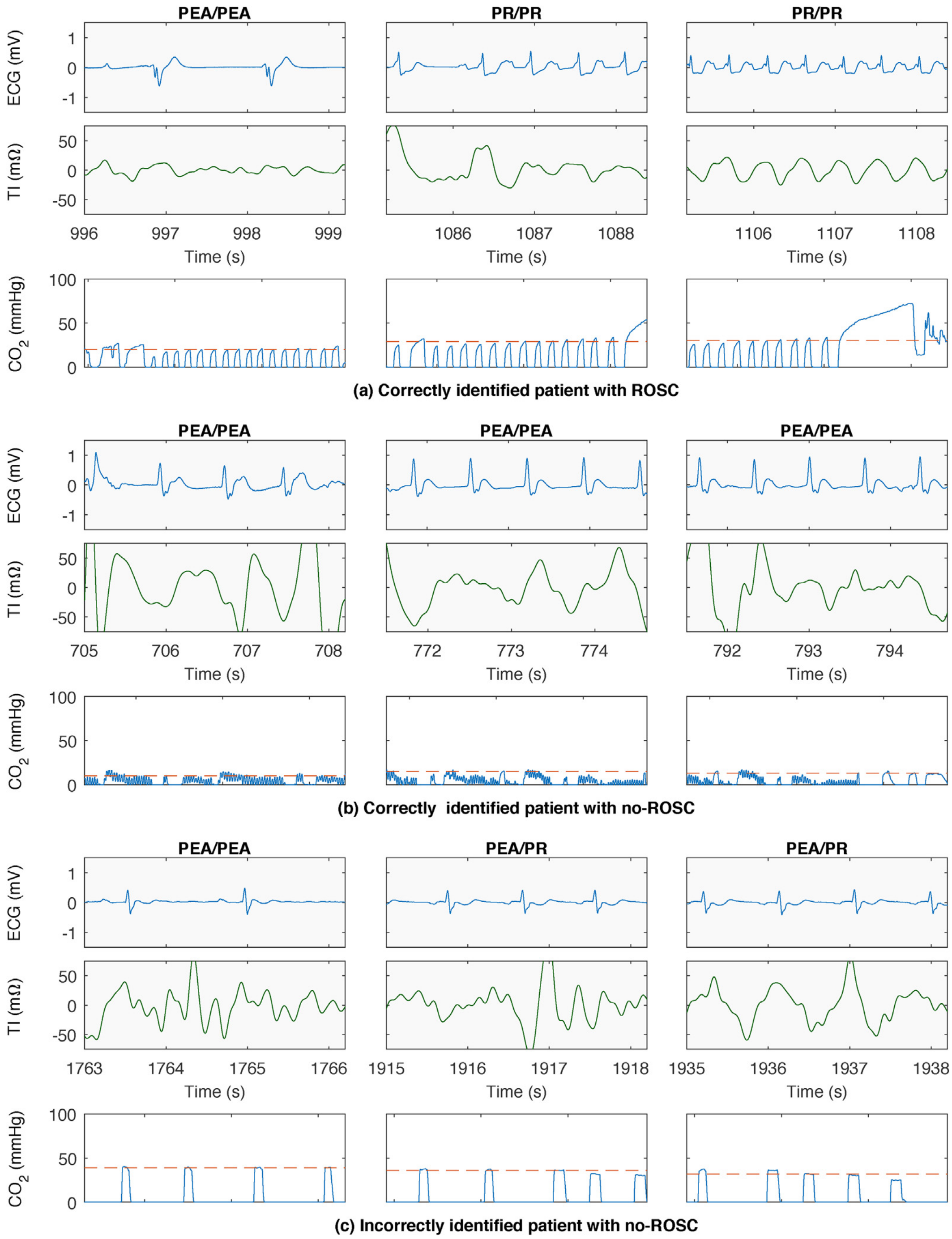

Fig. 4 – Examples of the case study. Panels (a), (b) and (c) show a correctly identified patient with ROSC, a correctly identified patient without ROSC, and a patient without ROSC incorrectly identified, respectively. Each panel depicts the three consecutive PEA/PR segments analysed. The text on top of each segment indicates its true label followed by the predicted label by the classifier. The capnogram corresponds to the minute before the onset of the segment and the dashed horizontal line represents the MEtCO$_2$.

characteristics and EtCO$_2$ values.[33–39] This type of border rhythm challenges the design of an accurate classifier. An experiment supporting these conclusions is detailed in the supplementary file. The p_{pr} obtained from the classifier was significantly lower for PEA in no-ROSC cases, and as shown in Fig. 5, the median value of p_{pr} increases for PEA in ROSC patients as the patient approaches ROSC onset. This indicates that the p_{pr} obtained from the RF classifier may serve as a potential surrogate hemodynamic marker that could measure the evolution of PEA in response to therapy.

The analysis of the MEtCO$_2$ values for the intervals around ROSC (Fig. 2a) showed that EtCO$_2$ values increase as the patient approaches ROSC, and the rise is higher closer to ROSC onset, in line with previous findings.[12,13] We also observed that EtCO$_2$ levels were maintained after ROSC, or even decreased if ventilation rates

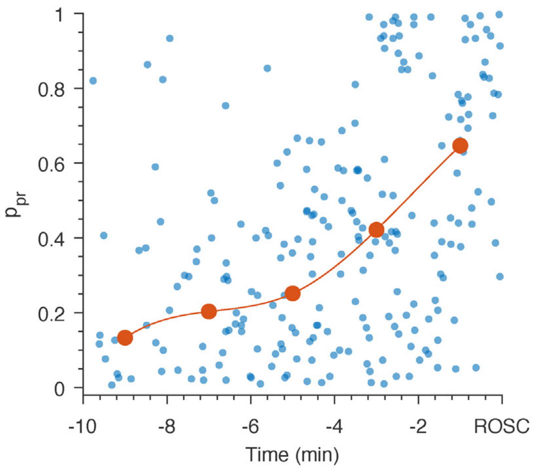

Fig. 5 – Time evolution of p_{pr} for the PEA segments as the patients approach ROSC. Blue dots indicate values for each segment, and the red curve is fitted to the median values of p_{pr} every 2 min.

were high. Abrupt increases in $EtCO_2$ can be used to identify ROSC onset, but are of little use in a PR/PEA classifier due to its short period utility time. During both PR and PEA, $EtCO_2$ may increase or decrease around high (PR) or low (PEA) baseline levels. However, interrupting chest compressions only after a sudden increase in $EtCO_2$ to check for an organized rhythm facilitate early detection of ROSC and minimize hands-off intervals by avoiding unnecessary chest compressions pauses to check for pulse.[9,14] The $EtCO_2$ levels reported in this study were high, which may be caused by the inclusion criteria applied to the data that contained those patients with sustained ROSC.

The overall performance of the PR/PEA discriminator is high (AUC > 0.9), but slightly below the scores reported by other methods based exclusively on the ECG[27] or combination of ECG and TI.[21,22] Those studies used segments selected ad-hoc for the processing of the ECG or the TI, which might have introduced a positive bias in the results. Our dataset was automatically selected, including all segments classified as organized rhythm by a commercial AED algorithm, and segment labelling was based exclusively on ROSC annotations made by clinicians on site. In fact, when we applied the method proposed in Ref.[27] to the dataset of this study, the SE/SP were 78.8%/84.1%, well below the 88.4%/89.7% reported in the original paper. This dataset reflects a more realistic and difficult scenario for PR/PEA classification.

As an example of applicability of the PR/PEA classifier, a simple automatic tool to retrospectively identify cases with ROSC was proposed. In our 426 cases, a simple method was over 95% accurate, yielding a 96.6% SE and a 94.5% SP for the retrospective detection of ROSC. These values are well above the 73.9% SE and 58.4% SP reported for an automatic algorithm based on capnography trends alone.[15]

Finally, the accuracy of the PR/PEA classifier supports its applicability as an automatic decision support tool to aid clinicians in the identification of ROSC. The algorithm uses only a 3.2-s analysis interval without chest compressions, so it can be used during CPR with minimal interruptions to chest compressions. Furthermore, we used an automatic CO_2 based ventilation detector that identifies the offset/onset of ventilations. This allows us to measure the $EtCO_2$ level as the maximum value during the alveolar plateau in the capnography, which avoids some of the problems associated with $EtCO_2$ readings (capnometry) at the end of the expiratory phase when chest compression artefacts are present in the CO_2 waveform.[40] Each ventilation was delineated using the algorithm proposed in,[23] a software-based algorithm that could be integrated in any equipment without hardware modifications. The algorithm is launched once the AED algorithm has detected an organized rhythm, and it only requires waveform characteristics of the 3.2-s long ECG and TI signals and the median of the $EtCO_2$ values in the minute prior to the analysis.

6 Limitations

This study shows three limitations. Firstly, the data were collected with the capnography module of the Philips HeartStart MRx monitor/defibrillator. Using another capnometer might alter the levels of $EtCO_2$. Secondly, our ground truth for all the experiments was the time of ROSC annotated by the clinician on scene. Using an independent gold standard for circulation, such as invasive blood pressure, would result in more robust conclusions. Lastly, there were no data available on the advanced airway technique used on each patient. However, the reported $EtCO_2$ values might be affected by the used airway management technique (supraglottic/endotracheal).

7 Conclusions

The results of this study demonstrate the added value of the capnogram for the automatic detection of ROSC in OHCA. The $EtCO_2$ level added discriminative power to the PR/PEA classifier based on the ECG and the TI. The accuracy of the models increased significantly when $MEtCO_2$ levels were added. This study shows that an automatic algorithm that uses capnography can be implemented to reliably detect ROSC.

Conflict of interest

Dr. Idris receives research grants from the US National Institutes of Health (NIH) and serves as an unpaid volunteer on the American Heart Association National Emergency Cardiovascular Care Committee and the HeartSine, Inc. Clinical Advisory Board.

Acknowledgements

This work has been partially supported by the Spanish Ministerio de Economía y Competitividad, jointly with the Fondo Europeo de Desarrollo Regional (FEDER), project TEC2015-64678-R, by the University of the Basque Country via the Ayudas a Grupos de InvestigaciónGIU17/031, and by the Basque Government through the grant PRE_2017_1_0112.

Appendix A. Signal processing and feature extraction

Nine features (v_1–v_9) were computed from the ECG ($s[n]$) and the TI ($z[n]$) signals. The ECG was filtered between 0.5 Hz and 30 Hz using zero-phase filtering to remove baseline component and high frequency noise. The TI was resampled to 250 Hz and filtered between 0.7 and 7 Hz to remove fluctuations caused by ventilations and enhance the circulation component.

Six different features, v_1–v_6, were calculated from the ECG as recently proposed in[27].

- The first difference of the signal ($s_\Delta = s[n] - s[n-1]$) was computed and the mean of its absolute value was the first feature:

$$v_1 = \frac{1}{N}\sum_{n=1}^{N} |s_\Delta[n]| \quad (A.1)$$

where N is the length of the segment in samples.

- The standard deviation of $s_\Delta[n]$:

$$v_2 = \sqrt{\frac{\sum_{n=0}^{N-2}(s_\Delta[n] - v_1)^2}{N-3}} \quad (A.2)$$

- The kurtosis (tailedness) of the square and averaged (with a 125 ms moving average filter) of s_Δ was v_3.
- Amplitude spectrum area (AMSA) is the sum of spectral amplitudes weighted by their frequency components. The spectral amplitudes at f_i,A_i, were calculated using the N_F = 4096 point FFT of the Tuckey windowed $s[n]$ segment:

$$v_4 = \sum_i A_i \cdot f_i, \quad 2 < f_i < 30 \quad (A.3)$$

- The energy of $s[n]$ at frequencies higher than 17.5 Hz:

$$v_5 = \frac{f_s}{2N_F}\sum_i A_i^2, \quad 17.5 < f_i < 30 \quad (A.4)$$

- Fuzzy entropy of $s[n]$, a measure of its regularity, was the v_6 feature.

PEA is defined as absence of palpable pulse when organized electrical activity of the heart is present. The TI signal shows small fluctuations for every effective heartbeat. Many efforts have been made to extract the circulation component of the signal using adaptive filters or ensemble averaging,[21,20,41] but all of them need accurate QRS detection. Ruiz et al. and Alonso et al. considered the circulation component as a quasi-periodic signal and estimated its Fourier coefficients using least mean squares or recursive least squares algorithms. The instantaneous heart rate was computed from the QRS complexes. Risdal et al. applied ensemble averaging to the TI signal around QRS instants to extract the circulation component. However, in this study we considered only features independent of QRS complex detection, in particular those proposed in[17,28,22]:

- The mean power of the two half segments of $z[n]$ were computed and the minimum value assigned to v_7.[22]
- The power spectrum of the first difference of $z[n]$ was computed, and v_8 was its peak amplitude in the 1.5–4.5 Hz range.[17]
- The normalized cross-correlation function was computed as follows:

$$r_{sz}(l) = \frac{1}{\sqrt{r_{ss} r_{zz}}}\sum_{n=1}^{N} s[n] z[n-l], \quad l = 0, \pm1, \ldots, \pm N-1 \quad (A.5)$$

where $r_{ss} = \sum_{n=1}^{N}(s[n])^2$ and $r_{zz} = \sum_{n=1}^{N}(z[n])^2$. The maximum peak of $r_{sz}[l]$ was v_9.[28]

Appendix B. Supplementary data

Supplementary data associated with this article can be found, in the online version, at https://doi.org/10.1016/j.resuscitation.2019.03.048.

REFERENCES

1. Perkins GD, Stephenson B, Hulme J, Monsieurs KG. Birmingham assessment of breathing study (BABS). Resuscitation 2005;64:109–13.
2. Ruppert M, Reith MW, Widmann JH, et al. Checking for breathing: evaluation of the diagnostic capability of emergency medical services personnel, physicians, medical students, and medical laypersons. Ann Emerg Med 1999;34:720–9.
3. Nyman J, Sihvonen M. Cardiopulmonary resuscitation skills in nurses and nursing students. Resuscitation 2000;47:179–84.
4. Eberle B, Dick W, Schneider T, Wisser G, Doetsch S, Tzanova I. Checking the carotid pulse check: diagnostic accuracy of first responders in patients with and without a pulse. Resuscitation 1996;33:107–16.
5. Ochoa FJ, Ramalle-Gomara E, Carpintero J, Garcıa A, Saralegui I. Competence of health professionals to check the carotid pulse. Resuscitation 1998;37:173–5.
6. Babbs CF. We still need a real-time hemodynamic monitor for CPR. Resuscitation 2013;84:1297–8.
7. Christenson J, Andrusiek D, Everson-Stewart S, et al. Chest compression fraction determines survival in patients with out-of-hospital ventricular fibrillation. Circulation 2009;120:1241–7.
8. Berg RA, Sanders AB, Kern KB, et al. Adverse hemodynamic effects of interrupting chest compressions for rescue breathing during cardiopulmonary resuscitation for ventricular fibrillation cardiac arrest. Circulation 2001;104:2465–70.
9. Soar J, Nolan JP, Böttiger BW, et al. European resuscitation council guidelines for resuscitation 2015: section 3. Adult advanced life support. Resuscitation 2015;95:100–47.
10. Hartmann SM, Farris RW, Di Gennaro JL, Roberts JS. Systematic review and meta-analysis of end-tidal carbon dioxide values associated with return of spontaneous circulation during cardiopulmonary resuscitation. J Intensive Care Med 2015;30:426–35.
11. Sheak KR, Wiebe DJ, Leary M, et al. Quantitative relationship between end-tidal carbon dioxide and CPR quality during both in-hospital and out-of-hospital cardiac arrest. Resuscitation 2015;89:149–54.
12. Pokorná M, Nečas E, Kratochvíl J, Skřipsk`y R, Andrlík M, Franěk O. A sudden increase in partial pressure end-tidal carbon dioxide (PETCO2) at the moment of return of spontaneous circulation. J Emerg Med 2010;38:614–21.
13. Lui CT, Poon KM, Tsui KL. Abrupt rise of end tidal carbon dioxide level was a specific but non-sensitive marker of return of spontaneous circulation in patient with out-of-hospital cardiac arrest. Resuscitation 2016;104:53–8.
14. Davis DP, Sell RE, Wilkes N, et al. Electrical and mechanical recovery of cardiac function following out-of-hospital cardiac arrest. Resuscitation 2013;84:25–30.
15. Brinkrolf P, Borowski M, Metelmann C, Lukas RP, Pidde-Küllenberg L, Bohn A. Predicting ROSC in out-of-hospital cardiac arrest using

expiratory carbon dioxide concentration: is trend-detection instead of absolute threshold values the key. Resuscitation 2018;122:19–24.
16. Pellis T, Bisera J, Tang W, Weil MH. Expanding automatic external defibrillators to include automated detection of cardiac, respiratory, and cardiorespiratory arrest. Crit Care Med 2002;30:S176–8.
17. Cromie NA, Allen JD, Navarro C, Turner C, Anderson JM, Adgey AAJ. Assessment of the impedance cardiogram recorded by an automated external defibrillator during clinical cardiac arrest. Crit Care Med 2010;38:510–7.
18. Cromie NA, Allen JD, Turner C, Anderson JM, Adgey AAJ. The impedance cardiogram recorded through two electrocardiogram/defibrillator pads as a determinant of cardiac arrest during experimental studies. Crit Care Med 2008;36:1578–84.
19. Losert H, Risdal M, Sterz F, et al. Thoracic-impedance changes measured via defibrillator pads can monitor signs of circulation. Resuscitation 2007;73:221–8.
20. Risdal M, Aase SO, Kramer-Johansen J, Eftesol T. Automatic identification of return of spontaneous circulation during cardiopulmonary resuscitation. IEEE Trans Biomed Eng 2008;55:60–8.
21. Alonso E, Aramendi E, Daya M, et al. Circulation detection using the electrocardiogram and the thoracic impedance acquired by defibrillation pads. Resuscitation 2016;99:56–62.
22. Ruiz JM, de Gauna SR, González-Otero DM, et al. Circulation assessment by automated external defibrillators during cardiopulmonary resuscitation. Resuscitation 2018;128:158–63.
23. Aramendi E, Elola A, Alonso E, et al. Feasibility of the capnogram to monitor ventilation rate during cardiopulmonary resuscitation. Resuscitation 2017;110:162–8.
24. Ayala U, Eftestøl T, Alonso E, et al. Automatic detection of chest compressions for the assessment of CPR-quality parameters. Resuscitation 2014;85:957–63.
25. Alonso E, Ruiz J, Aramendi E, et al. Reliability and accuracy of the thoracic impedance signal for measuring cardiopulmonary resuscitation quality metrics. Resuscitation 2015;88:28–34.
26. Irusta U, Ruiz J, Aramendi E, de Gauna SR, Ayala U, Alonso E. A high-temporal resolution algorithm to discriminate shockable from nonshockable rhythms in adults and children. Resuscitation 2012;83:1090–7.
27. Elola A, Aramendi E, Irusta U, Del Ser J, Alonso E, Daya M. ECG-based pulse detection during cardiac arrest using random forest classifier. Med Biol Eng Comput 2019;57:453–62.
28. Wei L, Chen G, Yang Z, Yu T, Quan W, Li Y. Detection of spontaneous pulse using the acceleration signals acquired from CPR feedback sensor in a porcine model of cardiac arrest. PLoS One 2017;12: e0189217.
29. Breiman L. Random forests. Mach Learn 2001;45:5–32.
30. Stone M. Cross-validatory choice and assessment of statistical predictions. J R Stat Soc Ser B Methodol 1974;111–47.
31. Zou KH, O'Malley AJ, Mauri L. Receiver-operating characteristic analysis for evaluating diagnostic tests and predictive models. Circulation 2007;115:654–7.
32. Ruopp MD, Perkins NJ, Whitcomb BW, Schisterman EF. Youden, Index and optimal cut-point estimated from observations affected by a lower limit of detection. Biometr J 2008;50:419–30.
33. Kolar M, Križmarić M, Klemen P, Grmec Š. Partial pressure of end-tidal carbon dioxide successful predicts cardiopulmonary resuscitation in the field: a prospective observational study. Crit Care 2008;12:R115.
34. Touma O, Davies M. The prognostic value of end tidal carbon dioxide during cardiac arrest: a systematic review. Resuscitation 2013;84:1470–9.
35. Grmec Š, Klemen P. Does the end-tidal carbon dioxide ($EtCO_2$) concentration have prognostic value during out-of-hospital cardiac arrest? Eur J Emerg Med 2001;8:263–9.
36. Weiser C, Poppe M, Sterz F, et al. Initial electrical frequency predicts survival and neurological outcome in out of hospital cardiac arrest patients with pulseless electrical activity. Resuscitation 2018;125:34–8.
37. Skjeflo GW, Nordseth T, Loennechen JP, Bergum D, Skogvoll E. ECG changes during resuscitation of patients with initial pulseless electrical activity are associated with return of spontaneous circulation. Resuscitation 2018;127:31–6.
38. Elola A, Aramendi E, Irusta U, et al. ECG characteristics of pulseless electrical activity associated with return of spontaneous circulation in out-of-hospital cardiac arrest. Resuscitation 2018;130:e54.
39. Prosen G, Križmarić M, Završnik J, Grmec Š. Impact of modified treatment in echocardiographically confirmed pseudo-pulseless electrical activity in out-of-hospital cardiac arrest patients with constant end-tidal carbon dioxide pressure during compression pauses. J Int Med Res 2010;38:1458–67.
40. Raimondi M, Savastano S, Pamploni G, Molinari S, Degani A, Belliato M. End-tidal carbon dioxide monitoring and load band device for mechanical cardio-pulmonary resuscitation: Never trust the numbers, believe at the curves. Resuscitation 2016;103:e9–e10.
41. Ruiz J, Alonso E, Aramendi E, et al. Reliable extraction of the circulation component in the thoracic impedance measured by defibrillation pads. Resuscitation 2013;84:1345–52.

Supplementary file

The effect of the uncertainty on time of ROSC annotations in the PR/PEA classifier

This supplementary material provides an extended analysis to clarify the effect on PEA/PR classification of the uncertainty (lack of precision) in the annotation of time of ROSC (t_{ROSC}) made by clinicians on site. The assumption is that in some cases ROSC might have occurred some time (up to a few minutes) before the time annotated in the patient charts, since clinicians on site might not detect ROSC immediately when it occurs.

If that was the case some of the PEA segments near the annotated t_{ROSC} would actually correspond to PR segments, and these segments would most likely be labelled wrong by the classifier. It would also affect the training process of the classifier since it would learn based on some erroneous labels. An experiment was conducted to quantify the effect of the lack of precision in t_{ROSC} in the accuracy of the classifier. Let t_d be the delay in the detection of ROSC by the clinicians. For the experiment we discarded all segments t_d minutes before t_{ROSC}, making the assumption that these annotations are not completely reliable. We tested different t_d values, from 0 (no correction) up to 10-minutes, and the resulting models were evaluated in terms of sensitivity (Se), specificity (Sp) and specificity only for patients with ROSC (Sp_1). Figure 1 shows the results. Assuming a t_d of -5 minutes increased Sp_1 from 60% to 80%, and Sp by 4-points. Assuming longer delays did not increase Sp_1, which remained stable at 10% below the global Sp. These results suggest two interpretations:

- t_{ROSC} may not be precise, and a rough estimate based on our experiment is that the uncertainty in the actual annotations of ROSC could be of up to 5-minutes. This is the reason why Sp_1 increased by 20-points when t_d was increased up to 5-minutes, but remained stable for larger values of t_d.
- There are some intrinsic differences between PEAs that transition to ROSC and those that do not. That is why Sp_1 was 10-points lower than the overall Sp, regardless of the uncertainty in t_{ROSC} annotations. Previous studies have shown differences between these two types of PEA both in the ECG and in EtCO_2 values [1, 2]. Besides, small mechanical contractions may cause fluctuations in impedance, so impedance waveform characteristics may be different in

PEA and pseudo-PEA. Pseudo-PEA is more likely to transition to ROSC than pure PEA, so it is likely that more pseudo-PEAs are present in ROSC cases.

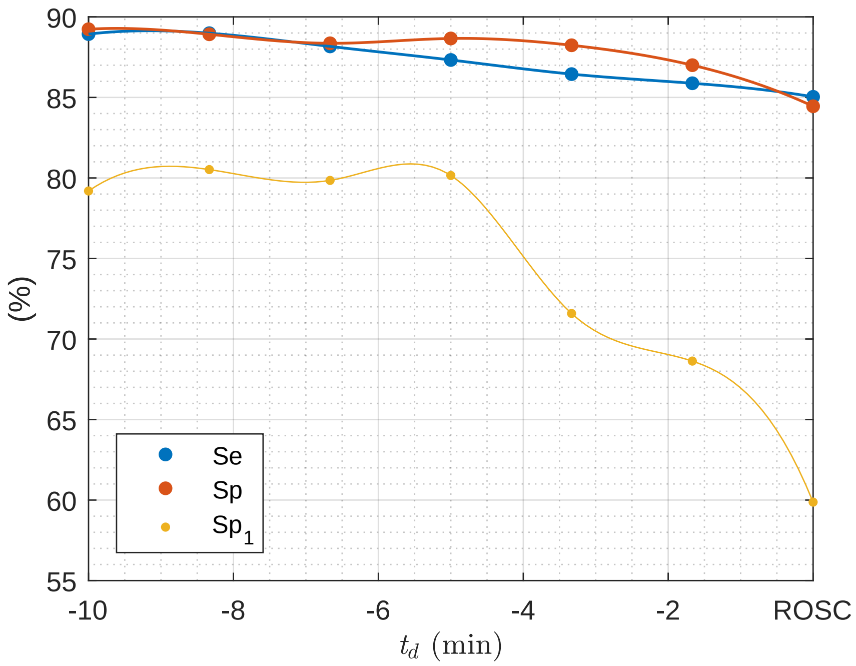

Figure .1: Effect of the uncertainty in the time of ROSC annotated by clinicians in the accuracy of the model. The value t_d is the assumed average delay in the detection of ROSC. $t_d = 0$ corresponds to the values reported in the manuscript.

References

[1] A. Elola, E. Aramendi, U. Irusta, E. Alonso, P. Owens, M. Chang, and A. Idris. ECG characteristics of pulseless electrical activity associated with return of spontaneous circulation in out-of-hospital cardiac arrest. *Resuscitation*, 130:e54, 2018.

[2] G. Prosen, M. Križmarić, J. Završnik, and Š. Grmec. Impact of modified treatment in echocardiographically confirmed pseudo-pulseless electrical activity in out-of-hospital cardiac arrest patients with constant end-tidal carbon dioxide pressure during compression pauses. *Journal of International Medical Research*, 38(4):1458–1467, 2010.

A.2.3 Bigarren helburuari lotutako aurreneko argitalpena nazioarteko konferentziak

A.7. Taula. Bigarren helburuari lotutako aurreneko argitalpena nazioarteko konferentzian.

	Argitalpena nazioarteko konferentzian
Erreferentzia	Andoni Elola, Elisabete Aramendi, Unai Irusta, Erik Alonso, Pamela Owens, Mary Chang, Ahamed Idris, "ECG characteristics of pulseless electrical activity associated with return of spontaneous circulation in out-of-hospital cardiac arrest", *Resuscitation 2018*, vol.130, p. e54.
Kalitate adierazleak	• **Argitalpen mota**: Nazioarteko konferentzia • **Kuartila**: Q1 (2/29) (*Web of Science* 2019) • **Inpaktu faktorea**: 4.572

through patient-wise 10-fold cross validation. The test set was used to compute the performance of the method in terms of sensitivity (SE) and specificity (SP). This procedure was repeated 500 times to estimate the distributions of SE and SP.

Results: The SVM showed a mean (standard deviation) SE and SP of 96.5% (2.5) and 97.0% (1.4), respectively. The method met the minimum performance requirements of the American Heart Association (SE > 90% and SP > 95%). The method required on average only 279 (36) ms per segment in a standard platform.

Conclusion: An automated method based on a state of the art machine learning technique accurately detects VF during OHCA. Its low computational cost makes it suitable for implementation into current defibrillators.

https://doi.org/10.1016/j.resuscitation.2018.07.096

AP055

Two-chambered blood pump for the heart-lung bypass machines

Zurab Chkhaidze *, Nodar Khodeli

Iv. Javakhishvili Tbilisi State University, Tbilisi, Georgia

Introduction: Development of blood pumps that provide artificial circulation with parameters approximated to those of physiological blood circulation is still a topical issue.

Materials and methods: The study concerns the development of a two-chambered blood pump of the volumetric pump category. It is a hybrid of a roller pump and a ventricular assist device. The main distinctive feature is the absence of any parts moving inside the blood flow, so there is no hemolysis. One of the important parts of the pump is the pulsator, which operates on the principle of cardiosynchronized (if needed) clamping of the outlet tube. The pump realizes both the pulsatile flow, which is close to the physiological arterial flow parameters, as well as the non-pulsatile flow typical to a venous flow. After the bench tests, the pump was successfully tested for a long (up to 8 h) heart-lung bypass on 14 sheep in three different experimental models with cardiac arrest.

Results: Pump characteristics during the bench test is:

Frequency 0–250 beats/min;

Output pressure 0–200 mmHg;

Blood flow 0–8 l/min.

Experimental studies in models of extracorporeal cardiopulmonary resuscitation (7 animals), “ex situ” machine perfusion preservation of isolated donor organs (2 animals) and “in situ” machine perfusion preservation of organ complexes (5 animals) confirmed the comparative “physiological” nature of the developed pump.

Conclusion: Hybrid double-chambered blood pump in standard perfusion schemes is able to provide both the systemic and the organ perfusion adapted as much as possible to the hemodynamic parameters of the experimental animal.

https://doi.org/10.1016/j.resuscitation.2018.07.097

AP056

ECG characteristics of Pulseless Electrical Activity associated with Return of Spontaneous Circulation in Out-of-Hospital Cardiac Arrest

Andoni Elola [1,*], Elisabete Aramendi [1], Unai Irusta [1], Erik Alonso [1], Pamela Owens [2], Mary Chang [2], Ahamed Idris [2]

[1] *University of the Basque Country, Bilbao, Spain*
[2] *University of Texas Southwestern Medical Center, Dallas, USA*

Purpose: Predicting the prognosis of Pulseless Electrical Activity (PEA) would allow optimally directing resuscitation efforts. Contradictory results have been reported regarding the association between PEA characteristics such as Heart Rate (HR) and Return of Spontaneous Circulation (ROSC). The aim of this study was to analyse the ECG characteristics of PEA that predict ROSC.

Materials and methods: Data from 173 out-of-hospital cardiac arrest patients were extracted, all of them recorded by the DFW Center for Resuscitation Research (UTSW, Dallas), and divided into ROSC/noROSC patients. The former showed sustained QRS complexes from the onset of ROSC (t_{ROSC}, annotated by clinicians) without chest compressions and the latter were annotated as died in field at the end of the episode (t_{end}). A total of 1439 artifact-free PEA ECG segments of 5 s were extracted during the last 10 min prior to t_{ROSC} (326, ROSC) or t_{end} (1113, noROSC). The HR, Mean Slope (MS) from the first difference of the ECG and Amplitude Spectrum Area (AMSA) were computed automatically for each segment, and combined in a Logistic Regression (LR) model. Patient-wise 10-fold cross validation was adopted to train and test the model, and its performance was evaluated in terms of Sensitivity (Se), Specificity (Sp) and Area Under the Curve (AUC).

Results: Three features showed different distributions for ROSC/noROSC groups ($p < 0.001$), mean (SD) were: 66.6 (40.0)/54.8 (33.72), 5.5 (3.5)/2.4 (1.8) and 43.1 (22.6)/18.0 (11.3) for HR, MS and AMSA respectively. AUC values were 0.56, 0.80 and 0.84. The LR model had Se/Sp/AUC of 80.3%/78.6%/0.85, and the posterior probability of ROSC measured using the model increased as time approached t_{ROSC} (see Fig. 1).

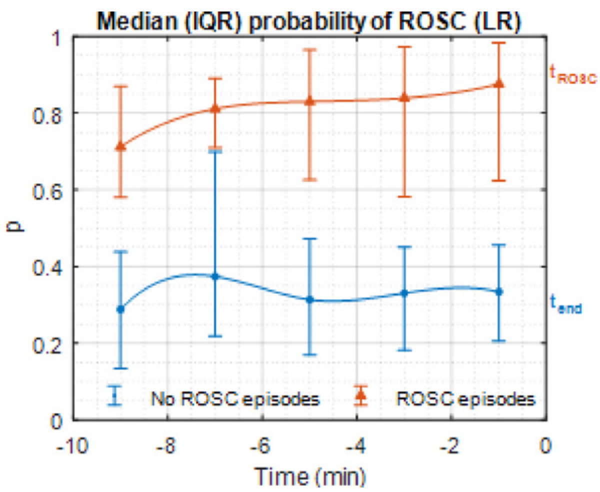

Fig. 1.

Conclusions: PEA characteristics are good prognostic markers of ROSC. The best ECG feature was AMSA, but combining all features provides a better prediction.

https://doi.org/10.1016/j.resuscitation.2018.07.098

A.2.4 BIGARREN HELBURUARI LOTUTAKO BIGARREN ARGITALPENA NAZIOARTEKO KONFERENTZIAN

A.8. Taula. Bigarren helburuari lotutako bigarren argitalpena nazioarteko konferentzian.

	Argitalpena nazioarteko konferentzian
Erreferentzia	Andoni Elola, Elisabete Aramendi, Unai Irusta, Per Olav Berve, Frefrik Arnwald, Lars Wik, Fred W Chapman, "Using the Thoracic Impedance to Predict Measures From Invasive Arterial Blood Pressure in Out-Of-Hospital Cardiac Arrest", *Circulation 2019*, vol.140, no. Suppl_2, p. A237.
Kalitate adierazleak	• **Argitalpen mota**: Nazioarteko konferentzia • **Kuartila**: Q1 (1/138) (*Web of Science* 2019) • **Inpaktu faktorea**: 23.603

Circulation

FREE ACCESS | ABSTRACT

POSTER ABSTRACT PRESENTATIONS
SESSION TITLE: CPR 5

Abstract 237: Using the Thoracic Impedance to Predict Measures From Invasive Arterial Blood Pressure in Out-Of-Hospital Cardiac Arrest

Andoni Elola, Elisabete Aramendi, Unai Irusta, Per-Olav Berve, Fredrik K Arnwald, Lars Wik, Fred W Chapman

Originally published 11 Nov 2019 | Circulation. 2019;140:A237

Abstract

Background: During cardiopulmonary resuscitation (CPR), pulse detection can be challenging. Invasive blood pressure measurements (IBP) can help monitoring patient hemodynamics, but arterial catheter placement is difficult. Transthoracic impedance (TI) measured between the defibrillator pads can detect circulation activity. We hypothesized that TI changes can predict the corresponding IBP, and potentially be used to non-invasively detect pulse during CPR.

Materials and methods: We included 28 out of hospital cardiac arrest patients receiving CPR by the Oslo Emergency Service who had concurrent recordings of IBP (radial artery, BD, 20G, US) and TI (via defibrillator pads, LP15, Stryker, US). 5-second segments with stable and CPR artefact free signals were extracted (Figure). The circulation component of the TI signal (Figure, red line) was extracted using a Kalman smoother. Ten waveform features were computed per segment and fed into a random forest regressor to predict systolic and diastolic arterial pressures (SAP, DAP), their difference (DifAP) and area of the IBP signal (ArAP). Pearson correlation coefficients between the regression model and the IBP metrics were computed. Data were divided by patient into training/test sets to fit and evaluate the model, respectively, and the process was repeated 500 times.

Results: 235 minutes (2261 segments) were extracted with median (Q1-Q3) values of 71.3(39.2-88.1) mmHg for SAP, 44.2(30.0-50.0) mmHg for DAP, 25.6(7.1-38.8) mmHg for DifAP and 63.4(17.0-85.9) mmHg*sec for ArAP. The correlation coefficients between TI-predicted and IBP-measured SAP, DAP, DifAP and ArAP were 0.62 (0.49-0.72), 0.36 (0.22-0.49), 0.69 (0.57-0.76) and 0.64 (0.50-0.73), respectively.

Conclusions: Different hemodynamic phases can be observed in both TI and IBP (Figure). TI-based predictions showed good correlation with IBP measures. This could lead to new non-invasive methods to monitor different phases of circulation based on the TI.

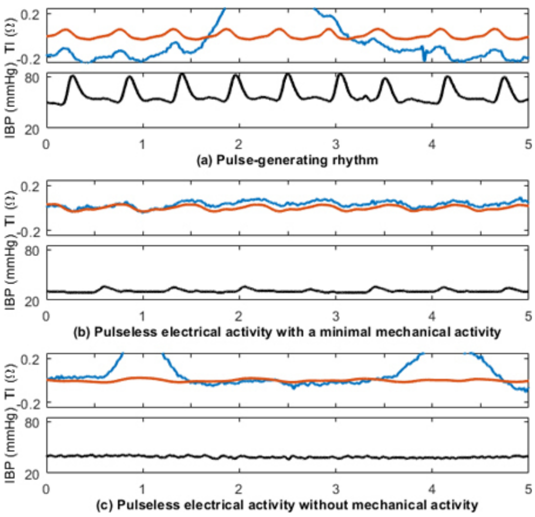

Download figure

Footnotes

For author disclosure information, please visit the AHA Resuscitation Science Symposium 2019 Online Program Planner and search for the abstract title.

Circulation

November 19, 2019
Vol 140, Issue Suppl_2

Article Information

Download: 0

Originally published November 11, 2019

Check for updates

Keywords

A.2.5 BIGARREN HELBURUARI LOTUTAKO HIRUGARREN ARGITALPENA NAZIOARTEKO ALDIZKARIAN

A.9. Taula. Bigarren helburuari lotutako hirugarren argitalpena nazioarteko aldizkarian.

	Argitalpena nazioarteko aldizkarian
Erreferentzia	Andoni Elola, Elisabete Aramendi, Unai Irusta, Per Olav Berve, Lars Wik, "Multimodal algorithms for the classification of circulation states during out-of-hospital cardiac arrest", *IEEE Transactions on Biomedical Engineering 2020*.
Kalitate adierazleak	• **Argitalpen mota**: JCRen indexatutako aldizkari artikulua • **Kuartila**: Q1 (14/87) (*Web of Science* 2019) • **Inpaktu faktorea**: 4.424

Multimodal algorithms for the classification of circulation states during out-of-hospital cardiac arrest

Andoni Elola, Elisabete Aramendi*, *Member IEEE*, Unai Irusta, *Member IEEE*, Per Olav Berve, Lars Wik

***Abstract*— *Goal:* Identifying the circulation state during out-of-hospital cardiac arrest (OHCA) is essential to determine what life-saving therapies to apply. Currently algorithms discriminate circulation (pulsed rhythms, PR) from no circulation (pulseless electrical activity, PEA), but PEA can be classified into true (TPEA) and pseudo (PPEA) depending on cardiac contractility. This study introduces multi-class algorithms to automatically determine circulation states during OHCA using the signals available in defibrillators. *Methods:* A cohort of 60 OHCA cases were used to extract a dataset of 2506 5-s segments, labeled as PR (1463), PPEA (364) and TPEA (679) using the invasive blood pressure, experimentally recorded through a radial/femoral cannulation. A multimodal algorithm using features obtained from the electrocardiogram, the thoracic impedance and the capnogram was designed. A random forest model was trained to discriminate three (TPEA/PPEA/PR) and two (PEA/PR) circulation states. The models were evaluated using repeated patient-wise 5-fold cross-validation, with the unweighted mean of sensitivities (UMS) and F_1-score as performance metrics. *Results:* The best model for 3-class had a median (interquartile range, IQR) UMS and F_1 of 69.0% (68.0-70.1) and 61.7% (61.0-62.5), respectively. The best two class classifier had median (IQR) UMS and F_1 of 83.9% (82.9-84.5) and 76.2% (75.0-76.9), outperforming all previous proposals in over 3-points in UMS. *Conclusions:* The first multiclass OHCA circulation state classifier was demonstrated. The method improved previous algorithms for binary pulse/no-pulse decisions. *Significance:* Automatic multiclass circulation state classification during OHCA could contribute to improve cardiac arrest therapy and improve survival rates.**

***Index Terms*— Random Forest, Machine Learning, Cardiac arrest, pulsed rhythm (PR), pulseless electrical activity (PEA), pseudo pulseless electrical activity.**

I. INTRODUCTION

OUT of hospital cardiac arrest (OHCA) is a major public health problem in the industrialized world, with an annual incidence of 41 (range 19-104) cases treated per 100 000 persons in Europe [1], and more than 350 000 cases reported annually by the resuscitation outcome consortium in the USA [2]. Despite recent advances in treatment and monitoring, survival rates with good functional status remain around 9% in adults [2]. Cardiac arrest can happen without warning. The patient abruptly loses the respiratory and cardiovascular functions, leading to unconciousness and ultimately death if the patient is not treated within a few minutes. The chain of survival metaphor specifies the key steps to improve OHCA survival rates. Those steps are: early recognition of the arrest, early treatment including cardiopulmonary resuscitation (CPR) and defibrillation, and post-resuscitation care. CPR includes effective chest compressions and ventilations, coordinated with defibrillation therapy provided with either basic automated external defibrillators (AED) or advanced monitor/defibrillators. Specialized interventions may include advanced monitoring, pharmacological treatment, and if spontaneous circulation is restored, transport to a hospital for post-resuscitation care [3], [4].

The objective of resuscitation therapies is to restore spontaneous circulation (ROSC) or pulse, i.e. the cardiac function of the patient. However, during therapy OHCA patients undergo frequent and dynamic rhythm transitions [5]. It is therefore key to recognize and monitor the patient's response to treatment, particularly the identification of spontaneous pulse. Rapid recognition of ROSC would avoid unnecessary chest compressions that could lead the patient into VF again [6], and would anticipate the benefit of post-resuscitation treatment [7]. More specifically, algorithms or methods are needed to discriminate pulseless electrical activity (PEA) from pulse generating rhythms (PR) [8], [9]. During PEA, patients present a (quasi)-normal electrocardiogram with discernible heartbeat activity (QRS complexes), but no associated mechanical contractions. A state known as electromechanical dissociation.

Pulse detection in OHCA patients is challenging. Palpation techniques have a low specificity (55%) and require long interruptions (> 10 s) in therapy [10]–[12]. Automated pulse identification using the electrocardiogram (ECG) is challenging because PEA and PR rhythms show an organized ECG with discernible QRS complexes [13]. Chest conductivity is affected by transport of oxygenated blood, so the thoracic impedance (TI) signal is also of value to identify pulse

Manuscript submitted June, 2020; accepted October, 2020. This work was supported by the Spanish Ministerio de Ciencia, Innovación y Universidades through grant RTI2018-101475-BI00, jointly with the Fondo Europeo de Desarrollo Regional (FEDER), and by the Basque Government through grants IT1229-19 and PRE_2019_2_0100

Asterisk indicates corresponding author.
*E. Aramendi is with the Department of Communications Engineering, University of the Basque Country UPV/EHU, Ingeniero Torres Quevedo Plaza, 1, 48013, Bilbao, Spain (e-mail: elisabete.aramendi@ehu.eus).
A. Elola and U. Irusta are with the Department of Communications Engineering, University of the Basque Country UPV/EHU, Ingeniero Torres Quevedo Plaza, 1, 48013, Bilbao, Spain.
Per Olav Berve and Lars Wik are with the Norwegian National Advisory Unit on Prehospital Emergency Medicine (NAKOS), Norway.

during OHCA [8]. In the last decade, various algorithms have been proposed for PEA/PR discrimination during OHCA using only the ECG [13], [14], the thoracic impedance [15], [16] or a combination of both signals [8], [9], [17]. More recently, physiological signals affected by cardiac output like capnography or photoplethysmography have been incorporated to PEA/PR discrimination algorithms [18], [19].

One key limitation of all these contributions is to define a binary circulation state (pulse/no-pulse). PEA can be further classified into true-PEA (TPEA) and pseudo-PEA (PPEA) [20]. During PPEA echocardiography studies show that the electrical activity of the heart produces mechanical contractions, although of insufficient strength to maintain consciousness and adequate organ perfusion [21]. The two states of PEA have very different prognosis and treatment [22]–[24], and since PEA is the initial rhythm in up to 60% of OHCA cases [25], discriminating PPEA from TPEA is of great clinical interest. Echocardiography and invasive blood pressure (IBP) are the key technologies to discriminate PEA states, but they are rarely available during OHCA. Other methods based on ECG variables and end-tidal-CO2 ($EtCO_2$) values have also been proposed, but with inconclusive results [24], [26]–[28]. There is a need for automated circulation state classification algorithms that differentiate TPEA, PPEA and PR rhythms.

This study introduces a new multi-modal solution to classify circulation states during OHCA using concurrent information derived from the ECG, the TI and the capnogram. The solution allows the classification into two classes (PR/PEA) or three classes (TPEA/PPEA/PR), with the final aim of monitoring the circulation state of the patient and the response to resuscitation treatment. The study is based on an unique dataset that includes IBP signals measured using arterial lines during OHCA to provide an accurate ground truth clinical annotation of the circulation state.

II. Data collection and preprocessing

A. Dataset

The source of the data was a randomized OHCA clinical trial (No. NCT02479152), that investigated the hemodynamics of patients in cardiac arrest treated with manual cardiopulmonary resuscitation and mechanical chest compression devices. Data were recorded between 2015 and 2017 by the doctor manned car, part of the Air ambulance department of the Oslo Emergency Medical System (EMS) under the supervision of the principal investigator of the trial (coauthor Dr L. Wik). A total of 210 patients were included, from whom four signals were concurrently recorded using the Lifepak 15 (Stryker Ltd.) monitor-defibrillator: the ECG and the TI (recorded through the defibrillation pads), the sidestream capnogram, and the IBP signal acquired via onsite radial/femoral cannulation. In 135 cases cerebral oxygen saturation was continuously monitored in the right and left frontal lobes using the ForeSight Elite monitor (Casmed, Inc).

All signals were first converted to a common sampling rate of $f_s = 250\,\text{Hz}$, and the capnogram was time-aligned with the ECG and the TI. Then signal intervals with the following characteristics were extracted: minimum duration 5-s, ECG in an organized rhythm (QRS complexes), and free of chest compression artefacts.

The ECG, TI and capnogram were used to develop the algorithms. A clinician and two expert biomedical engineers used all other sources of information to annotate the circulation state (TPEA, PPEA, PR) for each interval, including: clinical patient charts with annotated ROSC intervals, the IBP waveform, and cerebral oxygen saturation when available. Systolic (Sys), diastolic (Dias) and pulse pressure ($\text{PP} = \text{Sys} - \text{Dias}$) were computed for each cardiac cycle and averaged to be displayed during annotation. The distinction between the three circulation states was possible using the objective values obtained from the IBP because systolic and pulse pressures are higher for PR than for PEA, and within PEA higher values are observed for PPEA than for TPEA. Fig. 1 shows a 150-s period with the signals recorded by the LifePak monitor, in which two intervals without chest compressions (as seen in the impedance) were extracted: a short 10-s PPEA interval (orange) around 15:39:00 with Sys/Dias/PP values of 54/34/20 mmHg, and a longer 40-s PR interval (green) around 15:40:40 with Sys/Dias/PP values of 147/67/80 mmHg.

A total of 300 intervals were identified from the 60 patients that had an IBP waveform. A median (interquartile range, IQR) of 5 (3-7) intervals was extracted per patient, with a median (IQR) duration of 27.6 (11.2-76.0) s. They were labeled as TPEA (129, from 37 patients), PPEA (75, from 26 patients) and PR (96, from 31 patients). The median (IQR) blood pressure values for the three circulation states in the extracted intervals are summarized in Table I. When the distributions were compared using a Mann-Whitney U test the systolic pressure and pulse pressure values were significantly higher for PR than for PPEA ($p < 0.001$), and for PPEA than for TPEA ($p < 0.001$).

TABLE I
Systolic (Sys), diastolic (Dias) and pulse pressure (PP) values for the three groups considered in this study

	TPEA	PPEA	PR
Sys (mmHg)	32.5 (24.6-41.7)	40.4 (35.0-49.1)	95.5 (68.9-148.7)
Dias (mmHg)	27.2 (19.5-36.4)	28.1 (25.9-33.7)	51.1 (40.0-75.9)
PP (mmHg)	4.1 (0.0-6.8)	11.3 (8.0-16.4)	45.4 (29.4-68.1)

The intervals were further divided into non overlapping 5-s segments. These segments were separated by 1-s in TPEA and PPEA for which the signals and the circulatory state of the patient are very variable. The PR segments were separated by 15-s because once a patient recovers pulse the circulatory state is more stable. As reference, the median duration of the PR and PEA intervals were 129-s and 15-s, respectively. These segments were used to design and validate the three (TPEA/PPEA/PR) and two (PEA/PR) circulation state classifiers. A total of 2506 5-s segments were obtained, for a median (IQR) of 42 (16-62) segments per patient, whereof 679 were TPEA, 364 PPEA and 1463 PR. Fig. 2 shows one example for each class. In the PPEA and PR segments there is a visible correlation between the ECG, the IBP and the impedance circulation component (ICC) (see Section III-B). For the TPEA the IBP is nearly flat, and there is no circulation

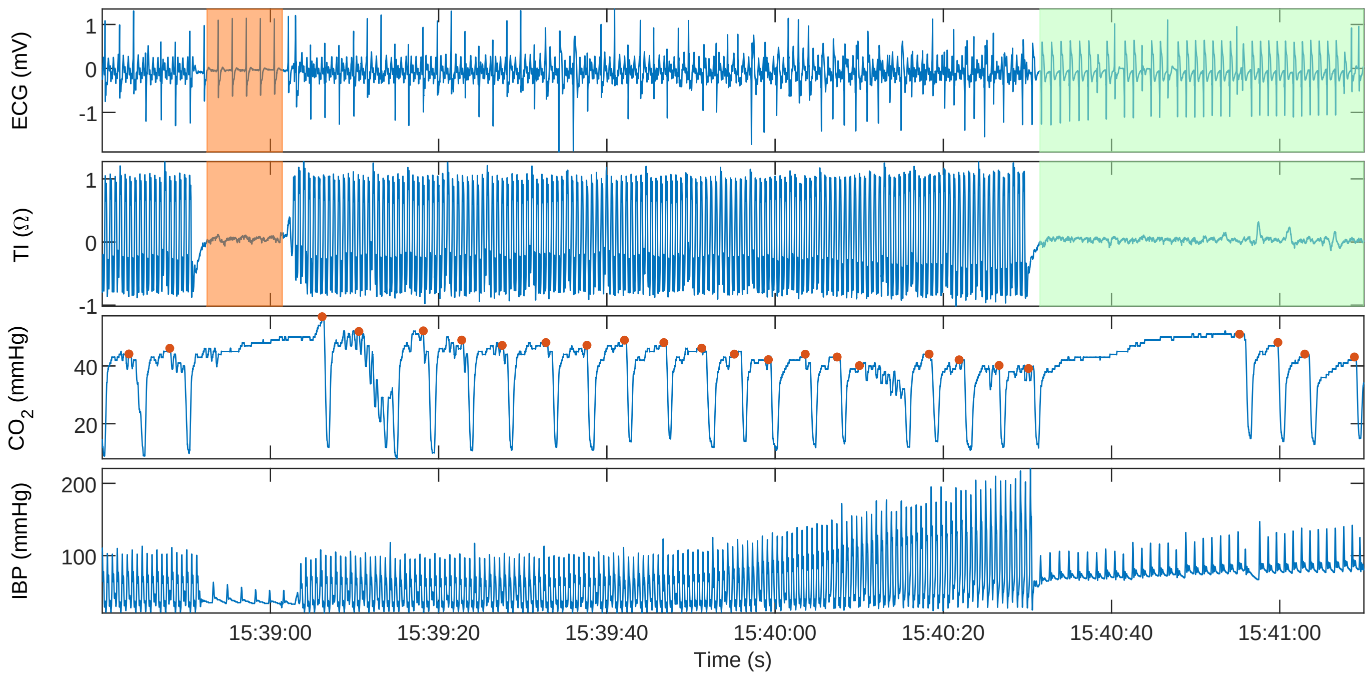

Fig. 1. A period of 150 s from a patient in OHCA is shown, where the ECG, the thoracic impedance (TI), and the capnogram can be observed together with IBP waveform, i.e. the signal used to annotate the pulse states. Two intervals are marked, a PPEA (in red) around 15:39:00 and a PR (in green) around 15:40:40. In the capnogram the EtCO$_2$ values computed for each ventilation are marked as dots (in red).

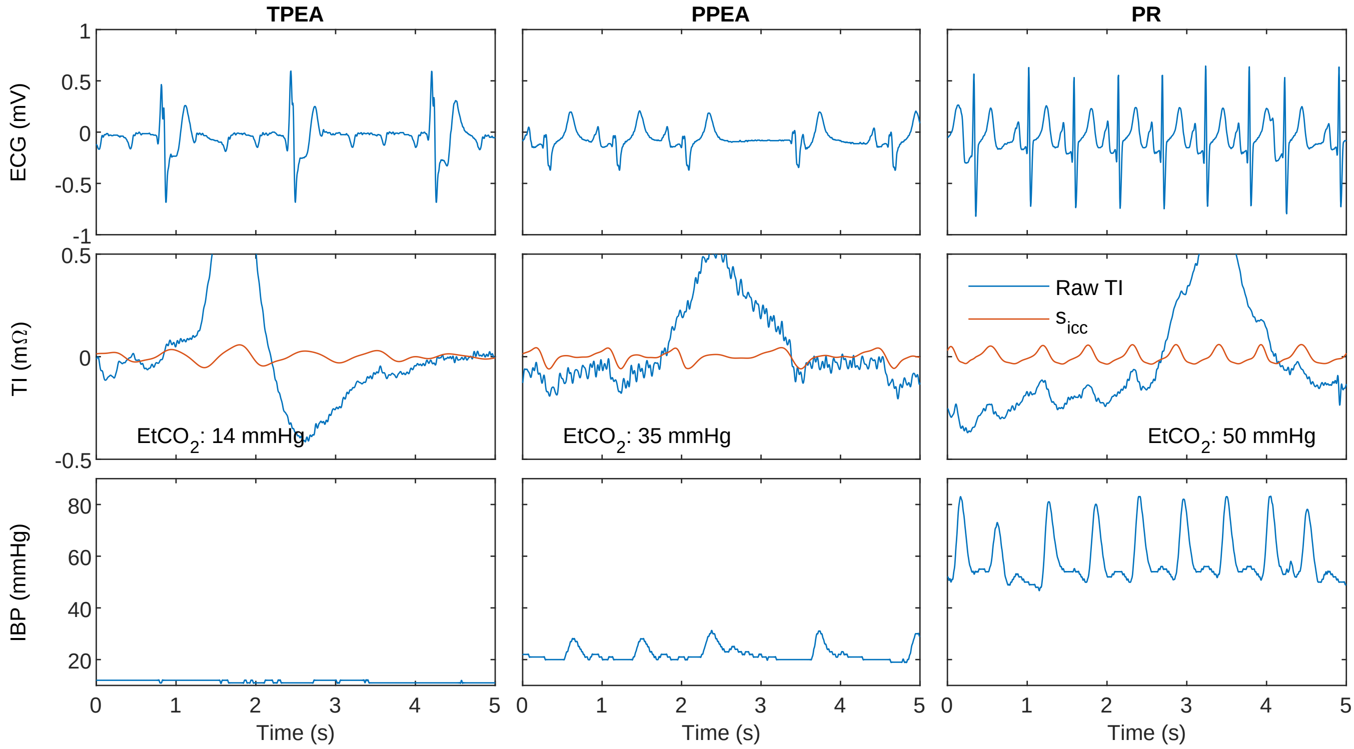

Fig. 2. Examples of segments annotated as true PEA (TPEA), pseudo PEA (PPEA) and PR. The ECG, the TI andthe extracted circulation component (s_{icc}) are used by the algorithm together with the average EtCO$_2$ associated to each segment. The invasive blood pressure (IBP) permitted the labeling of the segments in the three classes.

component in the impedance. In addition the EtCO$_2$ values are displayed in the figure; these values were computed by averaging the EtCO$_2$ values of the ventilations in the previous minute [19].

III. Signal preprocessing

The ECG and TI were preprocessed to denoise the signals and extract components of interest. Multiresolution analysis based on stationary wavelet transform (SWT) was used to obtain the sub-band components or detail coefficients, and to denoise the signals using soft thresholding [29]. A Daubechies 4 mother wavelet was adopted [30].

A. The ECG

The ECG was decomposed in 8 levels of detail coefficients ($d_{1,\mathrm{ecg}}$-$d_{8,\mathrm{ecg}}$) and the threshold was estimated using $d_{2,\mathrm{ecg}}$ to denoise $d_{3,\mathrm{ecg}}$-$d_{8,\mathrm{ecg}}$. A denoised ECG (s_{ecg}) was reconstructed using the denoised $d_{3,\mathrm{ecg}}$ to $d_{8,\mathrm{ecg}}$, which is equivalent to using the $0.5-31.25$ Hz bandwidth, adequate for the detection of pulse [13]. Fig. 3 shows the raw ECG, the denoised detail components $d_{3,\mathrm{ecg}}$-$d_{7,\mathrm{ecg}}$ and s_{ecg} for a PR case.

B. TI denoising and ICC extraction

The TI signal was first band-pass filtered in the 0.8-10 Hz band to remove baseline fluctuations and high frequency noise [8], [9], and then the ICC was obtained. The ICC shows the changes in TI produced by blood flow, and is associated to mechanical ventricular contractions [31]. The ICC can be modeled as a Fourier series, with a time changing fundamental frequency equal to the instantaneous heart rate [9], [32]. For a sampling period T_s and the discretized time axis $t_j = j \cdot T_s$, the ICC component at time t_j is expressed as [9]:

$$s_{\mathrm{icc}}(t_j) = \sum_{k=1}^{K} a_k(t_j)\cos(2\pi k f(t_j){\cdot}t_j){+}b_k(t_j)\sin(2\pi k f(t_j){\cdot}t_j) \tag{1}$$

where $f(t_j)$ is the beat-to-beat heart rate in Hz, and $a_k(t_j)$ and $b_k(t_j)$ are time-varying Fourier coefficients that will be estimated using Kalman filtering and smoothing, and the model uses K harmonics. The Kalman state vector $\boldsymbol{x}_j$ and the observation vector $\mathbf{H}_j$ are then:

$$\boldsymbol{x}_j = [a_1(t_j), \ldots, a_K(t_j), b_1(t_j), \ldots, b_K(t_j)]^T \tag{2}$$

$$\begin{aligned}\mathbf{H}_j = [&\cos(2\pi f(t_j)t_j), \ldots, \cos(2\pi f(t_j)Kt_j),\\ &\sin(2\pi f(t_j)t_j), \ldots, \sin(2\pi f(t_j)Kt_j)]\end{aligned} \tag{3}$$

In this work we assume a_k and b_k are gaussian processes [33], that can be updated as:

$$a_k(t_j) = \psi_j a_k(t_{j-1}) + w_j \tag{4}$$

$$b_k(t_j) = \psi_j b_k(t_{j-1}) + w_j \tag{5}$$

where w_j is a gaussian process with zero mean and standard deviation σ, and $\psi_j = \exp(-\lambda(t_j - t_{j-1}))$. The dynamic model can be expressed as:

$$\boldsymbol{x}_j = \boldsymbol{\Psi}_j \boldsymbol{x}_{j-1} + \mathbf{Q}_j \tag{6}$$

where $\boldsymbol{\Psi}_j = \psi_j \cdot \mathbf{I}_{2K}$, $\mathbf{Q}_j = \sigma \cdot \mathbf{I}_{2K}$ and $\mathbf{I}_{2K}$ is the identity matrix of order $2K \times 2K$.

The a_k and b_k coefficients were estimated using Rauch-Tung-Striebel smoother, as described in [33], [34], and $K = 5$ harmonics, $\lambda = 0.05$ and $\sigma = 0.01$ were used. The instantaneous heart rate, $f(t_j)$, was measured by detecting the R peaks in the ECG signal using the Hamilton-Tompkins algorithm [35].

The circulation component was reconstructed using $d_{5,\mathrm{icc}} - d_{7,\mathrm{icc}}$ ($\approx 1-8$ Hz). Fig. 3 shows the s_{icc} and detail coefficients for a PR case. As shown in the figure, the Kalman smoother is capable of obtaining the circulation component even in the presence of low frequency TI variations caused by ventilation, as observed in the band-passed impedance signal, s_{TI}.

C. The capnogram

$EtCO_2$ values were automatically computed in the capnogram using the algorithm described in Aramendi et al. [36]. For each ventilation the $EtCO_2$ value was marked as the maximum value of the capnogram in the expiration plateau, as shown by red dots in Fig. 1.

IV. Feature Engineering and Classification

A pletora of features, both described in the literature for PEA/PR discrimination, and new features proposed in this study for the same task were implemented.

A. State of the art features

A set of 37 features described in [8], [9], [13], [15], [17], [19], [32] were computed using the ECG, TI, ICC and capnography signals:

- **ECG:** Mean RR interval (`MeanRR`), variance of RR intervals (`VarRR`), mean and standard deviation of QRS peak-to-peak amplitudes (`MeanPP` and `StdPP`), median signal length (`MedianSL`), mean and variance of QRS width, QRS amplitude to duration ratio (`SlopeQRS`), median and variance of the signal after normalizing between 0 and 1 (`MSnorm` and `StdSnorm`), mean value of the signal, mean and standard deviation of the absolute value of the first difference of the signal (`MeanAbs1` and `StdAbs1`), the kurtosis of the averaged slope (`KurtSlp2`), amplitude spectrum area (`AMSA`), energy above 17.5 Hz (`HfP`) and Fuzzy entropy (`FuzzEn`).
- **TI:** Variance and cross-power (`XPwr`) as described in [17], peak of the power spectrum of the first difference of the signal in $1.5\,\mathrm{Hz} < f < 4.5\,\mathrm{Hz}$ range (`PkF`), and 10 features from the ensemble averaged signal as described in [8].
- **ICC:** Area per sample and mean area of s_{icc} and its first difference, Δs_{icc}. Mean and standard deviation of the peak-to-peak fluctuations of every beat in s_{icc} (`MeanPP` and `StdPP`), and the mean of Δs_{icc} (`MeanPP1`) [9], [32].
- **Capnogram:** The median value of the $EtCO_2$ measured in the previous minute, $MEtCO_2$, as described in [19].

B. Novel features

Pulsatility is associated to ECGs with narrower QRS complexes of larger amplitudes, and to waveforms in the ICC correlated to the heartbeats (QRS complexes). These differences should produce different characteristic waveforms in the detail coefficients for TPEA, PPEA and PR. The following features were extracted from s_{ecg}, $d_{3,\mathrm{ecg}} - d_{7,\mathrm{ecg}}$, s_{icc} and $d_{5,\mathrm{icc}} - d_{7,\mathrm{icc}}$ [37]–[39].

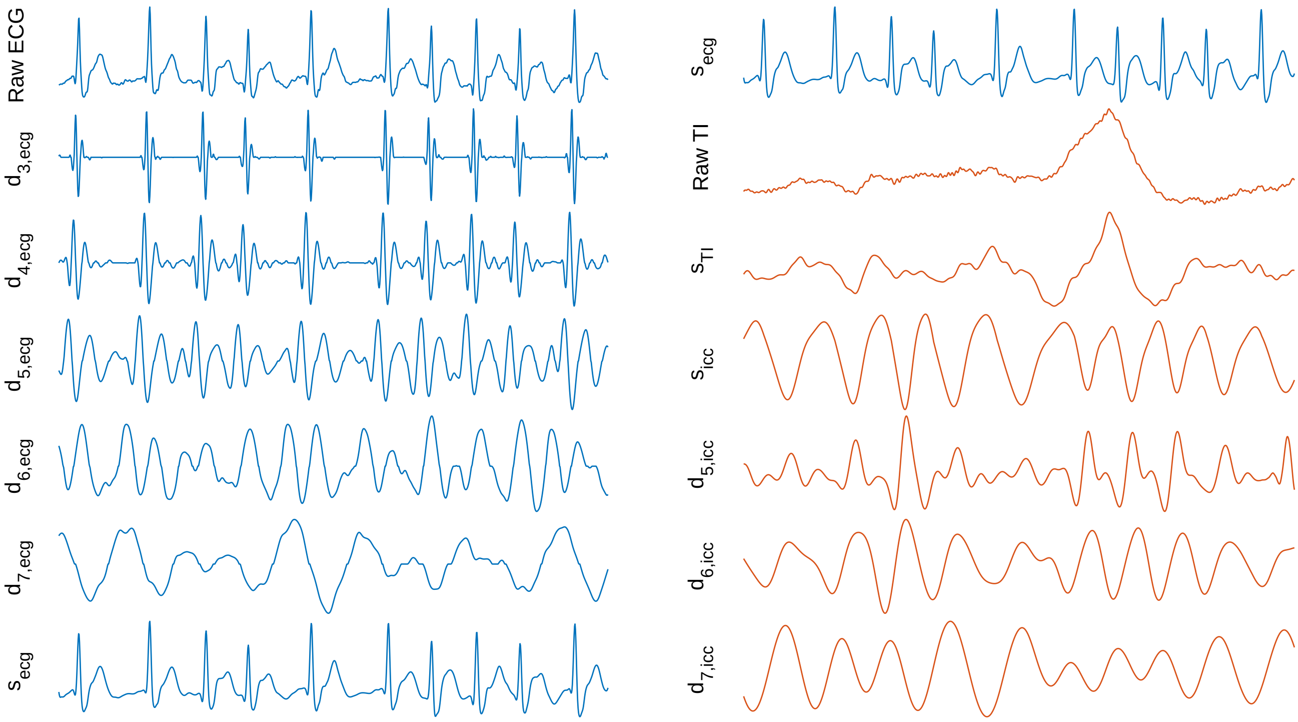

Fig. 3. Decomposition of the ECG and the TI signal into detail components using the stationary wavelet transform. The denoised ECG ($\boldsymbol{s}_{\mathbf{ecg}}$) and TI ($\boldsymbol{s}_{\mathbf{TI}}$) and the impedance circulation component ($\boldsymbol{s}_{\mathbf{icc}}$) are also shown.

- Interquartile range (`IQR`).
- Sample entropy (`SampEn`) with an embedding dimension of 2 and tolerance of 0.2.
- Mean and standard deviation of the absolute value after normalizing to unit variance (`NMeanAbs` and `NMeanSd`).
- Mean and standard deviation of the absolute value of the first difference after normalizing to unit variance (`NMeanAbs1` and `NMeanSd1`).
- Skewness (`Skew`) and kurtosis (`Kurt`).
- Hjorth mobility (`Hmb`) and complextity (`Hcmp`).
- Phase-space representation was computed using Taken's time-delay embedding method with $\tau = 2$ and the skewness of pairwise distances was calculated (`SkewPS`).

Two extra features were computed for s_{ecg} and s_{icc}:

- The error of estimating the spectral power of the signal with a 4th order autorregresive Burg model (`ARErr`), best fit to signals with spectra concentrated around a fundamental frequency and its harmonics.
- The smoothed nonlinear energy operator (`SNEO`) as described in [40], which shows higher values for signals with higher amplitudes.

C. Feature selection and classification

The Random Forest (RF) classifier was adopted for both feature selection and classification. A RF is an ensemble of B decision trees that produce uncorrelated predictions, and uses a majority vote of the trees to produce the final label. Each tree was trained using the bootstrapping method with replacement and 50% of the data. The minority classes were over-sampled to have equal number of observations per class when training each tree and address class imbalance.

Data were partitioned patient-wise in a quasi stratified way into 5-fold cross validation partitions, and the procedure was repeated 100 times to statistically characterize the performance of the classifiers. In the training phase two RF classifiers were trained. The first RF classifier was trained using only the ECG and TI features, and was used for feature selection using permutation feature importance. At this stage minority classes were not over-sampled. The second RF classifier (final model) was trained using the most important N_f features and MEtCO_2, and now the minority classes were over-sampled. Note that the total number of features in the final model was $N_f + 1$ when the MEtCO_2 was considered.

D. Model evaluation

The models were evaluated using the per class sensitivity (Se) and F_1-score. The unweighted mean of sensitivities (UMS) and the mean of the per class F_1-scores ($\text{F}_{1\text{m}}$) were used as global performance metrics. For the 2-class problem the area under the receiver operating characteristic curve (AUC) was also computed. The number of segments varied across patients, so all metrics were computed weighting each patient equally.

A multimodal model was evaluated integrating the three signals, ECG, TI and capnogram. Simple defibrillators and AEDs do not include a capnography module, so models based on the ECG and TI only were also developed. Finally, some lower cost AEDs do not record the TI with sufficient amplitude resolution to obtain the ICC [9], [13], so models using only the ECG were also developed.

V. Results

A. Detailed classification of circulation states

The performance metrics for the detailed circulation state classifier are shown in Fig. 4 for models with an increasing number of features. The results in terms of UMS improved by less than 0.3-percent points for the models with more than $N_f = 30$ features, which had a median (IQR) F_{1m} and UMS of 61.5% (60.8-62.4) and 68.8% (67.7-69.8), respectively. The confusion matrix in Fig. 5 shows the detailed classification per group for the model with $N_f = 30$ features. The intermediate circulation state (PPEA) was the hardest to classify, since it may present PR or TPEA like characteristics depending on the degree of cardiac contraction.

The novel ICC feature extraction provided relevant information to classify circulation states. Fig. 6 shows the average feature ranking for all training partitions for a model with $N_f = 30$ features. The ranking was obtained as the probability of being included in the model after feature selection. As shown in the figure, our model for 30 features included 7 ICC features, but 3 of those were the ones with the highest probability to be included in the model. Some of the features were already proposed in the state of the art for PEA/PR classification, but other important features were first used in this study for circulation state classification. Note that $MEtCO_2$ was not included in the feature selection process and was added manually, so it is not present in Fig. 6.

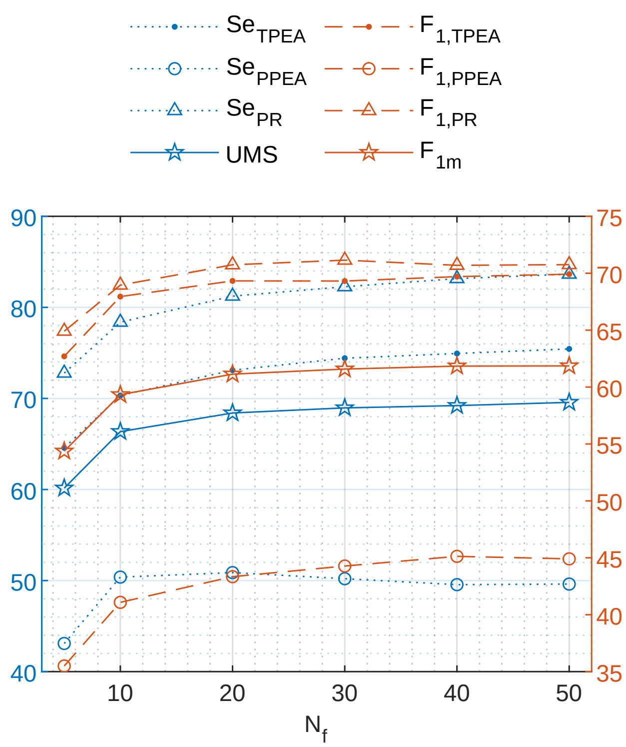

Fig. 4. Performance (%) of the prediction model in terms of the number of features included (N_f) for the three-class classification problem.

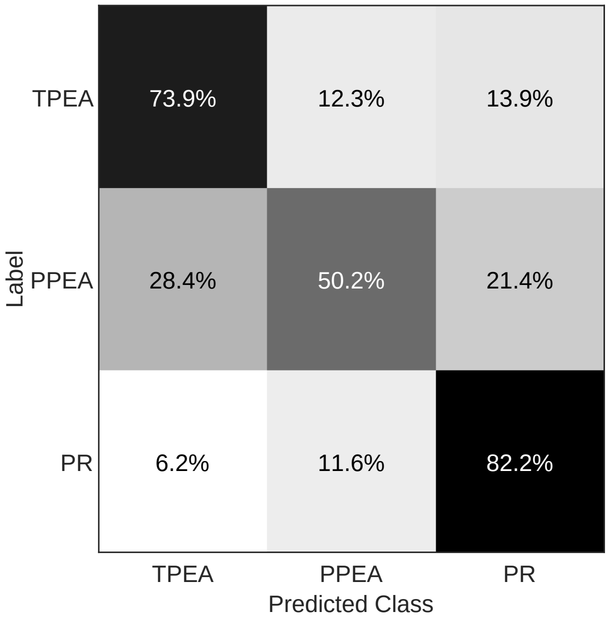

Fig. 5. Confusion matrix of the three-class circulation state classifier.

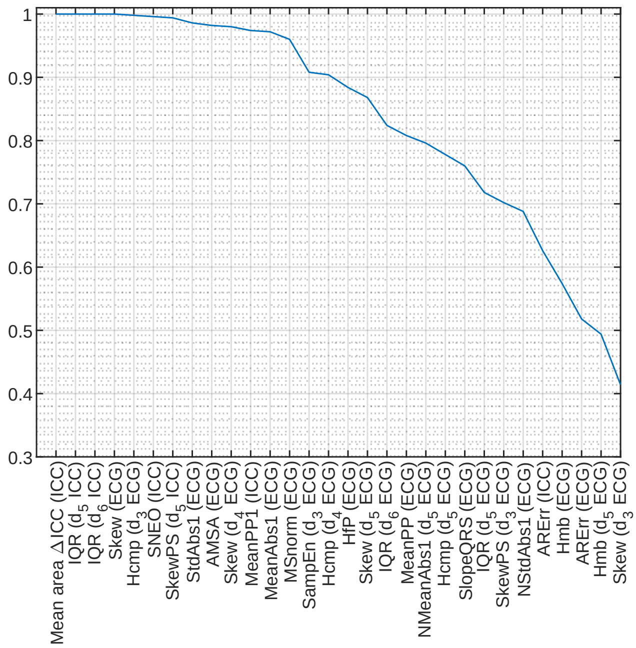

Fig. 6. Probability of selection for each feature when $N_f = 30$ and three classes were considered (TPEA/PPEA/PR)

The detailed (three-class) classification results depending on the available information (source signals) are shown in Table II. The TPEA and PPEA classes were most affected by constrained signal models, removing $MEtCO_2$ information decreased the F_1-score for TPEA by 3 points and for PPEA by 2 points. Further removing the TI produced a decrease in F_1-score of over 12 points for TPEA and 8 points for PPEA. The ECG only and ECG+TI models presented a UMS of 58.6% and 66.9%, 25 and 33 points above that of a random guess.

This article has been accepted for publication in a future issue of this journal, but has not been fully edited. Content may change prior to final publication. Citation information: DOI 10.1109/TBME.2020.3030216, IEEE Transactions on Biomedical Engineering

TABLE II
PERFORMANCE METRICS REPRESENTED AS MEDIAN (IQR) FOR THE THREE-CLASS CLASSIFICATION PROBLEM

Signals	N_f	Se_{TPEA}	Se_{PPEA}	Se_{PR}	UMS	$F_{1,TPEA}$	$F_{1,PPEA}$	$F_{1,PR}$	F_{1m}
ECG, TI, CO_2	10*	70.3 (4.8)	50.4 (5.5)	78.4 (2.9)	66.2 (2.8)	67.9 (4.0)	41.1 (4.4)	69.0 (2.7)	59.2 (2.4)
ECG, TI, CO_2	20*	73.1 (3.7)	50.9 (4.6)	81.2 (2.4)	68.6 (2.4)	69.3 (2.4)	43.3 (3.3)	70.7 (2.5)	61.2 (1.8)
ECG, TI, CO_2	30*	74.4 (3.6)	50.2 (4.2)	82.3 (1.9)	68.8 (2.1)	69.3 (2.9)	44.3 (2.9)	71.1 (2.0)	61.5 (1.6)
ECG, TI, CO_2	40*	74.9 (3.7)	49.6 (3.7)	83.2 (1.5)	69.0 (2.1)	69.7 (2.8)	45.1 (3.0)	70.7 (1.7)	61.7 (1.5)
ECG	30	57.5 (4.5)	37.2 (5.5)	80.9 (2.7)	58.6 (2.6)	57.1 (2.8)	35.7 (4.4)	68.9 (1.9)	53.8 (2.2)
ECG, TI	30	71.8 (3.4)	47.7 (5.6)	81.5 (2.1)	66.9 (2.6)	65.8 (2.5)	42.9 (4.1)	70.8 (2.3)	59.8 (2.1)

* The final model included $N_f + 1$ features (MEtCO_2)

Another key variable when identifying the circulation state is the duration of the signal segment. Chest compression therapy must be interrupted for the analysis to avoid artefacts in the ECG and TI. But these interruptions compromise blood flow in deteriorated circulation states and may negatively affect patient survival [41]. Consequently, the shorter the analysis segment the better. Fig. 7 shows the median (IQR) of per class F_1 scores of a $N_f = 30$ feature model as the duration of the analysis segment is shortened. From 1-s to 5-s windows F_1 increased only one point for PR, but almost 5 points for TPEA and PPEA. Increasing the analysis window was beneficial to discriminate the most challenging class, PPEA.

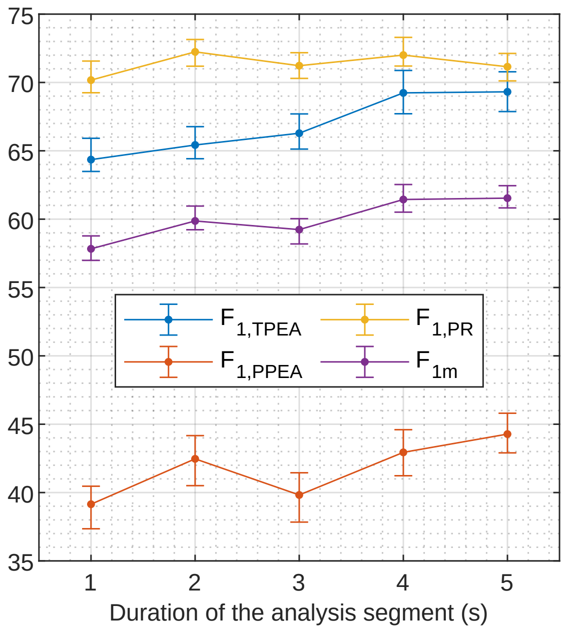

Fig. 7. Median (IQR) of per class F_1 in terms of the duration of the analysis segment.

B. Binary classification of circulation states

Binary classification of circulation states (PEA/PR or pulse/no-pulse classification) is a well known field of study in biosignal analysis applied to cardiac arrest [8], [9], [14]. Our model for this problem was constructed joining the TPEA and PPEA classes. The performance metrics as a function of the number of features in the RF model are shown in Fig. 8. The accuracy of the model increased substantially

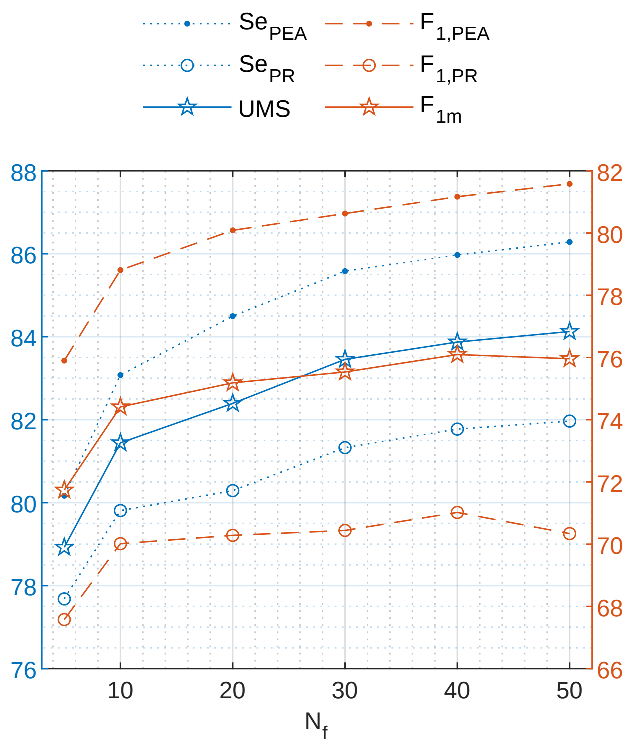

Fig. 8. Performance (%) of the prediction model in terms of the number of features included (N_f) for the two-class classification problem

when going from a 5-feature to a 50-feature model, with an increase of 5 points in UMS. As reference, the performance of our model was compared in our dataset to those of the reference studies in binary circulation state classification [8], [9], [13], [19]. The results are shown in Table III. Moreover, since these methods ranged from ECG only to multimodal methods including ECG, TI and CO_2 the analysis was further stratified to include models with features from the different signals. Our model outperformed the state of the art PEA/PR classification models. The UMS/F_{1m} of our models were 5/6 and 4/3 points larger than the next best methods based on ECG+TI and ECG+TI+CO_2, respectively. In all cases the AUC of our models was 1 to 4 points larger.

Fig. 9 shows the average feature ranking for all training partitions for a model with 30 features. It can be observed that the model includes 7 ICC features, 3 of which have the highest probability. Some of the most important features were first proposed in this study for PEA/PR classification.

This article has been accepted for publication in a future issue of this journal, but has not been fully edited. Content may change prior to final publication. Citation information: DOI 10.1109/TBME.2020.3030216, IEEE Transactions on Biomedical Engineering

TABLE III
PERFORMANCE METRICS REPRESENTED AS MEDIAN (INTERQUARTILE RANGE) FOR THE TWO-CLASS CLASSIFICATION PROBLEM

	Signals	N_f	Se_{PEA}	Se_{PR}	UMS	$F_{1,PEA}$	$F_{1,PR}$	F_{1m}	AUC
Risdal et al. [8]	ECG, TI	17	78.8 (2.7)	78.0 (3.1)	78.3 (2.2)	74.0 (1.8)	64.9 (2.0)	69.4 (1.7)	0.84 (0.02)
Risdal et al. [8]	ECG, TI	12	80.1 (3.2)	77.6 (2.2)	78.6 (2.2)	74.6 (2.3)	65.1 (2.0)	69.7 (1.8)	0.84 (0.02)
Alonso et al. [9]	ECG, TI	6	68.8 (1.7)	77.3 (1.4)	73.1 (1.4)	67.7 (1.3)	65.7 (1.9)	66.7 (1.4)	0.84 (0.02)
Elola et al. [13]	ECG	9	77.9 (2.2)	80.2 (2.6)	78.9 (1.6)	74.6 (1.2)	67.9 (1.8)	71.2 (1.5)	0.84 (0.01)
Elola et al. [19]	ECG, TI, CO_2	10	79.9 (2.2)	81.1 (2.2)	80.4 (1.9)	77.0 (2.0)	79.4 (2.0)	73.0 (1.7)	0.87 (0.01)
This study	ECG, TI, CO_2	10*	83.1 (3.0)	79.8 (2.8)	81.5 (1.8)	78.8 (2.5)	70.0 (2.9)	74.5 (1.9)	0.87 (0.02)
This study	ECG, TI, CO_2	20*	84.5 (2.5)	80.3 (2.3)	82.4 (1.7)	80.1 (1.7)	70.3 (2.5)	75.3 (1.5)	0.88 (0.01)
This study	ECG, TI, CO_2	30*	85.6 (2.4)	81.3 (2.0)	83.2 (1.9)	80.6 (1.7)	70.4 (2.5)	75.6 (1.8)	0.89 (0.01)
This study	ECG, TI, CO_2	40*	86.0 (2.1)	81.8 (2.1)	83.9 (1.7)	81.2 (1.7)	71.0 (2.6)	76.2 (1.8)	0.89 (0.01)
This study	ECG	30	76.4 (2.6)	80.4 (4.0)	78.4 (2.2)	74.4 (1.8)	68.5 (2.1)	71.4 (1.6)	0.85 (0.01)
This study	ECG, TI	30	85.9 (2.2)	80.5 (2.3)	83.1 (1.8)	80.6 (1.5)	70.3 (2.7)	75.5 (1.8)	0.88 (0.01)

* The final model included $N_f + 1$ features ($MEtCO_2$)

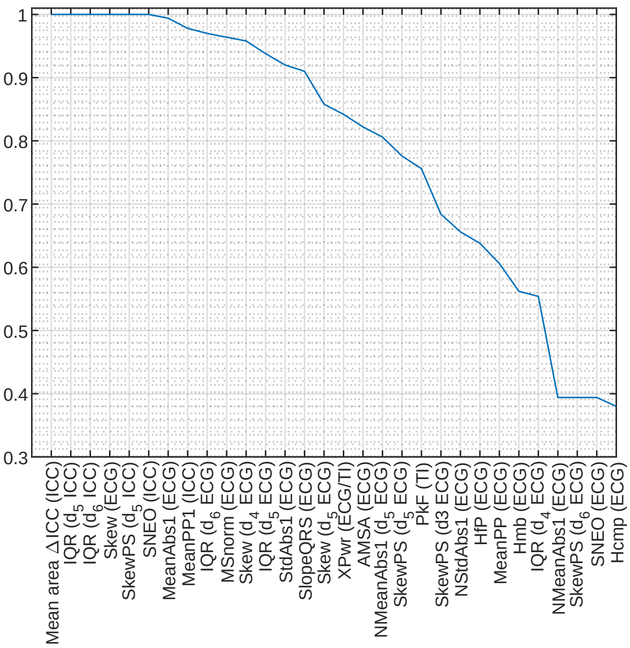

Fig. 9. Probability of selection for each feature when $N_f = 30$ and two classes were considered (PEA/PR).

VI. DISCUSSION

This study is, to the best of our knowledge, the first to address detailed circulation state classification models during OHCA. One of the key difficulties when assessing the circulation state during OHCA is the lack of a reliable source of information for the ground truth annotations. We were able to circumvent this difficulty by using a rich experimental biomedical signal dataset of 210 OHCA cases, in which patients were cannulated and the IBP signal was recorded in a prehospital setting. Then, the models to determine the circulation state were developed using signals routinely acquired during OHCA treatment like the ECG, TI or the capnogram. Moreover, different models were designed for ECG only, ECG+TI and ECG+TI+CO_2 situations, to address the differences in availability of biomedical signals in current defibrillator models used to treat OHCA.

Our best model to classify circulation states had a median F_{1m} and UMS of 61.5% and 68.8%, i.e. 35-points above a random guess for a 3-class problem. The model used ECG, TI and CO_2 features, in fact $MEtCO_2$ was important to differentiate TPEA and PPEA. For a 30 feature model removing the $MEtCO_2$ lowered the TPEA and PPEA sensitivities from 74.4% to 71.8%, and from 50.2% to 47.7%, respectively. The $MEtCO_2$ values were significantly larger in PPEA than in TPEA, with median values of 32.1 (25.2-42.8) mmHg and 9.2 (5.0-24.1) mmHg, respectively. These conclusions are coherent with those observed in previous studies [19], [24]. In fact, $EtCO_2$ showed positive correlations with blood pressure measurements [42], which may explain its value to differentiate circulation states during PEA.

In this study we introduced a novel feature extraction method from the ECG and TI combining multiresolution waveform analysis based on the SWT and a Kalman smoother to obtain the ICC. When our methods were compared to those proposed in the literature for the binary classification of circulation states (PEA/PR) [8], [9], [13], [19], our models outperformed all previous models (see Table III). This proves the value of the feature extraction methods introduced in this study, in particular the value of the Kalman smoother to obtain the ICC. When compared to a previous approach to obtain the ICC based on the RLS method [9] and following the same procedure, our Kalman smoother improved the median UMS by 4.5 and 2 points for the detailed and the binary classification of circulation states, respectively.

The detailed automatic classification of circulation states of OHCA patients may contribute to improve treatment, particularly, in guiding the administration of vasoconstrictors like epinephrine. Currently, the European Resuscitation Council and the American Heart Association recommend different treatments for pseudo and true PEA [4], [43]. The distinction between PEA states, and the identification of spontaneous circulation, are currently done by expert clinicians in stressful treatment conditions, it is not very accurate, and involves long interruptions in therapy [44]–[46]. Integrating the algorithms introduced in this study in current monitor defibrillators would contribute to a better identification of circulation states, and could serve experts as a clinical decision support tool during OHCA treatment.

The proposed algorithms provided Se values of 86% and

81.8% for PEA and PR, respectively. However, for clinical practice minimum accuracy figures would be required. For instance, the American Heart Association recommends sensitivities above 90% and 95% for the automatic shock/no-shock decision algorithms before being used in automated external defibrillators [47]. No such recommendations exist for pulse detection algorithms, but our algorithms, despite outperforming state of the art solutions, are still far from the accuracies needed in clinical practice. However, if the algorithms were to be used as a diagnosis support tool by the rescuer in combination with other information provided by the defibrillator, the accuracy requirements could be relaxed and the solution integrated in every day practice.

The precision of the classification algorithms could benefit from further research. Including a larger dataset to develop the models, or using advanced machine learning techniques could enhance the performance of the classifiers. Obtaining a larger patient cohort is a difficult task, as IBP is rarely acquired in OHCA. However, unlabeled data could be used to augment the datasets using techniques like semi-supervised learning [48], as the ECG, TI and the capnogram are routinely acquired signals. Deep learning algorithms have already been proven to outperform binary classifiers of circulation states [14], and other signals such as the PPG have shown promising results [18]. Future solutions might benefit from additional signals in the classification model and more sophisticated machine learning architectures.

VII. Conclusions

This study introduces multimodal biosignal processing and machine learning algorithms for the classification of circulation states during OHCA, and it is the first time that the automatic detection of detailed circulation states is addressed. These algorithms could serve as an important clinical decision tool for clinicians for the adequate administration of medication during OHCA treatment, and in decisions such as transport to hospital for post-resuscitation care.

Appendixes, if needed, appear before the acknowledgment.

Acknowledgment

Authors are gratefull to collaborators Fred.W. Chapman and Fredrick Arnwald for their support and valuable contributions to this study.

References

[1] J.-T. Gräsner, R. Lefering, R. W. Koster, S. Masterson, B. W. Böttiger, J. Herlitz, J. Wnent, I. B. Tjelmeland, F. R. Ortiz, H. Maurer *et al.*, "EuReCa ONE: 27 Nations, ONE Europe, ONE Registry: A prospective one month analysis of out-of-hospital cardiac arrest outcomes in 27 countries in europe," *Resuscitation*, vol. 105, pp. 188–195, 2016.

[2] E. J. Benjamin, S. S. Virani, C. W. Callaway, A. M. Chamberlain, A. R. Chang, S. Cheng, S. E. Chiuve, M. Cushman, F. N. Delling, R. Deo *et al.*, "Heart disease and stroke statistics-2018 update: a report from the american heart association." *Circulation*, vol. 137, no. 12, p. e67, 2018.

[3] G. D. Perkins, A. J. Handley, R. W. Koster, M. Castrén, M. A. Smyth, T. Olasveengen, K. G. Monsieurs, V. Raffay, J.-T. Gräsner, V. Wenzel *et al.*, "European resuscitation council guidelines for resuscitation 2015: Section 2. adult basic life support and automated external defibrillation," *Resuscitation*, vol. 95, pp. 81–99, 2015.

[4] J. Soar, J. P. Nolan, B. W. Böttiger, G. D. Perkins, C. Lott, P. Carli, T. Pellis, C. Sandroni, M. Skrifvars, G. Smith *et al.*, "Section 3. adult advanced life support: European resuscitation council guidelines for resuscitation 2015." *Resuscitation*, 2015.

[5] E. Skogvoll, T. Eftestøl, K. Gundersen, J. T. Kvaløy, J. Kramer-Johansen, T. M. Olasveengen, and P. A. Steen, "Dynamics and state transitions during resuscitation in out-of-hospital cardiac arrest," *Resuscitation*, vol. 78, no. 1, pp. 30–37, 2008.

[6] J. Berdowski, J. G. Tijssen, and R. W. Koster, "Chest compressions cause recurrence of ventricular fibrillation after the first successful conversion by defibrillation in out-of-hospital cardiac arrest," *Circulation: Arrhythmia and Electrophysiology*, vol. 3, no. 1, pp. 72–78, 2010.

[7] J. P. Nolan, J. Soar, A. Cariou, T. Cronberg, V. R. Moulaert, C. D. Deakin, B. W. Bottiger, H. Friberg, K. Sunde, and C. Sandroni, "European resuscitation council and european society of intensive care medicine guidelines for post-resuscitation care 2015: section 5 of the european resuscitation council guidelines for resuscitation 2015," *Resuscitation*, vol. 95, pp. 202–222, 2015.

[8] M. Risdal, S. O. Aase, J. Kramer-Johansen, and T. Eftesol, "Automatic identification of return of spontaneous circulation during cardiopulmonary resuscitation," *IEEE Transactions on Biomedical Engineering*, vol. 55, no. 1, pp. 60–68, 2008.

[9] E. Alonso, E. Aramendi, M. Daya, U. Irusta, B. Chicote, J. K. Russell, and L. G. Tereshchenko, "Circulation detection using the electrocardiogram and the thoracic impedance acquired by defibrillation pads," *Resuscitation*, vol. 99, pp. 56–62, 2016.

[10] B. Eberle, W. Dick, T. Schneider, G. Wisser, S. Doetsch, and I. Tzanova, "Checking the carotid pulse check: diagnostic accuracy of first responders in patients with and without a pulse," *Resuscitation*, vol. 33, no. 2, pp. 107–116, 1996.

[11] J. Tibballs and P. Russell, "Reliability of pulse palpation by healthcare personnel to diagnose paediatric cardiac arrest," *Resuscitation*, vol. 80, no. 1, pp. 61–64, 2009.

[12] M. Ruppert, M. W. Reith, J. H. Widmann, C. K. Lackner, R. Kerkmann, L. Schweiberer, and K. Peter, "Checking for breathing: evaluation of the diagnostic capability of emergency medical services personnel, physicians, medical students, and medical laypersons," *Annals of emergency medicine*, vol. 34, no. 6, pp. 720–729, 1999.

[13] A. Elola, E. Aramendi, U. Irusta, J. Del Ser, E. Alonso, and M. Daya, "ECG-based pulse detection during cardiac arrest using random forest classifier," *Medical & Biological Engineering & Computing*, vol. 57, no. 2, pp. 453–462, Feb. 2019.

[14] A. Elola, E. Aramendi, U. Irusta, A. Picón, E. Alonso, P. Owens, and A. Idris, "Deep Neural Networks for ECG-Based Pulse Detection during Out-of-Hospital Cardiac Arrest," *Entropy*, vol. 21, no. 3, p. 305, Mar. 2019.

[15] N. A. Cromie, J. D. Allen, C. Turner, J. M. Anderson, and A. A. J. Adgey, "The impedance cardiogram recorded through two electrocardiogram/defibrillator pads as a determinant of cardiac arrest during experimental studies*," *Critical Care Medicine*, vol. 36, no. 5, p. 1578, May 2008.

[16] A. Elola, E. Aramendi, U. Irusta, A. Picón, E. Alonso, I. Isasi, and A. Idris, "Convolutional Recurrent Neural Networks to Characterize the Circulation Component in the Thoracic Impedance during Out-of-Hospital Cardiac Arrest," in *2019 41st Annual International Conference of the IEEE Engineering in Medicine and Biology Society (EMBC)*, Jul. 2019, pp. 1921–1925.

[17] J. M. Ruiz, S. R. de Gauna, D. M. González-Otero, P. Saiz, J. J. Gutiérrez, J. F. Veintemillas, J. M. Bastida, and D. Alonso, "Circulation assessment by automated external defibrillators during cardiopulmonary resuscitation," *Resuscitation*, vol. 128, pp. 158–163, 2018.

[18] R. W. Wijshoff, A. M. van Asten, W. H. Peeters, R. Bezemer, G. J. Noordergraaf, M. Mischi, and R. M. Aarts, "Photoplethysmography-based algorithm for detection of cardiogenic output during cardiopulmonary resuscitation," *IEEE Transactions on Biomedical Engineering*, vol. 62, no. 3, pp. 909–921, 2014.

[19] A. Elola, E. Aramendi, U. Irusta, E. Alonso, Y. Lu, M. P. Chang, P. Owens, and A. H. Idris, "Capnography: A support tool for the detection of return of spontaneous circulation in out-of-hospital cardiac arrest," *Resuscitation*, vol. 142, pp. 153–161, Sep. 2019.

[20] T. Aufderheide, N. Paradis, and H. Halperin, "Etiology, electrophysiology, and myocardial mechanics of pulseless electrical activity," *Cardiac arrest: the science and practice of resuscitation medicine*, vol. 22, p. 426, 2007.

[21] N. A. Paradis, G. B. Martin, M. G. Goetting, E. P. Rivers, M. Feingold, and R. M. Nowak, "Aortic pressure during human cardiac arrest:

identification of pseudo-electromechanical dissociation," *Chest*, vol. 101, no. 1, pp. 123–128, 1992.

[22] R. J. Myerburg, H. Halperin, D. A. Egan, R. Boineau, S. S. Chugh, A. M. Gillis, J. I. Goldhaber, D. A. Lathrop, P. Liu, J. T. Niemann *et al.*, "Pulseless electric activity: definition, causes, mechanisms, management, and research priorities for the next decade: report from a national heart, lung, and blood institute workshop," *Circulation*, vol. 128, no. 23, pp. 2532–2541, 2013.

[23] U. A. P. Flato, E. F. Paiva, M. T. Carballo, A. M. Buehler, R. Marco, and A. Timerman, "Echocardiography for prognostication during the resuscitation of intensive care unit patients with non-shockable rhythm cardiac arrest," *Resuscitation*, vol. 92, pp. 1–6, 2015.

[24] G. Prosen, M. Križmarić, J. Završnik, and Š. Grmec, "Impact of modified treatment in echocardiographically confirmed pseudo-pulseless electrical activity in out-of-hospital cardiac arrest patients with constant end-tidal carbon dioxide pressure during compression pauses," *Journal of International Medical Research*, vol. 38, no. 4, pp. 1458–1467, 2010.

[25] M. Y. C. Chia, T. P. W. Kwa, W. Wah, S. Yap, N. E. Doctor, Y. Y. Ng, D. R. Mao, B. S.-H. Leong, H. N. Gan, L. P. Tham *et al.*, "Comparison of outcomes and characteristics of emergency medical services (ems)-witnessed, bystander-witnessed, and unwitnessed out-of-hospital cardiac arrests in singapore," *Prehospital Emergency Care*, vol. 23, no. 6, pp. 847–854, 2019.

[26] C. Weiser, M. Poppe, F. Sterz, H. Herkner, C. Clodi, C. Schriefl, A. Warenits, M. Vossen, M. Schwameis, A. Nürnberger *et al.*, "Initial electrical frequency predicts survival and neurological outcome in out of hospital cardiac arrest patients with pulseless electrical activity," *Resuscitation*, vol. 125, pp. 34–38, 2018.

[27] L. Littmann, D. J. Bustin, and M. W. Haley, "A simplified and structured teaching tool for the evaluation and management of pulseless electrical activity," *Medical Principles and Practice*, vol. 23, no. 1, pp. 1–6, 2014.

[28] D. Bergum, G. W. Skjeflo, T. Nordseth, O. C. Mjølstad, B. O. Haugen, E. Skogvoll, and J. P. Loennechen, "Ecg patterns in early pulseless electrical activity-associations with aetiology and survival of in-hospital cardiac arrest," *Resuscitation*, vol. 104, pp. 34–39, 2016.

[29] D. L. Donoho and J. M. Johnstone, "Ideal spatial adaptation by wavelet shrinkage," *biometrika*, vol. 81, no. 3, pp. 425–455, 1994.

[30] I. Daubechies, *Ten lectures on wavelets*. Siam, 1992, vol. 61.

[31] H. Losert, M. Risdal, F. Sterz, J. Nysæther, K. Köhler, T. Eftestøl, C. Wandaller, H. Myklebust, T. Uray, S. O. Aase *et al.*, "Thoracic-impedance changes measured via defibrillator pads can monitor signs of circulation," *Resuscitation*, vol. 73, no. 2, pp. 221–228, 2007.

[32] J. Ruiz, E. Alonso, E. Aramendi, J. Kramer-Johansen, T. Eftestøl, U. Ayala, and D. González-Otero, "Reliable extraction of the circulation component in the thoracic impedance measured by defibrillation pads," *Resuscitation*, vol. 84, no. 10, pp. 1345–1352, 2013.

[33] Z. Zhao, S. Särkkä, and A. B. Rad, "Spectro-temporal ecg analysis for atrial fibrillation detection," in *2018 IEEE 28th International Workshop on Machine Learning for Signal Processing (MLSP)*. IEEE, 2018, pp. 1–6.

[34] S. Haykin, *Kalman filtering and neural networks*. John Wiley & Sons, 2004, vol. 47, ch. 1.

[35] P. S. Hamilton and W. J. Tompkins, "Quantitative investigation of qrs detection rules using the mit/bih arrhythmia database," *IEEE transactions on biomedical engineering*, no. 12, pp. 1157–1165, 1986.

[36] E. Aramendi, A. Elola, E. Alonso, U. Irusta, M. Daya, J. K. Russell, P. Hubner, and F. Sterz, "Feasibility of the capnogram to monitor ventilation rate during cardiopulmonary resuscitation," *Resuscitation*, vol. 110, pp. 162–168, 2017.

[37] I. Isasi, U. Irusta, A. Elola, E. Aramendi, U. Ayala, E. Alonso, J. Kramer-Johansen, and T. Eftestøl, "A machine learning shock decision algorithm for use during piston-driven chest compressions," *IEEE Transactions on Biomedical Engineering*, vol. 66, no. 6, pp. 1752–1760, 2018.

[38] I. Isasi, U. Irusta, A. B. Rad, E. Aramendi, M. Zabihi, T. Eftestøl, J. Kramer-Johansen, and L. Wik, "Automatic cardiac rhythm classification with concurrent manual chest compressions," *IEEE Access*, vol. 7, pp. 115 147–115 159, 2019.

[39] A. B. Rad, T. Eftestøl, K. Engan, U. Irusta, J. T. Kvaløy, J. Kramer-Johansen, L. Wik, and A. K. Katsaggelos, "Ecg-based classification of resuscitation cardiac rhythms for retrospective data analysis," *IEEE Transactions on Biomedical Engineering*, vol. 64, no. 10, pp. 2411–2418, 2017.

[40] B. Chicote, U. Irusta, E. Aramendi, I. Isasi, D. Alonso, F. Vicente, and M. Sanchez, "Nonlinear energy operators for defibrillation shock outcome prediction," in *2016 Computing in Cardiology Conference (CinC)*. IEEE, 2016, pp. 61–64.

[41] C. Vaillancourt, S. Everson-Stewart, J. Christenson, D. Andrusiek, J. Powell, G. Nichol, S. Cheskes, T. P. Aufderheide, R. Berg, I. G. Stiell *et al.*, "The impact of increased chest compression fraction on return of spontaneous circulation for out-of-hospital cardiac arrest patients not in ventricular fibrillation," *Resuscitation*, vol. 82, no. 12, pp. 1501–1507, 2011.

[42] C. P. Kheng and N. H. Rahman, "The use of end-tidal carbon dioxide monitoring in patients with hypotension in the emergency department," *International journal of emergency medicine*, vol. 5, no. 1, p. 31, 2012.

[43] M. S. Link, L. C. Berkow, P. J. Kudenchuk, H. R. Halperin, E. P. Hess, V. K. Moitra, R. W. Neumar, B. J. O'Neil, J. H. Paxton, S. M. Silvers *et al.*, "Part 7: adult advanced cardiovascular life support: 2015 american heart association guidelines update for cardiopulmonary resuscitation and emergency cardiovascular care," *Circulation*, vol. 132, no. 18_suppl_2, pp. S444–S464, 2015.

[44] F. Lapostolle, P. Le Toumelin, J. M. Agostinucci, J. Catineau, and F. Adnet, "Basic cardiac life support providers checking the carotid pulse: performance, degree of conviction, and influencing factors," *Academic emergency medicine*, vol. 11, no. 8, pp. 878–880, 2004.

[45] E. J. Clattenburg, P. Wroe, S. Brown, K. Gardner, L. Losonczy, A. Singh, and A. Nagdev, "Point-of-care ultrasound use in patients with cardiac arrest is associated prolonged cardiopulmonary resuscitation pauses: a prospective cohort study," *Resuscitation*, vol. 122, pp. 65–68, 2018.

[46] M. A. H. in't Veld, M. G. Allison, D. S. Bostick, K. R. Fisher, O. G. Goloubeva, M. D. Witting, and M. E. Winters, "Ultrasound use during cardiopulmonary resuscitation is associated with delays in chest compressions," *Resuscitation*, vol. 119, pp. 95–98, 2017.

[47] R. E. Kerber, L. B. Becker, J. D. Bourland, R. O. Cummins, A. P. Hallstrom, M. B. Michos, G. Nichol, J. P. Ornato, W. H. Thies, R. D. White *et al.*, "Automatic external defibrillators for public access defibrillation: recommendations for specifying and reporting arrhythmia analysis algorithm performance, incorporating new waveforms, and enhancing safety: a statement for health professionals from the american heart association task force on automatic external defibrillation, subcommittee on aed safety and efficacy," *Circulation*, vol. 95, no. 6, pp. 1677–1682, 1997.

[48] X. Zhaia, Z. Zhoua, and C. Tina, "Semi-supervised learning for ecg classification without patient-specific labeled data," *Expert Systems with Applications*, p. 113411, 2020.

A.2.6 Bigarren helburuari lotutako hirugarren argitalpena nazioarteko konferentzian

A.10. Taula. Bigarren helburuari lotutako hirugarren argitalpena nazioarteko konferentzian.

	Argitalpena nazioarteko konferentzian
Erreferentzia	Andoni Elola, Elisabete Aramendi, Unai Irusta, Henry Wang, Ahamed Idris, "Automated Detection of Patients with Return of Spontaneous Circulation in the Retrospective Analysis of Resuscitation Episodes", *Circulation 2020*, vol. 142, no. Suppl_4, p. A308.
Quality indices	• **Argitalpen mota**: Nazioarteko konferentzia • **Kuartila**: Q1 (1/138) (*Web of Science* 2019) • **Inpaktu faktorea**: 23.603

POSTER ABSTRACT SESSIONS
SESSION TITLE: OUTCOME PREDICTIONS

Abstract 308: Automated Detection of Patients with Return of Spontaneous Circulation in the Retrospective Analysis of Resuscitation Episodes

Andoni Elola, Elisabete Aramendi, Unai Irusta, Henry E Wang, Ahamed H Idris

Originally published 9 Nov 2020 | https://doi.org/10.1161/circ.142.suppl_4.308 | Circulation. 2020;142:A308

Abstract

Introduction: Retrospective analysis of out-of-hospital cardiac arrest episodes is important to evaluate the performance of resuscitation teams, and to advance research. Large numbers of electronic files are compiled in cardiac arrest registries and identifying patients with return of spontaneous circulation (ROSC) is expensive and time-consuming. The aim of this study was to analyze the feasibility of automatically annotating ROSC using the signals recorded by defibrillators.

Materials and methods: A set of 893 patients (261 with ROSC, of which 127 were transient) recorded by the Dallas-Fort Worth Center for Resuscitation Research using Philips HeartStart MRx devices were included. Every record contained the ECG and the thoracic impedance (TI) signals. ROSC was automatically identified as follows: 1) chest compression pauses longer than 60 s were identified using either the TI or the compression depth signals. 2) Organized ECG rhythms were identified using a comercial defibrillator's algorithm. 3) Pulsatile rhythms were identified using a published machine learning algorithm based on the ECG or the ECG and TI signals. The model uses up to 9 features, extracted from both the ECG (6) and the TI (3) signals. ROSC was identified when a 10s-interval was classified as pulsatile and the ROSC onset was set at the beginning of the pause. The performance was assessed in terms of Sensitivity (Se, ROSC patients), Specificity (Sp, no ROSC patients) and overall F1-score. Error in the ROSC onset was calculated comparing the automatically detected onset to the reviewed time of the clinical annotation of ROSC.

Results: The algorithm based exclusively on ECG showed Se, Sp and F1 scores of 90.0%, 92.7% and 90.5%, respectively. The algorithm that included both ECG and TI improved scores to 91.2%, 94.3% and 92.1%. For the set of patients with transient ROSC the algorithm showed a Se of 81.9% (95.6% for permanent ROSC) using the ECG and TI signals. The median (IQR) absolute error on the time of first ROSC onset was 0.8 (0.6-8.2) s.

Conclusions: An accurate algorithm to automatically identify patients with ROSC is demonstrated. This technique could be useful for retrospective analysis of cardiac arrest registries.

Footnotes

Author Disclosures: For author disclosure information, please visit the AHA Resuscitation Science Symposium 2020 Online Program Planner and search for the abstract title.

Previous | Back to top | Next

Circulation

November 17, 2020
Vol 142, Issue Suppl_4

Article Information

https://doi.org/10.1161/circ.142.suppl_4.308

Originally published November 9, 2020

A.3 Hirugarren helburuari lotutako argitalpenak

A.3.1 Hirugarren helburuari lotutako aurreneko argitalpena nazioarteko konferentzian

A.11. Taula. Hirugarren helburuari lotutako aurreneko argitalpena nazioarteko konferentzian.

	Argitalpena nazioarteko konferentzian
Erreferentzia	Andoni Elola, Elisabete Aramendi, Unai Irusta, Naroa Amezaga, Jon Urteaga, Pamela Owens, Ahamed Idris, "Automated Detection of Patients with Return of Spontaneous Circulation in the Retrospective Analysis of Resuscitation Episodes", *Circulation 2019*, vol. 140, no. Suppl_2, p. A127.
Kalitate adierazleak	• **Argitalpen mota**: Nazioarteko konferentzia • **Kuartila**: Q1 (1/138) (*Web of Science* 2019) • **Inpaktu faktorea**: 23.603

Circulation

November 19, 2019
Vol 140, Issue
Suppl_2

POSTER ABSTRACT PRESENTATIONS
SESSION TITLE: DEFIBRILLATION 2

Abstract 127: Machine Learning Techniques to Predict Cardiac Re-Arrest in Out-Of-Hospital Setting

Andoni Elola, Elisabete Aramendi, Unai Irusta, Naroa Amezaga, Jon Urteaga, Pamela Owens, Ahamed H Idris

Originally published 11 Nov 2019 | Circulation. 2019;140:A127

Abstract

Background: Re-arrest occurs when a cardiac arrest patient being treated by the emergency medical services experiences another cardiac arrest after return of spontaneous circulation (ROSC).The incidence of re-arrest is high, close to 40% in out-of-hospital cardiac arrest (OHCA), and it is associated with lower survival. Prediction of re-arrest could improve prehospital care. The aim of this study was to develop a re-arrest prediction model based on heart rate variability (HRV) features.

Materials and methods: OHCA cases treated by Dallas-FortWorth Center of Resuscitation Research were analyzed. Patients with at least two minutes of ROSC were included. Re-arrest was ascertained by the presence of life-threatening ECG and/or presence of chest compressions within 12 minutes after ROSC. Eighteen HRV characteristics for 1 min and 2 min intervals after ROSC were computed. Features were fed into a Random Forest (RF) classifier with 100 trees to predict re-arrest cases. Ten-fold cross-validation with 30 repetitions was applied to train the model and assess the performance in terms of area under the curve (AUC).

Results: Inclusion criteria were met by 98 patients, 41 of which suffered re-arrest. The median time (interquartile range) to re-arrest from ROSC onset was 5 (3-7) min. The re-arrest prediction model showed a median AUC of 0.71 and 0.75 for 1 and 2 min post ROSC intervals, respectively. The most important HRV features in the RF predictor were the SD1/SD2 ratio (where SD1 and SD2 are the dispersions of points both perpendicular and parallel to the line-of-identity in the Poincaré plot), SD2, the interquartile range of the RR intervals, peak frequency in the high frequency band (0.15-0.4 Hz) and coefficient of variation of RR intervals (the ratio between the mean and standard deviation of RR intervals).

Conclusions: HRV metrics predict re-arrest in OHCA. Further studies with larger datasets are needed to better understand re-arrest dynamics and confirm conclusions.

Article Information

Originally published November 11, 2019

Keywords

Footnotes

For author disclosure information, please visit the AHA Resuscitation Science Symposium 2019 Online Program Planner and search for the abstract title.

AHA Journals

Arteriosclerosis, Thrombosis, and Vascular Biology (ATVB)
Circulation
Circ: Arrhythmia and Electrophysiology
Circ: Genomic and Precision Medicine
Circ: Cardiovascular Imaging
Circ: Cardiovascular Interventions
Circ: Cardiovascular Quality & Outcomes
Circ: Heart Failure
Circulation Research
Hypertension

A.3.2 Hirugarren helburuari lotutako aurreneko argitalpena nazioarteko aldizkarian

A.12. Taula. Hirugarren helburuari lotutako aurreneko argitalpena nazioarteko aldizkarian.

	Argitalpena nazioarteko aldizkarian
Erreferentzia	Andoni Elola, Elisabete Aramendi, Enrique Rueda, Unai Irusta, Henry Wang, Ahamed Idris, "Towards the Prediction of Rearrest during Out-of-Hospital Cardiac Arrest", *Entropy 2020*, vol. 22, no. 7, p. 758.
Kalitate adierazleak	• **Argitalpen mota**: JCRen indexatutako aldizkari artikulua • **Kuartila**: Q2 (33/85) (*Web of Science* 2019) • **Inpaktu faktorea**: 2.494

entropy

MDPI

Article

Towards the Prediction of Rearrest during Out-of-Hospital Cardiac Arrest

Andoni Elola [1,*], Elisabete Aramendi [1], Enrique Rueda [1], Unai Irusta [1], Henry Wang [2] and Ahamed Idris [3,†]

1 Department of Communications Engineering, University of the Basque Country, 48013 Bilbao, Spain; elisabete.aramendi@ehu.eus (E.A.); enrique.rueda@ehu.eus (E.R.); unai.irusta@ehu.eus (U.I.)
2 Department of Emergency Medicine, University of Texas Health Science Center, Houston, TX 77030, USA; henry.e.wang@uth.tmc.edu
3 Department of Emergency Medicine, University of Texas Southwestern Medical Center, Dallas, TX 75390, USA; ahamed.idris@utsouthwestern.edu
* Correspondence: andoni.elola@ehu.eus; Tel.: +34-946-01-39-56
† A.I. serves as an unpaid volunteer on the American Heart Association National Emergency Cardiovascular Care Committee and the HeartSine, Inc. Clinical Advisory Board.

Received: 21 May 2020; Accepted: 7 July 2020; Published: 9 July 2020

check for updates

Abstract: A secondary arrest is frequent in patients that recover spontaneous circulation after an out-of-hospital cardiac arrest (OHCA). Rearrest events are associated to worse patient outcomes, but little is known on the heart dynamics that lead to rearrest. The prediction of rearrest could help improve OHCA patient outcomes. The aim of this study was to develop a machine learning model to predict rearrest. A random forest classifier based on 21 heart rate variability (HRV) and electrocardiogram (ECG) features was designed. An analysis interval of 2 min after recovery of spontaneous circulation was used to compute the features. The model was trained and tested using a repeated cross-validation procedure, on a cohort of 162 OHCA patients (55 with rearrest). The median (interquartile range) sensitivity (rearrest) and specificity (no-rearrest) of the model were 67.3% (9.1%) and 67.3% (10.3%), respectively, with median areas under the receiver operating characteristics and the precision–recall curves of 0.69 and 0.53, respectively. This is the first machine learning model to predict rearrest, and would provide clinically valuable information to the clinician in an automated way.

Keywords: out-of-hospital cardiac arrest (OHCA); rearrest; electrocardiogram (ECG); heart rate variability (HRV); random forest (RF)

1. Introduction

Cardiac arrest remains a major public health problem with more than 275,000 out-of-hospital cardiac arrest (OHCA) cases treated yearly in Europe [1], and survival rates below 10% [2,3]. Prompt treatment is crucial because the probability of survival decreases by 10% for every minute treatment is delayed [4,5]. Current cardiopulmonary resuscitation (CPR) guidelines define chain of survival to ensure a prompt OHCA treatment, with five important links [6]: early recognition of the arrest, CPR with chest compressions and ventilations, rapid defibrillation, basic/advanced emergency medical treatment, and post-cardiac arrest care.

The final aim of the treatment provided by the emergency medical services is to achieve the return of spontaneous circulation (ROSC), and to then proceed to the last link of the chain of survival, post-arrest treatment, and transportation to hospital. CPR manoeuvres, defibrillation, and drugs produce changes in the patient's state, which are reflected in the cardiac rhythm. For instance, defibrillation may bring a patient from ventricular fibrillation to a rhythm with spontaneous pulse, that is, to ROSC.

Rearrest is experienced by patients who achieve ROSC and suffer a subsequent cardiac arrest during their prehospital care. Rearrest is frequent in the prehospital setting with observed incidences between 24% and 43% [7–10]. Moreover, rearrest is associated to poorer patient outcomes, both for hospital discharge and neurological state at follow up [7–11]. The prediction of rearrest would contribute to better outcomes by providing adequate medical treatment to better stabilize the patient, and by delaying transport to hospital, as providing adequate care is more difficult when rearrest occurs in an ambulance during transport to hospital.

Several characteristics observable in the electrocardiogram (ECG) are associated to rearrest risk factors: low heart rate, increased heart rate variability, long QRS complexes, irregular beats, etc. Nevertheless, very few automated methods have been proposed to predict rearrest. Some important contributions by Salcido et al. in the use of heart rate variability (HRV) features and morphology features of the ECG [9,12] showed the potential of the ECG in this context. Other studies focused on the transition between cardiac rhythms, including the transition from pulse-generating rhythms (ROSC) to non-pulsatile rhythms, that is, rearrest [13].

In this paper, a machine learning technique is developed to predict rearrest in OHCA patients. A solution based on a random forest (RF) classifier is adjusted for 1 and 2 min of ECG signal acquired by the defibrillation pads, a signal commonly recorded by all defibrillators in OHCA scenarios. In the Materials section, the source of the OHCA cases and the ECG signals is described. The HRV features and the design of the RF classifier is detailed in Methods, and the Results are given next. In the Discussion section, the clinical importance and implications in OHCA treatment of this algorithm are elaborated.

2. Data Collection

The data used in this study were a subset of a large OHCA episode collection gathered in the Dallas–Fortworth area by the DFW center for resuscitation research (UTSW, Dallas). Every episode was recorded using the Philips HeartStart MRx device, which acquires the ECG signal and the thoracic impedance through the defibrillation pads. The ECG signal was acquired with a sampling frequency of 250 Hz and a resolution of 1.03 μV per least significant bit. Additionally, some episodes included the chest compression depth signal, which in conjunction with the impedance signal, permitted identifying the intervals with chest compressions.

There were a total of 797 episodes with concurrent ECG and impedance signals. Episodes with ROSC were identified based on the instant of ROSC (t_{ROSC}) annotated by clinicians on the scene. No rearrest episodes (NoRA) corresponded to patients with sustained ROSC according to the clinical information in the patient's chart, and no chest compressions until the end of the episode. A minimum duration of 2 min was required for the ROSC interval. Rearrest episodes (RA) were identified if ROSC was lost in an interval of 12 min after ROSC. Patients that suffered a rearrest after 12 min from the ROSC onset were considered in the NoRA group. Figure 1 shows a RA case, where spontaneous pulse was lost t_{RA} seconds after the onset of ROSC, t_{ROSC}. The final patient cohort included 162 patients, 107 NoRA, and 55 RA cases. In the NoRA cases, the median (first quartile–third quartile) duration from the onset of ROSC to the end of episode was 300 (240–874) s. In the RA cases the median duration from ROSC onset to RA was 303 (195–410) s.

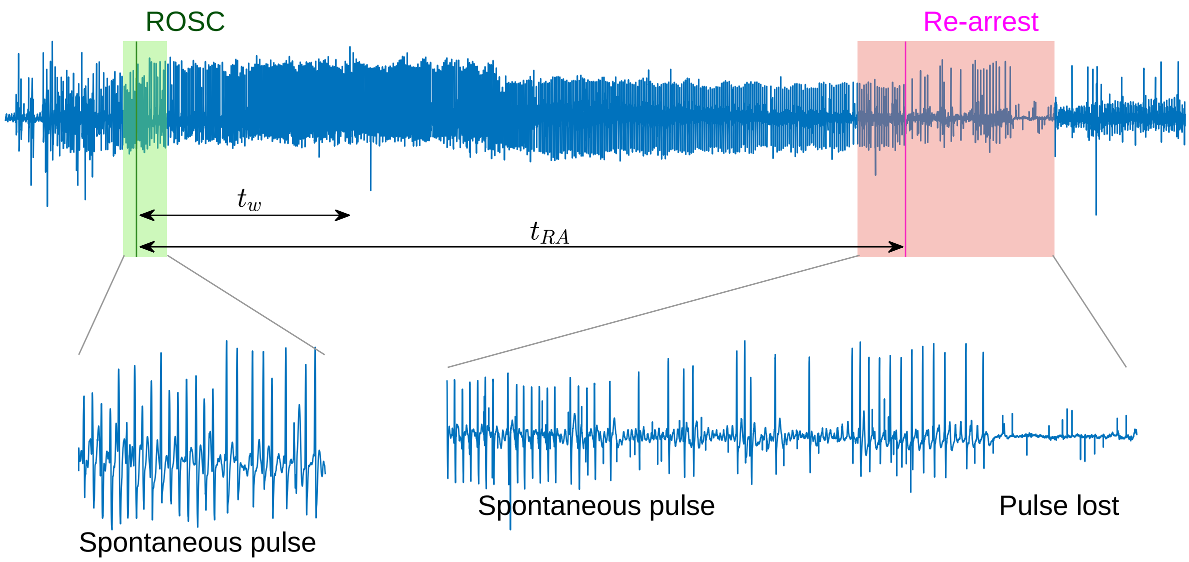

Figure 1. Out-of-hospital cardiac arrest (OHCA) episode where the instant of return of spontaneous circulation (ROSC), t_{ROSC}(s), is associated to the pulse generating rhythm (green), and rearrest (RA) occurs t_{RA}(s) later when the rhythm degenerates into a pulseless activity and asystole (red). The segment of analysis is noted with a duration of t_w(s).

3. Methods

The rearrest prediction algorithm proposed in this manuscript was applied to segments of t_w minutes of ECG signal extracted right after t_{ROSC}, as shown in Figure 1. For case number i a vector of 21 features, $\mathbf{v}_i = \{v_{i,1}, \cdots, v_{i,21}\}$, was computed for each segment and a machine learning classifier applied for the binary classification ($y_i = \{0, 1\} = \{\text{NoRA}, \text{RA}\}$). Two segment lengths were considered in the model, $t_w = 1$ min and $t_w = 2$ min.

3.1. ECG Processing and Feature Extraction

A total of 21 features (Table 1) were extracted to vectorize the ECG segment: 17 were based on HRV metrics as proposed in [14], and four new features were incorporated based on the ECG waveform.

First, the ECG signal was filtered between 0.5 and 40 Hz using order 4 Butterworth (zero-phase) filter to remove baseline wander and high frequency noise. Second, HRV features were computed using the R peaks detected using the well-known Hamilton–Tompkins QRS detector [15]. A variance-based correction was applied to prevent false negative heartbeat detections caused by large amplitude changes in the R-peaks. The impact of spiky artifacts in the adaptive thresholding of the QRS detector was thus reduced and the RR series were constructed. Examples of RR series for a RA and a NoRA case can be observed in Figure 2.

The HRV features computed using the RR series can be divided into three groups [16]:

- **Time domain features.** The classic metrics of RR variability were computed: mean RR interval (v_1), standard deviation (v_2), root mean square of the successive differences (v_3), coefficient of variation ($v_4 = v_2/v_1$) [17], number of RR intervals that differ more than 50 ms (v_5), and the interquartile range of RR intervals (v_6).
- **Frequency domain features.** First, the spectrum of the RR sequence was computed using the Lomb–Scargle periodogram for unevenly sampled signals [18]. Then, two different frequency bands were analyzed, the low-frequency or LF band (0.04–0.15 Hz) and the high-frequency or HF band (0.15–0.4 Hz). The computed features were the absolute and relative power in the LF band (v_7 and v_8), the absolute and relative power in the HF band (v_9 and v_{10}), the relation between LF and HF power (v_{11}), and the peak frequencies in LF and HF bands (v_{12} and v_{13}).

- **Nonlinear features.** Self similarity of the RR samples was evaluated using the Poincaré plot and entropy-based features. From the Poincaré plot the variability was measured with the width, $SD1^2$, and depth, $SD2^2$, of the ellipse, v_{14} and v_{15}, respectively. Their relation was computed as v_{16}. The sample entropy of the RR series (v_{17}) was computed from a cubic interpolation of the RR series to form a uniformly sampled series (10 Hz), and $m = 1$ and $r = 0.2$ were used [19].

Additionally, four features were computed using the ECG signal, three of them proposed in [13] (v_{18}, v_{19}, and v_{21}). They were computed as follows.

- The centroid frequency, v_{18}, was computed based on the power spectral density (PSD) of the ECG signal. The PSD was estimated for the f_i frequencies using Welch's periodogram with a signal window of 12 s, an overlap of 50% and a fast Fourier transform of 4096 points:

$$v_{18} = \frac{\sum_i PSD(f_i) \cdot f_i}{\sum_i PSD(f_i)} \tag{1}$$

- The mean of the absolute values of the samples of the ECG segment, v_{19}.
- The relative QRS-power, as the power of the signal concentrated in the frequency band corresponding to the QRS complexes (5–14 Hz) [15,20]:

$$v_{20} = \frac{\sum_{f_i=5}^{f_i=14} PSD(f_i)}{\sum_i PSD(f_i)} \tag{2}$$

- The variability of the duration of the QRS complexes. QRS complexes were delineated using a wavelet based algorithm [21] and the standard deviation of their durations was v_{21}.

Table 1 provides a quick reference for the meaning of the v_i features.

Table 1. Overview of the computed features.

Time-domain HRV features	**Non-linear HRV features**
v_1 : Mean RR	v_{14} : $SD1^2$
v_2 : Standard deviation RR	v_{15} : $SD2^2$
v_3 : RMSSD	v_{16} : $SD1^2/SD2^2$
v_4 : Coefficient of variation	v_{17} : Sample entropy
v_5 : nNN50	**Signal-level features**
v_6 : Interquartile range RR	v_{18} : Centroid frequency
Frequency-domain HRV features	v_{19} : Signal amplitude
v_7 : LF absolute power	v_{20} : Relative QRS power
v_8 : LF relative power	v_{21} : Standard deviation of QRS width
v_9 : HF absolute power	
v_{10} : HF relative power	
v_{11} : LF/HF power	
v_{12} : LF peak frequency	
v_{13} : HF peak frequency	

Figure 2 shows the ECG segment and the RR sequence for $t_w = 1$ min in an RA and NoRA case. The RR instants (marked), the RR spectrum (LF and HF highlighted), and the Poincaré diagram are plotted. Larger variability of the RR series, a more disperse Poincaré plot, and more power concentration in the high frequency band were all associated to RA.

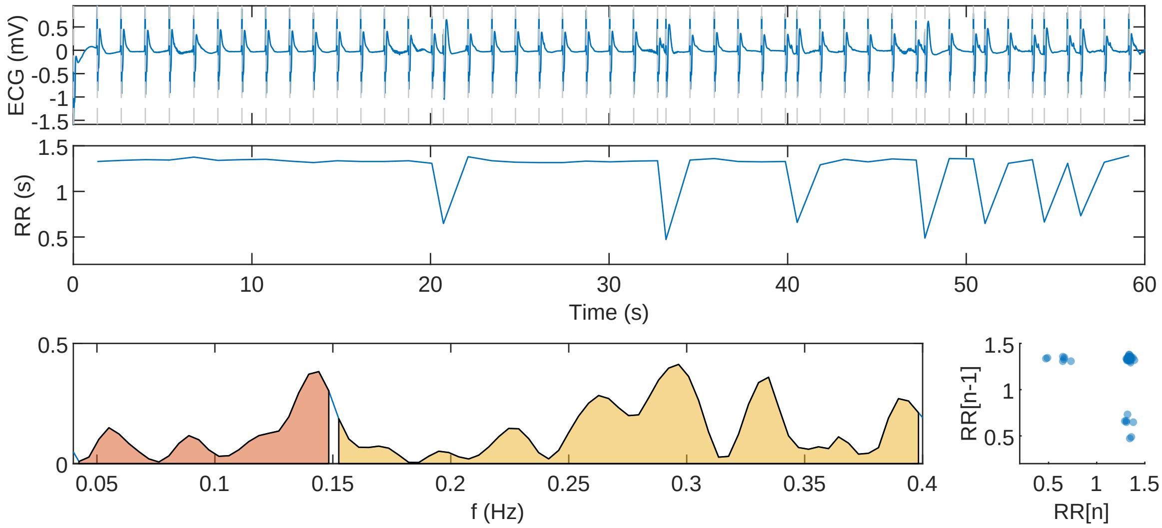

(a) Case leading to rearrest

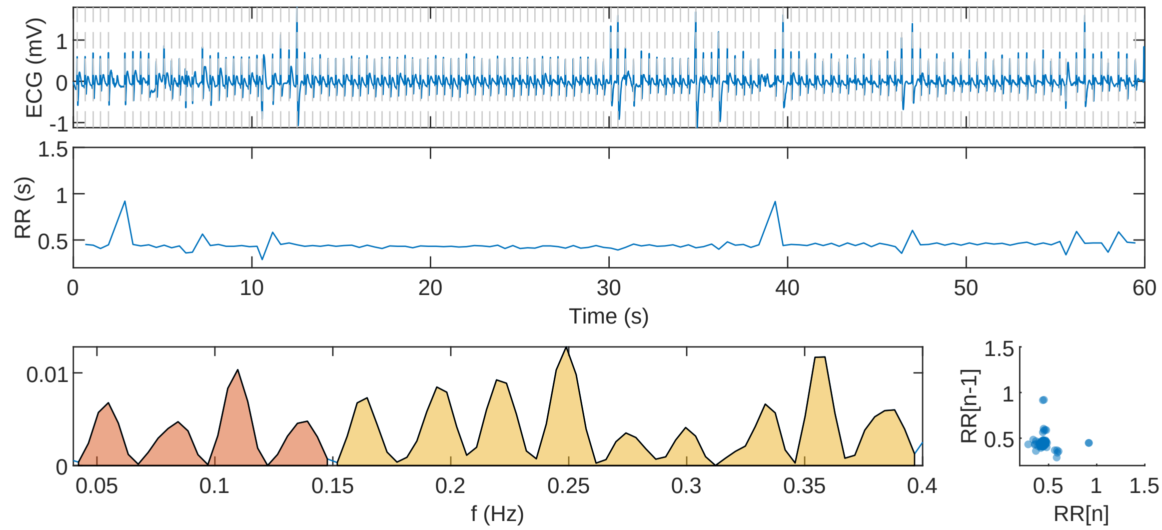

(b) A case with no rearrest.

Figure 2. Signals corresponding to RA and no rearrest (NoRA) cases are plotted in panels (**a**,**b**), respectively. The ECG signal for $t_w = 1\,\text{min}$, the RR sequence, its power spectrum and and the Poincaré plot are shown.

3.2. Building the RF Classifier

First, an univariate analysis was carried out to analyze the power of each feature to discriminate RA and NoRA cases. A cost-sensitive logistic regression classifier was fitted using a single feature in the training set and the performance metrics were obtained for that model in the test set (see Section 3.3). Then, a Random Forest (RF) classifier was used to combine all the features for several reasons: it can learn nonlinear mappings, it can be easily adapted for imbalanced datasets, and, besides allowing an embedded feature selection, feature importance can be estimated. Moreover, in our preliminary tests with other machine learning models the RF produced the best classification results. The RF classifier is an ensemble of B decision trees (weak learners) that produce uncorrelated predictions, and the final label is decided by majority voting [22]. Uncorrelated decisions are made by using different bootstraps of the training data to train each weak learner, and also a limited set of randomly selected features are used at each tree split. The importance of each feature can be estimated by permuting the values of each feature and looking at the increase in the out-of-bag error (error measured using the data that each weak learner did not see during the training process). The following two steps were followed.

- The RF was trained using the training dataset at hand and the importance of each feature was computed and correspondingly sorted.
- The RF was trained again using the same training data and using only the most important N_f features from the previous ranking. Considering the class imbalance in our study (≈34/66%), the number of instances per class were balanced when creating the bootstraps to train each tree by oversampling the minority class. The RF model was evaluated with the testing dataset in hand.

Both RFs were trained using $B = 300$ weak learners and each tree was trained using only 5% of the data. Bootstrapping was made using sampling with replacement, i.e., repeated instances were possible. For binary classification problems, the number of trees that predicted that a certain instance is positive divided by B can be interpreted as the probability or likelihood of the instance being positive.

3.3. Evaluation

The RF model was trained and tested using patient-wise and stratified 5-fold cross-validation data partition. Data were divided in five nonoverlapping groups, one was used for testing and the other four for training. This is repeated five times so every patient is used in the training and test sets. The procedure was repeated 100 times to estimate the statistical distributions of the performance metrics in terms of median (interquartile range (IQR)). The standard metrics for binary classification problems were considered.

The classification problem in this study involved two unbalanced classes: a negative class with the majority of the instances (NoRA), and a minority positive class (RA). In this scenario, two diagnostic tools are helpful to evaluate the models: receiver operating characteristics (ROC) and precision–recall (PR) curves. These curves are calculated evaluating corresponding performance metrics for different thresholds of the likelihoods given by the RF classifier. The following metrics were considered; sensitivity (Se) or recall (probability of detecting a RA case correctly), specificity (Sp, probability of detecting a NoRA case correctly), precision (probability that a positive detection corresponds to a positive case) and the harmonic mean between precision and recall (F_1 score). Areas under both curves, area under receiver operating characteristics curve (AUROC) and area under precision–recall curve (AUPRC), are good representative metrics to evaluate the performance of the model. Every metric is given as percentage.

4. Results

In the QRS detection, the variance based filter only changed the detections of the Hamilton-Tompkins algorithm in five cases (3% of episodes), and less than 0.3% of the samples were modified in those cases. To asses the quality of QRS detection and the RR series derived thereof, a signal quality index was adopted, the proportion of beats that are detected by two different QRS detectors over all detected beats [23]. As proposed by the authors of [23], we used a QRS detector robust to noise (Hamilton–Tompkins [15]) and a detector based on a length transform proposed by Zong et al. [24], which is more sensitive at lower signal-to-noise ratios. Median (first quartile–third quartile) agreement between the QRS detectors was 98.4% (90.7–99.6%), showing the good quality of the data.

The analysis of the logistic regression classifier for single features yielded median AUROC and AUPRC values for $t_w = 1$ min in the range of 52.0 to 65.1 and 29.3 to 50.3, respectively. Similar results were obtained for $t_w = 2$ min, with AUROC in the range of 53.7 to 66.2 and AUPRC in the range of 28.2 to 50.1. A random classifier in this case would correspond to AUROC = 50.0 and AUPRC = 34.0. Table 2 shows the distributions and median AUROC/AUPRC for the top 10 features (highest harmonic mean between AUROC and AUPRC) for $t_w = 1$ min and $t_w = 2$ min, respectively. It can be observed that time features like v_2 and v_4 were important for both values of t_w, showing that the variability of the RR sequence is a powerful discriminative feature. Nonlinear features measured through Poincaré plots and entropy (v_{15} and v_{17}) also showed high AUROC with medians of 65.0 and 65.5, respectively.

The correlation analysis between the features, based on the Pearson coefficient, r^2, showed high correlation between features in the same or different domains. Thus, v_2 showed good correlation ($r^2 > 0.75$) with v_3, v_4, v_{14} and v_{15}, and also v_4 with v_{14}.

The median (IQR) values of the features showed that RA patients presented more variable RR intervals, reflected in higher values of time HRV features, v_2 and v_4, and in a wider Poincaré plot as measured by v_{15}. The entropy of the RR series (v_{17}) was lower in RA cases, suggesting a more regular/predictable time series.

Table 2. Distributions of the values for the top 10 features, represented as median (IQR) for each class, and their median area under receiver operating characteristics curve (AUROC) and area under precision–recall curve (AUPRC) values. Results for $t_w = 1$ min and $t_w = 2$ min are shown.

$t_w = 1$ min					$t_w = 2$ min				
Feature	**NoRA**	**RA**	**AUROC**	**AUPRC**	**Feature**	**NoRA**	**RA**	**AUROC**	**AUPRC**
v_{15}	0.01 (0.02)	0.03 (0.10)	65.0	50.3	v_2	0.08 (0.12)	0.21 (0.37)	66.2	50.1
v_2	0.07 (0.10)	0.15 (0.25)	64.9	50.2	v_4	0.16 (0.19)	0.29 (0.40)	65.7	49.4
v_7	0.00 (0.00)	0.00 (0.01)	63.3	49.4	v_6	0.06 (0.11)	0.14 (0.26)	63.4	48.7
v_4	0.14 (0.17)	0.23 (0.24)	64.2	48.9	v_{17}	0.31 (0.45)	0.18 (0.27)	65.5	47.4
v_9	0.00 (0.00)	0.01 (0.03)	62.4	47.8	v_3	0.57 (0.23)	0.71 (0.49)	63.3	48.4
v_{14}	0.05 (0.06)	0.09 (0.18)	61.9	47.8	v_{14}	0.05 (0.09)	0.11 (0.20)	64.0	47.7
v_{17}	0.35 (0.51)	0.20 (0.30)	65.1	45.9	v_{15}	0.01 (0.02)	0.05 (0.22)	61.7	47.0
v_3	0.56 (0.26)	0.68 (0.45)	60.3	48.2	v_{20}	0.38 (0.20)	0.28 (0.22)	64.5	45.4
v_1	0.55 (0.24)	0.63 (0.38)	59.3	46.8	v_5	216 (81)	180 (104)	61.6	46.6
v_5	106 (45)	93 (54)	59.4	45.4	v_7	0.00 (0.00)	0.01 (0.03)	60.7	46.4

Figure 3 shows the median AUROC and AUPRC for the RF classifier as a function of the number of features considered in the model, N_f. Adding features to the model improved both metrics.

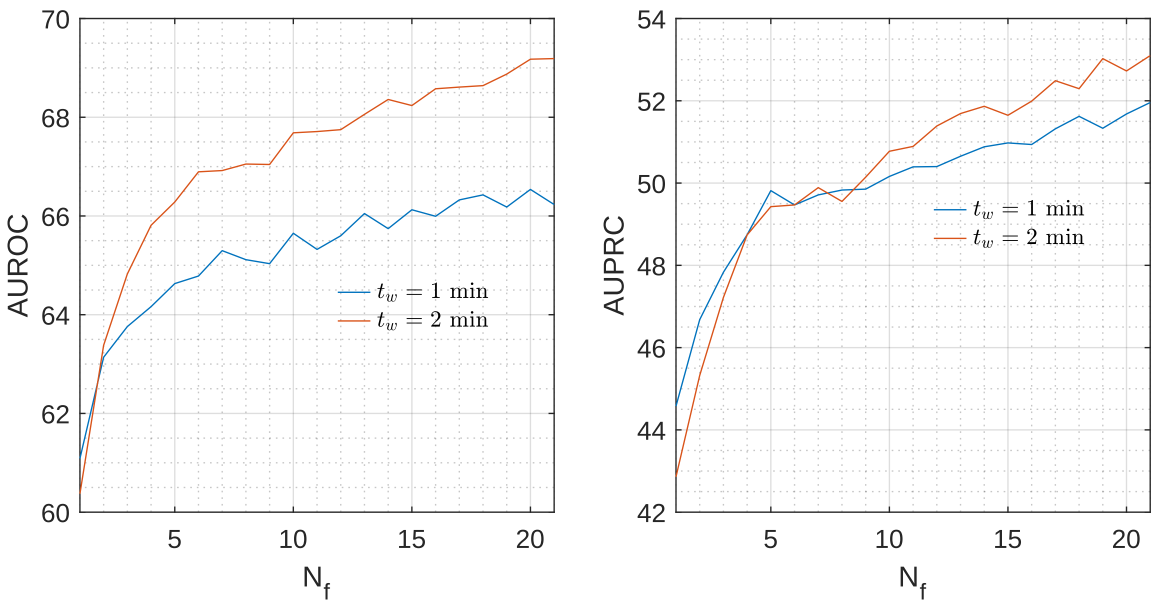

Figure 3. AUROC and AUPRC for the random forest (RF) classifier in function of the number of features of the model, N_f, for $t_w = 1$ min and $t_w = 2$ min.

Figure 4 shows the ROC and PR curves for the repetition closest to the median performance. The AUROC and AUPRC increased a median of 2 and 1 points for $t_w = 2$ min, showing that longer intervals improved the accuracy of the features in general and that of the spectral features in particular. The distributions of importance for each feature, depicted in Figure 5, show that most of the features had a positive importance and were relevant for the RF model. Features like v_{20}, v_{17}, v_7, v_{15}, or v_2 were in the top 10 when analyzed individually (see Table 2). Others, like v_{16}, were relevant when combined with the rest in the predictive model and when considering a RF classifier instead of a cost-sensitive logistic regression classifier.

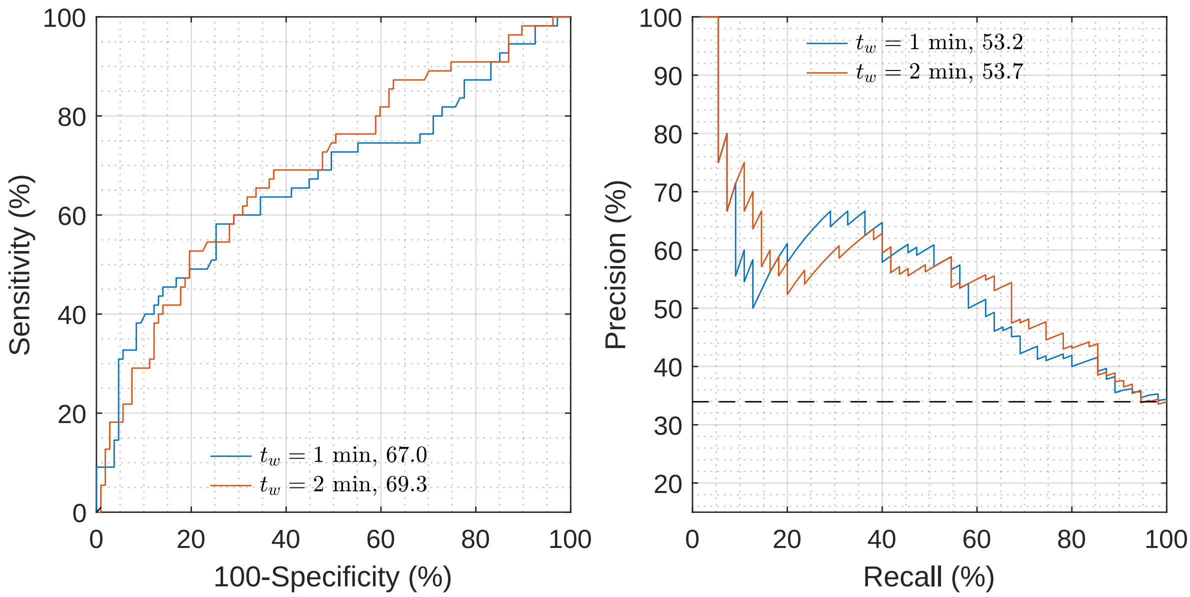

Figure 4. Receiver operating characteristics (ROC) and precision–recall (PR) curves for both values of t_w. The repetition that was closest to the median AUROC or AUPRC was chosen to depict the curves. The AUROC and AUPRC increased from 67.0 to 69.3, and from 53.2 to 53.7, respectively, when $tw = 2$ min were considered.

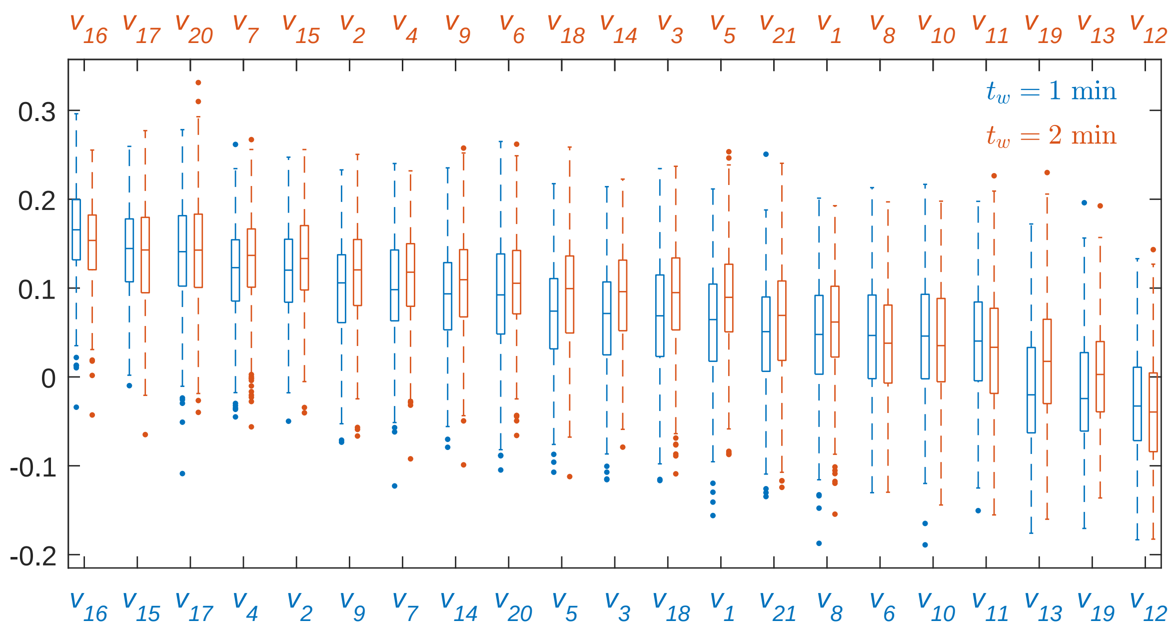

Figure 5. Distributions of feature importances given by the RF classifier sorted by importance for $t_w = 1$ min (blue) and $t_w = 2$ min (red).

Table 3 shows the overall metrics for the RF classifier for the thresholds that maximized the F_1 score. Adding the ECG features, v_{18}–v_{21}, to the HRV features significantly increased Se for both t_w values ($p < 0.05$ according to the Mann–Whitney test). For $t_w = 2$ min the AUROC and AUPRC increased 2 points, and the Se almost 6 points, meaning that 20% of the missclassified RA cases would be correctly detected.

Table 3. Performance metrics for the RF model in median (IQR) using only the HRV features and using all the features for both interval analyses, $t_w = 1$ min and $t_w = 2$ min.

	t_w	Se or Recall (%)	Sp (%)	Precision (%)	F_1 (%)	AUROC	AUPRC
HRV features	1 min	57.3 (11.8)	75.7 (14.5)	54.5 (9.8)	55.8 (2.8)	65.4 (2.3)	51.2 (2.9)
	2 min	61.8 (6.4)	72.9 (6.1)	54.4 (4.6)	57.6 (2.0)	67.3 (2.0)	50.7 (2.7)
All features	1 min	63.6 (15.5)	69.2 (20.6)	51.5 (10.0)	55.4 (3.1)	66.2 (2.2)	52.0 (2.6)
	2 min	67.3 (9.1)	67.3 (10.3)	51.4 (5.3)	57.9 (1.7)	69.2 (1.6)	53.1 (3.0)

5. Discussion

The final objective of prehospital treatment of OHCA is to recover spontaneous pulse. However, many detrimental factors may induce a secondary cardiac arrest, or rearrest, before arrival to hospital. These rearrest events reduce the probability of survival to hospital discharge [7,8,25–27]. Currently, clinicians apply expert knowledge on scene to foresee if a patient who has achieved ROSC should be transported immediately, or if the patient requires longer on-site treatment. Defibrillators show physiologic signals on screen but do not provide tools to assist clinicians on the prediction of a secondary arrest. To the best of our knowledge, this study provides the first automated method based on the ECG to predict rearrest. This is important because the ECG is routinely recorded in all defibrillators. The method is based on a RF classifier using HRV features and ECG waveform features, and showed a Se and Sp of 67%.

Fluctuating heart rates are frequent in organized rhythms during cardiac arrest. When spontaneous circulation is restored the QRS complexes may still be irregular in morphology and rate. ECG features associated to the heart rate have been used to successfully predict time to RA [12], especially the standard deviation of the measured heart rate. The standard deviation of the RR intervals (v_2) is a similar measure, and was also one of the most important features of the RF classifier. Moreover, v_2 alone showed a median AUROC of 66.2 (65.3–67.0) and median AUPPRC of 50.1 (49.3–50.7).

HRV features have been widely used in non-arrest situations to detect and predict cardiac arrhythmias [20,28,29]. They were originally designed to analyze long intervals, minutes, or even hours, in hemodynamically stable patients. Interestingly, in this study, HRV features have been proven to be good predictors of RA even with segments as short as $t_w = 1$ min. The spectral HRV features showed better performance for $t_w = 2$ min due the better resolution of the RR spectrum associated to longer analysis segments. We observed median increases of 1–2 points in the AUROC when the segment was increased from $t_w = 1$ min to $t_w = 2$ min.

In a post-cardiac arrest scenario, the patient may not be breathing spontaneously after ROSC, and rescuers should artificially ventilate the patient. This may cause reduced respiratory-related heart rate dynamics and may influence HRV features. However, more studies are needed to analyze the relationship between the HRV metrics and ventilation metrics of the patient.

During treatment of OHCA patients many rhythm transitions occur, such as from an initial ventricular fibrillation to recovery of spontaneous pulse. Many studies have focused on the analysis of the prevalence and the prediction of rhythm transitions [30,31], including the transition from ROSC to another cardiac rhythm, that is, rearrest. A short time predictor was proposed in [13] using features v_{18}, v_{19}, and v_{21} to predict the rhythm in the next 3 s with an AUROC of 73. Our clinical context was different as we developed a model for patients that recovered a stable spontaneous pulse, and applied our model to predict a rearrest occurring on average 5 (6–7) min later. This is a much more challenging scenario, but of great clinical importance as it would allow clinicians to make more informed decision on transport to hospital after spontaneous pulse is recovered.

In this study, we also confirmed that the ECG waveform features significantly improved the performance of the RF model. Compared to the RF based exclusively on HRV features that we proposed in [14], the combination of HRV and ECG features improved the AUROC and AUPRC in 2 points when we increased the number of patients in the dataset by 65%. These are the first results of a machine learning solution to predict rearrest, and the RF model showed that including more features increased the accuracy of the method. The prediction of rearrest is a clinically important topic in OHCA treatment, and our results show that it is a challenging one. In the future, more sources of information available during treatment could be added to the models, including measures of the respiratory function (capnogram), cerebral state (cerebral oximetry or EEG-based bispectral analysis), or even blood pressure. These signals are not universal in OHCA treatment, but could be used to provide complementary information to that derived from HRV/ECG analysis.

The duration of the analysis interval of the ECG is important to predict rearrest. Our results showed that the performance improved when longer analysis windows were used, with differences of 2 points in AUROC when the duration of the analysis window was increased from 1 min to 2 min. In order to confirm that hypothesis, we replicated the analysis using the typical short window for HRV parameter calculations ($t_w = 5$ min). This reduced the sample size to 98 (26 RA and 72 NoRA). In this subset the AUC when $t_w = 5$ min was 8 points larger than for $t_w = 2$ min. This shows that longer analysis intervals improve the accuracy for the prediction of rearrest. However, in an OHCA scenario, time to clinical decisions and interventions is critical for survival, so a trade-off must be found between the detection of critical situations (rearrest) and the time needed to identify those situations. Longer delays to transport the patient in sustained ROSC to a hospital for a percutaneous coronary intervention may substantially lower the probability of survival of the patient [32]. Consequently, short analysis intervals (if sufficient for a diagnosis) should always be adopted.

This study has several limitations. The first one is the small patient cohort (162 cases), which, albeit being the largest cohort studied to date for this purpose, is still insufficient to draw conclusive results. Further studies on larger cohorts are needed, based on the evidence provided in this study. Second, the interpretation of the HRV parameters in a cardiac arrest context is controversial. Our results show they convey important information on the prediction of rearrest, but their physiological interpretation as measures of how cardiac arrest affects the autonomic nervous system are unclear. Third, in OHCA, time constraints in clinical interventions are of life and death importance; this limits the time available for the decisions and thus the segment lengths to compute HRV metrics. Short segments under 5-min should be used to compute HRV metrics, which further complicates the accuracy and interpretability of these measures. Finally, the conditions in which the ECG is recorded in a prehospital setting (hygiene, electrode contact, movement, and interventions) make QRS detection and thus RR-series calculations more challenging than in controlled hospital or laboratory conditions.

6. Conclusions

A RF model to predict a secondary arrest in the out-of-hospital setting is proposed using only 1 or 2 min of ECG signal right after return of spontaneous circulation. This manuscript shows that ECG signal and HRV metrics contain information about rearrest events, further studies are needed to confirm and improve our results.

Author Contributions: A.E. and E.A. conceived and designed the study. A.E. programmed the experiments and obtained the results. E.A. and E.R. participated in the curation and annotation of datasets. E.A., E.R., and U.I. helped with the interpretation of the experiments. A.I. and H.W. provided the datasets from the defibrillators, and helped with the interpretation of the biomedical signals and the clinical information. All authors contributed to the writing of the manuscript. All authors have read and agreed to the published version of the manuscript.

Funding: This work was supported by the Spanish Ministerio de Ciencia, Innovación y Universidades through grant RTI2018-101475-BI00, jointly with the Fondo Europeo de Desarrollo Regional (FEDER), and by the Basque Government through grants IT1229-19, PRE_2019_2_0100 and PRE_2019_1_0262. A.I. receives research grants from the US National Institutes of Health (NIH).

Conflicts of Interest: The funders had no role in the design of the study; in the collection, analyses, or interpretation of data; in the writing of the manuscript, or in the decision to publish the results.

Abbreviations

The following abbreviations are used in this manuscript:

AUROC	area under ROC curve
AUPRC	area under PR curve
CPR	cardiopulmonary resuscitation
ECG	electrocardiogram
HF	high frequency
HRV	heart rate variability
LF	low frequency
NoRA	no rearrest
OHCA	out-of-hospital cardiac arrest
PR	precision–recall
RA	rearrest
RF	random forest
ROC	receiver operating characteristics
ROSC	return of spontaneous circulation

References

1. Atwood, C.; Eisenberg, M.S.; Herlitz, J.; Rea, T.D. Incidence of EMS-treated out-of-hospital cardiac arrest in Europe. *Resuscitation* **2005**, *67*, 75–80. [CrossRef]
2. De Vreede-Swagemakers, J.J.; Gorgels, A.P.; Dubois-Arbouw, W.I.; Van Ree, J.W.; Daemen, M.J.; Houben, L.G.; Wellens, H.J. Out-of-hospital cardiac arrest in the 1990s: A population-based study in the Maastricht area on incidence, characteristics and survival. *J. Am. Coll. Cardiol.* **1997**, *30*, 1500–1505. [CrossRef]
3. Myat, A.; Song, K.J.; Rea, T. Out-of-hospital cardiac arrest: Current concepts. *Lancet* **2018**, *391*, 970–979. [CrossRef]
4. Valenzuela, T.D.; Roe, D.J.; Cretin, S.; Spaite, D.W.; Larsen, M.P. Estimating effectiveness of cardiac arrest interventions: A logistic regression survival model. *Circulation* **1997**, *96*, 3308–3313. [CrossRef] [PubMed]
5. Waalewijn, R.A.; De Vos, R.; Tijssen, J.G.; Koster, R.W. Survival models for out-of-hospital cardiopulmonary resuscitation from the perspectives of the bystander, the first responder, and the paramedic. *Resuscitation* **2001**, *51*, 113–122. [CrossRef]
6. Perkins, G.D.; Handley, A.J.; Koster, R.W.; Castrén, M.; Smyth, M.A.; Olasveengen, T.; Monsieurs, K.G.; Raffay, V.; Gräsner, J.T.; Wenzel, V.; et al. European Resuscitation Council Guidelines for Resuscitation 2015: Section 2. Adult basic life support and automated external defibrillation. *Resuscitation* **2015**, *95*, 81–99. [CrossRef] [PubMed]
7. Brooke Lerner, E.; O'Connell, M.; Pirrallo, R.G. Rearrest after prehospital resuscitation. *Prehospital Emerg. Care* **2011**, *15*, 50–54. [CrossRef]
8. Salcido, D.D.; Sundermann, M.L.; Koller, A.C.; Menegazzi, J.J. Incidence and outcomes of rearrest following out-of-hospital cardiac arrest. *Resuscitation* **2015**, *86*, 19–24. [CrossRef]
9. Salcido, D.D.; Schmicker, R.H.; Kime, N.; Buick, J.E.; Cheskes, S.; Grunau, B.; Zellner, S.; Zive, D.; Aufderheide, T.P.; Koller, A.C.; et al. Effects of intra-resuscitation antiarrhythmic administration on rearrest occurrence and intra-resuscitation ECG characteristics in the ROC ALPS trial. *Resuscitation* **2018**, *129*, 6–12. [CrossRef] [PubMed]
10. Bhardwaj, A.; Ikeda, D.J.; Grossestreuer, A.V.; Sheak, K.R.; Delfin, G.; Layden, T.; Abella, B.S.; Leary, M. Factors associated with re-arrest following initial resuscitation from cardiac arrest. *Resuscitation* **2017**, *111*, 90–95. [CrossRef]
11. Vyas, A.; Chan, P.S.; Cram, P.; Nallamothu, B.K.; McNally, B.; Girotra, S. Early coronary angiography and survival after out-of-hospital cardiac arrest. *Circ. Cardiovasc. Interv.* **2015**, *8*, e002321. [CrossRef] [PubMed]
12. Salcido, D.; Sundermann, M.; Koller, A.; Menegazzi, J. Towards predicting the time and rhythm of rearrest after out-of-hospital cardiac arrest. *Resuscitation* **2015**, *96*, 10. [CrossRef]
13. Alonso, E.; Eftestøl, T.; Aramendi, E.; Kramer-Johansen, J.; Skogvoll, E.; Nordseth, T. Beyond ventricular fibrillation analysis: Comprehensive waveform analysis for all cardiac rhythms occurring during resuscitation. *Resuscitation* **2014**, *85*, 1541–1548. [CrossRef] [PubMed]

14. Elola, A.; Rueda, E.; Amezaga, N.; Aramendi, E.; Irusta, U. Análisis de la Variabilidad del Ritmo Cardiaco para la Predicción de la Parada Cardiaca Extrahospitalaria Recurrente. In Proceedings of the Libro de actas, XXXVII Congreso Anual de la Sociedad Española de Ingeniería Biomédica, Santander, Spain, 27–29 November 2019; pp. 127–130.
15. Hamilton, P.S.; Tompkins, W.J. Quantitative investigation of QRS detection rules using the MIT/BIH arrhythmia database. *IEEE Trans. Biomed. Eng.* **1986**, *12*, 1157–1165. [CrossRef]
16. Shaffer, F.; Ginsberg, J. An overview of heart rate variability metrics and norms. *Front. Public Health* **2017**, *5*, 258. [CrossRef] [PubMed]
17. Tateno, K.; Glass, L. Automatic detection of atrial fibrillation using the coefficient of variation and density histograms of RR and ΔRR intervals. *Med. Biol. Eng. Comput.* **2001**, *39*, 664–671. [CrossRef]
18. VanderPlas, J.T. Understanding the lomb—Scargle periodogram. *Astrophys. J. Suppl. Ser.* **2018**, *236*, 16. [CrossRef]
19. Richman, J.S.; Moorman, J.R. Physiological time-series analysis using approximate entropy and sample entropy. *Am. J. Physiol. Heart Circ. Physiol.* **2000**, *278*, H2039–H2049. [CrossRef]
20. Zabihi, M.; Rad, A.B.; Katsaggelos, A.K.; Kiranyaz, S.; Narkilahti, S.; Gabbouj, M. Detection of atrial fibrillation in ECG hand-held devices using a random forest classifier. In Proceedings of the 2017 Computing in Cardiology (CinC), Rennes, France, 24–27 September 2017; IEEE: Piscataway, NJ, USA, 2017; pp. 1–4.
21. Martínez, J.P.; Almeida, R.; Olmos, S.; Rocha, A.P.; Laguna, P. A wavelet-based ECG delineator: Evaluation on standard databases. *IEEE Trans. Biomed. Eng.* **2004**, *51*, 570–581. [CrossRef]
22. Breiman, L. Random forests. *Mach. Learn.* **2001**, *45*, 5–32. [CrossRef]
23. Li, Q.; Mark, R.G.; Clifford, G.D. Robust heart rate estimation from multiple asynchronous noisy sources using signal quality indices and a Kalman filter. *Physiol. Meas.* **2007**, *29*, 15. [CrossRef] [PubMed]
24. Zong, W.; Moody, G.; Jiang, D. A robust open-source algorithm to detect onset and duration of QRS complexes. In Proceedings of the Computers in Cardiology, Thessaloniki Chalkidiki, Greece, 21–24 September 2003; IEEE: Piscataway, NJ, USA, 2003; pp. 737–740.
25. Salcido, D.D.; Stephenson, A.M.; Condle, J.P.; Callaway, C.W.; Menegazzi, J.J. Incidence of rearrest after return of spontaneous circulation in out-of-hospital cardiac arrest. *Prehospital Emerg. Care* **2010**, *14*, 413–418. [CrossRef] [PubMed]
26. Hartke, A.; Mumma, B.; Rittenberger, J.; Callaway, C.; Guyette, F. Incidence of re-arrest and critical events during prolonged transport of post-cardiac arrest patients. *Resuscitation* **2010**, *81*, 938–942. [CrossRef]
27. Chestnut, J.M.; Kuklinski, A.A.; Stephens, S.W.; Wang, H.E. Cardiovascular collapse after return of spontaneous circulation in human out-of-hospital cardiopulmonary arrest. *Emerg. Med. J.* **2012**, *29*, 129–132. [CrossRef]
28. Shao, M.; Bin, G.; Wu, S.; Bin, G.; Huang, J.; Zhou, Z. Detection of atrial fibrillation from ECG recordings using decision tree ensemble with multi-level features. *Physiol. Meas.* **2018**, *39*, 094008. [CrossRef] [PubMed]
29. Owis, M.I.; Abou-Zied, A.H.; Youssef, A.B.; Kadah, Y.M. Study of features based on nonlinear dynamical modeling in ECG arrhythmia detection and classification. *IEEE Trans. Biomed. Eng.* **2002**, *49*, 733–736. [CrossRef] [PubMed]
30. Skogvoll, E.; Eftestøl, T.; Gundersen, K.; Kvaløy, J.T.; Kramer-Johansen, J.; Olasveengen, T.M.; Steen, P.A. Dynamics and state transitions during resuscitation in out-of-hospital cardiac arrest. *Resuscitation* **2008**, *78*, 30–37. [CrossRef]
31. Nordseth, T.; Bergum, D.; Edelson, D.P.; Olasveengen, T.M.; Eftestøl, T.; Wiseth, R.; Abella, B.S.; Skogvoll, E. Clinical state transitions during advanced life support (ALS) in in-hospital cardiac arrest. *Resuscitation* **2013**, *84*, 1238–1244. [CrossRef]
32. Cournoyer, A.; Notebaert, É.; De Montigny, L.; Ross, D.; Cossette, S.; Londei-Leduc, L.; Iseppon, M.; Lamarche, Y.; Sokoloff, C.; Potter, B.J.; et al. Impact of the direct transfer to percutaneous coronary intervention-capable hospitals on survival to hospital discharge for patients with out-of-hospital cardiac arrest. *Resuscitation* **2018**, *125*, 28–33. [CrossRef]